# THE ROLE OF TAF PROTEINS DURING EARLY ZEBRAFISH DEVELOPMENT

by

ANDREAS ZAUCKER

A thesis submitted to

The University of Birmingham

for the degree of

DOCTOR OF PHILOSOPHY

College of Medicine & Dentistry

The University of Birmingham

April 2011

# Abstract

Replacement of the prototype promoter recognition factor (PRF) TFIID by alternative PRFs or changes in its subunit composition have recently been implicated in differentiation processes during development. TFIID is composed of TBP (TATA-binding protein) and 13 TAFs (TBP-associated factors). I comprehensively studied the roles of Tafs during vertebrate development using zebrafish model.

Taf knock down (kd) phenotypes generated in an antisense morpholino oligonucleotide (MO) screen suggest differential functions of Tafs during zebrafish development. The kd phenotypes also propose a special requirement of DNA-binding Tafs during zebrafish development.

In conjunction with zygotic mutant phenotype analysis of zebrafish *taf8*-mutants compared to *taf6*-mutants I investigated a potential coactivator function of Taf8 for Pparγ, which has been suggested by *in vitro* data. Oil Red O (ORO) stainings of 5 dpf (days post fertilisation) *taf8*- and *taf6*-mutant larvae revealed a specific lipogenesis defect in liver and intestine of *taf8*-mutant larvae. The results from treatments with a PPARγ inhibitor suggest that this lipogenic process is Pparγ-dependent. To convincingly establish a coactivator function of Taf8 for Pparγ during early zebrafish development, future work has to link the 5 dpf lipogenesis phenotype of *taf8*-mutants to defects in Pparγ-dependent transcription.

# Acknowledgements

# Table of contents

# List of illustrations

List of tables

# List of abbreviations

## Abbreviations for model organisms

| | |
|---|---|
| *C. elegans* | *Caenorhabditis elegans* |
| *Drosophila* | *Drosophila melonagaster* |
| *Xenopus* | *Xenopus laevis* |
| mouse | *Mus musculus* |
| yeast | *Saccharomyces cerevisiae* |
| zebrafish | *Danio rerio* |

## Other abbreviations

| | |
|---|---|
| bp | base pair(s) |
| CD36 | CD36 antigen (thrombospondin receptor) |
| cDNA | complementary DNA |
| CNC | cephalic neural crest |
| CRE | *cis*-regulatory element |
| DBD | DNA binding domain |
| DNA | deoxyribonucleic acid |
| dpf | days post fertilisation |
| FABP | fatty acid-binding protein |
| gDNA | genomic DNA |
| GFP | green fluorescent protein |

| | |
|---|---|
| GTF | general transcription factor |
| HFD | histone fold domain |
| hpf | hours post fertilisation |
| Inr | initiator |
| kb | kilobase(s) |
| kDa | kilo Dalton |
| kd | knock down |
| LOF | loss of function |
| LPL | lipoprotein lipase |
| Mb | megabase(s) |
| MBT | mid-blastula transition |
| MO | morpholino oligonucleotide |
| MZT | maternal-to-zygotic transition |
| NFW | nuclease-free water |
| O/N | over night |
| PCR | polymerase chain reaction |
| PHD | plant homeodomain |
| PIC | preinitiation complex |
| Pol II | DNA-dependent RNA-polymerase II |
| PPAR | peroxisome proliferator-activated receptor |
| PRF | promoter recognition factor |
| qPCR | quantitative PCR |

| | |
|---|---|
| RNA | ribonucleic acid |
| RT-PCR | reverse transcription PCR |
| RXR | retinoid x receptor |
| SAGA | Spt-Ada-Gcn5-Acetyltransferase |
| SLC27A1 | solute carrier family 27 (fatty acid transporter), member 1; FATP1 |
| TAF | TBP-associated factor |
| *taf*-mutants | *taf8*- and *taf6*-mutants |
| Taf8up | set of genes from the 4 dpf microarray experiment, which are significantly up-regulated in *taf8*-mutants |
| Taf8down | set of genes from the 4 dpf microarray experiment, which are significantly down-regulated in *taf8*-mutants |
| Taf6up | set of genes from the 4 dpf microarray experiment, which are significantly up-regulated in *taf6*-mutants |
| Taf6down | set of genes from the 4 dpf microarray experiment, which are significantly down-regulated in *taf6*-mutants |
| TBP | TATA-binding protein |
| TF | transcription factor |
| TSS | transcription start site |
| UTR | untranslated region |
| WISH | whole-mount *in situ* hybridisation |

# 1   Introduction

## 1.1   Transcriptional regulation on the core promoter level

### 1.1.1   Overview of transcriptional regulation

The first step in the utilisation of the information encoded by the DNA (deoxyribonucleic acid) is its transcription into RNA (ribonucleic acid). This process ultimately results in macromolecules (gene products), RNAs and proteins, which determine the identity and behaviour of the cell. Transcription of genomic DNA in eukaryotes is carried out by three different DNA-dependent RNA-polymerases (Pol I, II, or III), each of them responsible for the production of different types of transcripts (rRNA, mRNA and small RNAs respectively). If not stated otherwise, the transcription of protein coding genes by Pol II is discussed in this thesis. The genomic DNA not only encodes for proteins (genomic code) but also contains a code for the spatiotemporal control of transcription, the regulatory code. The regulatory code is contained in sequences controlling the transcription of their target genes mostly in *cis*. Those sequences are therefore called *cis*-regulatory elements (CREs). The *cis*-regulatory elements are recognised and interpreted by *trans*-acting factors. *Trans*-acting factors are mostly proteins and protein-complexes, but RNAs can also be involved. Some of these proteins, so called transcription factors (TF), can directly bind to small sequence motifs within CREs. CREs can be classified into three categories, based on distance to the transcription start site (TSS):

1. Core promoter elements (or motifs) are located within the core promoter of genes. The core promoter is defined as the minimal sequence required for directing accurate transcription initiation by Pol II *in vitro*. The core promoter encompasses the sequences 40 bp (base pairs) upstream and downstream of the TSS.

2. Proximal Elements are CREs within several hundreds of base pairs upstream of the TSS.

3. Distal Elements are CREs located further away from the TSS. They can be several kilobases (kb) up to megabases (Mb) away from the TSS of their target genes. There is no clear functional distinction between distal and proximal promoter.

CREs and *trans*-acting factors are embedded in so called gene regulatory networks, which control the expression of the genes within the network.

Transcription is to a great extent regulated at the step of transcription initiation. However, the transcription of many genes, up to one third, might also to be regulated at the elongation step (Levine, 2011). The regulation of transcription initiation is a very complex process, involving various multiprotein complexes and CREs (Figure 1.1). Some of the multiprotein complexes, e.g. the chromatin modifying and the chromatin remodelling complexes, control if the chromatin template is in a state, which is accessible for the transcription machinery. The order and the cause effect relationship of the events are not fully understood, but all these regulatory inputs converge on the core promoter, to either block or facilitate the formation of a preinitiation complex (PIC). The PIC recruits and activates Pol II for transcription of the downstream gene.
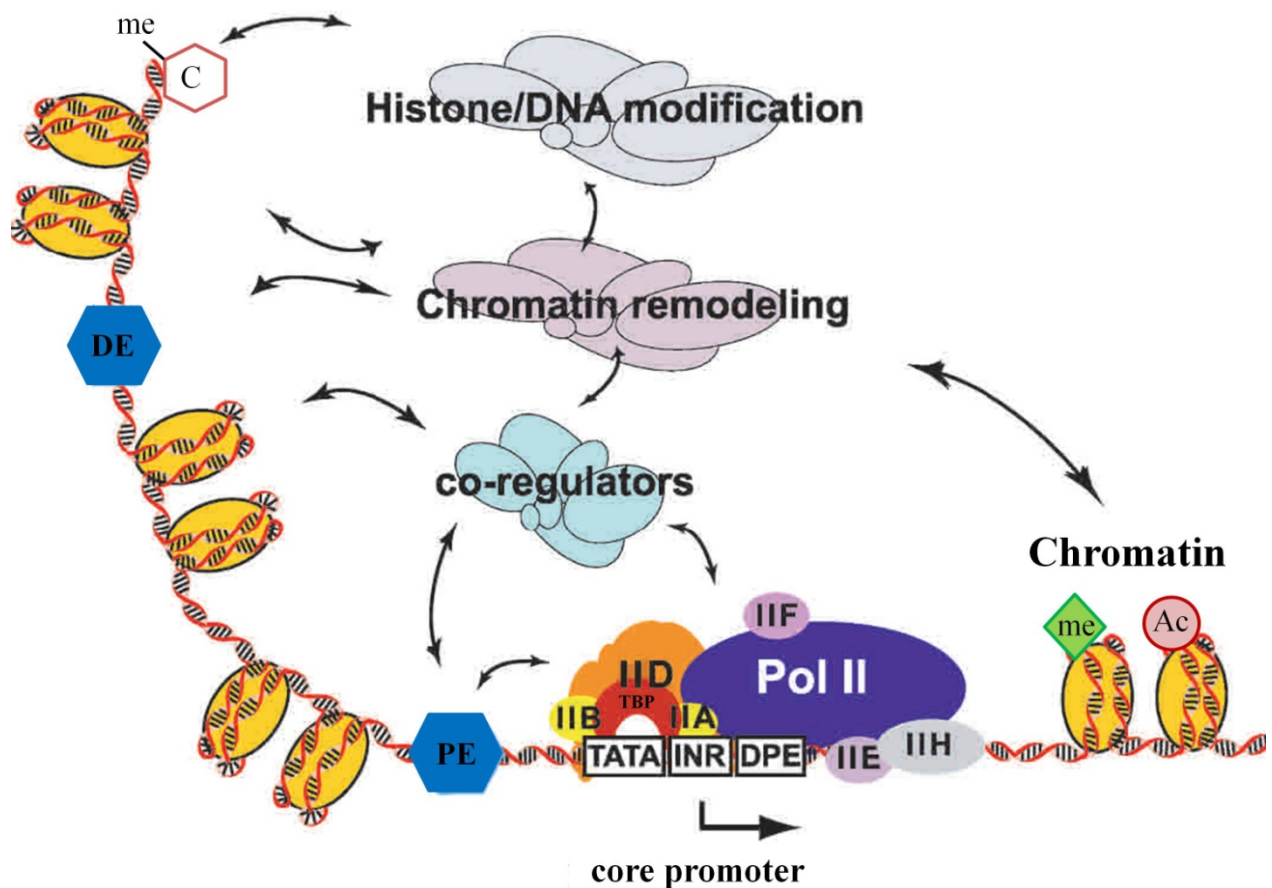
**Figure 1.1 – Multiprotein complexes involved in transcriptional regulation**

Schematic representation of protein complexes and *cis*-regulatory elements involved in the regulation of transcription initiation. The regulatory code embedded in distal elements (DE), proximal elements (PE), the core promoter and also the chromatin, is interpret by transacting protein complexes. There is an extensive interplay of the components involved, represented by the arrows in the figure. This interplay and the order of these regulatory events are not fully understood. But generally can be said that the formation of a preinitiation complex on the core promoter is either stimulated or blocked, depending on the protein-protein interactions on the *cis*-elements. Figure modified from (Hochheimer and Tjian, 2003).

## 1.1.1.1 Chromatin as a regulator of transcription

*In vivo* the template for Pol II is not DNA, but chromatin, which is a complex of DNA and proteins. The principal subunit of chromatin is the nucleosome. A nucleosome consists of ≈146 bp of DNA wrapped around a histone-octamer, which is a complex of a histone H3/H4-tetramer

3

sandwiched between two histone H2A/H2B-dimers. The site where the DNA enters and leaves the octamer is covered by histone H1. Chromatin plays a major role in transcriptional regulation, as it can switch between states which do, or do not favour transcription. It can be in an open, nucleosome depleted state, which is accessible for the transcription machinery and recruits factors with an activating effect on transcription. The opposite, silenced state is characterised by densely packed nucleosomes. This chromatin is less accessible for the transcription machinery and recruits factors with a silencing effect on transcription.

Many of the changes between the two states are associated with posttranslational modifications of the N-terminal domains (histone tails) of the histones in nucleosomes. Postranslational modifications described for histones are: Acetylation, methylation, phosphorylation, monoubiquitination, sumoylation and ADP-ribosylation ((Smith and Shilatifard, 2010) and references therein)). A histone modifications which is associated with transcriptionally active chromatin is H3K4me3 (histone H3 tri-methylated at lysine K4), whereas the H3K27me3 modification is indicative of a repressed state (Mikkelsen et al., 2007, Rosenfeld et al., 2009). Both marks can be found together in the promoter regions of a set of genes in ESCs (Embryonic Stem Cells) which is enriched for developmental regulators (Bernstein et al., 2006). It has been hypothesised that bivalent promoters facilitate the rapid activation of genes in certain lineages during development. However, the significance of bivalent domains is under debate (B. M. Lee and Mahadevan, 2009). Histone acetylation, in particular H3K9ac, is associated with an open chromatin state on regulatory regions and with transcription (Roh et al., 2005). Proteins involved in transcriptional regulation often contain domains which can bind to modified residues of histones. Bromodomains for example bind to acetylated lysines (Mujtaba et al., 2007), whereas chromodomains, MBT (mid-blastula transition) repeats and PHD-fingers (plant homeodomain)

4

bind to methylated lysines (Bonasio et al., 2010, Champagne and Kutateladze, 2009, Yap and Zhou, 2011).

## 1.1.1.2    Proteins and complexes on enhancers

Enhancers are *cis*-regulatory sequences with stimulating effect on the transcription rate of their target genes. Accordingly, they contain binding sites for so called (transcriptional) activators. Activators are transcription factors, a class of proteins which bind to DNA to regulate transcription of a subset of genes, which are regarded as the TF's target genes. The structure of TFs is modular, comprising a DNA-binding domain (DBD) and a (trans)activation domain (AD). The TF uses the DBD to bind to short (6-12 bp) sequence motifs. The sequence motifs are called transcription factor binding sites (TFBS). The DBD is not unique for each TF. Only a limited number of DBDs seem to have evolved in nature, some of them are found only in certain branches of the tree of life, like the Dof domain proteins in plants (Yanagisawa, 2004). Accordingly most of the TFs in a given organism share their DBD with other TFs and the DBD can be used to classify TFs. The DNA-binding domain is the hallmark of a TF and the sequence motif encoding for it can be used to identify TFs in a sequenced genome. The AD, as the name suggests, is a domain responsible for the activating function of the activator on the transcription rate of its target genes. This domain provides surfaces for protein-protein interactions with either co-regulators or the PIC on the core promoter. A reoccurring principle is that TFs often bind to enhancers in combination with other activators, to form a complex on the enhancer called enhanceosome (Panne, 2008). The specific combination of TFs in the enhanceosome is thought to define the specific function of the enhancer.

### 1.1.1.3 Co-regulators and protein complexes linking enhancers to promoters

How do activators bound to distal sites influence the transcription rate of their target genes? The current view is that they do this in two ways:

1. Activators recruit co-regulators with enzymatic activities which render the chromatin into an open state, which is accessible for the transcription machinery (Visel et al., 2009).

2. Activators directly, or indirectly via co-regulators, interact with general transcription factors (GTFs) to stabilise the PIC. GTFs and their subunits are all the proteins within the PIC, which do not belong to Pol II (Wright and Tjian, 2009).

Both principles require that the enhancer and promoter come in close proximity to each other, which would result in a looping of the DNA. Indeed DNA-loops have been demonstrated (Carter et al., 2002). The higher order organisation of chromatin defines which sequences can potentially interact with each other. Factors which are shaping the higher order organisation of chromatin, like CTCF (CCCTC-binding factor) and cohesin, have accordingly been implicated in transcriptional regulation (Kagey et al., 2010, Phillips and Corces, 2009).

One mechanism for the regulation of transcription by co-regulators lies within their histone modifying activities. Histone actylation and deacytylation have been shown to have an inverse effect on transcription. Histone acetylation weakens the interaction of histones with DNA. This resolves the repressive effect of chromatin on transcription. The opposite is the case for histone deacetylation. Accordingly, many transcriptional co-regulators are themselves HATs (histone acetyl transferases), or they recruit HATs. The inverse is the case for co-reppressors, which often are HADCs (Anamika et al., 2010, Viswakarma et al., 2010).
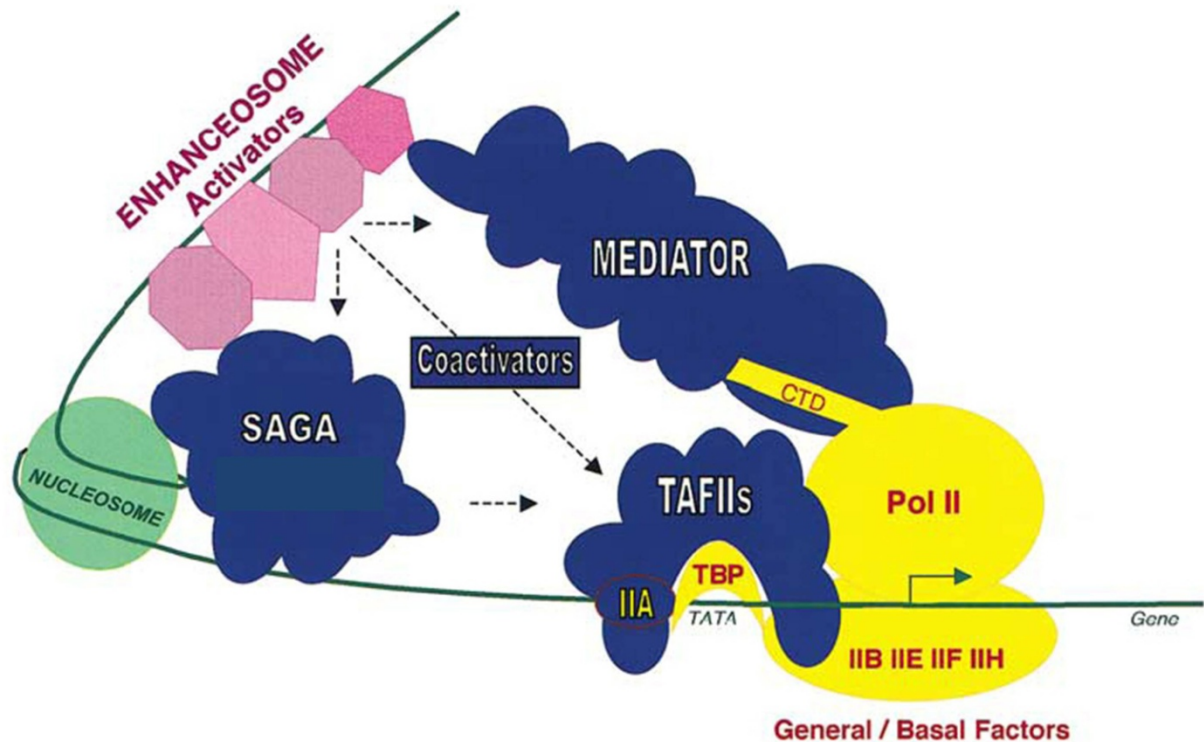
**Figure 1.2 – Coactivators of transcription**

The figure depicts the various types of coactivators which have been described in the literature. Some of those coactivators are mediating interactions between transcriptional activators and the basal transcription machinery (TAFs, Mediator, TFIIA and SAGA). Others have a chromatin modifying activity (HAT) which opens up the chromatin to facilitate transcription (SAGA, TAFs). Modified from (Martinez, 2002).

One complex mediating the indirect interaction of enhancers with promoters is called Mediator

Complex. The Mediator complex interacts with numerous activators and Pol II, such forming a

bridge between the enhancer and the basal transcription machinery on the core promoter. Another

class of such complexes is the SAGA complex (Spt-Ada-Gcn5-Acetyltransferase). SAGA first

has been described in yeast, followed by the discovery of complexes (TFTC, STAGA, PCAF),

with an overall very similar subunit composition, in other organisms. Therefore, it has been

suggested to collectively refer to them as SAGA, or SAGA-like complexes (Pijnappel and

7

Timmers, 2008). Furthermore these complexes harbour the yeast histone acetyl transferase Gcn5 (general control nonderepressable 5), or homologs of it.

### 1.1.1.4 Promoter recognition factors

Pol II itself does not recognise promoters and requires accessory factors for site-specific transcription initiation. Those accessory factors ( TFIIA, TFIIB, TFIID, TFIIE, TFIIF and TFIIH) have been biochemically purified in human HeLa cells. They are collectively referred to as GTFs. Their naming uses following nomenclature: TF (transcription factor) II (Pol II-driven transcription) X (chromographic fraction of isolation). All GTFs, except TFIIE, are themselves multiprotein complexes. One component of a PIC has to be able to distinguish promoters from the rest of the genome, based on sequence motifs and/or histone marks, and to nucleate PIC assembly (promoter recognition factor). The classical promoter recognition factor is TFIID, which is composed of TATA-binding protein and up to 13-14 TAFs. In the classical model of PIC formation TFIID, bound to core-promoters via its subunit TBP, nucleates the assembly of a stereotypic set of GTFs and Pol II into a PIC. There are two models for the precise order of PIC assembly (Thomas and Chiang, 2006):

The sequential assembly pathway suggests a stepwise assembly of the PIC. TFIID nucleates PIC assembly via binding to the promoter, followed by entry of TFIIB and TFIIA. A TFIID/A/B-TFIIF/Pol II complex forms on the promoter, which then recruits TFIIE and finally TFIIH.

The Pol II holoenzyme pathway (two component pathway) suggests that a preassembled Pol II holoenzyme complex (various compositions described), containing a subset of GTFs, associates with a second complex, containing the rest of the GTFs, to form a PIC.

## 1.1.2   Diversity of the core Pol II promoter binding machinery
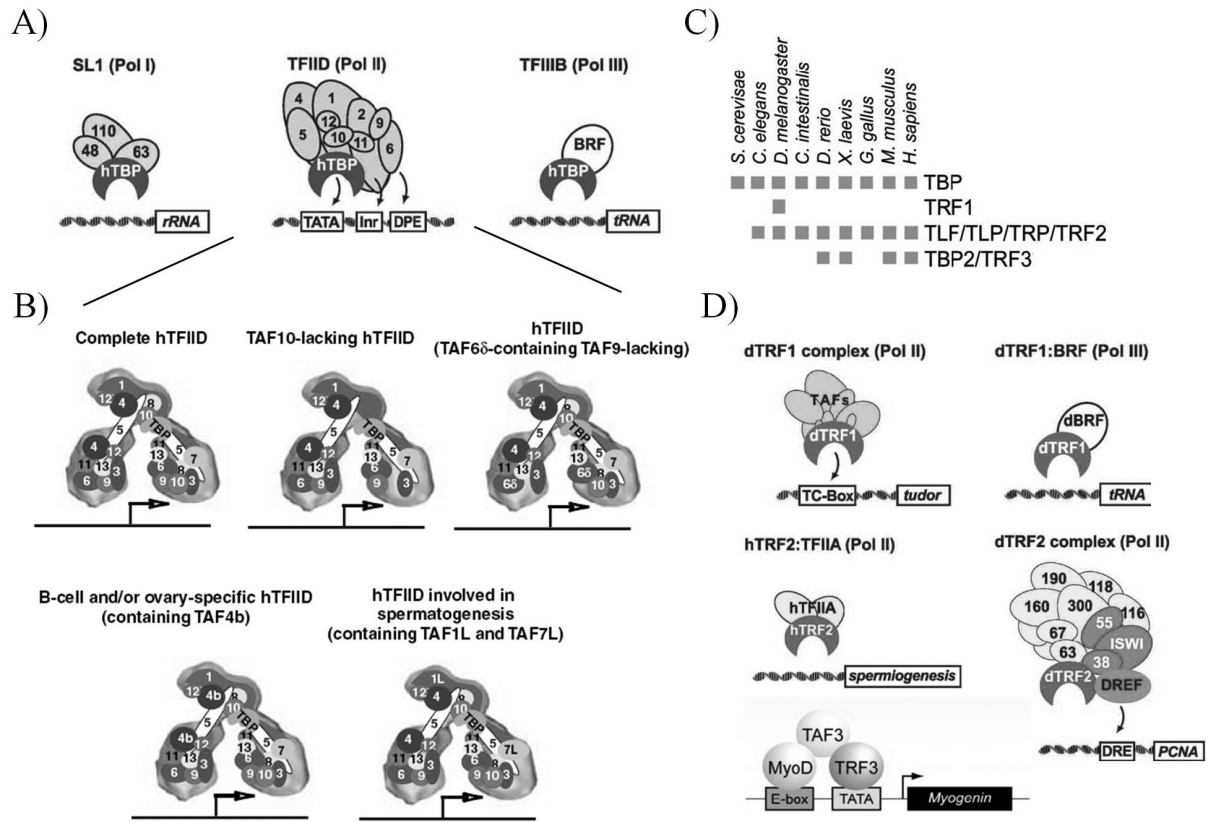


**Figure 1.3 – Diversity of core promoter binding machinery**

This figure illustrates the variety of PRFs which have been described in the literature. **A)** shows the three TBP-containing complexes, which are involved in the initiation of transcription from Pol I, Pol II and Pol III-dependent promoters, respectively. **A)** is taken from (Hochheimer and Tjian, 2003). **B)** is taken from (Muller and Tora, 2004). It illustrates the dynamic composition of TFIID, which differs between cell-types and might change upon exogenous stimuli (e.g. apoptotic stimuli). **C)** depicts the conservation of TBP-family proteins from yeast to humans. The figure is taken from (Bartfai et al., 2004). **D)** taken from (Hochheimer and Tjian, 2003) and (Hart and Green, 2008), depicts some of the various TBP-paralog containing complexes described in the literature.

## 1.1.2.1     TBP family of proteins

TBP can be seen as the central transcription factor in eukaryotic transcription, as it is involved in transcription catalysed by all three major eukaryotic RNA-polymerases, Pol I, II and III. It associates with different sets of other proteins to form specific complexes for the recruitment of the different Polymerases to the promoters of the specific types of genes they transcribe (Figure 1.3). Those TBP containing complexes are SL1 for Pol I, TFIID for Pol II and TFIIIB for Pol III. TBP is highly conserved from yeast to humans. TBP got its name from the fact that it was found to bind to the common eukaryotic promoter motif called TATA-box, which carries its consensus sequence (not the exact one) in its name. The DBD of TBP (C-terminal), also called the core-domain, has a saddle-shaped structure. It binds to DNA with its inner, concave side and binding forces the DNA double strand to kink in 90°. This is thought to assist in opening up the double strand for transcription initiation. The outer convex side is thought to provide interaction surfaces for other GTFs and proteins. TBP also carries a N-terminal domain. TBP is not required for all Pol II transcribed genes (Ferg et al., 2007, Jacobi et al., 2007, Martianov et al., 2002, Muller et al., 2001, Veenstra et al., 2000). In line with that finding, only a minority of ≈10-20% of Pol II core promoters appears to carry a TATA-Box (Ohler and Wassarman, 2010).

Numerous biochemical and genetic studies have been carried out on yeast TBP and TFIID. More recently, paralogs of TBP have been discovered in several metazoan species. The first one was TBP-related factor 1 (TRF1) in *Drosophila* (Crowley et al., 1993). It is an insect specific factor (or possibly Diptera-specific). Besides in *Drosophila* it only has been found in *Anopheles*. TRF1 interacts with TFIIA and B and directs TATA-dependent transcription *in vitro* (Hansen et al., 1997). TRF1 is ubiquitously expressed during embryogenesis and in adults, with higher

expression levels in the adult nervous system and in the male germline (Hansen et al., 1997). A TRF1 containing complex directing transcription from an alternative, TFIID-independent, promoter of the tudor gene has been described (Holmes and Tjian, 2000). However, on a global scale, ChIP-chip experiments suggest that TRF1 plays only a minor role in Pol II dependent transcription. The more important role of TRF1 seems to be in replacing TBP for Pol III dependent transcription (Isogai et al., 2007b, Takada et al., 2000).

A metazoan-specific factor called TBP-like factor (TLF) has been described nearly simultaneously by several authors (Dantonel et al., 1999, Maldonado, 1999, Moore et al., 1999, Rabenstein et al., 1999), causing a little bit of confusion with the naming. TRF2, TBP-related protein (TRP), TBP-related factor 2 (TRF2) and TBP-like protein 1 (TBPL1), all are synonyms for this factor. The core domain of human TLF shows only 42% sequence identity with the core domain of human TBP. Critical residues for the interaction with the DNA of the TATA-box are altered, so that TLF neither binds to the TATA-box, nor does it direct TATA-dependent transcription. Its biological role has been studied in several model organisms, revealing significant differences between mammals (mouse) and lower vertebrates (*Xenopus*, fish) and organisms. It seems to be essential for early development of lower vertebrates (Muller et al., 2001, Veenstra et al., 2000), as well as *C. elegans* (Kaltenbach et al., 2000) and *Drosophila* (Kopytova et al., 2006) In mouse it is dispensable for early development and plays a role in spermiogenesis. In *Drosophila* TLF interacts with DREF (DNA replication-related element binding factor). The DREF/TLF-complex can direct transcription from an alternative promoter of the PCNA gene (Proliferating cell nuclear antigen). This complex seems to play a significant role for Pol II transcription in *Drosophila* (Isogai et al., 2007a). In *Xenopus* and in *C. elegans* TLF is

required for the transcription of many genes during development (Jacobi et al., 2007, Kaltenbach et al., 2000).

The newest member of the TBP family is the vertebrate-specific TBP2 (TRF3, TBPL2)(Persengiev et al., 2003). Its core domain in humans is nearly identical to the one of TBP (91% identity). Accordingly it binds to the TATA-box, directs TATA-dependent transcription and interacts with TFIIA and B. This suggests redundant functions between TBP and TBP2. And indeed TBP2 substitutes TBP for Pol II dependent transcription in *Xenopus* oocytes (Akhtar and Veenstra, 2009). But there is a significant difference between TBP and TBP2. TBP2 lacks the N-terminal domain, suggesting roles of TBP2 beyond redundancy with TBP. Indeed specific functions of TBP2 have been described. A TBP2/TAF3 has been found to replace TFIID during myogenesis *in vitro* (Deato and Tjian, 2007). Also, the expression of TBP2 in *Xenopus* and zebrafish during gastrulation is restricted to the ventral half, which may contribute to the observed hematopoietic role of a TBP2/TAF3-complex in zebrafish and mouse embryonic stem cells (Hart et al., 2007, Hart et al., 2009). Similar to what has been described for TLF, TBP2 is essential during development in lower vertebrates (Bartfai et al., 2004, Hart et al., 2007, Jallow et al., 2004) but not in mouse. TBP2 ko mice show no obvious phenotype except of defects in oogenesis (Gazdag et al., 2009). TBP2's specific role in oocytes is supported by the observation that TBP2 is the predominantly expressed TBP-family member in vertebrate oocytes (Bartfai et al., 2004, Gazdag et al., 2007, Xiao et al., 2006). The mouse ko phenotype contradicts the findings about the role of TBP2 for the myogenic and hemtopoietic differentiation of mouse cells *in vitro* and caused an ongoing controversy about that issue. The reason for different observations might be due to different antibodies and protein extraction methods used in different laboratories (Goodrich and Tjian, 2010).

The two TBP paralogs in mouse seem to control transcriptional programmes in the context of meiosis, with TLF in the male and TBP2 in the female germline. While in lower vertebrates those two factors are also is essential during early development.

**Table 1.1 – Specific functions of TBP family members**
**adapted from (Goodrich and Tjian, 2010)**

| Factor | System studied | Functions discussed | References |
|---|---|---|---|
| TBP | HeLa cells | Mitotic bookmarking | (Xing et al., 2008) |
| | zebrafish | Key regulator of maternal to zygotic transition | (Ferg et al., 2007) |
| TRF1 | *Drosophila* | Pol III-dependent transcription | (Crowley et al., 1993), (Hansen et al., 1997) |
| TLF | *C. elegans, Xenopus,* zebrafish | Early embryogenesis | (Kaltenbach et al., 2000), (Veenstra et al., 2000), (Muller et al., 2001) |
| | *Drosophila* | Germ cell differentiation, metamorphosis | (Kopytova et al., 2006), (Bashirullah et al., 2007), |
| | *Drosophila* S2 cells | Transcription (e.g. histone H1) | (Hochheimer et al., 2002), (Isogai et al., 2007a) |
| | mouse | Spermatogenesis | (Zhang et al., 2001), (Martianov et al., 2001) |
| TBP2 | *Xenopus* | Gastrulation | (Jallow et al., 2004), (Xiao et al., 2006) |
| | zebrafish | Embryogenesis, haematopoiesis | (Bartfai et al., 2004), (Hart et al., 2007) |
| | mouse ESCs | Haematopoiesis | (Hart et al., 2009) |
| | mouse C2C12 cells | Myogenesis | (Deato and Tjian, 2007), |
| | mouse | Oogenesis | (Xiao et al., 2006), (Gazdag et al., 2009) |

## 1.1.2.2 Structural function of TAFs in TFIID

All proteins in TFIID other than TBP are so called TBP-associated factors, TAFs. They were first described as "coactivators associated with the TATA-binding protein that mediate transcriptional activation"(Dynlacht et al., 1991). The set of TAFs within TFIID is highly conserved from yeast to human and a unified nomenclature system exists, numbering them from 1-15 (Tora, 2002). Exceptions are Taf14, which is only found in yeast, and TAF15, which is also not found in all organisms. So the actual set of TAFs within TFIID in different organisms ranges between 13 and 14. TAFs are a quite heterogeneous group of proteins. However, 9 out of the 13 TAFs in TFIID carry a region with striking similarity to core histones, the histone fold domain (HFD). Via their HFDs TAFs form five pairs of heterodimers: TAF3/10, TAF4/12, TAF6/9, TAF8/10 and TAF11/13. Interestingly, all HFD-containing TAFs are present in more than one copy within TFIID, while HFD-less are present in single copies. The exception is the HFD-less TAF5. Our structural knowledge about TFIID is limited to low resolution (23-32Å) structures elucidated by electron microscopy (EM) of human and yeast TFIID. The structure of TFIID seems to resemble a horseshoe-shaped molecular clamp. The combination of EM with immunolabelling facilitated the localisation of individual TAFs within this structure. The TAFs within TFIID form a complicated network of protein-protein interactions resulting in its assembly and organisation. The current model suggests a modular assembly of TFIID. In this model a stable core complex, composed of most, if not all, of the TAF heterodimers and a TAF5 homodimer, associates with a TAF1-TAF7-TBP module and TAF2 to form TFIID. Several versions of this core complex have been described, comprising either 5 TAFs (Wright et al., 2006), 7 TAFs (Demeny et al., 2007) or

9 Tafs (yeast). However, the homo-dimerisation of TAF5 is under discussion and also whether the TAF3/10 heterodimer is really part ofTFIID (Cler et al., 2009).

The relative contribution of the subunits to the stability of TFIID has not been thoroughly investigated for all TAFs. There is some evidence that TAF4, TAF5 and TAF10 are each crucial for the assembly and the integrity of TFIID.

**Figure 1.4 – Structure of TAFs and model of TFIID-assembly**

In **A)** the domain structures of human TAFs, TAF paralogs (TAFb) and TAF-like proteins (TAFL) are depicted. Known domains are highlighted in different colours and their names are given in the according legend. TAFs which are part of the 7 TAF core complex are labelled with an asterisk. **B)** shows the current model of TFIID assembly. A core complex module associates with a TAF1-TAF7-TBP module and TAF2 to form full TFIID. Modified from (Cler et al., 2009).

## 1.1.2.3 Molecular and biological functions of TAFs

As a promoter recognition factor nucleating PIC-assembly, TFIID needs to be able to bind to promoter chromatin. It is well established that TBP binds to the TATA-box, but most of the promoters lack a detectable TATA-box.

The current view is that TFIID binds to TATA-free promoters via interactions of its TAF-subunits with other promoter elements and/or histone marks enriched around promoters. TAF2, alone or in a subcomplex with TAF1, binds to the Initiator (Inr) promoter element found around the TSS of many genes (Papai et al., 2009). Furthermore an interaction of the TAF6/9-heterodimer with the downstream promoter element (DPE) has been demonstrated (Burke and Kadonaga, 1997). Several of the TAFs contain structural domains for interactions with chromatin. TAF1, itself a HAT, interacts with actylated histone H4 via its tandem (double) bromodomain (Jacobson et al., 2000). TAF3 was shown to bind the histone mark H3K4me3, which is enriched at promoters of actively transcribed genes, via its PHD-finger (Vermeulen et al., 2007).
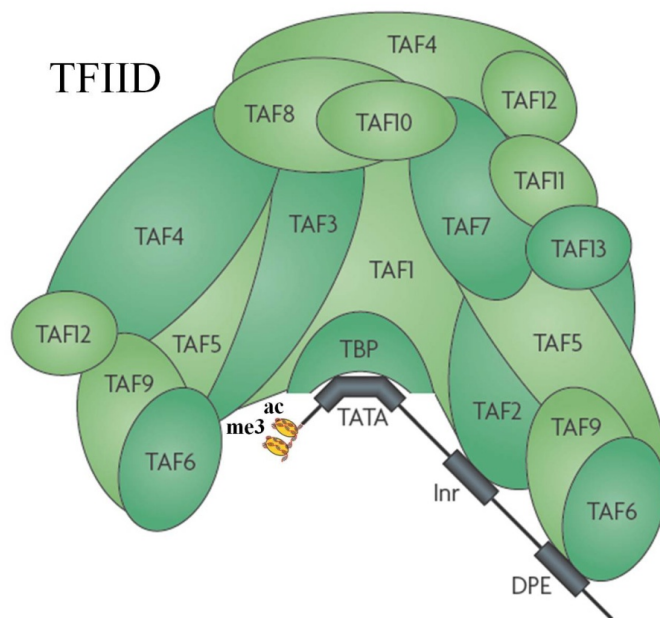
**Figure 1.5 – Promoter recognition by subunits of TFIID**

The figure shows a summary of what is known about promoter recognition by TFIID subunits. Binding of TAF2 together with TAF1 to the Inr has been demonstrated. The TAF6/9 heterodimer binds to the DPE. TAF3 was found to bind to the H3K4me3 histone mark and TAF1 binds to acetylated histone tails. These mechanisms might be essential for promoter recognition of TATA-less promoters. The figure is modified from (Goodrich and Tjian, 2010).

TAFs have initially been identified as coactivators required together with TBP for activated transcription. For some of the TAFs direct interactions with activators have been reported. Human TAF4 interacts with several activators like SP1 and CREB, via a well conserved domain (TAFH), which binds to a short hydrophobic motif often present in transcriptional regulators (X. Wang et al., 2007). TAF3, as part of a TBP2/TAF3 complex has been shown to be a coactivator for the myogenic factor MyoD in cultured mouse cells (Deato et al., 2008). For the *Drosophila* orthologs of TAF4 and TAF3 different coactivator functions have been described. TAF4 has been placed at the end of protein-protein interactions leading to activated transcription of a Wnt target gene (Wright and Tjian, 2009). TAF3 interacts with the hox gene *Antennapedia* (*Antp*) (Prince et al., 2008). For TAF7 interactions with numerous activators, including SP1, YY1, USF and CTF,

18

have been reported (Chiang and Roeder, 1995). Also in yeast interactions of Tafs with activators have been observed. Yeast TFIID serves as a coactivator for Rap1, via interactions of several of its subunits, the two Taf4/12 heterodimers and the two Taf5 molecules, with Rap1 (Garbett et al., 2007). Furthermore Taf12 has been shown to interact with the acidic activators Gal4 and Gcn4 (Reeves and Hahn, 2005).

Emerging from what is discussed above is the following picture of the general transcription factor TFIID: TFIID is a promoter recognition factor, recruited to core promoters via interactions of its subunits with core promoter motifs and with histone marks. Specific interactions of its numerous subunits with other transcriptional regulators enable TFIID to serve as an integration point for the various regulatory and signalling events acting on the regulation of transcription initiation on the core promoter.

But roles of TFIID subunits beyond the above described principle have been reported. In early embryos of *C. elegans*, transcription is globally repressed by sequestration of TAF-4 into the cytoplasm via interactions with OMA proteins (Guven-Ozkan et al., 2008). This principle, that the localisation of a TAF is controlled by its interaction partners is not new. The nuclear import of TAF10, which lacks a nuclear import signal (NLS), is dependent on its interactions with the NLS bearing TAF8 or TAF3 (Soutoglou et al., 2005). TAF12 has been implicated in an active DNA demethylation mechanism of promoter DNA (Schmitz et al., 2009). A splice variant of TAF6 called TAF6δ seems to be induced and incorporated into TFIID upon apoptotic stimuli (Wilhelm et al., 2008).

**Table 1.2 – Specific functions proposed for TAFs and homologs**

| Principle process | | Specific process discussed | Factor | References |
|---|---|---|---|---|
| Promoter Recognition | Binding to promoter motifs | Binding to initiator element (Inr) | TAF1, TAF2 | (Chalkley and Verrijzer, 1999) |
| | | Binding to downstream promoter element (DPE) | TAF6/9 heterodimer | (Burke and Kadonaga, 1997) |
| | | Binding to downstream core-promoter element (DCE) | TAF1 | (D. H. Lee et al., 2005) |
| | Binding to histone marks | Binding to acetylated histone H4 tails | TAF1 | (Jacobson et al., 2000) |
| | | Binding to H3K4me3 | TAF3 | (Vermeulen et al., 2007) |
| Coactivator | | Indirect coactivator for Wnt | TAF4 | (Wright and Tjian, 2009) |
| | | Fuctional interaction with ANTP | TAF3 | (Prince et al., 2008) |
| Differentiation process | | Myogenesis | TAF3 | (Deato and Tjian, 2007) |
| | | Hematopoiesis | | (Hart et al., 2009) |
| | | Adipogenesis | TAF8 | (Guermah et al., 2003) |
| Gametogenesis | | Mouse gametogenesis | TAF4b | (Falender et al., 2005) |
| | | Spermatogenesis | TAF7L | (Pointud et al., 2003) |
| | | *Drosophila* spermatogenesis | Several | (V. C. Li et al., 2009) |
| Others | | Active promoter DNA demethylation | TAF12 | (Schmitz et al., 2009) |
| | | Suppression of transcription in early embryos by sequestration of TAF-4 into the cytoplasm | TAF-4 | (Guven-Ozkan et al., 2008) |

## 1.1.3   TAF8

TAF8 protein is conserved from yeast to humans. The human protein is a 43 kDa (kilo Dalton) protein. It contains a histone fold domain at its N-terminus. The histone fold domain provides

surfaces for protein-protein interactions with other histone fold containing TAFs and proteins. Less is known about the function of the proline-rich domain.

The role of TAF8 during development has been investigated in mouse model, where a mutant allele has been generated by an insertion of a gene trap cassette, which disrupts the protein after 66 amino acids. The investigation of the mouse *Taf8* mutant phenotype revealed a specific requirement of TAF8 for the survival of the inner cell mass (ICM) of E3.75 blastocysts. Late blastocysts appear empty because of the lacking ICM. This resemblance of an empty nut, properly prompted the investigators to call the mouse phenotype of TAF8 "Taube Nuss", which is a german idiom for "empty nut" without a core (or someone with an empty head). The gene trap cassette used for the insertional mutagenesis also contained a LacZ reporter gene, which expression patterns should resemble the one of TAF8. Using the LacZ reporter gene the authors of that study found that TAF8 was ubiquitously expressed at very low levels throughout embryonic mouse development. The reporter gene appeared to be expressed a little bit higher in the inner cell mass, the developing heart and adult hippocampus.

Within TFIID TAF8 is present as a heterodimer with TAF10. TAF8 is not part of SAGA, where it is replaced by SPT7 as a hetero-dimerisation partner for TAF10. Recently a small TAF complex (SMAT) containing all three factors (TAF8, TAF10, SPT7L) has been described, which might be a storage complex to scavenge unincorporated TFIID and SAGA subunits (Demeny et al., 2007).

Very little is known about zebrafish Taf8. The gene is present as a single copy in the genome. The HFD is present in the protein but not the TAF8 proline-rich domain. Amongst the scarce experimental data specifically about Taf8 are the expression patterns of *taf8* determined by

whole- mount *in situ* hybridisation (Thisse, 2004) and analysis of the expression of a P$_{taf8}$:EGFP reporter gene in transgenics (Burket et al., 2008).

## 1.1.4 Hypothesis of transcriptional regulation on the core promoter

Research carried out during the last decade has revealed a substantial diversity of core promoter structures and of complexes forming on them. This phenomenon is thought to reflect transcriptional regulation on the core promoter. Transcriptional regulation on the core promoter level is based on the concept that the set of promoter recognition factors present in a given cell-type, to a certain extent restricts the transcriptional programmes, which can be carried out in that cell-type. The set of PRFs defines which promoters are used and how responsive those promoters are to regulatory input from other regulatory sites like enhancers. This differential responsiveness is thought to be based on the compatibility of complexes forming on enhancers and promoters.

### 1.1.4.1 Developmental transcription on the core promoter level

Several lines of evidence point towards a differential requirement of GTFs during development. Prototype TFIID seems to be required for transcription in early embryos. During lineage specification and differentiation this requirement of prototype (full) TFIID gradually diminishes. The reduction or entire depletion of the protein levels of TFIID-subunits has been observed in several differentiation processes: During the all-*trans* retinoic acid induced differentiation of F9 embryonal carcinoma cells into primitive endodermal cell-types (Perletti et al., 2001), the differentiation of 3T3-L1 preadipocytes into adipocytes (Guermah et al., 2003), the

differentiation of myoblasts into myotubes (Deato and Tjian, 2007) and the differentiation of hepatoblasts into hepatocytes (D'Alessio et al., 2011). In extreme cases, like during meiosis and myogenesis in mammals, an entire replacement of the basal transcription machinery has been reported (Deato and Tjian, 2007, Gazdag et al., 2009). One possible explanation for the observed phenomena is that full TFIID is required for transcriptional activation in mitotically dividing cells (Cler et al., 2009). TFIID is required for the activation (transcription initiation) of a gene during ontogeny, by providing an integration point for all the possible regulatory inputs, but is dispensable for reinitiation in certain differentiated cell-types.
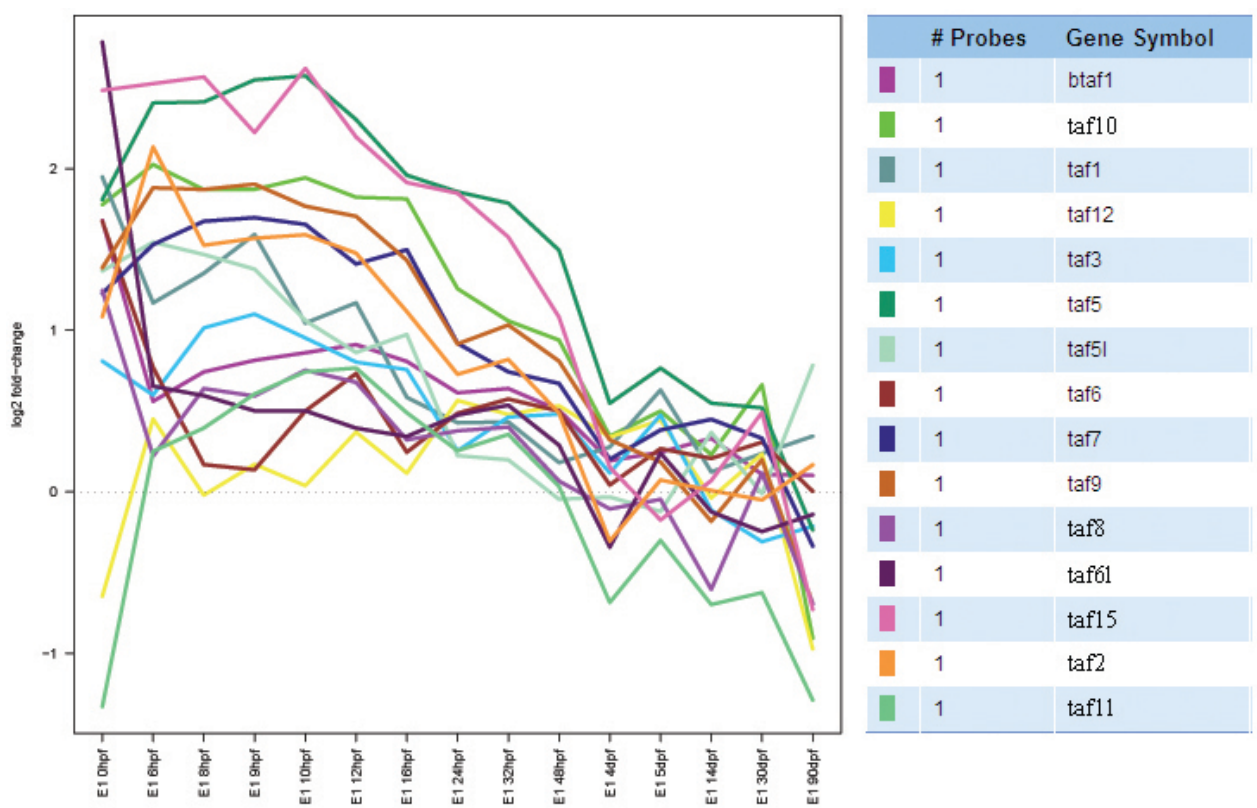


**Figure 1.6 – Decrease of *taf* transcript levels during zebrafish development**

Expression profile of *taf* transcripts during zebrafish development, from 0 hpf (hours post fertilisation) to 90 dpf. Most of the *tafs* show an expression profile where the transcript levels are steadily decreasing during development. The data is derived from single color experiments using an Affimetrix zebrafish array. Modified from web-tool ZF-Espresso (Max-Planck-Institute for Developmental Biology, Marc Saric, Robert Geisler, 2005).
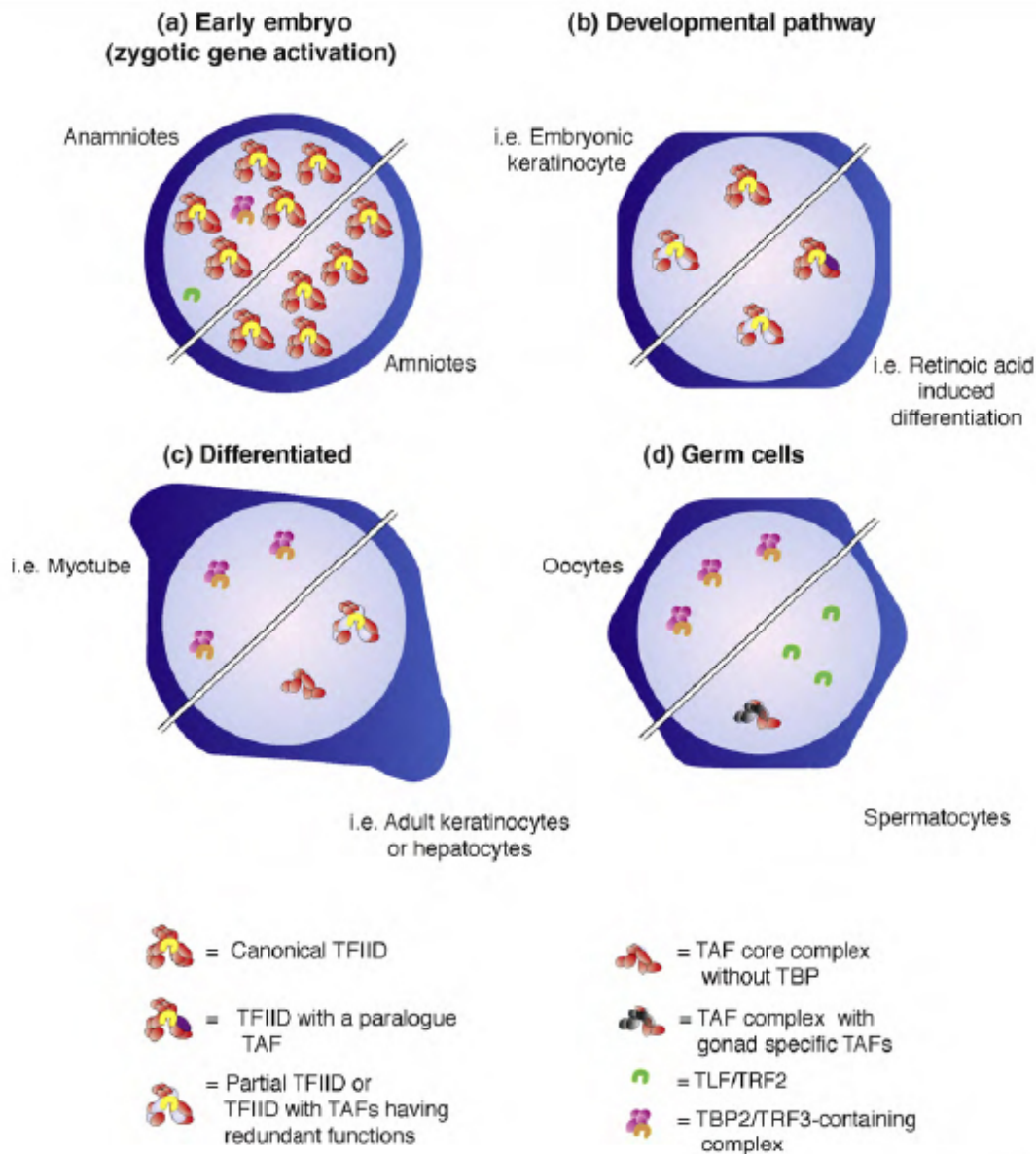
**Figure 1.7 – Regulation of developmental transcription on the core promoter level**

A) Early zygotic transcription in the pluripotent state largely follows the classical model of transcription initiation by canonical TFIID. B) With the appearance of enhancer-activated, spatially and temporally restricted transcription, differential roles of TAFs and TAF homologs have been demonstrated. This is paralleled by a decrease of TFIID components. C) In terminally differentiated cells an alternative promoter recognition factor replacing TFIID (TBP2/TAF3-complex) and partial TFIID complexes have been found. D) A highly specialised general transcription machinery seems to be acting in germ cells, in the context of meiosis. In the mouse gonads, TBP is replaced by TBP2 in oocytes and by TLF in spermatocytes. Figure is taken from (Muller and Tora, 2004).

## 1.2    Zebrafish Model

Zebrafish has been introduced as a model for developmental genetics by George Streisinger at the University of Oregon in the early 1980s (Chakrabarti et al., 1983, Streisinger et al., 1981, C. Walker and Streisinger, 1983). Zebrafish is a vertebrate model organism and its body plan and organ-systems therefore closer resemble the one of humans than do non-vertebrate models like *Drosophila* and *C. elegans*. Its major advantage over mammalian models is its *ex utero* development combined with optical transparency of the developing embryo. This allows studying complex processes like organogenesis or gene expression during development, *in situ,* in a whole developing organism, with single cell resolution. The embryo lacks membranes obscuring the view, which makes it possible to follow its development using simple light microscopy and to do experimental manipulations early on. Its development is rapid. After hatching between 2 to 3 days post fertilisation most organs are present at least as primordia and at 5 dpf the larva starts feeding. Furthermore the small fish can be maintained relatively cheap in high numbers under laboratory conditions. This model provides high numbers of embryos for experiments, as healthy females lay 200-300 eggs on a weekly basis throughout the year. A further advantage, which also renders zebrafish suitable for genetics, is the short generation time of zebrafish of around three months.

Because zebrafish is amenable for large scale mutagenesis screens it later became a very successful model for developmental genetics. A wealth of mutants has been generated in big mutagenesis screens, using either ENU to generate point mutations (Haffter et al., 1996), or pseudotyped retroviruses, to generate insertional mutants (Amsterdam et al., 1999). With the availability of the first assemblies of the zebrafish genome (1.9 Giga bases on 25 chromosomes)

and a powerful method to block the translation of mRNAs using morpholino oligonucleotides (MO, or just morpholino), zebrafish also became amenable for studying gene function by reverse genetics. Today there is a wealth of resources available, all accessible via the zebrafish model organism database ZFIN (zebrafish information network) and links therein: The genomic sequence via genome browsers (Ensembl, UCSC); genes, their transcripts and expression patterns; mutant, transgenic and wildtype lines; zebrafish anatomy and methodology.

Zebrafish is an excellent model to study the function of *cis*-regulatory elements *in vivo*, partly because transgenesis is relatively easy achievable (Abe et al., 2011). Reporter constructs, where the CRE is controlling the expression of a fluorescent reporter gene, can be used for transient or stable transgenesis. The way the CRE controls reporter gene expression can then be analysed by fluorescent microscopy in living zebrafish larvae, providing spatiotemporal resolution. CREs often function in a modular fashion and transgenesis using BACs, containing the full set of CREs controlling the expression of a gene, can yield transgenic lines recapitulating the full expression patterns of a gene. The labelling of certain cell-lineages with fluorescent reporter genes combined with time lapse confocal microscopy is a powerful tool to perform lineage tracing experiments and to study organogenesis in great spatiotemporal resolution (J. Y. Bertrand et al., 2010). Zebrafish experiments can be performed in well-plate formats, what predestines this model as the vertebrate model of choice for high throughput screens (HTS).

## 1.2.1    General LOF-phenotype for cell-essential genes

Early embryogenesis in animal models is driven by cellular components, which have been deposited in the egg during oogenesis. These maternal products (RNAs, proteins, mitochondria)

are collectively called maternal factors. During embryogenesis there is a transition phase during which the zygotic genome is activated and embryonic development gradually becomes controlled by factors produced by the embryo itself. This transition event is synonymously called MZT (maternal-to-zygotic transition) or ZGA (zygotic gene activation). In some animals (e.g. zebrafish and *Xenopus*) it is accompanied with another developmental event, the MBT. MZT and ZGA solely describe transcriptional phenomena, while the MBT also comprises phenomena like lengthening of the cell cycle and loss of synchrony of cell divisions. The extent to which embryogenesis is reliant on maternal factors differs between animal models. In mouse the zygotic genome becomes transcribed already at the two cell stage, whereas in zebrafish, the MZT happens around the 1000 cell stage. Obviously there is a significant difference in the number of cell divisions controlled by maternal factors in mouse and zebrafish. Interestingly, taking a different scale, zebrafish MZT happens much earlier than in mouse. The zebrafish genome becomes activated around 3.5 hpf, the mouse genome 18 hpi (hours post insemination) (Kimmel et al., 1995). The maternal impact on embryonic development in zebrafish is substantial and it has been shown that maternal factors contribute to embryonic development at least up to 3 dpf (Ryu et al., 2005). At least 8 000 maternal transcripts have been identified in zebrafish (Aanes et al., 2011) and maternally controlled processes include axis-specification and specification of the germline (Marlow, 2010).

In line with a substantial contribution of maternal gene products to early zebrafish development is the fact, that zygotic zebrafish mutants of supposedly cell-essential genes, often show surprisingly mild phenotypes (see http://web.mit.edu/hopkins/). The mutation still is lethal, but the mutants survive till 5 dpf and beyond. Those mutants display very similar, pleiotropic phenotypes, which I would like to call "general phenotype". In the general phenotype most, if not

all of the structures and organs are underdeveloped comparing mutants to wildtypes. Due to the substantial maternal contribution to embryonic development in zebrafish, many mutant phenotypes and morphants (MO-induced phenotypes) probably do not reflect the full loss of function (LOF) phenotype for that gene. To achieve a LOF-phenotype, where the gene product is completely lacking in the embryo, maternal zygotic mutants for the gene need to be generated. This very rarely is done because in many cases it is not trivial to generate a maternal mutant, as a prerequisite to study maternal zygotic phenotypes.

Many zygotic phenotypes studied in zebrafish in fact might be partial LOF-phenotypes, where maternal supply of the respective gene product compensates for loss of the zygotic gene. This is not necessarily a disadvantage. It enables investigators to study late functions of genes in downstream processes which couldn't be studied in more drastic null mutant phenotypes. Zebrafish mutants can be used to study the function of genes in organogenesis, whose mouse mutant counterparts die during or before gastrulation. The role of *hdac1* in liver development could for example only be revealed by studying the zebrafish mutant and not the more drastic mouse mutant phenotype for Hdac1 (Noel et al., 2008).

## 1.2.2    MO-mediated knock down technology

Morpholino oligonucleotides are synthetic analogues of nucleic acids, containing the same nucleobases, but differing in the structure of the backbone. The backbone of MOs is composed of morpholine rings (which carry the nucleobases) connected by phosphorodiamidate groups. This synthetic backbone renders MOs resistant to enzymatic degradation, because it is not recognised by any natural nucleases. However, they hybridise to complementary sequences just like their

natural counterparts. This hybridisation to complementary sequences is the basis for the use of MOs for a very efficient antisense-mediated knock down technique using MOs. Especially in research using zebrafish model, where the alternative RNAi (RNA interference) not could be established, the use of MOs for gene knock downs is very popular.

The target of MOs is usually a single stranded RNA molecule, where it can hybridise to complementary target sequences. Depending on the nature of the target sequence, the MO can interfere with various aspects of RNA biology. With the target sequence laying upstream or covering the start codon (AUG), MOs are used to block translation. Targeting splice donor or splice acceptor sites can induce aberrant splice products of the pre-mRNA (precursor mRNA), which are instable or do not encode for a functional protein (Morcos, 2007). The target sequence does not have to lie in a transcript of a protein-coding gene. MOs can also be used to target non-coding RNAs, like miRNAs (micro RNAs), or snRNAs (small nuclear RNAs) (Flynt et al., 2007, Konig et al., 2007).
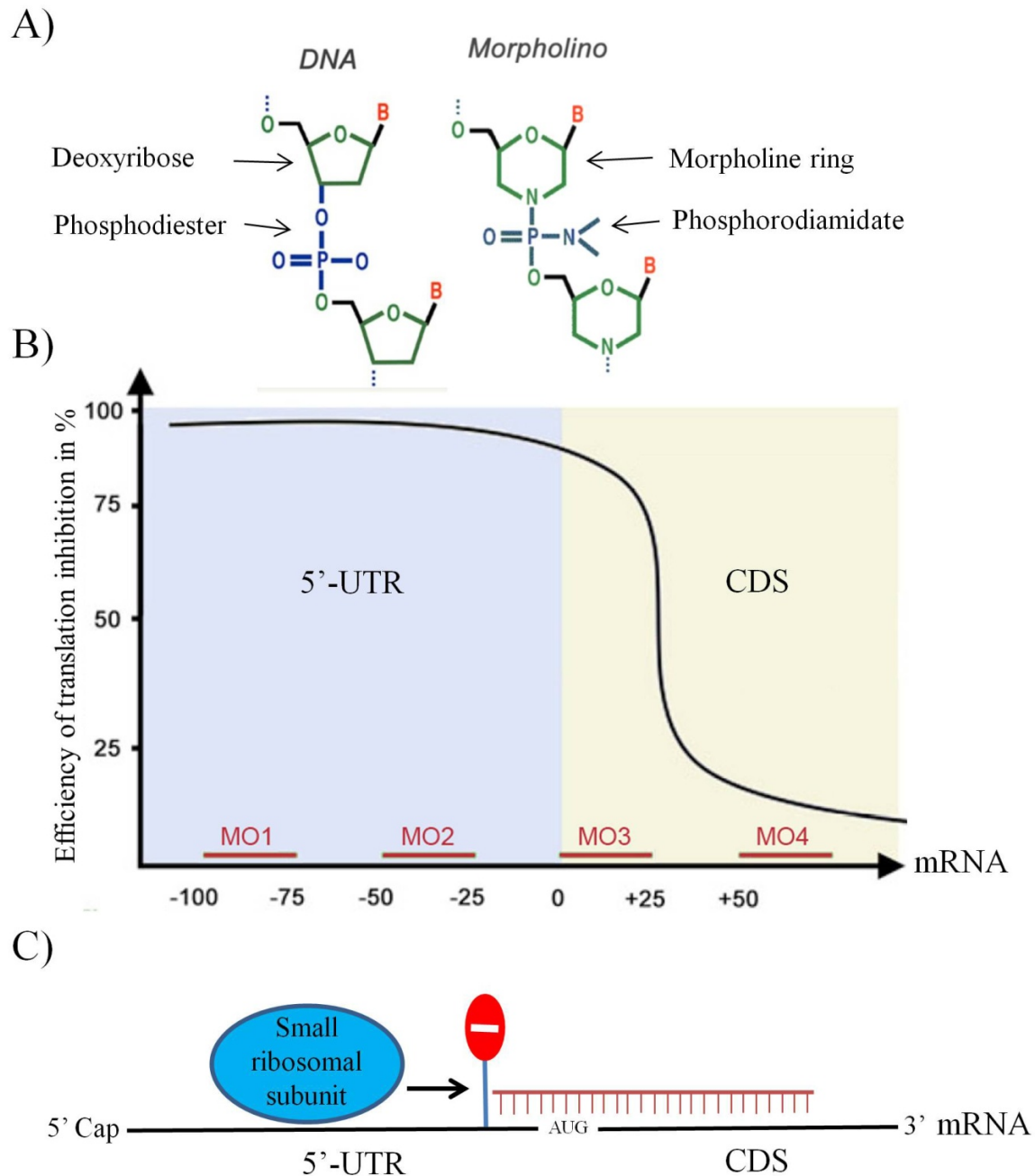
**Figure 1.8 – MO-mediated block of mRNA translation**

**A)** MOs are nucleic acid mimics, containing the same nucleobases, but with a different, nuclease-resistant backbone. **B)** Only MO-sequences targeting sequences upstream, or including the start codon AUG (first 25 nucleotides) are efficiently blocking the translation of the targeted mRNA. **C)** The reason for that lies within the mechanism of MO-mediated block of translation. The MO blocks the movement of the small ribosomal subunit, which is scanning for the start codon from the 5'-Cap. Adapted from (Seyffert, 2003).

Relevant for this thesis is only the use of MOs to block translation of mRNA, thereby generating LOF-phenotypes for the gene of the targeted transcript. The gold standard for controlling the specificity of morphant phenotypes is the following:

- Two targeting MOs inducing the same morphant phenotype.

- A MO, with 5 mismatches in its sequence, compared to one of the targeting MOs. These MOs will serve as a negative control MO and should not induce a morphant phenotype.

- The morphant phenotype should, at least partially, be rescued by co-injection of mRNA encoding for the wildtype protein. Best is it to use a mRNA, which is resistant to being targeted by the MO, for the rescue experiments.

If all the above mentioned criteria are fulfilled, the morphant phenotype is well controlled and therefore specific. The actual kd of the gene, the loss of the protein, has to be validated by western blot. This requires an antibody for the protein, which, especially for zebrafish, is not always available. Because of the other, stringent, methods to control the specificity of the morphant phenotypes, the validation of the kd is not mandatory. However, MO-induced aberrant splicing can be validated by RT-PCR (reverse transcription polymerase chain reaction). If primers are used for the RT-PCR, framing the aberrantly spliced part of the transcript, then the amplicon sizes on an agarose gel will differ between wildtype and mis-spliced transcript. This is for example the case if introns are included, or exons are excluded from the transcript. What also can be observed using MOs targeting splice sites is the loss or reduction of transcript levels, because a substrate for non-sense mediated decay is produced by the mis-splicing event.

# 1.3 Potential coactivator function of TAF8 for PPARγ

The lab of Laszlo Tora at the IGBMC Strasburg, a close collaborator of our group, is studying the role of TBP-type factor- and TAF-containing complexes in initiation Pol II-depending transcription. The studies of the Tora group include work on the identification of interaction partners of TAF proteins. During his time in the Tora lab Mate Demeny was working on interaction partners of TAF8. TAF8 was found to be a positive regulator of adipogenesis based on following observations:

1. TAF8 is dramatically and selectively (relative to other TAFs) induced and sequestered within TFIID upon *in vitro* differentiation of 3T3-L1 preadipocytes into adipocytes

2. The histone fold domain of TAF8 acts as a dominant-negative mutant and selectively inhibits the adipogenic differentiation of 3T3-L1 preadipocytes

3. Over-expression of wildetype TAF8 rescues the phenotype caused by its histone fold domain.

This suggests TAF8 as a potential interaction partner for the master regulator of adipocyte biology, PPARγ. Indeed, work carried out by Mate Demeny suggests a functional interaction of TAF8 with the nuclear receptor PPARγ. Flag-tagged human TAF8 can be co-immunoprecipitated together with PPARy and vice versa (Figure 1.9). Furthermore overexpressed TAF8 can potentiate the expression of a PPARγ responsive reporter gene in a dose dependent manner (Figure 1.10).
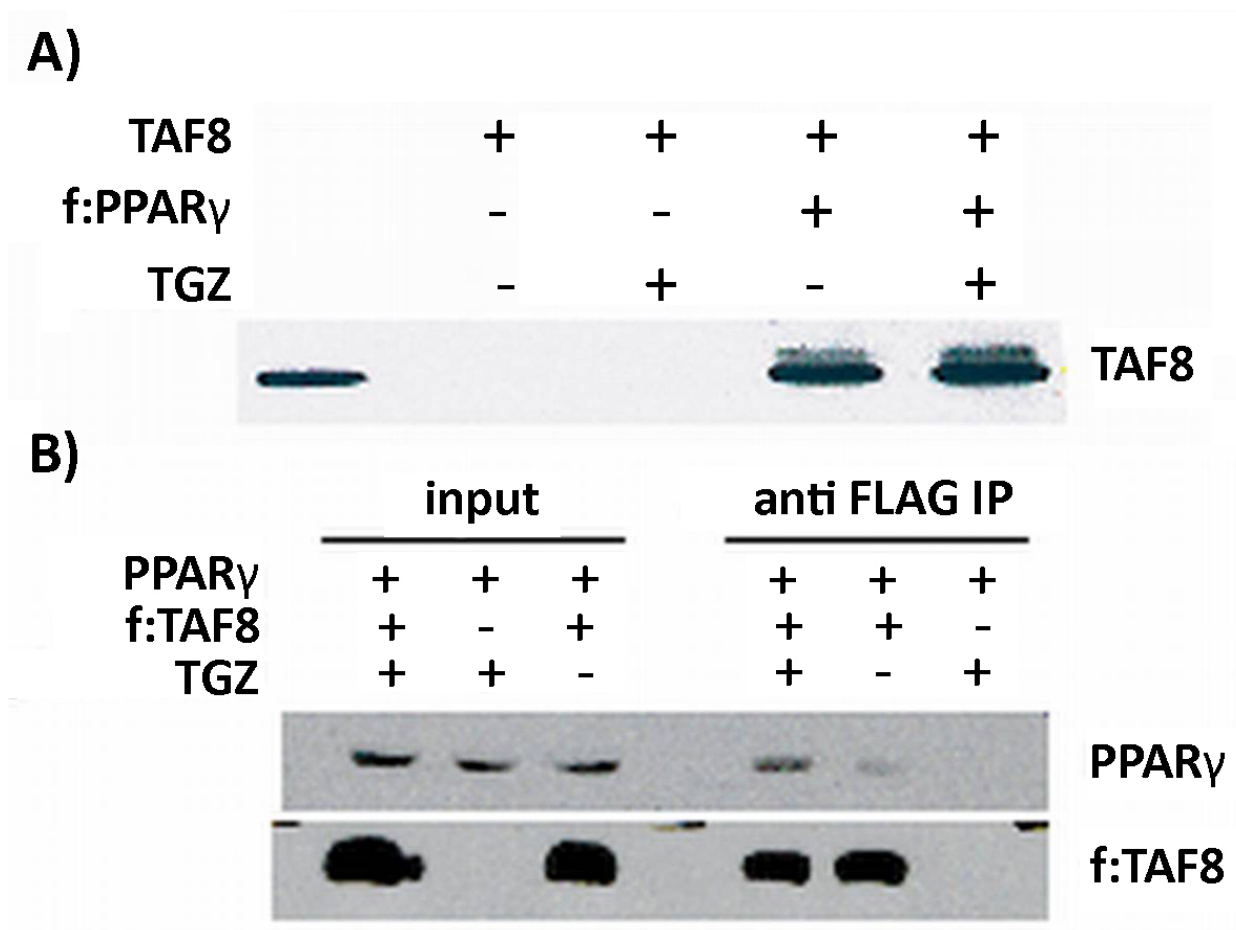
**Figure 1.9 – Interaction of human TAF8 with PPARγ demonstrated by CoIP (co-immunoprecipitation)**

**A)** Flag-tagged PPARγ co-immunoprecipitates with TAF8 when co-expressed in SF9 cells
**B)** Flag-tagged TAF8 co-immunoprecipitates with PPARγ when co-expressed in Cos-1 cells
These experiments have been performed at the IGBMC Strasburg by Mate Demeny.
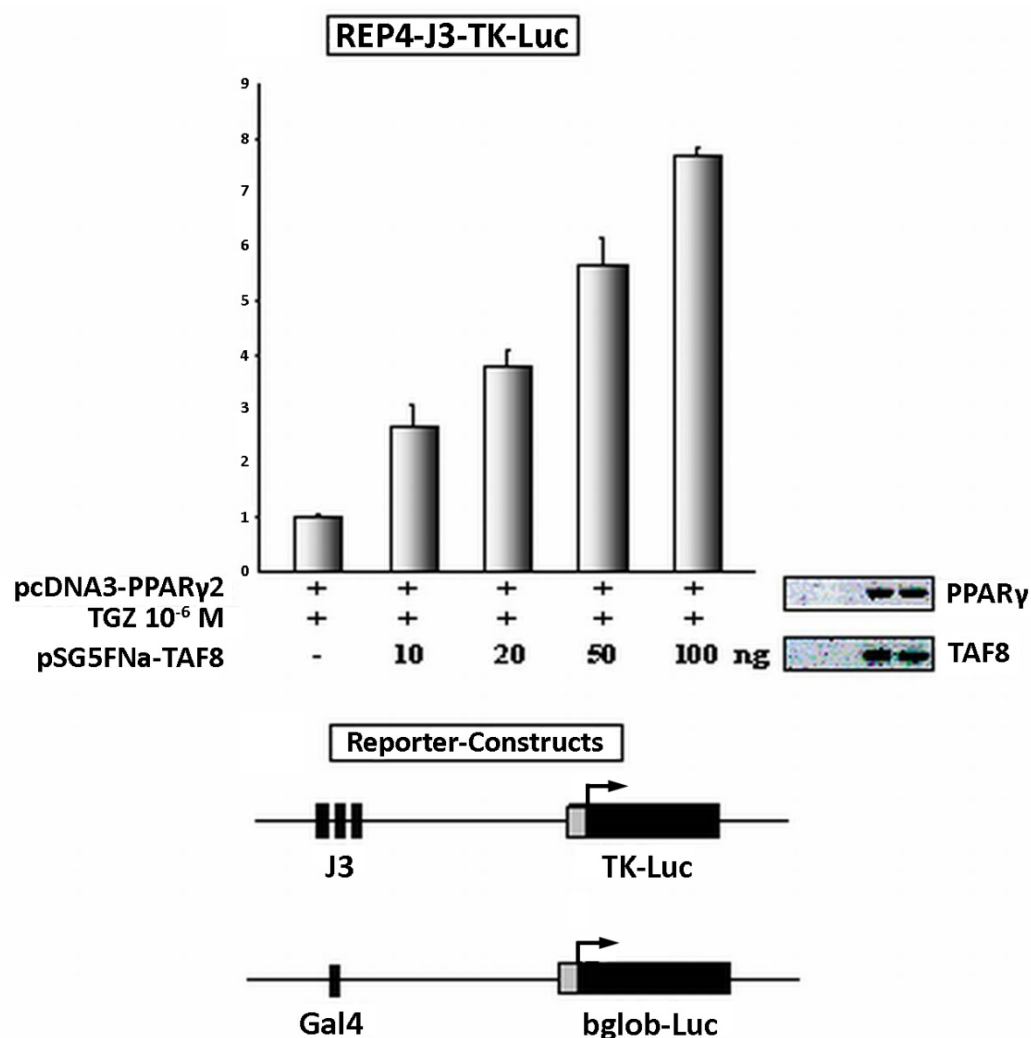
**Figure 1.10 – Luciferase assays suggests functional interaction between TAF8 and PPARγ**

Shown in the bar chart are the results from luciferase assays after the co-transfection of expression vectors for PPARγ, TAF8 and a PPARγ-responsive reporter (shown below). The PPARγ-responsive luciferase reporter is stimulated by TAF8 overexpression in a dose-dependent manner. These experiments have been performed by Mate Demeny.

## 1.3.1    NRs (nuclear receptors)

Nuclear Receptors are ligand regulated transcription factors. They link transcriptional regulation, and thereby cellular behaviour, to extracellular signals, like hormones and compounds with hormone like function. The central role in physiology and organismal homeostasis, together with

34

the fact that their activity can be modulated with endogenous and synthetic ligands, makes them excellent drug targets. Nuclear receptors have a modular structure:

A/B in Figure 1.11 is the N-terminal regulatory domain. The A/B domain is highly variable in sequence between nuclear receptors and contains activation function 1 (AF1), which itself produces only a weak transcriptional activation, but synergises with activation function 2 (AF2) in the E domain. The activity of the AF1 can be modulated by signalling pathways, which target certain phosphorylation sites within the A/B domain. C in Figure 1.11 is the DNA binding domain. It is a highly conserved domain, which is binding to DNA-sequences called hormone response elements (HRE) via two zink fingers. D in Figure 1.11 is the hinge region. The hinge region is a flexible domain linking domains C and E. The hinge region of some nuclear receptors binds to DNA sequences upstream of the HRE (Chandra et al., 2008). E in Figure 1.11 is the ligand binding domain (LBD). The LBD of nuclear receptors is moderately conserved in its primary structure but highly conserved in its tertiary structure. As the name suggests, this domain contains a ligand binding cavity. It also harbours activation function 2 (AF2), which is modulated by the presence of bound ligand. Furthermore it contributes to the dimerisation interface and interacts with co-regulators. F in Figure 1.11 is C-terminal domain. The C-terminal domain varies a lot between NRs.

Nuclear receptors form a so called superfamily of proteins and there are 48 genes which encode a nuclear receptor encoded by the human genome. There are several ways to classify this large group of proteins. Mechanistically they can be grouped into two major classes. One class is in the absence of ligand trapped in the cytoplasm, in a complex with heat shock proteins. Upon ligand binding the heat shock proteins dissociate and the NR is translocated into the nucleus, where it binds to its HRE as a homodimer. A second class is bound to its response element even in the

absence of ligand, as a heterodimer with RXR (retinoid x receptor). In this state it is associated with corepressor complexes and binding of ligand causes the replacement of these corepressor complexes with coactivator complexes, thereby leading to activated transcription of its target genes.

An alternative historical classification of NRs is based on the knowledge about their ligands. One class, the endocrine receptors, comprises the classical NRs, which are regulated by endocrine hormones like adrenal and gonadal steroids. Then there are the orphan receptors, which have been identified as a NR based on homology, without any knowledge about their ligands. Once a ligand for these orphan receptors has been found it is reclassified as a so called adopted orphan receptor. One interesting aspect of the adopted orphan receptors is the fact that they respond to exogenous compounds as ligands, e.g. dietary lipids. This links organismal physiology to environmental factors.

**Figure 1.11 – Nuclear receptors**

**A)** The five classical domains of a NR from N-terminus ($NH_2$) to C-terminus (COOH).
**B)** Classification of nuclear receptors according to the history of their identification and knowledge about their ligands. Endocrine receptors are the classical receptors and bind to hormonal lipids of the endocrine system. Orphan receptors can be identified as nuclear receptors based on homology, but their ligands are unknown. They are taken out of orphanage when their ligand is found and then become adopted orphan receptors. Figure modified from (Evans, 2004).

## 1.3.1.1    PPARs

In 1990 one of the orphan NRs was found to bind chemicals known to induce peroxisome proliferation (Issemann and Green, 1990). It was named peroxisome proliferator-activated receptor (PPAR) and later, after two closely related receptors have been discovered, PPARα (Nicolakakis and Hamel, 2010). The other two members of the family are called PPARβ (also called PPARδ) and PPARγ. Following the nomenclature for NRs the PPARs belong to nuclear receptor subfamily 1, group C. There is a wealth of published data about PPARs. A search in the pubmed database with PPAR as search term yields 12780 hits, while PPARγ alone as query retrieves 9812 publications (pubmed 10.02.2011). The reason why PPARs gain so much attention is certainly because they are regarded as extremely valuable drug targets, also against disorders associated with Metabolic Syndrome (Syndrome X). In the affluent societies of the industrialised nations obesity is an ever growing problem. Obesity is a risk factor to suffer from disorders like: Insulin resistance, which can progress into type 2 diabetes mellitus; dyslipidemia (high triglycerides and low high density lipoproteins); hypertension; atherosclerosis.
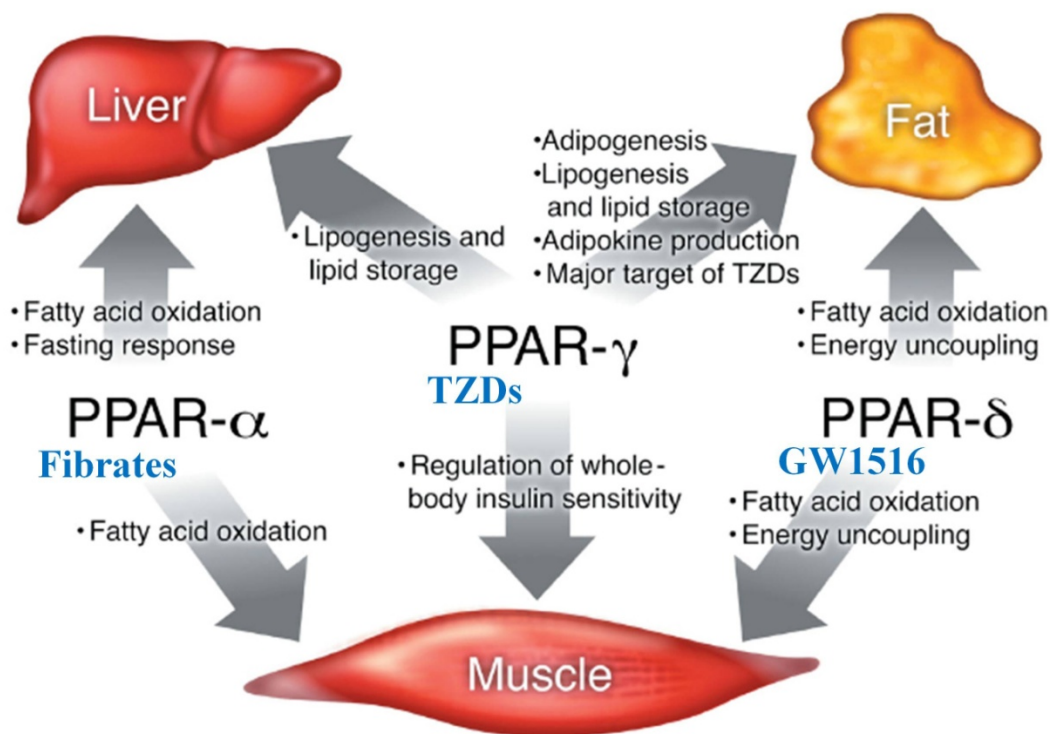
**Figure 1.12 – The role of PPARs in lipid-physiology**

This figure depicts the role of the three PPAR subtypes in three central tissues of lipid- and glucose-metabolism. The activities of PPARα and PPARβ lead to an increase in fatty acid catabolism for the production of energy equivalents (fat burning). Activation of PPARγ, in contrast, leads to an increase of intracellular neutral lipids, particularly in adipocytes (fat cells). All three NRs are drug targets for drugs against disorders associated with the metabolic syndrome, like the lipid-lowering fibrates and the insulin-sensitising TZDs. Recently also drugs targeting PPARβ became available (GW1516). Figure modified from (Evans et al., 2004).

## 1.3.1.2 PPARα

PPARα is the name giving member of this subgroup of NRs. Its activation leads to peroxisome proliferation in rodent livers. This effect is not observed in humans. PPARα is predominantly expressed in liver and to a lesser extend in heart and muscle. Its target genes are involved in fatty acid catabolism for energy production via β-Oxidation. Accordingly, PPARα knockout mice

suffer from hyperlipidemia and fatty liver. PPARα is the drug-target of the lipid-lowering fibrates (clofibrate, ciprofibrate).

### 1.3.1.3    PPARβ (PPARδ)

PPARβ, like PPARα, plays a role in energy expenditure via fatty acid catabolism (β-Oxidation). PPARβ is ubiquitously expressed, with low levels in liver. In contrast to PPARα, it also has been implicated in adaptive thermogenesis. Mice, in which PPARβ has been knocked out, show reduced energy uncoupling and are prone to obesity.

### 1.3.1.4    PPARγ

This member of the PPAR family plays a somewhat opposing role in lipid metabolism to the other two subtypes. Where PPARα and PPARβ are playing a role in fatty acid catabolism, in fat burning, PPARγ plays a role in fat storage. Accordingly it is predominantly expressed in adipose-tissue. PPARγ exists in two major isoforms in mammals, PPARγ1 and PPARγ2. PPARγ1 is broadly expressed, including liver, skeletal muscle, heart and adipocyte tissue. PPARγ2, which contains an extended N-terminus compared to PPARγ1, is mainly expressed in adipocytes In humans two more isoforms, called PPARγ3 and 4, encoding for the same protein like PPARγ1 have been found (Desvergne and Wahli, 1999). There is plenty of evidence that PPARγ is a master regulator of adipocyte biology (white fat tissue). It is essential for the formation (adipogenesis) and the function (lipid-handling, adipokine production) of white fat tissue. With the 3T3-L1 cell line an excellent *in vitro* model for adipogenesis is available. This preadipocyte cell line can be hormonally (adipogenic inducers) stimulated to differentiate into mature

adipocytes, which accumulate triglycerides in lipid droplets and express marker genes typical for mature adipocytes. From this model, it is known that PPARγ plays a major role during adipogenesis together with members of the CCAAT/enhancer binding protein (C/EBP) family. It appears that hormonal stimulation leads to the induction of a central regulatory loop in mature adipocytes, where PPARγ and C/EBPα mutually are keeping up their expression levels, leading to a robust high expression of those two factors. C/EBPβ and C/EBPδ are involved in the initiation of this regulatory loop and can be considered as early markers for adipogenesis, although a role for C/EBPβ in mature adipocytes has been described recently. There is a substantial overlap of genomic sites co-occupied be PPARγ and C/EBP members, suggesting that these factors cooperatively regulate the expression of adipocyte target genes. Indeed, around half of the genes induced during adipogenesis appear to be regulated by PPARγ, highlighting its role as master regulator of this differentiation process.
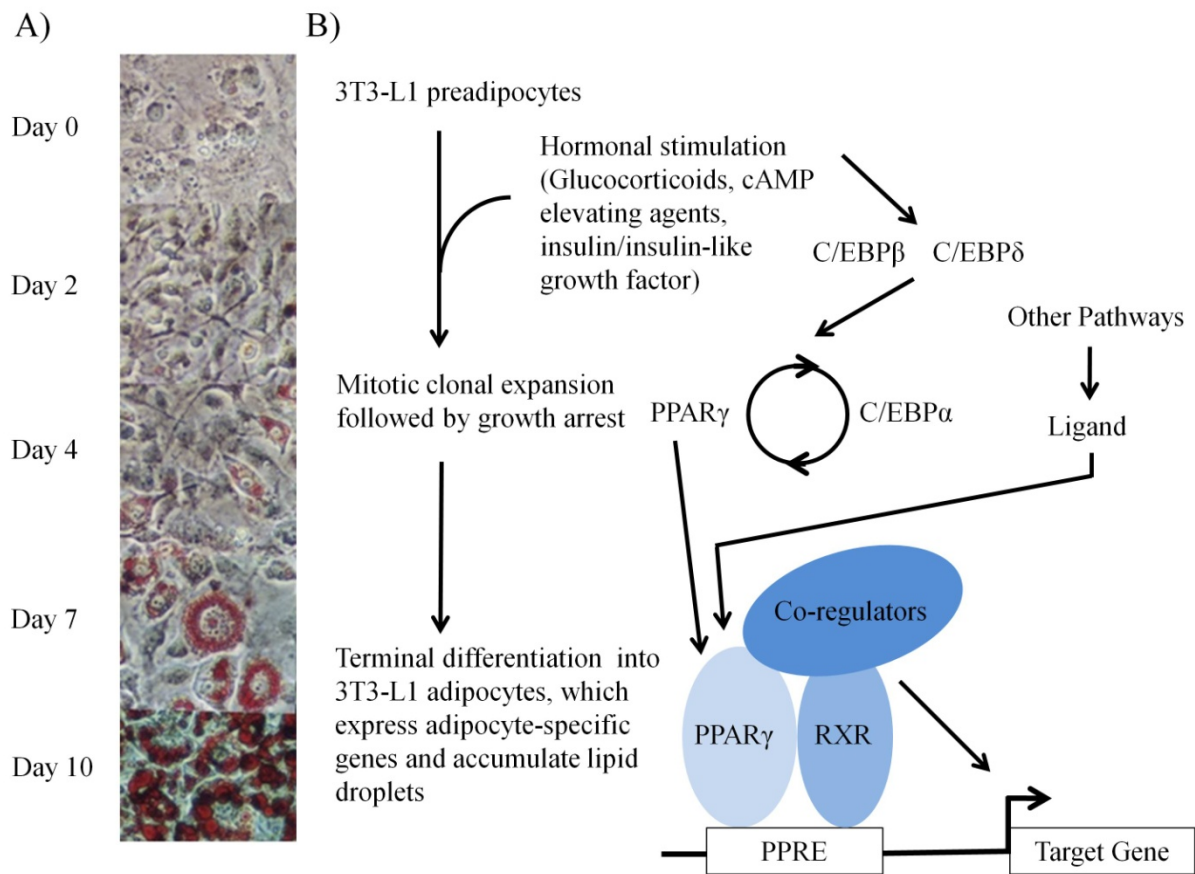
**Figure 1.13 – The 3T3-L1 model for adipogenesis**

**A)** Light microscopy pictures of 3T3-L1 cells at different days post hormonal stimulation for adipogenic differentiation. The cells have been stained with the red lipid stain ORO to reveal the accumulation of lipids in mature adipocytes (days 7 and 10). Note the change of the fibroblast like morphology to the roundish shape of mature adipocytes during the differentiation. The time course experiment shown in **A)** has been performed by Mate Demeny.
**B)** Shown on the left is the order of cell biological events during the differentiation process. Hormonal stimulation of 3T3-L1 preadipocytes leads to several rounds of clonal expansion, followed by growth arrest and terminal differentiation into mature adipocytes. Shown on the right is the order of molecular events leading to establishment of the mature adipocyte transcriptional programme. These molecular events involve PPARγ and C/EBP family members.

The biological role of PPARγ *in vivo* extensively has been studied using mouse-model. PPARγ

null mice revealed essential functions for PPARγ during pre-natal and post-natal development.

During mouse development substantial expression of PPARγ is first detected in the placenta at

E8.5. The first expression in the embryo is observed around E14.5 in the interscapular brown fad pad. Mice lacking PPARγ die around E9.5 because of a placental pathology. The placental trophoblast fails to differentiate properly and the placenta does not become vascularised. The fetus in turn, where PPARγ is not expressed at that stage, displays cardiomyopathies (premature cardiomyocyte differentiation and ventricular hypoplasia). This early phenotype can be rescued by placental reconstitution with tetraploid chimeras. PPARγ does not seem to be essential for further embryonic development. However, a knockout mouse surviving to term dies within one week and displays lipodystrophy, fatty liver and haemorrhages (Barak et al., 1999).

Tissue-specific KOs of PPARγ in mouse made clear that not only the adipocyte PPARγ, but also PPARγ in other tissues plays an important role in lipid- and glucose-homeostasis (see Figure 1.12). Interestingly, an adipocyte-specific KO revealed that PPARγ is essential for maintenance of the adipocyte-phenotype and for the survival of adipocytes. Humans with one PPARγ mutant allele display partial lipodystrophy and insulin resistance.

PPARγ in mammals is expressed in macrophages, where it is involved in a certain aspect of cholesterol metabolism. The lipid transport system of fish, like the one of mammals, consists of an exogenous (dietary) loop as well as an endogenous loop. The lipids are transported as lipoprotein (particles). Chylomicrons are the lipoproteins of the exogenous loop. They are composed of triacylglycerols (TAGs), cholesterol, cholesterol-esters and apolipoprotein B-48 (Apob-48). Nascent chylomicrons bypass the liver via lymphatic vessels but later enter the blood circulation. After they have delivered their TAG-content to peripheral tissues (skeletal muscle, adipose tissue) the chylomicron remnants are taken up by the liver. In the liver, lipids are packaged into particles of similar composition like chylomicrons, except for a different apolipoprotein component, Apob-100. This lipoprotein, released from the liver into the

circulation, is called very low density lipoprotein (VLDL). While delivering its TAG-cargo (low density) to peripheral tissues the density of this lipoprotein successively increases. The VLDL goes over IDL (Intermediary Lipoprotein) to LDL (Low Density Lipoprotein). Macrophage PPARγ is involved in a process by which macrophages convert oxLDL (bad cholesterol), which contains ligands for PPARγ, into HDL (good cholesterol). HDL, high density lipoprotein, is considered as good cholesterol, because it transports cholesterol to the liver, where it can be secreted together with the bile. This is one of the few processes by which excess cholesterol, which has been associated with artheromatous diseases, can be removed from the body.
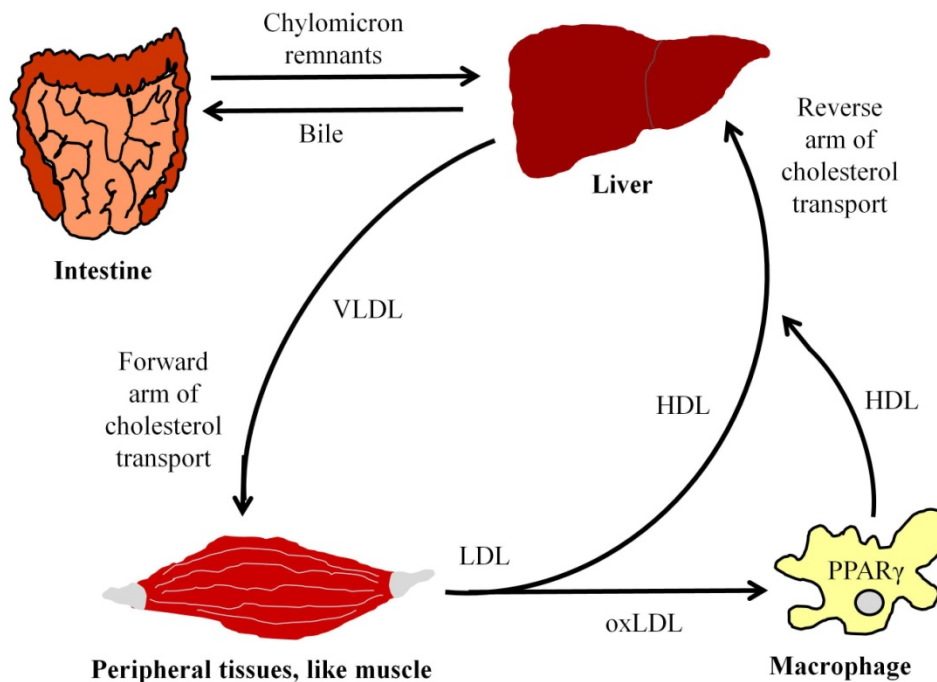


**Figure 1.14 – PPARγ and cholesterol transport**

Depicted is a schematic of the lipid transport system, with emphasis on cholesterol transport and the role of PPARγ in clearance of "bad" cholesterol. Dietary cholesterol reaches the liver in chylomicron remnants. In the liver it is repacked into VLDL and released into the circulation. As TAGs (triacyl glycerols) are lost to peripheral tissues VLDL becomes the denser LDL. LDL components can become oxidised with time. Macrophages can take up oxidised LDL (oxLDL, bad cholesterol) and release it as HDL (good cholesterol). This process involves PPARγ, which is activated by certain components of oxLDL (Evans, 2004).

## 1.3.2    Transcriptional regulation by PPARγ

PPARs form a heterodimer with members of the RXR-family (nuclear receptor subfamily 2, group B). Especially the interaction with RXRα seems to be important for PPARγ-regulated transcription (Chawla et al., 2001, Lefterova et al., 2008). The principal mechanism for ligand-dependent transcriptional regulation by PPARs is the following:

In the unliganded state the PPAR/RXR-heterodimer, bound to the PPRE (peroxisome proliferator response element) is associated with a corepressor complex containing HDACs. Upon ligand-binding the corepressor complex is replaced with coactivator complexes like Mediator and complexes containing HATs (Viswakarma et al., 2010).

The PPRE consists of two hexameric half sites, direct repeats of an AGGTCA consensus, separated by one nucleotide. Such a HRE is called DR1-element (Heinaniemi et al., 2007). PPARγ occupies the 5' half site and the RXR the 3' half site, while the hinge region of PPARγ makes additional contacts with the AAACT element found up-stream of some PPREs (Chandra et al., 2008).

Several mechanisms for transrepression by PPARγ (PPARγ/RXR-heterodimer) have been described in the literature (Schmidt et al., 2010):

1. PPARγ directly binds to other TFs like AP-1 and NFκB, which prevents them from binding to their response elements (P. Wang et al., 2001).

2. PPARγ interferes with transcriptional regulation by competing for general coactivators with other TFs which rely on those coactivators (Kodera et al., 2000).

3. Sumoylated PPARγ has been connected to transrepression of NFκB-dependent transcription by preventing the removal of the NCoR/SMRT corepressor complex from the promoter region of pro-inflammatory genes (Jennewein et al., 2008).

4. PPARγ inhibits the phosphorylation of JNK and p38 in the MAPK pathway by an unknown mechanism. Thereby, PPARγ indirectly represses the transcription of pro-inflammatory genes (Desreumaux et al., 2001).

It is increasingly being recognised that the activity of PPARγ is regulated by post translational modifications (PTMs) (van Beekum et al., 2009). PPARγ contains two known phosphorylation sites, Serine 112 and Serine 273 (number of residues is for PPARγ2). Serine 112 lies within AF1 and is a target of MAPKs and the CDKs (cyclin-dependent kinases) CDK7 and CDK9. Phosphorylation of Serine 112 by MAPKs seems to predominantly decrease the transcriptional function of PPARγ, while phosphorylation of the same residue by CDK7/9 has the opposite effect. Serine 273 is a target of CDK5. Phosphorylation of Ser273 by CDK5 causes dysregulation of a subset of PPARγ target genes, including genes which are dysregulated in obesity, like the insulin-sensitising adiponectin. Some of the PPARγ-targeting insulin-sensitising drugs, e.g. Rosiglitazone, block the phosphorylation of Ser273 by CDK5. Two sumoylation sites have been found in PPARγ. Sumoylation of K107 has a repressive effect on transcription, while sumoylation of K395 is connected to transrepression of NFκB target genes (Pascual et al., 2005, van Beekum et al., 2009).
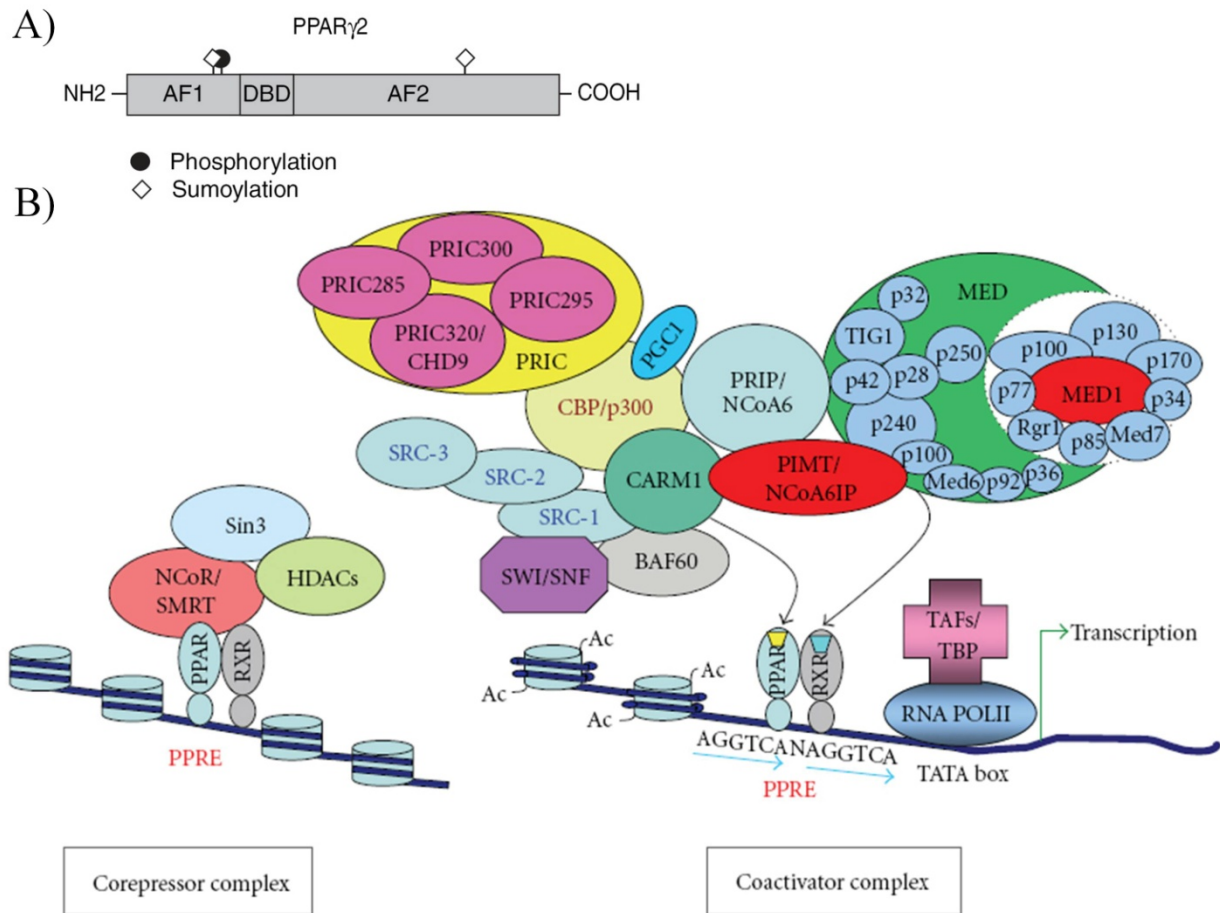
**Figure 1.15 – Transcriptional regulation by PPARγ**

**A)** Schematic representation of the PPARγ2 protein structure. The positions of known post translational modifications of this protein (Ser112/Ser273 phosphorylation and K107/K395 sumoylation) are shown. These PTMs influence the transcriptional activity of PPARγ.

**B)** Principle mechanism of transcriptional regulation by PPARs. Upon ligand binding HDAC-containing corepressor complexes are replaced with HAT-containing coactivator complexes and complexes linking PPAR/RXR to the basal transcription machinery (Mediator). **A)** was taken from (van Beekum et al., 2009) and **B)** from (Viswakarma et al., 2010).

# 1.3.3 Zebrafish as model for lipid-metabolism and adipocyte biology

## 1.3.3.1 PPARγ in zebrafish

The zebrafish genome contains orthologs for all three PPAR subtypes. Due to the whole genome dublication event in the teleost lineage, there are two copies for *pparα* (*pparαa*, *pparαb*) and *pparβ* (*pparβa*, *pparβb*). Zebrafish *pparγ* is a single copy gene, like its mammalian ortholog. So far, no splice variants for *pparγ* have been described. The spatiotemporal expression patterns of zebrafish NRs together with their most important co-regulators during embryonic development have been comprehensively studied (S. Bertrand et al., 2007). The study revealed that NRs are often more specifically expressed than their co-regulators. There is hardly any expression of *pparα* during embryonic zebrafish development. *Pparβa* is highly expressed in the liver, whereas its dublicate *pparβb* is weakly expressed throughout the body and stages. *Pparγ* shows a broad expression during embryonic stages, but in early larvae becomes more restricted to endodermal organs like gut, intestinal bulb, liver and swim-bladder.

The expression of Ppars has also been comprehensively studied in adult zebrafish (Ibabe et al., 2002). In this study the expression patterns of the Ppars only partly resembled the ones observed in mammals. Zebrafish Pparα is expressed mainly in liver, kidney, intestine and pancreas. Pparβ is ubiquitously expressed and for Pparγ weak expression in pancreas, intestine and gonads has been observed.

### 1.3.3.2    Zebrafish as a model for adipocyte research

The best studied biological function of PPARγ is its role in fat cells. Models mainly used in adipocyte research are rodents and *in vitro* models. The preadipocyte cell line 3T3-L1 can *in vitro* be stimulated to differentiate into adipocytes and is used as an *in vitro* model for adipogenesis. Zebrafish model only recently has been established as a model for adipocyte research.

Adipogenesis during early zebrafish development has been studied by several investigators using slightly different approaches. They also used different criteria for the identification of adipocytes and the stage, where the first adipocytes are observed, differs between the studies.

In one study Li et al. investigated the role of the RA (retinoic acid) and PPARγ signalling pathways acting on CNC (cephalic neural crest). Their findings indicate that cephalic osteoblasts and adipocytes share a common precursor, CNC. Modulating the activity of both pathways using respective ligands, they observed a reciproke relationship between cephalic adipogenesis and osteogenesis, where increased adipogenesis goes at an expense of osteogenesis and vice versa. In this study the first cephalic adipocytes were observed at 5 dpf using marker gene expression (*pparγ*, *cebpa*) and lipid accumulation (ORO) as criteria to identify adipocytes (N. Li et al., 2010). Flynn et al. monitored the appearance of adipocytes during early zebrafish development. They used lipid accumulation (nile red), marker gene expression (*pparγ* and *fabp11a*) and histological criteria to identify mature adipocytes. In this study the first adipocytes were observed in close proximity to the pancreas at 8 dpf. Another finding of that study was that exogenous nutrition seems to be required for the appearance of the first preadipocytes close to the pancreas at 6 dpf (Flynn et al., 2009). Finally Imrie et al. studied the development of WAT (white adipose tissue) in zebrafish. They determined the position of the WAT-depots in zebrafish and their

appearance during development. The authors of this study used similar criteria for the identification of adipocytes like Flynn et al. but additionally checked for the expression of the adipokines adipsin and adiponectin. They found that the first WAT-depot in zebrafish appears around 12 dpf in the pancreas (Imrie and Sadler, 2010).

### 1.3.3.3    Zebrafish as model for hepatobiliary diseases

Like other organs in zebrafish the liver develops rapidly and is fully functional by 5 dpf (Chu and Sadler, 2009). Zebrafish liver development can be subdivided into two principal phases, budding and growth (Field et al., 2003). Unlike in mammals hepatic vasculature and hematopoiesis are not essential for hepatogenesis in zebrafish (Chu and Sadler, 2009). However, a functional blood-circulation is required for late stages of liver development, during the growth phase (Korzh et al., 2008). Furthermore, endothelial cells seem to contribute to the establishment of properly separated vascular and biliary networks by assisting in apicobasal polarisation of hepatocytes (Sakaguchi et al., 2008). A single layer of hepatocytes lies between those two networks, their apical membranes facing the biliary network, their basal membranes facing the vascular network. The anatomical architecture, the arrangement of cells and vasculature, differs between mammalian and teleost livers (Hinton and Couch, 1998, Lorent et al., 2004). The subdivision of this organ into functional units differs, but the function of the hepatic cell-types and the overall function of the organ is the same (Sadler et al., 2005). Also the biliary tree resembles its mammalian counterpart and is composed of extra- and intrahepatic ducts and ductules. However, in teleosts, a specialised branch of the biliary tree, the preductular epithelial cell, analogous to the Canal of Hering, seems to connect canaliculi and ductules (Sadler et al., 2005).

**Table 1.3 – Zebrafish as a model for hepatobiliary diseases**

The table is adapted from (Chu and Sadler, 2009).

| Gene | LOF-phenotype | Defects observed (model for disease, syndrome) | Reference |
|---|---|---|---|
| *vps33b* | Morphant | Cholestasis (ARC-Syndrome) | (Matthews et al., 2005) |
| *foie gras* | Mutant | Hepatic steatosis (fatty liver disease) | (Sadler et al., 2005) |
| *nf2* | Mutant | Choledochal cysts | |
| *vps18* | Mutant | Hepatomegaly, biliary paucity | |
| *dtp* | Mutant | Hepatic steatosis and degeneration | (Matthews et al., 2009) |
| *Jagged* and *notch* | Morphants (compound knock downs) | Biliary paucity (Alagille-Syndrome) | (Lorent et al., 2004) |

# 1.4    Objectives

## 1.4.1    Distinct roles of TAFs in development

In chapter 1.1.4 I introduced the concept of transcriptional regulation on the core promoter level. Although there is accumulating evidence suggesting a participation of the core promoter binding machinery in transcriptional regulation also during development , only a few studies have shown how changes in the core promoter binding machinery lead to the establishment of cell-type specific transcriptional programmes. TBP- and TAF-paralog containing complexes for example seem to drive transcriptional programmes in the context of meiosis. Also replacement of the canonical TFIID complex during myogenesis has been described (Deato and Tjian, 2007). However, this finding was not confirmed by the mouse ko (knock out) phenotype of TBP2, which only displays defects in gametogenesis in females. Therefore, there is a need to study the function of components of the basal transcription machinery *in vivo*, in the context of a whole developing organism.

I chose zebrafish as an *in vivo* model to study the role of Taf proteins during early zebrafish development due to the advantages of this model for that purpose. LOF-phenotypes can be easily generated and analysed in this model (chapter 1.2) using MO-mediated kd technology.

The systematic study of Tafs would, to our knowledge, be the first comprehensive analysis of the role of TAF-proteins during development of a vertebrate organism. I hypothesised, that besides the relative contribution of the distinct Taf-subunits to early zebrafish development, the study might reveal some interesting specific phenotypes for certain Tafs, similar to the implication of Taf3 in hematopoiesis (Hart et al., 2009). Furthermore it will be interesting to analyse the Taf-

morphants in the light of the knowledge about structure and composition of the different TAF-containing complexes.

## 1.4.2 Exploring the potential role of Taf8 in Pparγ-dependent gene regulation

The advantages of zebrafish as a model organism, especially the possibility to visualise and study complex developmental and physiological processes *in vivo*, are increasingly utilised for lipid research. Staining methods to visualise the distribution of neutral lipids in living embryos/larvae (Nile Red, (Jones et al., 2008)) or in fixed embryos/larvae (ORO, (Schlegel and Stainier, 2006)) can be deployed in zebrafish. Importantly a collection of lipids conjugated with the fluorochrome BODIPY are available to study their distribution and conversion *in vivo* by live imaging (Holtta-Vuori et al., 2010). Utilising its advantages and the available resources, zebrafish has successfully been established as a model for various lipid-related diseases: Atherosclerosis (Stoletov et al., 2009), obesity (Song and Cone, 2007), diabetes (Elo et al., 2007, Gleeson et al., 2007), cholesterol metabolism (Schlombs et al., 2003), acute alcoholic liver disease (Passeri et al., 2009) and non-alcoholic fatty liver disease (Sadler et al., 2005).

I want to study the phenotype of the zebrafish *taf8*-mutant with focus on *in vivo* evidence for a potential coactivator function of Taf8 for Pparγ, a key-regulator of lipid-metabolism. This might provide valuable information about the mechanism of PPARγ-regulated transcription, by further linking PPARγ to the basal transcription machinery, additionally to its known interactions with the Mediator complex (Ge et al., 2002, Grontved et al., 2010). TAF8 has been implicated in adipogenesis, a differentiation process for which PPARγ is essential. *In vivo* evidence of a

functional interaction of Taf8 with Pparγ in the context of adipogenesis would strengthen the role of TAF8 as a pro-adipogenic factor.

## 1.4.3 Zebrafish as a genetic model for studying metabolic disorders involved in ARC-syndrome

Macrophage PPARγ is linked to cholesterol metabolism via a process by which oxLDL is cleared from the circulation. Zebrafish becomes increasingly used as a model for disorders related to lipid-metabolism. Cholestasis and malabsorption of lipids are lipid-related features of the multisystem disorder ARC-syndrome (arthrogryposis renal dysfunction and cholestasis-syndrome). The kd phenotype for the zebrafish ortholog of the gene which is mutated in the majority of the cases of classical ARC-syndrome (*vps33b*) shows some resemblance to the lipid-related defects found in ARC-syndrome (Matthews et al., 2005). We want to compare the kd phenotype of the zebrafish ortholog of the gene which is mutated in the remaining cases of classical ARC-syndrome (*vipar*, VPS33b Interacting Protein involved in Apical protein Restriction) to the *vps33b* kd phenotype. Similarities and differences between the phenotypes would allow conclusions on the question if the two genes act in the same pathway.

The studies on analysing the *taf8*-mutants and *vipar*-morphants for lipid-metabolism related defects might contribute to the establishment of zebrafish as a model for lipid research.

## 1.4.4 New methods to interfere with maternal effect genes

Many zebrafish phenotypes of supposedly cell-essential genes show a surprisingly mild general phenotype (chapter 1.2.1). This phenotype might reflect a mixture of a general cellular defect,

which is attenuated by the substantial maternal supply of the gene product, and a specific phenotype, reflecting specific functions of the respective gene. I want to explore if detailed analysis of general phenotypes can reveal distinct, non-general features, which may indicate specific functions. Given the modest nature of phenotype observed for numerous cell-essential genes, the maternal contribution needs to be addressed.

In collaboration with Zsolt Csenki we want to develop a method which circumvents the need of a zygotic mutant as a prerequisite to study maternal gene function by direct manipulation of isolated early stage oocytes. This requires the reintroduction of the oocytes into the ovary of surrogate mothers to allow for normal oogenesis. We explored if a novel transplantation method for early stage oocytes may allow the development of fertilisable eggs.

# 2   Material and Methods

## 2.1   Material

### 2.1.1   Chemicals

If not otherwise stated chemicals were ordered from Sigma-Aldrich (Poole, UK) or Fisher Scientific (Loughborough, UK). Commonly used chemicals, like salts and organic solvents, are not listed.

| Chemical | Catalogue Number | Supplier |
|---|---|---|
| Ampicillin | | Sigma-Aldrich, Poole, UK |
| Albumin, bovine serum, Fraction V, $\approx 99\%$ | A3059-10G | Sigma-Aldrich, Poole, UK |
| dNTPs | | 5Prime, Nottingham, UK |
| 37% Formaldehyde Solution | | Sigma-Aldrich, Poole, UK |
| Nuclease-Free Water | 9914G | Applied Biosystems, Warrington, UK |
| Nuclease-Free Water | P1193 | Promega, Southampton, UK |
| Paraformaldehyde | | Sigma-Aldrich, Poole, UK |
| Phenol red solution | | Sigma-Aldrich, Poole, UK |
| N-Phenylthiourea | | Sigma-Aldrich, Poole, UK |
| Kanamycin | | Sigma-Aldrich, Poole, UK |
| Hydrogen peroxide, 30 wt.%solution in water | 21, 676-3 | Sigma-Aldrich, Poole, UK |
| TRIzol Reagent | 15596-018 | Invitrogen, Paisley, UK |
| Phenol:Chloroform:Isoamyl Alcohol 25:24:1 Saturated with 10 | P3803-100ML | Sigma-Aldrich, Poole, UK |

| | | |
|---|---|---|
| mM Tris, pH 8.0, 1mM EDTA | | |
| Phenol:Chloroform 5:1, Acid-equilibrated: pH 4.7 | P1944-400ML | Sigma-Aldrich, Poole, UK |
| GW9662 (PPARγ antagonist) | M6191-5MG | Sigma-Aldrich, Poole, UK |
| Troglitazone (PPARγ agonist) | T2573-5MG | Sigma-Aldrich, Poole, UK |
| Gentamycin Sulfate | BP918-1 | Fisher Scientific, Loughborough, UK |
| 10x DPBS without $CaCl_2$ and $MgCl_2$ | 14200-083 | Invitrogen, Paisley, UK |
| Phosphate Buffered Saline (Dulbecco A) | BR0014G | Oxoid Limited, Basingstoke, UK |
| Guanidine Thiocyanate | G9277 | Sigma-Aldrich, Poole, UK |
| Alizarin Red S | A5533-25G | Sigma-Aldrich, Poole, UK |
| Alcian Blue 8GX | A5268-10G | Sigma-Aldrich, Poole, UK |
| N-Phenylthiourea, Grade I, ≈ 98% | P7629-10G | Sigma-Aldrich, Poole, UK |
| Phenol red Solution, 0.5% in DPBS | P0290 | Sigma-Aldrich, Poole, UK |
| Citric Acid (Monohydrate) | C-1909 | Sigma-Aldrich, Poole, UK |
| Formamide | F5686-1L | Sigma-Aldrich, Poole, UK |
| TWEEN 20 | P1379 | Sigma-Aldrich, Poole, UK |
| Dimethyl sulfoxide DMSO | D8418 | Sigma-Aldrich, Poole, UK |
| pH indicator sticks | FB33003 | Fisher Scientific, Loughborough, UK |
| 3.0 ml Graduated Pasteur Pipette | E 1414-0300 | Starlab, Milton Keynes, UK |
| 3.0 ml Fine Tip Pasteur Pipette | E 1414-1300 | Starlab, Milton Keynes, UK |
| Ethyl 3-aminobenzoate, methanesulfonic acid salt, 98% MESAB | E10521-50G | Sigma-Aldrich, Poole, UK |
| Ribonucleic acid, transfer, Type V, From Wheat Germ | R7876-10KU | Sigma-Aldrich, Poole, UK |
| 1 kb DNA Ladder | N3232S | New England Biolabs, Hitchin, UK |
| 100 bp DNA Ladder | N3231S | New England Biolabs, Hitchin, UK |

| | | |
|---|---|---|
| Optical 96-Well Reaction Plate | N801-0560 | Applied Biosystems, Warrington, UK |
| Optical Adhesive Film | 4311971 | Applied Biosystems, Warrington, UK |
| Oil Red O | 00625-25G | Sigma-Aldrich, Poole, UK |
| Oligo (dT)15 Primer 500 μg/ml | C110A | Promega, Southampton, UK |
| rRNasin RNase Inhibitor 40 u/μl | N251B | Promega, Southampton, UK |
| Gel Loading Dye Blue (6x) | B7021S | New England Biolabs, Hitchin, UK |
| Gel Loading Buffer II | 8546G | Applied Biosystems, Warrington, UK |
| Ampicillin sodium salt | A9518-25G | Sigma-Aldrich, Poole, UK |
| TURBO DNase 2 u/μl with Ammonium Acetate Stop Solution | 2238G2, 9075G | Applied Biosystems, Warrington, UK |
| DIG RNA Labeling Mix, 10x, Digoxigenin-UTP | 11 277 073 910 | Roche Diagnostics, Burgess Hill, UK |
| Trypsin from bovine pancreas | T9201-100MG | Sigma-Aldrich, Poole, UK |
| BCIP (5-Bromo-4-chloro-3-indolyl-phosphate), 3 ml (150 mg) | 11 383 221 001 | Roche Diagnostics, Burgess Hill, UK |
| NBT (4-Nitro blue tetrazolium chloride) | 11 383 213 001 | Roche Diagnostics, Burgess Hill, UK |
| Random Hexamers 100 μl 50 μM | N808-0127 | Applied Biosystems, Warrington, UK |
| Heparin 100 mg | H3400-100MG | Sigma-Aldrich, Poole, UK |

## 2.1.2    Enzymes

| Enzyme | Catalogue Number | Supplier |
|---|---|---|
| Pfu Polymerase | | |
| Protease, Type XIV: Bacterial, | | Sigma-Aldrich, Poole, UK |

| From *Streptomyces griseus* (pronase) | | |
|---|---|---|
| Proteinase K | | Sigma-Aldrich, Poole, UK |
| Restriction Enzymes | | Invitrogen, Paisley, UK<br>New England Biolabs, Hitchin, UK<br>Promega, Southampton, UK |
| RNaseA | | Sigma-Aldrich, Poole, UK |
| Power SYBR Green PCR Master Mix | 4367659 | Applied Biosystems, Warrington, UK |
| M-MLV RT, RNase H(-) Point Mutant 200 U/µl with M-MLV RT 5x Buffer | M368B, M531A | Promega, Southampton, UK |
| RQ1 RNase-Free DNase 1 u/µl with 10x Reaction Buffer and Stop Solution | M610A, M198A, M199A | Promega, Southampton, UK |
| GoTaq DNA Polymerase 5 u/µl with 5x Green GoTaq Reaction Buffer | M830A, M791B | Promega, Southampton, UK |
| T7 RNA Polymerase | 10881767001 | Roche Diagnostics, Burgess Hill, UK |
| SP6 Polymerase | 114 876 710 01 | Roche Diagnostics, Burgess Hill, UK |

## 2.1.3    Equipment and Consumables

| Equipment for microinjections | | |
|---|---|---|
| Equipment | Catalogue Number | Supplier |
| Analogue gas microinjector | | Tritech Research, Los Angeles, USA |
| Borosilicate glass capillaries (OD 1 mm, ID 0.78 mm) | 300035 | Harvard Apparatus, Kent, UK |
| Flaming-Brown needle puller | | Sutter Instruments, Novato, USA |

| | | |
|---|---|---|
| Nanosep Centrifugal Devices (modified nylon membrane) | 516-8554 | VWR, Lutterworth, UK |
| Microloader Filling Tips | 524 295 6003 | Eppendorf, Hamburg, Germany |

| Equipment for microarray | | |
|---|---|---|
| Equipment | Catalogue Number | Supplier |
| Unrestricted AMADID Release GE 4x44K 60mer, 1X244K features, sold in multiples of 1-1'x3' slides per kit, 1 micrroarray per slide | G2519F | Agilent, Waldbronn, Germany |
| LRILAK PLUS, two-Colour Low RNA Input Linear Amplification Kit PLUS | 5188-5340 | |
| Pack of 5 Backings, 4 Arrays/Slide | G2534-60011 | |
| Gene Expression Hybridization Kit | 5188-5242 | |
| Two Color RNA Spike-in Kit | 5188-5928 | |
| Gene Expression Wash Buffer Kit | 5188-5327 | |
| Stabilization and Drying Solution | 5185-5979 | |
| RNeasy mini kit | 74106 | Quiagen, Crawley, UK |

| Equipment | Supplier |
|---|---|
| Stereomicroscope SMZ800 with digital camera DXM1200 controlled by ACT-1 Version 2.70 software | Nikon |
| Stereoscopic Zoom Microscope SMZ 1500 with Epi-fluorescence Attachment and digital camera DS-Qi1Mc controlled by NIS Elements software | Nikon |
| Stereomicroscope SMZ645 | Nikon |
| Heraeus Megafuge 11R Centrifuge | Thermo Scientific |
| Heraeus Incubator (used for zebrafish embryos/larvae) | Thermo Scientific |

| Milli-Q$_{PLUS}$ 185, Ultra Pure Water System | Millipore, Watford, UK |
|---|---|
| Multi Genius, Bio Imaging System controlled by GeneSnap sofware | Syngene, Cambridge UK |
| NanoDrop ND-1000 | Peqlab, Erlangen, Germany |

| Equipment for PCR (polymerase chain reaction) | |
|---|---|
| Equipment | Supplier |
| iQ5 Multicolor Real-Time PCR Detection System | BIO-RAD, Hemel Hempstead, UK |
| DNA Engine Tetrad 2 Peltier Thermal Cycler | BIO-RAD, Hemel Hempstead, UK |
| iQ5 software | BIO-RAD |
| Optical well plates | Applied Biosystems, Warrington, UK |
| Optical films | Applied Biosystems, Warrington, UK |
| PCR strips | |
| Single PCR tubes | |
| Optical well plates | Applied Biosystems, Warrington, UK |
| TripleMaster PCR System | Eppendorf, Hamburg, Germany |

## 2.1.4    Kits

| Kit | Catalogue Number | Supplier |
|---|---|---|
| Plasmid Maxi Kit | | Quiagen, Crawley, UK |
| First Choice RLM-RACE | AM1700 | Applied Biosystems, Warrington, UK |
| TOPO TA Cloning Kit (with pCR2.1-TOPO) | K4500-01 | Invitrogen, Paisley, UK |
| Wizard SV Gel and PCR Clean-Up System | A9282 | Promega, Southampton, UK |
| nMESSAGE mMACHINE SP6 | AM1340 | Applied Biosystems, Warrington, UK |

| | | | |
|---|---|---|---|
| TURBO DNA-free | AM1907 | Applied Biosystems, Warrington, UK | |
| Wizard Plus SV Minipreps DNA Purification System | | Promega, Southampton, UK | |

## 2.1.5    Morpholino oligonucleotides

| Targeted Gene | Morpholino | Morpholino type | Sequence |
|---|---|---|---|
| *taf1* | *taf1*ATG | targeting | TCATCACTGTCCGAGTCTGACATTC |
| | *taf1*ATGmm | mismatch control | GCATCCCTGTCAGAGTATGACTTTC |
| | *taf1*UTR | targeting | CTCTCCTCTTGAAGTAAACCGGCAC |
| *btaf1* | *btaf1*ATG | targeting | AGATAAAGAGACGTTCTAACCGCAT |
| | *btaf1*mm | mismatch control | AGAaAAAcAcACcTTCTAACCcCAT |
| *taf2* | *taf2*ATG | targeting | CCCTTGTCTTTCTTGCGGTTCATTC |
| | *taf2*ATGmm | mismatch control | ACCTTTTCTTTATTGCTGTTCCTTC |
| | *taf2*UTR | targeting | CCCTTAAGTCCATTTCGTCATGTCC |
| *taf3* | *taf3*ATG | targeting | GCGCGAAGCTCTCACACATCTCTCC |
| | *taf3*ATGmm | mismatch control | TCGCGACGCTCGCACAAATCTATCC |
| | *taf3*UTR | targeting | GGGCTTTGTTTTGGCCACTCACATC |
| *LOC100149942 (taf4l)* | *taf4l*ATG | targeting | ACGTCCCGATCAAAGTAGTTACCAT |
| | *taf4l*mm | mismatch control | ACcTCCCcATgAAAcTAcTTACCAT |
| *taf5* | *taf5*ATG | targeting | CCATCCTGCACAGCCGCCATTTTTC |
| | *taf5*ATGmm | mismatch control | ACATCATGCAAAGCCTCCATTTTTC |
| *taf5l* | *taf5l*ATG | targeting | GGACACGCTTCATCTCTGCATAATC |
| | *taf5l*UTRmm | mismatch control | AGTGAAGGCCTTTCCTTGAGACAAG |
| | *taf5l*UTR | targeting | CGTGAATGCCTGTCCTGGAGAAAAG |
| *taf6* | *taf6*ATG | targeting | TCTGTCTGCGTTCCTCTGCCATTTC |
| | *taf6*ATGmm | mismatch control | GCTGTATGCGGTCCTATGCCCTTTC |
| | *taf6*UTR | targeting | CAGCTATGTCTATTTAAAGCTGCCG |
| *taf6l* | *taf6l*ATG | targeting | GCCGTTCCTCCCTCTCGGTCATCTT |
| | *taf6l*ATGmm | mismatch control | GCCcTTgCTgCCTCTgGcTCATCTT |
| *taf7* | *taf7*ATG | targeting | TCCCACTTTTGTTTTTGAGGTCATC |
| | *taf7*ATGmm | mismatch control | NA |
| | *taf7*UTR | targeting | ATCAGAGAACAGCTAAATTGAGCAC |
| *taf8* | *taf8*ATG | targeting | ATCATTACCGAGTCTGCCATTTTAG |

| | taf8ATGmm | mismatch control | ATCATTAGCGACTGTGCGATTTTAC |
|---|---|---|---|
| *taf9* | *taf9*ATG | targeting | TTCGGAGACGCCATTTTTCACTCCT |
| | *taf9*ATGmm | mismatch control | TTCcGAcACGCgATTTTTgACTgCT |
| | *taf9*UTR | targeting | AGCGAGCGATCAGCCTTACCCAGAC |
| *si:dkey-72l14.8* *(taf10)* | *taf10*ATG | targeting | CGGTCTGCGTGAGATCCACGTTCAT |
| | *taf10*ATGmm | mismatch control | CGcTCTcCGTGAcATCCACcTTgAT |
| | *taf10*UTR | targeting | TTCCCGGCTTAGTTTATGTATTGCA |
| *taf11* | *taf11*ATG | targeting | GGGTCTGCCATGATTTCAGCTCAGA |
| | *taf11*ATGmm | mismatch control | TGGTCGGCCATTATTTAAGCTAAGA |
| | *taf11*UTR | targeting | CGACAACCGCGTTGAAAATAATGTT |
| *taf12* | *taf12*ATG | targeting | GCTGGATACTGGGTCATACTATGCT |
| | *taf12*ATGmm | mismatch control | TCTGGCTACTTGGTCCTACTCTGCT |
| | *taf12*UTR | targeting | TGTCAAATGTCACAAGCCTCTTCAG |
| *taf13* | *taf13*ATG | targeting | CGGGATCATCTTCTTCCTCGACCAT |
| | *taf13*ATGmm | mismatch control | AGGGAGCATCGTCTTACTCGCCCAT |
| | *taf13*UTR | targeting | ACACAAACAAACCAGCAGGAAACGC |
| *zgc:158363* *(taf15)* | *taf15*ATG | targeting | GTAGCCTGAATCTGAGGCCATCGTT |
| | *taf15*ATGmm | mismatch control | TTAGCATGAAGCTGAGTCCATAGTT |
| | *taf15*UTR | targeting | ATTAAAAACCCGGCACGAGCGAAAC |

## 2.1.6    PCR Primers (oligonucleotides)

AZ: Andreas Zaucker.
(1): from Adam Amsterdam (MIT, personal communication).
(2): taken from (Jones et al., 2008).
(3): taken from (McCurley and Callard, 2008).

| Primer name | Gene | Sequence 5'-3' | $T_M$ in °C | Amplicon in bp | Design |
|---|---|---|---|---|---|
| (gDNA) Taf8 fw | *taf8* | CTCTTTCCTTCACCCTGCTG | 60 | 396 | AZ |
| (gDNA) Taf8 rev | *taf8* | GCTAACCCAATTCTCCATGC | 58 | | AZ |
| (gDNA) Taf6 fw | *taf6* | TAGCGGTAACGCACAGACAA | 58 | 390 | AZ |
| (gDNA) Taf6 rev | *taf6* | CTTTCAGGCAACAACCCATC | 58 | | AZ |
| Insert rev | gtvirus, t5virus | CTGTTCCATCTGTTCCTGAC | 58 | 186/148 (with Taf8 fw) 246 (with Taf6 fw) | (1) |

| Primer Name | Gene | Sequence 5'-3' | $T_M$ in°C | Amplicon from cDNA/gDNA in bp | Design |
|---|---|---|---|---|---|
| Taf8 fw | *taf8* | TGATAGCGCTGAGAAAGCTG | 58 | 187/953 | AZ |
| Taf8 rev | | TTTGGCGTACACTGGAAGAG | 58 | | AZ |
| Taf6 fw | *taf6* | TCGGAACTAAATGGGCTGTG | 58 | 188/ (N/A) | AZ |
| Taf6 rev | | GCTTCTGTCTGCGTTCCTCT | 60 | | AZ |
| Bactin1 fw | *bactin1* | TCTTCACTCCCCTTGTTCAC | 58 | 198/1565 | AZ |
| Bactin1 rev | | GGAGTCTTTCTGTCCCATGC | 58 | | AZ |
| Bactin1 II fw | | CGAGCAGGAGATGGGAACC | 62 | 102/102 | (3) |
| Bactin1 II rev | | CAACGGAAACGCTCATTGC | 58 | | (3) |
| Fabp11a fw | *fabp11a* | CACCTTCAAAACCACCGAGA | 58 | 203/(1781 and 1772) | AZ |
| Fabp11a rev | | CCACATCACCCATCTTGCAT | 58 | | AZ |
| Fabp11b fw | *fabp11b* | TGAGCAGGGCGTCATCACTATGAA | 65 | 176/1121 | (2) |
| Fabp11b rev | | TTGTGGTCTTTCCTTCCCAGGTCT | 65 | | (2) |
| Cd36 fw | *cd36* | GAACAGCTTGGTTGGAGCTT | 58 | 318/4847 | AZ |
| Cd36 rev | | GCATCAACAGGCAGCAAGTA | 58 | | AZ |
| Lpl fw | *lpl* | TTACCCAACATCAGCCTCCT | 58 | 249/1173 | AZ |
| Lpl rev | | GCGTCGTCTGGAGAAAGAGT | 60 | | AZ |
| Pparγ fw | *pparγ* | TGCCGCATACACAAGAAGAG | 58 | 240/11029 | AZ |
| Pparγ rev | | GGCTTTGGTCAGAGGGAAGT | 60 | | AZ |
| Slc27a1a fw | *slc27a1a* | TCAGCAAGCTCTTCCTCCAT | 58 | 188/7941 | AZ |
| Slc27a1a rev | | GCTCCTCGTTGACAAGTTCG | 60 | | AZ |
| Ef1a fw | *ef1a* | CTTCTCAGGCTGACTGTGC | 59 | 358/(N/P) | (3) |
| Ef1a rev | | CCGCTAGCATTACCCTCC | 58 | | (3) |
| Fabp2 fw | *fabp2* | ATTCTCTGGCAGACGGCACT | 61 | 166/2368 | AZ |
| Fabp2 rev | | TTGGCCTCGACTCCATCATA | 58 | | AZ |

## 2.1.7    Zebrafish lines

| Line | Description |
|------|-------------|
| AB | Wildtype line |
| *taf8*<sup>hi3079Tg</sup> | Mutant line generated by insertional mutagenesis. The foreign sequence (GT transgenic construct) inserted into the first intron. |
| *taf8*<sup>hi4055Tg</sup> | Mutant line generated by insertional mutagenesis. The foreign sequence (GT transgenic construct) inserted into the first intron. |
| *taf6*<sup>hi80aTg</sup> | Mutant line generated by insertional mutagenesis. The foreign sequence (F5 transgenic construct) inserted into the first intron. |
| *fli1a:EGFP gata1:dsRed* | Double transgenic line with *fli1a:EGFP* driven expression of enhanced GFP (green fluorescent protein) in the blood vasculature, the dorsal aorta, the posterior cardinal vein and the thoracic duct . The *gata1:dsRed* transgene drives expression of dsRed in the dorsal aorta, the erythroid cell lineage and in the posterior cardinal vein (Rampon et al., 2009, Yaniv et al., 2007). |

The *taf8*-mutants used in this thesis were a mix of the two *taf8*-mutant lines. The difference between the two mutant alleles (*taf8*$^{hi3079Tg}$ and *taf8*$^{hi4055Tg}$) is negligible. The two independent insertions occurred in very close proximity in the first intron of the *taf8* gene. There are only 38 bp between the insertion sites. Both alleles are mutant alleles, it shouldn't matter for the experiments in this thesis, which combination of two *taf8*-mutant alleles generates the mutant phenotype as long as it is a *taf8* LOF phenotype. Because this is the case for all combinations the term *taf8*-mutant in this thesis refers to *taf8*-mutants irrespective of the exact combination of mutant alleles.

```
acaccaaatacagtttttagcAAACGCAGAACGCACAATGAGTTTATTTG
CGAATGCTAAACATCAGAGGAAAAACCACTAGAGTTCTAAAATGGCAGAC
TCGGTAATGATGGGGAGCGGATCTTTAAACTCCGGAAGCgtacgttaaat
atctcctttcattaacgctaacgttactctttccttcaccctgctggctc
agcc
hi4055 (5п-3п)
aaacaatactaactttagttttttgatcaaaattagac
hi3079 (5п-3п)
ttaaaggcacttgtgtaatatatttttaaagcagacaccgtatcgtatgta
aacacgtctgtatatatatatatatatatatatatatatatatatatata
tatatatatatatatatatatatatatatatatcaattatatagtgag
ctgcggcagatcagtgtcgtcaaacagtgttttatata

approx 2 kb to next exon
```

**Figure 2.1 – Insertion sites of the *hi4055* and *hi3079* alleles**

Shown are the insertion sites of the two nearly identical *taf8*-mutant alleles, *taf8*$^{hi3079Tg}$ and *taf8*$^{hi4055Tg}$. The information is taken from the Hopkins lab web page (http://web.mit.edu/hopkins/).

## 2.1.8 Web-based databases and bioinformatic tools

| | |
|---|---|
| Ensembl | http://www.ensembl.org/index.html |
| NCBI | http://www.ncbi.nlm.nih.gov/ |
| UCSC | http://genome.ucsc.edu/ |
| DAVID | http://david.abcc.ncifcrf.gov/home.jsp |
| OligoCalc | http://www.basic.northwestern.edu/biotools/oligocalc.html |
| Primer3 | http://frodo.wi.mit.edu/primer3/ |
| BioVenn | http://www.cmbi.ru.nl/cdd/biovenn/ |
| ZFIN | http://zfin.org/cgi-bin/webdriver?MIval=aa-ZDB_home.apg |
| KEGG | http://www.genome.jp/kegg/kegg2.html |
| ZF-Espresso | http://zf-espresso.tuebingen.mpg.de/ |
| Nancy Hopkins web page | http://web.mit.edu/hopkins/ |

## 2.1.9    Software

SigmaStat for Windows Version 3.5 (Systat Software, Inc)

Serial Cloner 1.3-11

Bio-Rad iQ5

ImageJ software

Microsoft Excel 2007

# 2.2    Zebrafish methodology

## 2.2.1    Production of embryos

Zebrafish embryos can be easily obtained by crossing adult fish. Females and males can be distinguished by body-shape and colour. Healthy, egg-producing females, have a big white belly and their colour is bluish grey. Males are slender and their colour is more yellowish golden. A female needs three stimuli to lay: Light (in the wild zebrafish lay in the morning), males and a not to low water temperature <20°C. If zebrafish are pair-wise put together directly from their communal tanks in the morning they lay with a big delay, or they do not lay at all. Both is not desired for experiments, where the time of the production of fertilised eggs needs to be controlled. If the pairs are put together in small crossing cages the day before, their laying behaviour is much better and they will start to mate as soon as there is light on the next morning. The crossing cages contain neatly fitting inlays with a mesh bottom, which separates the adult zebrafish from the eggs. This is necessary, because the adult zebrafish would eat the eggs. Furthermore, the inlay itself can be subdivided into two compartments using a divider. If female

and male were kept in separate compartments over night (O/N), they only can mate if the divider is removed. The experimentator thereby can control when eggs (embryos) are produced. This is especially important for experiments where synchronised and/or early (zygote, one cell stage) embryos are required, like microinjections.

## 2.2.2    Rearing zebrafish larvae

The cages used for crossings of adults fit in the top of small fish tanks such a way, that most of the cage is submerged into the water of the tank, but the fringe of the cage still stays above the surface level of the water in the tank. Thereby the temperature for egg incubation in the cages is controlled by the system. In those cages zebrafish embryos are reared. It is critical to rear embryos in a container with a low surface level of the medium. This allows early larvae to reach the surface for swallowing air, to initially inflate their swim bladders. The inflation of the swim-bladder allows larvae to stay at the surface for feeding. After approximately one month, they are then released from the cages into the communal tanks.

## 2.2.3    Microinjections

Microinjection of early zebrafish embryos was carried out manually, without micromanipulator. The embryos are readily accessible and there are no obstacles, like strong envelops or shells. The chorion is relatively weak until 2 cell stage. Thus, injection is carried out through the chorion into the cytoplasm, or into the unsegregated ooplasm 10-15 min after fertilisation. The embryos can be immobilised prior to injection by complete removal of the medium from the Petri dish.

## 2.2.3.1    Injection solutions

The injection solutions for the MO-screen were prepared the following way:

A 5% rhodamin solution was prepared dissolving the powder in nuclease free water. The 5% rhodamin solution was filtered through a microspin column to remove all undissolved rhodamin powder. Similarly, a 0.5% phenol red solution was prepared, spinning the stock solution through a microspin column to remove un-dissolved phenol red. Prior to use the 1 mM MO (in nuclease-free water, NFW) stock solutions were heated to 65°C for 5 min to bring any precipitated MO back into solution.

| MO injection solutions | | |
|---|---|---|
| Stock solution, concentration | Volume in µl | Final concentration |
| MO, 1 mM | 1 | 100 µM |
| Rhodamin, 5% | 1 | 0.5% |
| Phenol red, 0.5% | 2 | 0.1% |
| NFW | 6 | |
| Final Volume | 10 | |

## 2.2.3.2    Dechorionation of embryos and larvae

Early zebrafish embryos <1 hpf can be easily dechorionated by pronase digestion of the chorion, which is composed of glycoproteins. Later the chorion hardens and during gastrulation stages it is impossible to digest the chorion by pronase without damaging the embryos. From 24 hpf on the embryos can again be efficiently digested using pronase. An alternative to enzymatic dechorionation with pronase is manual dechorionation with forceps, which can be done from late somitogenesis stages onwards.

Dechorionated embryos ≤30 hpf are fragile and should not be kept in plain Petri dishes, where they might stick to the plastic and break when moved. Instead, they have to be kept in agarose gel-coated Petri dishes (agarose-plates). Agarose-plates are made by heating a 1% suspension of agarose in Hank's medium (140 mM NaCl, 5.4 mM KCl, 4.2 mM NaHCO$_3$, 1.3 mM CaCl$_2$, 1 mM MgSO$_4$, 440 µM KH$_2$PO$_4$, 250 µM Na$_2$HPO$_4$) till it forms a gel. The hot gel can then be poured into Petri dishes. When the gel has solidified the Petri dish is coated with an agarose gel.

Dechorionation of early embryos (zygote, 1 cell stage)

If dechorionated embryos younger than Prim-5 stage were needed for experiments, the embryos were dechorionated right after fertilisation. Freshly laid eggs are opaque and their chorion is not inflated. In this stage they can be easily damaged. When they had cleared up and their chorion had swollen up they were collected and put into non-coated small Petri dishes (Ø 6 cm). Extant liquid above the chorions was removed. Then 500 µl (for ≤500 embryos) or 1 000 µl (for more than 500 embryos) of pronase (10 mg/ml in Hank's) were added and the pronase evenly distributed by shaking. The pronase was preheated in hand warm water from the tap. The Petri dish then was left standing under the microscope till the first embryos (approximately5) can be seen, which have left the chorion. This should happen within the first 5 min after adding the pronase. Keeping the embryos for to long in pronase carries the risk to over-digest them. The Petri dish then was carefully submerged into a 500 ml beaker containing clean water from the system. Because the embryos break at the surface-tension, they have to stay submerged throughout. The water was decanted as far as possible and fresh water was added letting it run down the wall of the tilted beaker. The movement of the embryos generated by this stream helps

to dechorionate them. This washing step to remove the pronase was repeated two more times. After the last washing the embryos were transferred into agarose gel coated Petri dishes using plastic Pasteur pipettes.

## Dechorionation of embryos at 1 dpf

Embryos around or older than Prim-5 stage were either dechorionated manually using forceps, or by pronase digest. The 1 dpf embryos usually were digested in a similar way to the early embryos, but in large Petri dishes (Ø 9 cm), by adding 1 ml of pronase (10 mg/ml). In contrast to the early embryos the 1 dpf embryos were not kept standing under the microscope but were vigorously shaken approximately every minute till most had left the chorion. The washing steps again were the same like the ones for early embryos. Embryos younger than or in Prim-5 stage were transferred into agarose-plates, because they still are fragile. Embryos around or older than Prim-15 stage were transferred into plain Petri dishes.

## 2.2.3.3    Injections

To ensure an optimal, homogenous distribution of the injected material, it is critical to inject zebrafish embryos at the earliest possible time point. In the egg the cytoplasm (ooplasm) is mixed with the yolk. After fertilisation the cytoplasm separates from the yolk and forms the first blastomere (cell) at the animal pole. Structures called axial streamers are involved in this transport process of the ooplasm to the animal pole. In my experience, it is optimal to microinject the embryos as early as possible, at a time point before the beginning of separation of ooplasm and yolk (zygote), or while the first blastomere just begins to form. The injected material then

together with the ooplasm is transported into the first cell (blastomere). Because the first blastomere is fully formed already around 12 min after fertilisation, there is little time to dechorionate the embryos before injections. The microinjections performed for this thesis therefore all were done with non-dechorionated embryos, between zygote and 1 cell stage.

An alternative to the strategy described above is to inject the material directly into the first blastomere. Furthermore, axial streamers are still present at least up to the 8 cell stage (Fuentes and Fernandez, 2010) and the blastomeres are not completely separated from the yolk cell by a plasma membrane until the 8 cell stage (marginal cells even cycle 10) (Kimmel et al., 1995). Small molecules therefore can reach the cytoplasm of the blastomeres also when injected at later stages, by diffusion.

For microinjections through the chorion, embryos are collected with a net, right after the eggs have cleared up and the chorion has swollen up. The collected embryos then were placed into a small Petri dish. If the embryos are collected too early, they will be damaged during the microinjection process, because they are attached to the chorion. The embryos were collected in the middle of the Petri dish and the liquid was removed completely. This is necessary to prevent the embryos from rolling away while trying to inject them.

The embryos then were injected with the injection solutions using a nitrogen gas injector. This gas injector is a relatively simple system using the pressure from compressed nitrogen in a gas bottle to press (shoot) the injection solution, which was filled into an injection needle using microloader tips, into the embryo. Because I injected embryos before the 1 cell stage the injection solutions were injected at random positions, cortically, just under the plasma membrane. Material injected that way efficiently localised to the cytoplasm of the first cell. If the material is injected deeper into the embryo, it might be trapped there and not be transported into the first cell. The

phenol red in the injection solution serves to control the amount of solution injected. The diameter of the injected drop of injection solution was around one tenth of the diameter of the embryo. The amount injected with the gas injector system can be controlled using a valve, which opening is controlled by a pedal. The opening time when pressing the pedal can be controlled be a dial. The injections were done by free hand with an injection needle attached to a holder which is connected to the valve via a silicone tube. The injection needles were made from borosilicate capillaries using a needle puller.

## 2.2.3.4 *Vipar* knock down and rescue experiments

The experiments aiming for the characterisation of the zebrafish *vipar*-morphant were performed in collaboration with Andrew R. Cullinane and the Gissen group. A detailed description of the performed experiments can be found in Andrew R. Cullinane's PhD thesis: "Characterisation of the Role of VPS33B in Vesicular Trafficking in Polarised Epithelial Cells (University of Birmingham, 2009)".

MOs against the start codon (*vipar* ATG MO) and the intron2-exon3 splice junction (*vipar* Exon3 MO) injected into early embryos prior to the formation of the first blastomere. The concentration in the injection solutions was 10 μM for the ATG MO and 100 μM for the Exon3 MO. As a control MO served a MO with five mismatches in its sequence compared to the Exon3 MO. The concentration of the control MO was 100 μM in the injection solutions. The MO injection solutions contained 10 ng/μl CFP-mRNA (cyan fluorescent protein) as a injection control.

For rescue experiments half of the MO injected embryos were injected a second time with 100 ng/μl *vipar*-mRNA. This injection solution contained RFP-mRNA as a injection control. To

control the specificity of the rescue with *vipar*-mRNA, control rescue experiments with 120 ng/μl

RFP-mRNA were performed. Using the CFP and RFP fluorescence the embryos were sorted into

MO injected and double injected (MO + RNA) embryos at 1 dpf (Figure 2.2).
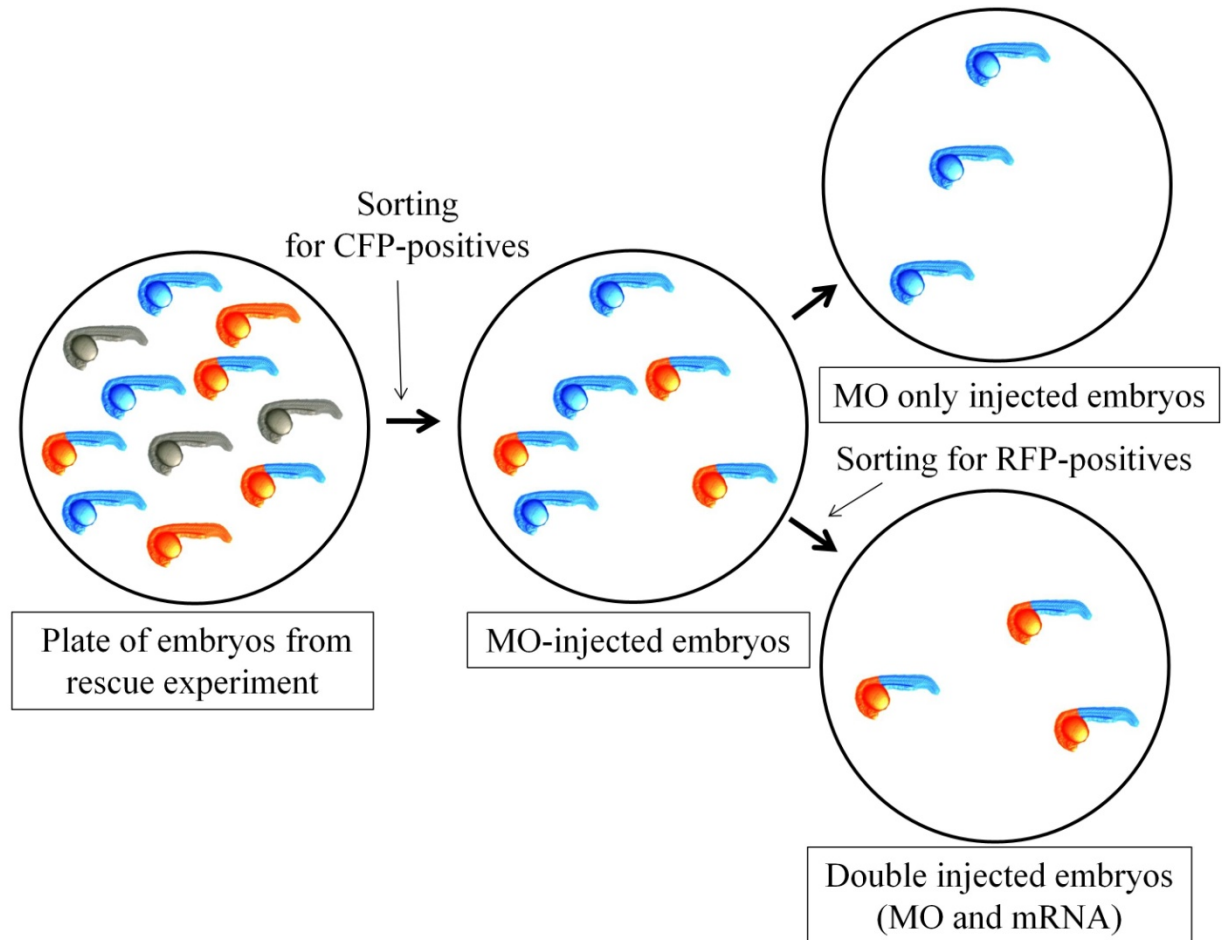


**Figure 2.2 – Fluorescence sorting of embryos from rescue experiments**

The injection solutions used for the rescue experiments of the *vipar*-morphants contained mRNAs encoding for fluorescent proteins. The MO injection solutions contained CFP-mRNA and the *vipar*-mRNA injection solutions contained also RFP-mRNA. The fluorescence then was used to distinguish MO only injected embryos (CFP positive) from embryos which were injected with both, the MO and the rescuing mRNA (CFP and RFP positive).

## 2.2.4    Imaging of embryos and larvae

All the imaging for this thesis was performed using the Stereomicroscope SMZ800 with the digital camera DXM1200 controlled by ACT-1 Version 2.70 software.

# 2.3    MO-screen

In the MO-screen we targeted 18 Taf proteins implicated in Pol II transcription, plus additional 13 non Taf targets. The experiments for the non Taf targets are not discussed in this thesis. Because of the scale of the experiment, 31 targets, we didn't carry out the full set of controls for a MO-mediated kd experiment. As specificity controls served mismatch MOs (5 mismatches) for the targeting MOs. But no rescue experiments were performed. All MOs used for the screen were translation blocking MOs, targeting the AUG or the 5'-UTR (untranslated region) sequence. The reason for not including splice interfering MOs is, that all Taf transcripts are already present in the unfertilised egg (unpublished CAGE data). Because the maternal Taf transcripts are already spliced, they cannot be targeted with splice MOs.

## 2.3.1    MO-screen protocol

Day 1: Injections

The MOs were injected through the chorion, into early (<1 cell stage) embryos, like it was described in (chapter 2.2.3.3). The injections usually were performed in the morning between 9.30 am and 12.30 pm. The injected embryos were obtained from crossings of the AB line. Because we were aiming at 100 embryos for phenotype analysis, between 100-200 embryos per

injection solution were injected. Twelve rounds of injections were performed to cover all injection solutions and the repeats of experiments.

After injections the embryos were kept at 28°C (incubator) in large Petri dishes containing Hank's medium supplemented with gentamicin (50 µg/ml). In the afternoon of the day of injection the Petri dishes were cleaned using plastic Pasteur pipettes. That means that everything what is not a developing embryo was removed: Non-fertilised eggs, fish scales, dead embryos, pieces of food and faeces. After cleaning, the Hank's medium (+ gentamicin) was replaced.

## Day2: Fluorescence sorting and 1 dpf phenotype analysis

In the morning, the Petri dishes were cleaned again by removing dead embryos. This in nearly all cases only were very few (<10 embryos) and is very unlikely to be caused by the MOs, but rather by damaging during injections or by maternal/paternal defects.

Under the fluorescence microscope, non-injected, or embryos with a non-homogenous, poor distribution of the rhodamin tracer (red fluorescence), were sorted out. In each Petri dish 5 non-injected embryos were left, to serve as wildtype reference embryos for the phenotype analysis. After the fluorescence sorting of embryos using rhodamin as an injection control, the embryos were enzymatically dechorionated like it is described in (2.2.3.2). The dechorionation was done after the fluorescence sorting because it is easier to sort embryos which are still in the chorion. After dechorionation the embryos were transferred into new Petri dishes and the medium used was changed to Hank's medium without gentamicin.

If a significant number of embryos at 1 dpf showed a phenotype, this phenotype was analysed.

## Day3: 2 dpf phenotype analysis

In some experiments the embryos not were dechorionated at 1 dpf but in the morning of the second day post fertilisation, either enzymatically or manually. Two dpf was the main stage for the analysis and documentation of the MO-induced phenotypes.

For the phenotype analysis the embryos were transferred into a large agarose-plate. Then the embryos were anesthetised by adding drops of MESAB (4 mg/ml tricaine in Hank's) to the medium in the agarose-plate and shaking the plate to distribute the MESAB in the medium. This procedure was repeated till the embryos stopped moving, but still had a relatively normal heart beat and blood circulation. In that condition the embryos can be left for hours to analyse their phenotype, without any adverse effects on their development, upon replacing medium afterwards. The embryos of each Petri dish (MO-injection) were separated into groups sharing same features of the phenotype, into categories of phenotypes. The numbers of embryos in each group (also the wildtype group) were documented and the phenotypes were described using the (non-injected) wildtype embryos as a reference. The 5 non-injected wildtype embryos were not taken into account when counting the embryos in each category of phenotypes. The imaging of the embryos and larvae was performed in agarose-plates. To obtain proper side view images, with the embryo/larvae in focus throughout, the yolk ball of the embryos/larvae was placed into a hole, which was cut out from the agarose gel using a small needle.

## 2.4    Histology Methods

### 2.4.1    Staining of cartilage with alcian blue

The larvae were fixed for 2 h in 4% PFA fixative, at RT. Afterwards they were washed once with 0.1% Tween 20 in $dH_2O$ for 5 min.

The larvae were stained in alcian blue staining solution (0.1 g/ml alcian blue, 0.1 N HCl, 0.1% Tween 20 in $dH_2O$) for two days at 4°C.

The larvae were bleached for two hours in bleach solution (0.3% $H_2O_2$, 1% KOH, 0.1% Tween 20 in $dH_2O$). Afterwards they were rinsed two times in 0.1% Tween 20 (in $dH_2O$).

The larvae were pre-incubated for 10 min in saturated sodium borate buffer (30% saturated Sodium Borate, 70% $dH_2O$, 0.1% Tween 20). Then the soft tissue was digested O/N at 4°C by the trypsin in the digestion solution (0.05 mg/ml Trypsin, 30% saturated Sodium Borate, 0.1% Tween 20 in $dH_2O$).

The stained larvae were stepwise (25%, 50%, 75%) transferred into 86% Glycerol. The stained larvae were imaged on a depression slide under the Stereomicroscope SMZ800, with the digital camera DXM1200 controlled by the ACT-1 Version 2.70 software.

### 2.4.2    Staining of lipids with Oil Red O

The Oil Red O stainings were performed by Nan Li. The drug treatments and the initial analysis of the stainings, pictures and defining staining categories, were performed by the candidate. Nan Li scored the phenotypes according to the staining categories.

Larvae were fixed O/N in 3.7% formaldehyde (in PBS) at 4°C. The formaldehyde was removed by washing the samples for 5 min in PBS (2.67 mM KCl, 1.47 mM $KH_2PO_4$, 137.93 mM NaCl, 8.06 mM $Na_2HPO_4$-$7H_2O$). Then the larvae were incubated for two hour at RT in Oil Red O staining solution (0.3% ORO in 70% 2-propanol).

## 2.4.2.1     GW9662-treatments (PPARγ inhibitor)

For treatments with PPARγ inhibitor the embryos were incubated for 72 hours in E3-medium (5 mM NaCl, 0.17 mM KCl, 0.33 mM $CaCl_2$ and 0.33 mM $MgSO_4$) which was either 0.5 or 5 µM for the PPARγ inhibitor GW9662. There were no statistically significant differences in the lipid staining behaviour between larvae treated with 0.5 or 5 µM GW9662. Because of that, the three experiments for 0.5 µM and the three experiments for 5 µM were analysed together as GW9662-treated larvae. Control groups were incubated in E3-medium which contained the same amount of DMSO which was added to the 5 µM GW9662 treated larvae as a solvent for GW9662.

## 2.4.3     Whole-mount *in situ* hybridisation with zebrafish ovaries

1. Fixation

Dissected zebrafish ovaries were fixed in BT-Fix (77 mM $Na_2HPO_4$, 23 mM $NaH_2PO_4$, 120 µM $CaCl_2$, 220 mM sucrose and 4% paraformaldhyde) O/N at 4°C. The next day the BT-Fix was replaced by 100% MeOH and the samples were kept O/N at -20°C.

2. Rehydration and hybridisation with digoxigenin-labelled antisense YFP-probe

The YFP-probe was generated by *in vitro* transcription of the reverse strand of the EYFP coding sequence inserted into pUT+ vector.

The ovaries stepwise were rehydrated via passing through a dilution series of MeOH in PTW (PBS with 901 µM $CaCl_2$, 493 µM $MgCl_2$-$6H_2O$ and 0.1% Tween 20) at RT. They were incubated for 5 min in each dilution (75%, 50%, 25% MeOH) to allow for equilibration. Then they were washed 3 times for 5 min in PTW.

Afterwards the ovaries were preblocked in 500 µl Hyb-Buffer (50% formamide, 5xSSC, 1 mg/ml yeast total RNA, 50 µg/ml Heparin, 9 mM Citric Acid and 0.1% Tween 20) for 4 h at 67°C (water bath). Then 1 µl of digoxigenin-labelled antisense YFP-probe was added to the Hyb-Buffer. The ovaries were incubated O/N at 67°C with that 1:500 dilution of YFP-probe.

3. Immunodetection of hybridised probe

Non-hybridised probe was washed out by the following washing steps in 20xSSC (3 M NaCl, 0.3 M trisodium citrate) dilutions at 67°C:

-   2x 30 min with Washing Buffer I (1xSSC, 50% formamide and 0,1% Tween 20)

-   1x 15 min with Washing Buffer II (2xSSC and 0,1% Tween 20)

-   2x 30 min with Washing Buffer III (0.2x SSC and 0,1% Tween 20)

Afterwards the ovaries were rinsed in Blocking Buffer (1% DMSO, 0.2% BSA and 0.1% Tween 20 in PBS). Then the ovaries were blocked in Blocking Buffer for 4 h at RT. In parallel a 1:400 dilution of antiDIG-antibody (Fab-fragment conjugated with AP) was preblocked in Blocking Buffer with fish powder. After removing the fish powder by spinning it down, the preblocked antibody was further diluted (1:4000) in Blocking Buffer. The ovaries were incubated O/N with that 1:4000 dilution of antibody at 4°C.

4. Alkaline phosphatase (AP) staining of the ovaries with BCIP/NBT chromogenic substrate

Unbound antibody was washed out by the following washing steps:

-   1x rinsing in PTW

- 6x washing in PTW for 20 min

Then the ovaries were equilibrated in the alkaline Staining Buffer (100 mM TrisHCl pH 9.5, 100 mM NaCl, 50 mM $MgCl_2$ and 0.1% Tween 20) for 5 min. Finally the ovaries were incubated in Staining Solution (306 µM NBT and 500 µM BCIP dissolved in Staining buffer) until a purple staining was visible (ca 1 h). The Staining was stopped by rinsing the ovaries with PTW followed by postfixing them with BT-Fix.

# 2.5 Preparation of cDNA (complementary DNA) from total RNA for qPCR and RT-PCR experiments

## 2.5.1 Total RNA preparation using the TRIzol method

Total RNA was prepared using the TRIzol Reagent (Invitrogen, Paisley, UK). This method can be used to simultaneously prepare RNA, DNA and protein from the same sample. For the work described in this thesis, it solely was used for RNA preparations. The preparations were done following the manufacturer's instructions for RNA-preparations from tissue-samples. For the comparative gene expression experiments at 2 dpf the amount of larvae from which total RNA was prepared ranged from 3-5 larvae per sample. For all 3 dpf experiments 12 larvae per sample were used. In the following the RNA-preparation protocol for the 3 dpf experiments is described. For the 2 dpf experiments all volumes were scaled down to half and 0.5 ml reaction tubes were used.

## Homogenisation

The samples were put on ice and 500 µl of TRIzol-Reagent were added. Then the sample was homogenised crushing the larvae in the TRIzol-Reagent with a pistil. Following this initial homogenisation, additional 500 µl of TRIzol-Reagent were added to the samples. The samples, now in 1 ml TRIzol, were further homogenised by sucking them up and down three times through a narrow hypodermic needle. After the homogenisation the tube was left at RT for at least 5 min to allow complete dissociation of nucleoprotein complexes.

## Phase Separation

200 µl Chloroform were added to the homogenate and the tube was vigorously shaken (vortexed). After vortexing the tubes were left at RT for 3 min. Then the tubes were spun with 12 000 g at 4°C for at 15 min. After the centrifugation the solution had separated into three phases, with the upper aqueous phase containing the RNA.

## Precipitation

For precipitation of the RNA, the aqueous phase (≈600 µl, 60% of volume of TRIzol reagent used) needs to be transferred into a fresh tube. To prevent carry-over of material from the other phases, only two thirds (400 µl) of the aqueous phase were pipetted into a fresh 1.5 ml reaction tube. The RNA was then precipitated by mixing the aqueous solution with 500 µl of added isopropanol, followed by inverting the tube several times. The tubes were spun shortly, to collect the solution from the wall of the tube and left at RT for around 10 min. The solution was then centrifuged with 12 000 g at 4°C for 10 min.

## Washing of pellet

The RNA was now visible as a pellet on the side wall of the bottom of the tube. The supernatant was removed completely and 1 ml of 75% ethanol in autoclaved $dH_2O$ was added. Then the tube

was vortexed to break the pellet and expose it to the washing solution. Afterwards the solution was spun with 7500 g at 4° for 5 min. This washing step was repeated once

Air-drying of pellet and redissolving of RNA pellet

The washing solution was removed completely and the tube was left with an open lid in a rack for air-drying of the pellet. When ethanol solution had evaporated completely (≤10 min), the RNA was redissolved in 20 µl NFW.

## 2.5.2    cDNA synthesis

The quality of the total RNA was checked on an agarose gel and the quantity of the total RNA was measured using a NanoDrop spectrophotometer.

The total RNA was reverse transcribed into cDNA using a reverse transcriptase (RT). These are retroviral enzymes, RNA-dependent DNA-polymerases, which use a single stranded RNA-template (retroviral genome) to synthesise the complementary DNA strand (cDNA). Reverse transcriptases are used in molecular biology to produce cDNA from RNA templates.

For reverse transcription of the total RNA from the samples the RT M-MLV (RNase H Minus, Point Mutant; Promega, Southampton, UK) was used. Like DNA polymerases, reverse transcriptases need a primer, an oligonucleotide which hybridises to the complementary sequence of a single stranded RNA/DNA molecule. This primer, when hybridised to its target, generates a double stranded starting point for the polymerase, with a 3'-end for the addition of the next complementary nucleotide. For reverse transcriptase reactions, one can choose from three types of primers:

1. Specific primers: Specific primers have a sequence which is complementary to a specific RNA template. In a RT reaction using specific primers only one type of RNA molecules will efficiently be reverse transcribed into cDNA, e.g. one specific mRNA.

2. oligo dT primers: These primers are used to reverse transcribe all mRNAs in a RNA preparation into cDNA. Oligo dT primers hybridise to the polyA tail of mRNA, providing a starting point for the RT at the 3'-end of the transcript. Because the reverse transcriptase only efficiently synthesises around 2 kb of the complementary sequence, only the 3'-ends of transcripts will be quantitatively represented in a cDNA preparation using oligo dT primers.

3. Random hexamers: Random hexamers are used to try to reverse transcribe all of the single stranded RNA molecules present in a RNA preparation into cDNA. As the name suggests, random hexamers are a mixture of hexamers of different, random sequence. By chance these random hexamers should target all RNA molecules and all regions of the RNA molecules in a RNA preparation. Thus, cDNA prepared using random hexamers should reflect the RNA used for the RT reaction.

The principle of the protocol for cDNA synthesis using M-MLV is shown Figure 2.3. A master mix for the RT reaction was prepared on ice in 1.5 ml tubes. In a PCR tube, the RNA template (total RNA) was mixed with primers for an annealing reaction. To prepare cDNA for qPCR (quantitative PCR) and RT-PCR oligo(dT)15 primers were used. After the annealing reaction the RT Master Mix was added to the Annealing Reaction Mix and the two solutions were mixed by pipetting up and down several times. The resulting RT Reaction Mix then was incubated at 40°C for the initial 10 min and then at 50°C for 50 min in a Tetrad Thermocycler.

**Annealing Reaction Mix**
• RNA template
• Primer
• Nfw

**RT Master Mix**
• Buffer
• M-MLV
• dNTPs
• RNase Inhibitor
• Nfw

Annealing of primers by heating to 70°C for 5 min followed by cooling on ice for 5 min

Prepared on ice

Mixing of both solutions
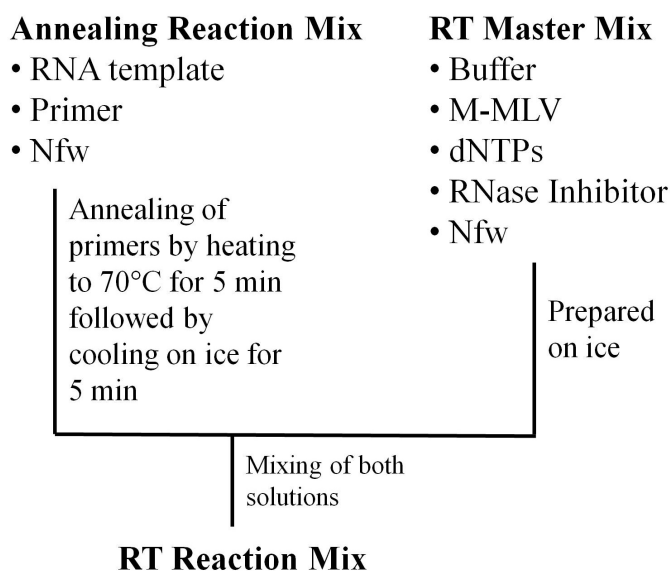
**RT Reaction Mix**

**Figure 2.3 – Preparation of RT Reaction Mix**

The Annealing Reaction Mix, in which the primers are annealed to the RNA template, was mixed with a RT Master Mix. That resulted in the RT Reaction Mix, in which the RNA template was reverse transcribed into cDNA.

| RT Reaction Mix | | |
|---|---|---|
| Component, Concentration | Volume in µl | Final Concentration |
| M-MLV RT 5x Reaction Buffer | 5 | 1x |
| dNTPs (10 mM each) | 1.25 | 400 nM |
| M-MLV (H⁻) point mutant (200 U/µl) | 0.5 | 4 U/µl |
| RNasin (40 U/µl) | 0.2 | 0.32 U/µl |
| Annealing Reaction Mix | 14 | |
| - 1 µg total RNA | <5 | 40 ng/µl |
| - 500 µg/ml OligodT$_{15}$ primer | 1 | 20 ng/µl |
| - NFW | fill up to 14 | |
| NFW | 4.05 | |
| Total volume | 25 | |

## 2.5.3　Agarose gel electrophoresis

DNA and RNA fragments can be separated by size by agarose gel electrophoresis. Because of the phosphodiester group in the backbone of nucleic acids, which has a very low pKa, nucleic acids are negatively charged at a wide range of pHs. When placed into the electric field between a cathode and an anode, the negatively charged nucleic acid molecule will be accelerated towards the positively charged anode. Because of the highly similar charge/mass ratio of nucleic acid fragments of different length, they would move with the same velocity, if there wouldn't be differential resistance acting on their movement. This differential resistance is generated by the matrix of an agarose gel, which lets fragments of a smaller size travel faster than fragments of a larger size. Parameters which influence the velocity with which the nucleic acid fragment will travel in the gel are: The percentage of the gel, the electric field applied (potential), the temperature, and besides the length of the nucleic acid fragment, also its geometry.

Agarose gel electrophoresis protocol

A suspension of agarose powder in TBE-Buffer, the running buffer for agarose gel electrophoresis, was prepared in a flask. The percentage of agarose was depending on the size of fragments to be separated on the gel. In most cases 1% gels were prepared. The suspension then was heated in a microwave till the solution was completely clear. The gel then was left on the bench to cool down (hand warm, ≤60°C), before 2 µl ethidiumbromide (500 µg/ml) per 50 ml gel were added. The ethidiumbromide was distributed homogenously by carefully shaking the flask. The gel then was pureed into a tray for solidification. Combs can be positioned over the tray that way, that their teeth generate little wells in the gel, after solidification.

The agarose gel then was placed in chamber between a cathode and an anode. The chamber was filled with TBE-Buffer till the gel just was covered with solution. Then the comb was removed. This generates little wells in the gel, which can be loaded with samples. After loading the samples, an electric field was applied by a power source. The voltage applied was depending on the length of the gel. The rule of thumb for the voltage is: 5-10 V per cm of distance between the electrodes. Usually samples are mixed with a (gel) loading buffer before loading. The loading buffer contains visible dyes, which running behaviour on the gel is comparable of DNA/RNA-fragments of a certain size. Usually a loading buffer contains one small, fast running and one large, slow running dye. Thus the dyes are demarcating the range where the DNA/RNA-fragments are running on the gel.

The ethidiumbromide is used to visualise the double stranded DNA/RNA molecules. It intercalates in between the stacks of base pairs in the double helix, which intensifies the fluorescence of ethidiumbromide about 20 fold. When placed in the dark on a certain UV tables, the UV light excites the fluorescence of the ethidiumbromide. Because the ethidiumbromide will be concentrated and stronger at accumulations of DNA fragments, DNA fragments of the same length will appear as fluorescent bands on the gel. The size of the fragments in those bands can be estimated by comparing their height on the gel to the bands of a marker (DNA/RNA ladder), which ran alongside the sample. Because the composition of the marker is known, the size of the fragment corresponding to each band of the marker is known. Comparing the height of a band to bands of the markers running at a similar height can give a good estimation of the size of a fragment.

# 2.6    Comparative gene expression analysis

## 2.6.1    Genotyping PCRs

The genotyping PCRs for the 2 dpf qPCR experiments were performed with a piece of tail, analogue to a colony-PCR. A small piece of tail was cut from the 2 dpf embryos using small hypodermic needles. The rest of the embryo was immediately homogenised in TRI-Reagent for total RNA preparation. The embryos were terminally anesthetised with MESAB just prior to the procedure to prevent RNA degradation in dead embryos. The small piece of tail was directly thrown into a genotyping PCR reaction mix.

The reaction mix contained three primers for the potential amplification of both alleles in the PCR, the wildtype and the mutant allele. The size of the PCR-products for the wildtype and the mutant allele were sufficiently different to be resolved on an agarose gel. The genotyping PCRs enabled us to prepare cDNAs from mutants and their wildtype siblings at a developmental stage, at which wildtypes and mutants are indistinguishable from each other.

| PCR reaction mix for the *taf8* genotyping PCRs | | |
|---|---|---|
| Component, Concentration | Volume in µl | Final concentration |
| 5x Taq Buffer (+ MgCl$_2$) | 4 | 1x |
| dNTPs (10 mM each) | 0.4 | 200 µM |
| gDNA Taf8 fw primer, 10 µM | 1.2 | 600 nM |
| gDNA Taf8 rev primer, 10 µM | 0.8 | 400 nM |
| Insert rev primer, 10 µM | 0.6 | 300 nM |
| Taq DNA Polymerase (5 U/µl) | 0.2 | 0.05 U/µl |
| Template, piece of tail | | |
| NFW | 12.8 | |
| Total volume | 20 | |

| PCR reaction mix for the *taf6* genotyping PCRs | | |
|---|---|---|
| Component, Concentration | Volume in µl | Final concentration |
| 5x Taq Buffer (+ MgCl$_2$) | 4 | 1x |
| dNTPs (10 mM each) | 0.4 | 200 µM |
| gDNA Taf8 fw primer, 10 µM | 1.2 | 600 nM |
| gDNA Taf8 rev primer, 10 µM | 0.6 | 300 nM |
| Insert rev primer, 10 µM | 0.6 | 300 nM |
| Taq DNA Polymerase (5 U/µl) | 0.2 | 0.05 U/µl |
| Template, piece of tail | | |
| NFW | 13 | |
| Total volume | 20 | |

| Thermocycler program for genotyping PCRs | | | |
|---|---|---|---|
| Step | Temperature in °C | Time | |
| Preheating | 95 | 5 min | |
| Template Melting | 95 | 30 s | |
| Annealing | 55 | 30 s | 36x |
| Extension | 72 | 30 s | |
| Final Extension | 72 | 10 min | |
| End | 4 | for ever | |

## 2.6.2   RT-PCR

RT-PCR is the combination of cDNA preparation in a RT-reaction and the subsequent amplification of a specific sequence from the cDNA. The sequence is amplified from the cDNA using a primer pair framing the sequence on the cDNA target in a conventional PCR. In this thesis RT-PCR was used to check total RNAs for substantial gDNA (genomic DNA) contamination. The reactions were performed analogous to the actual qPCR-reactions, with same primer concentrations, template concentration, annealing temperature and cycle number. The differences were that no SYBRGreen master mix was used and that the extension time was increased to allow amplification of gDNA.

| PCR reaction mix for RT-PCRs | | |
| --- | --- | --- |
| Component, Concentration | Volume in µl | Final concentration |
| 5x Taq Buffer (+ MgCl$_2$) | 4 | 1x |
| dNTPs (10 mM each) | 0.4 | 200 µM |
| Foward primer, 10 µM | 0.2 or 04 | 100 or 200 nM |
| Reverse primer, 10 µM | 0.2 or 0.4 | 100 or 200 nM |
| Taq DNA Polymerase (5 U/µl) | 0.2 | 0.05 U/µl |
| NFW | 15 or 14.6 | |
| Total volume | 20 | |

| Thermocycler program for RT-PCRs | | | |
| --- | --- | --- | --- |
| Step | Temperature in °C | Time | |
| Preheating | 95 | 3 min | |
| Template Melting | 95 | 30 s | 40x |
| Annealing | 60 | 30 s | |
| Extension | 72 | 2 min | |
| Final Extension | 72 | 10 min | |
| End | 4 | for ever | |

## 2.6.3    qPCR

The advantage of qPCR in comparison to conventional RT-PCR is that qPCR measures the amount of PCR-product during each cycle of the PCR-reaction. This ensures comparisons between samples during the quantitative, exponential phase of the PCR-reaction. Not the amount of DNA is measured by the thermocycler (Real Time machine) during each cycle, but a fluorescence signal which is proportional to the amount of DNA. There are several variants of qPCR. What was performed in this thesis is qPCR following the SYBR Green method. Like ethidiumbromide, SYBR Green is a fluorochrome which intercalates into double stranded DNA (nucleic acids). Therefore SYBR Green fluorescence can be used to measure the amount of PCR-product after each cycle. The disadvantage of the SYBR Green method is that there is no sequence specificity of the fluorescence signal. SYBR Green intercalates into any double stranded nucleic acid, regardless of the sequence.

### 2.6.3.1    Specificity controls for qPCR experiments

Because of this limitation of the SYBR Green method, the specificity of the qPCR-reaction needs to be thoroughly controlled. SYBR Green would intercalate into qPCR-products which are amplified from genomic DNA. In this work all primers were designed that way, that they target exons framing large introns ($\geq$1 kb). The amplification of the large PCR-product from gDNA is suppressed during the qPCR run. All primers used for the qPCRs in this thesis have a PCR-product larger than 1 kb from genomic DNA, except for Bactin1 II and Ef1a. The Ef1a primers cross exon-exon boundaries and do not anneal to genomic DNA.

Even if the amplification of gDNA is suppressed by primers framing large exons, differential contamination of samples with gDNA would have an impact on the quantification of transcript levels by qPCR, by differentially influencing the efficiency of the qPCR reaction. Therefore, additionally to the appropriate primer-design, also the DNA-contamination of the total RNA used for cDNA preparations needs to be minimised. All total RNAs used for this work, except for the 2 dpf experiments I and III, were subject to a DNA digest by DNase. The DNA digests was carried out using the Turbo DNA-Free Kit (Applied Biosystems, Warrington, UK) following the manufactures instructions.

The specificity of the qPCR reaction was controlled in three ways:

1. A dissociation curve was recorded after each qPCR run.

2. In some cases cDNA from –RT reactions were tested by conventional RT-PCR.

3. The correct product size of the qPCR-products was validated by agarose gel electrophoresis.

Dissociation curve (melting curve):

The melting curve is recorded after the amplification cycle during a qPCR run. The fluorescence is recorded by the Real Time Cycler while the temperature in the tubes increases from 55°C to 95°C. The that way recorded melting curve depicts RFUs (relative fluorescence units) over temperature. The RFUs decrease steadily over the increasing temperature because the amount of double stranded DNA with intercalated SYBR Green decreases. Around the melting point of the PCR-product the drop of fluorescence is dramatic (high negative slope). The melting point of the PCR-product is the turning point of that curve. The negative first deviation of the curve transforms this turning point into a peak. The results of melting curves are usually depicted as the

negative first deviation. A successful qPCR run shows only one peak, reflecting only one PCR-product.

In Figure 2.4 representative melting curves of the PCR-product for all primers used for qPCR in this thesis are shown. The melting curves contain only one peak, with five exceptions: Bactin1, Bactin1 II, Fabp11a, Pparγ and Taf6. The melting curves for Bactin1 and Pparγ contain small peaks indicative of a second PCR-product. It could be primer dimers, but the relatively high melting points of around 78.5°C (Bactin1) and 80°C (Pparγ) for the small peaks argue against it. The peaks are not recognised by the iQ5 software. Corresponding bands for these peaks are not observed, when PCR-product from PCRs using those primers is analysed by agarose gel electrophoresis (Figure 2.5). The size of those additional peaks is always very small, but proportional to the specific product. I therefore concluded that this not very substantial presence of a second PCR-product is unlikely to cause any asymmetrical miss-measurement of CT-values by qPCR. The broad single peak for Bactin1 II also contains a second peak, which is not always resolved by the melting curve. Also for the PCR-product derived from PCRs using Bactin1 II primers, no band corresponding to the second peak is observed on agarose gels (see Figure 2.5).

The melting curve for Fabp11a contains a clearly visible shoulder, which is indicative of a second PCR-product, besides the specific product. The Tm of around 78°C argues against primer dimers. When cDNA derived from a –RT reaction is analysed by qPCR, the peak corresponding to the shoulder and the specific product disappears from the melting curve, and a peak with a Tm indicative of primer dimers appears. This finding suggests that the second PCR-product is amplified from cDNA. All primers used for qPCR and RT-PCR were checked for specificity by running an *in silico* PCR against the zebrafish genome (Zv9), using the respective tool in the UCSC browser. The Fabp11a primer pair is the only primer pair for which the tool found two

PCR-products. The hits correspond to two different copies of the Fabp11a (*fabp11a*) gene in close vicinity on chromosome 19. The transcripts from the two different loci are nearly identical. The Fabp11a primer pair amplifies the same PCR-product from them. A second band is not visible when PCR-product from PCR-reactions using Fabp11a primers is analysed on an agarose gel and the size of the small shoulder is always proportional to the size of the specific product. The peak of the melting curve for Taf6 is suspiciously broad. The broad peak contains additional PCR-products, which are not resolved by the melting curve, but which are visible as additional bands on an agarose gel. However, these bands are very faint in comparison to the specific PCR-product (Figure 4.2).
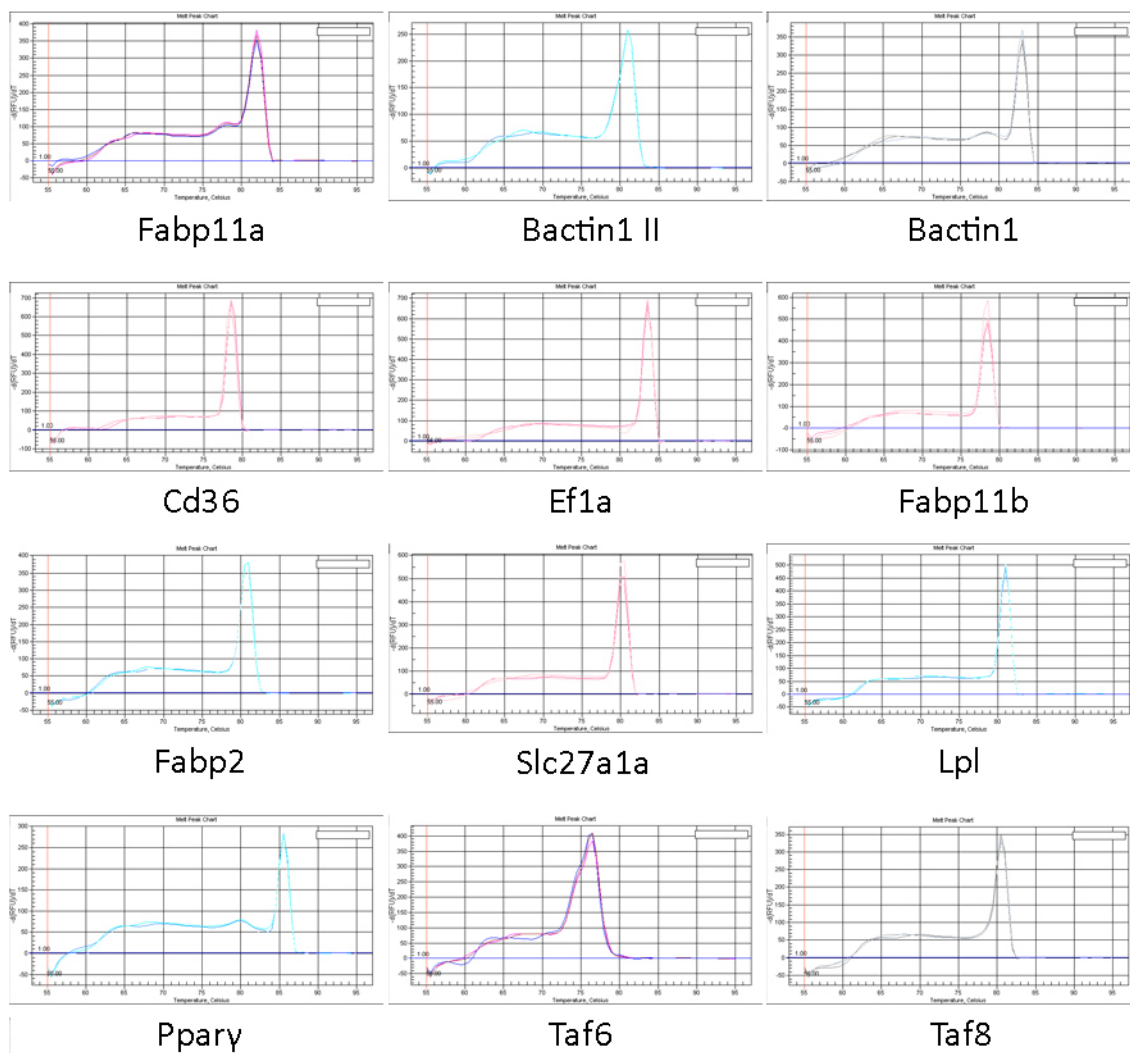
**Figure 2.4 – Representative melting curves**

Representative melting curves are depicted for each of the primer pairs used for qPCRs and/or RT-PCR in this thesis. The melting curves were recorded after qPCR runs in triplicates.

2. –RT-reaction

A –RT-reaction is performed like a RT-reaction for cDNA preparation, but the Reverse Transcriptase is replaced by NFW. Any template which is amplified from –RT cDNA is not derived from the reverse transcription of RNA and must therefore be DNA contamination. This fact can be utilised to assess the extent of DNA contamination in a total RNA preparation, when

96

cDNA from RT and –RT are compared by conventional PCR. Substantial DNA contamination would result in bands from the PCR-product of the PCR-reaction using the –RT cDNA. The size of the PCR-product is of the same size, or larger than the PCR-product using RT cDNA, depending on whether or not, the primers target the same, or different exons on the cDNA.

The DNA contamination of total RNA preparations prepared following the protocol described in (chapter 2.5) is usually not substantial. This has been tested by Heather Woodhouse in her masters project "Study of PPARγ-dependent transcription in Zebrafish embryos".

In Figure 2.5, RT and –RT cDNAs from the first 3 dpf experiment were compared by PCR amplifying Bactin1 II and Fabp11a. The Bactin1 II primers target sequences on the same exon of the *bactin1* cDNA. Therefore substantial gDNA contamination would result in amplification of a PCR-product of the same size like the one which is amplified from RT cDNA. No band (PCR-product) can be seen in the lanes with samples from the –RT-PCR in contrast to the RT-PCR where a band of the correct size (102 bp) can be seen. In this experiment also Fabp11a primers were used. They anneal to different exons. Consequently the expected product size from cDNA is 203 bp and from gDNA is 1781/1772 bp. No band indicative of a substantial contamination of the total RNA with gDNA can be seen. However, in the samples from the –RT there are bands running on the height of primer dimers, which are also seen in the non template control (NTC) for Fabp11a.
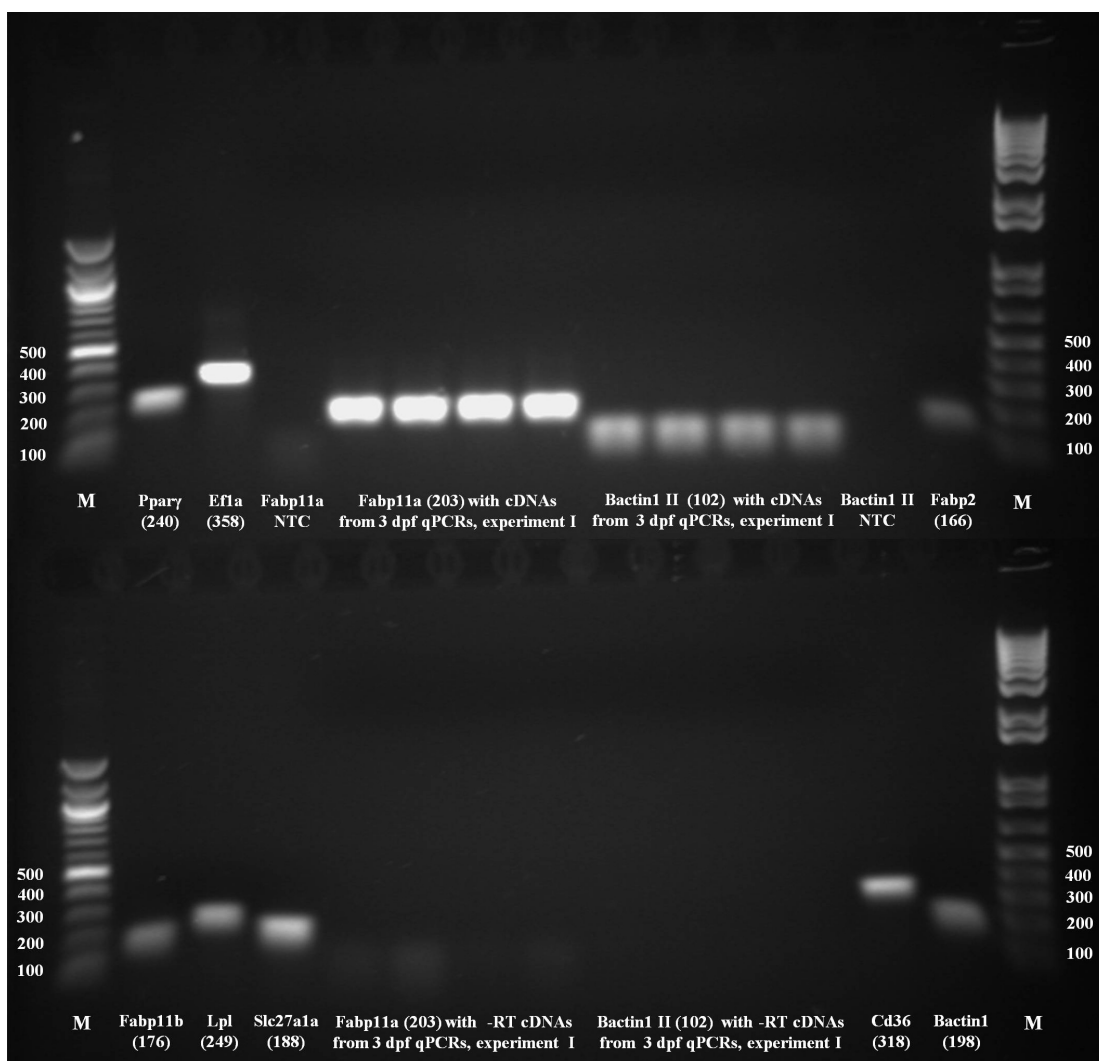
**Figure 2.5 – Specificity controls of qPCR reactions**

Analysed on this agarose gel were 10 µl of PCR-product from qPCR-reactions using following primer pairs: Pparγ, Ef1a, Fabp2, Fabp11b, Lpl, Slc27a1a, Cd36 and Bactin1. The expected product size is given in brackets. The lanes in the middle are loaded with 10 µl of PCR-product from RT-PCR reactions (lanes 5-12 upper part) using cDNA from the first 3 dpf qPCR experiment (*taf8*-mutants, *taf8*-wildtype siblings, *taf6*-mutants, *taf6*-wildtype siblings). Lanes 5-12 in the lower part of the gel were loaded with 10 µl PCR-product from corresponding -RT-PCR.

## 2.6.3.2    qPCR reaction

The primer concentration for each primer pair used for qPCR needs to be optimised to yield

optimal efficiency while maintaining specificity. In this thesis two concentrations for primer pairs

98

were used for qPCR 100 and 200 nM. The table below specifies which concentration was used for which primer pair.

| Name of primer pair | Final concentration of each primer in the qPCR reaction mix | Name of primer pair | Final concentration of each primer in the qPCR reaction mix |
|---|---|---|---|
| Taf8 | 200 nM | Taf6 | 100 nM |
| Slc27a1a | 200 nM | Pparγ | 100 nM |
| Lpl | 200 nM | Bactin1 | 100 nM |
| Fabp2 | 100 nM | Bactin1 II | 100 nM |
| Fabp11a | 100 nM | Cd36 | 100 nM |
| Fabp11b | 100 nM | Ef1a | 100 nM |

| qPCR Reaction | | |
|---|---|---|
| Component, Concentration | Volume in µl | Final concentration |
| Power SYBR Green Master Mix, 2x | 12.5 | 1x |
| Template (1:20 dilution of cDNA from RT) | 5 | 1:100 |
| Forward primer, 10 µM | 0.25 or 0.5 | 100 nM or 200 nM |
| Reverse primer, 10 µM | 0.25 or 0.5 | 100 nM or 200 nM |
| NFW | 7 or 6.5 | |
| Total volume | 25 | |

First a qPCR Master Mix was prepared, containing all components except the template. Then an (optical) 96-well plate was loaded with 5 µl Template. Finally 20 µl qPCR Master Mix were added to the template. After the plate was sealed with optical film (Applied Biosystems, Warrington, UK), the plates were spun down for one minute to collect the qPCR reaction mix at the bottom of the wells.

The 96-well plates were than placed into a iQ5 Multicolor Real-Time PCR Detection System (BIORAD, Hemel Hempstead, UK) for the qPCR run. The cycler program can be specified in the iQ5 software which

is controlling the Real Time machine. The cycler program is shown in Figure 2.6. The template used for the plates was instructing the machine to measure SYBR Green fluorescence in all 96 wells.
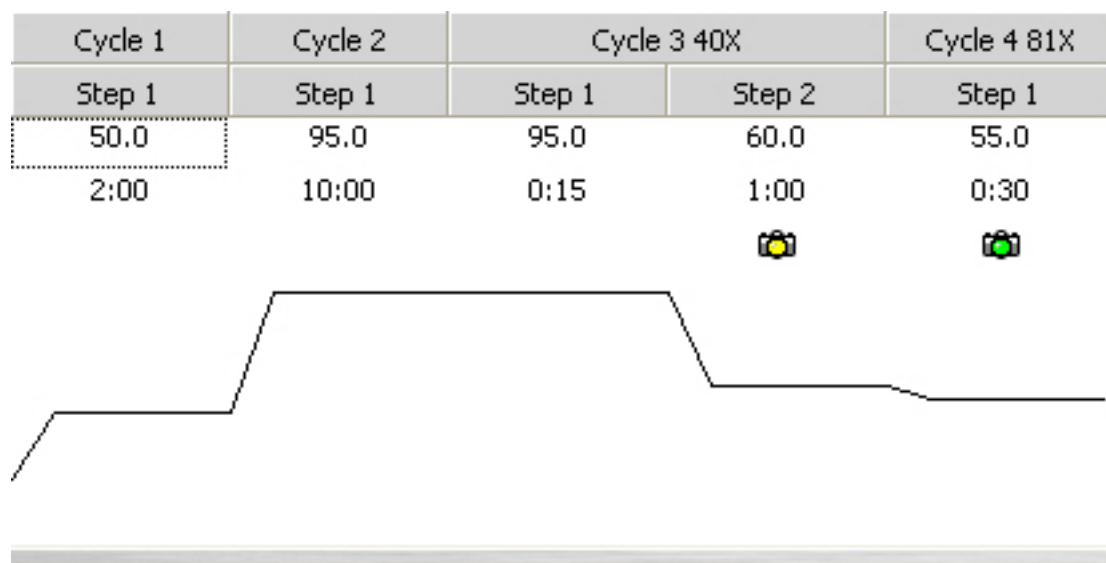


**Figure 2.6 – Cycler Program for Real Time PCRs**

Depicted is the cycler program used for all qPCRs. After an initial preheating step at 50°C for 2 min the polymerase is activated by heating up to 95 °C for 10 min. Next is the amplification cycle. It consists of cycles of template melting at 95°C for 15 s followed by a combined annealing elongation step at 60°C for 1 min. After the amplification cycle the dissociation curve is recorded. The respective cycle records the changes in fluorescence during the stepwise increase of the temperature from 55 to 95 °C in 0.5°C increments.

## 2.6.3.3    Analysis of qPCR experiments

Relative quantifications of transcript levels by qPCR assume that the PCR-product doubles with each cycle. The fluorescence signal, which is proportional to the PCR-product, doubles as well. If there was double as much template at the beginning of the reaction in one sample compared to a reference, then, at each cycle of the qPCR run, the fluorescence signal for the sample is double as high as the one for the reference. The reference would reach the same fluorescence signal one cycle later. This principle is the basis for calculating differences in transcript levels using CT-

values (cycle threshold). If a threshold of the fluorescence signal is set, the cycle when different samples reach that threshold can be used to infer differences in the amount of template in the samples. Double as much template in one sample results in a difference of one cycle ($\Delta CT = 1$) when the samples reach the threshold for the fluorescence. To correct for differences in the total amount of cDNA used for the qPCR reaction, the CT-values for the assayed gene is normalised to the CT of an internal standard. A good internal standard just reflects differences in the overall amount of template and is unaffected by the different conditions, which are compared by the qPCR (wildtype/mutant, treated/untreated). The internal standard used in this thesis was *bactin1*, which was described as a good internal standard for qPCR in zebrafish (McCurley and Callard, 2008).

The difference in the transcript level for one gene normalised to the internal standard can then be calculated using the $\Delta\Delta CT$-method using following equation:

$\Delta\Delta CT = \Delta CT_{sample} - \Delta CT_{reference} = (CT_{target} - CT_{internal\ standard})_{sample} - (CT_{target} - CT_{internal\ standard})_{reference}$

The fold change of the gene between sample and reference is then $2^{-\Delta\Delta CT}$.

This method contains the flaw that it assumes 100% efficiency of the reactions, meaning a doubling of the PCR-product with each cycle. If the efficiency of the qPCR reaction is not 100% it can cause miss-interpretation of qPCR results. This is especially the case if the efficiencies of the reactions for the assayed genes (target) and the internal standard differ greatly. To be able to correct for differences in the efficiency of the PCR reactions I determined the efficiency of the PCR reactions for each primer pair. The efficiency was inferred from the slope of a standard curve generated from qPCR with a dilution series of a mix of cDNAs used for qPCR in this thesis. The dilution series of cDNA diluted 1:10, 1:20, 1:40, and 1:80 should cover the range

where CTs where determined in qPCRs for this thesis. For all qPCR experiments 1:20 dilutions of cDNA were used as a template. The efficiencies of the qPCR reactions for each primer pair a shown in table below.

**Table 2.1 – Efficiencies of primer pairs used for qPCR**

| Gene | Efficiency |
|------|------------|
| Ef1a | 1.47 |
| Bactin1 II | 1.81 |
| Bactin1 | 1.69 |
| Fabp11a | 1.76 |
| Fabp11b | 1.77 |
| Fabp2 | 1.78 |
| Cd36 | 1.71 |
| Lpl | 1.76 |
| Taf8 | 1.81 |
| Taf6 | 1.93 |
| Slc27a1a | 1.83 |
| Pparγ | 1.70 |

Because the efficiencies between the target and the internal standard differed, fold changes were calculated using the Pfaffl-method (Pfaffl, 2001). The Pfaffl-method implements and therefore corrects for differences in the efficiencies of the PCR-reactions between the target and the internal standard. The formula used is the following:

Fold change = ((Efficiency target)$^{\Delta CT \text{ target}}$) / ((Efficiency internal standard)$^{\Delta CT \text{ internal standard}}$)

The optimal fluorescence threshold for the determination of CT-values was set relative to each gene. But for one gene the same threshold was used throughout all experiments. This ensures the comparability of different experiments performed on different plates. Two experiments were performed to test the comparability of experiments on different plates. An experiment using the Fabp11b primer pair and 8 samples from the 3 dpf experiments was repeated on another plate. The Pearson correlation coefficient for the CT-values derived from the repeats was 0.95. For a

similar experiment using 4 samples from the 2 dpf experiments and the Bactin1 primer pair, the Pearson correlation coefficient was 0.98. This good correlation between experiments on different plates justifies the comparison of data from different experiments on different plates.

For each sample qPCRs were performed in triplicates. The mean CT-value of this three technical repeats was used to calculate fold changes following the Pfaffl-method. If evaporation occurred in one well the corresponding data was discarded. Experiments with a standard deviation of the triplicate CT-values greater than 0.5, were discarded.

## 2.6.4    Microarray analysis

### 2.6.4.1    Preparation of total RNA for microarrays

Production of 4 dpf fish-larvae

Pairs of heterozygous *taf8*-mutants were crossed. Seven clutches of eggs were collected. The larvae were kept in large Petri dishes at 28.5°C. The medium used was Hank's without additions (antibiotics). The medium was changed at least once a day. At 2 dpf the embryos were dechorionated manually with fine forceps. At 3 dpf the larvae were separated into mutants and wildtypes (large Petri dishes).

Preparation of samples

Three different pools of 50 wildtype-larvae (*taf8*-mutant siblings) in small Petri dishes were generated mixing larvae from all of the seven large wildtypet Petri dishes. Three different pools of *taf8*-mutants were generated in a similar way. Now there were 3x50 wildtype and 3x50 *taf8*-mutant larvae in small Petri dishes. The larvae were transferred from the small Petri dishes into 2 ml reaction tubes (-> 6 samples). They were washed one time in Hanks. The samples were fixed

103

by snap-freezing them in liquid nitrogen (no MESAB used). They were kept at -80°C till they were further processed later the same day.

Homogenisation of samples

The samples were homogenised in 1 ml Trizol-Reagent (Invitrogen) using an IKA T 25 basic ULTRA-TURRAX mixer (setting 6, 24 000 rpm). The tubes with the samples were kept on dry ice till homogenisation. After homogenisation they stayed at RT. Always experimental pairs were homogenised one after the other (wildtype/mutant I, wildtype/mutant II, wildtype/mutant III). The homogenisation-procedure included the following steps:

1. Homogenisation of sample in 1 ml Trizol for 1 min.

2. Washing of mixer with 10 ml autoclaved $dH_2O$ in a 15 ml Falcon for 30 s.

3. Discarding $dH_2O$.

4. Washing mixer in 10 ml mixer wash solution (4 M guanidine thiocyanate) in a 15 ml tube for 1 min.

5. Washing of mixer with 10 ml 70% ethanol in a 15 ml tube for 30 s.

6. Discarding ethanol after each experimental pair (for example wildtype/mutant I).

7. Washing of mixer with 10 ml autoclaved $dH_2O$ in a 15 ml tube for 30 s.

Before usage the mixer was washed with steps 2-7. Also different mixer wash solutions were used after each sample.

Then total RNA was prepared as it is described in 2.5.1.

Analysis of quantity and quality of the RNA

The concentration of the total RNA in ng/µl and the 260/280 ratio were determined using a NanoDrop photometer, to assess the amount and the purity of the total RNA. The values are as follows:

| Measurement of concentration and purity of prepared total RNA | | |
|---|---|---|
| Sample | Concentration in ng/µl | 260/280 ratio |
| wildtype I | 1170.4 | 2.09 |
| wildtype II | 1024.3 | 2.09 |
| wildtype III | 1108.4 | 2.08 |
| *taf8*-mutant I | 871.0 | 2.09 |
| *taf8*-mutant II | 966.6 | 2.09 |
| *taf8*-mutant III | 757.9 | 2.08 |

## 2.6.4.2    Hybridisation of microarrays with labelled cRNA

This experiment was carried out by Lixin Yang.

Cy3/Cy5-labelled cRNA was synthesized using "Agilent Low RNA Input Linear Amplification Kit Plus (two color, Cat# 5188-5340)". The procedure was performed following the protocol for using a waterbath, not a thermocycler, in the respective manual (version 4.0).

Annealing of a T7 Promoter Primer and cDNA synthesis by RT

This step was performed exactly following Agilent's protocol. A 11.5 µl Annealing-Mix was pipetted together containing 2 µg of total RNA, 1.2 µl T7-Primer and the appropriate amount of either SpikeA or SpikeB-Mix. The Annealing-Mixes were heated to 65 °C for 10 min in a water bath. Afterwards they were cooled down for 5 min on ice. Now 8.5 µl cDNA Master Mix were added, resulting in a 20 µl cDNA Synthesis Mix. For the RT-reaction these cDNA Synthesis Mixes were incubated at 40 °C for 2h in a circulating water bath. Afterwards the M-MLV-RT was inactivated by heating the mixes to 65°C for 15 min in a water bath. Then the samples were cooled down for five minutes on ice.

Amplification by *in vitro* transcription incorporating Cyanin 3- or Cyanin 5-CTP

This step was not performed exactly following Agilent's protocol, because it was performed with 10µl cDNA instead of 20 µl. 30 µl of a cRNA Master Mix was added to 10 µl of the cDNA from the previous step resulting in 40 µl *in vitro* Transcription Reactions. The cRNA Master Mixes contained either Cyanin 3 or Cyanin 5-CTP. The *in vitro* Transcription Reactions were incubated for 2 h at 40°C in a water bath. The cDNA (and indirectly the underlying mRNA) is thereby amplified through *in vitro* Transcription into Cy3/Cy5-labelled cRNA.

Purification of the amplified cRNA

For the cRNA-purification Quiagen's RNeasy Mini Kit was used. The protocol used was the protocol for this Kit modified by Agilent. Again the procedure was performed with half the volume used in the Agilent-protocol. 10 µl of nuclease-free water were added to the 40 µl *in vitro* Transcription Reactions. For precipitation of the cRNA 175 µl RLT and then 125 µl ethanol were added. Then 350 µl of this mix were loaded on a RNeasy column. By centrifugation with 13 000 rpm for 30 s at 4 °C with a cooled centrifuge the precipitated cRNA was loaded onto the RNeasy mini column. It followed two washing steps with 250 µl RPE. The cRNA was eluted from the column pipetting 60 µl nuclease-free water directly on the membrane, followed by centrifugation with 13 000 rpm for 30 s at 4°C.

Quantification and QC of the synthesized cRNA

A ND-1000 spectrophotometer (NanoDrop Technologies, Rockland, DE) was used to determine the concentration of synthesized cRNA in ng/µl.

The samples then were hybridised to G2519F microarrays (see chapter 2.1.3) according to the manufacturer's instructions. The slides then were scanned with a GenePix4000B microarray scanner resulting in TIFF-files of the scans. The analysis of those TIFF-files (scans) with the GenePix software generated the raw data of the microarray experiments.

## 2.6.4.3 Analysis of microarrays

Analysis of the raw data

The analysis of the scanned microarray slides was carried out by Remo Sanges (Stazione Zoologica Anton Dohrn, Napoli) using the LIMMA library from the BioConductor collection of packages for the R statistical environment. The operations performed in the R statistical environment were:

1. Background subtraction.

2. Loess normalisation within arrays.

3. Quantile normalisation between arrays.

4. Differential expression significance analysis using linear models.

The analysis from Remo provided lists (Excel tables) for each microarray experiment containing information about differential expression of genes and the significance of the result.

| | A | B | C | D | E | F | G |
|---|---|---|---|---|---|---|---|
| 1 | Row | ID | Name | logFC | P.Value | adj.P.Val | GeneName |
| 2 | 291 | A_15_P107148 | NM_182891 | 3.028370208 | 9.53E-13 | 1.00E-09 | opn1mw2 |
| 3 | 28 | A_15_P107148 | NM_182891 | 2.911143012 | 9.58E-15 | 1.08E-10 | opn1mw2 |
| 4 | 311 | A_15_P103862 | TC347911 | 2.063089933 | 1.35E-10 | 3.76E-08 | TC347911 |
| 5 | 238 | A_15_P103862 | TC347911 | 2.053499571 | 2.99E-12 | 2.25E-09 | TC347911 |
| 6 | 139 | A_15_P100851 | NM_199481 | 1.793006795 | 6.63E-10 | 1.21E-07 | ccng1 |
| 7 | 363 | A_15_P100851 | NM_199481 | 1.727965276 | 6.13E-11 | 2.12E-08 | ccng1 |

**Figure 2.7 – Example for tables derived from microarray analysis**

Column **B** provides the Agilent ID for the probe on the array and column **C** links the identifier of a zebrafish transcript to the probe. The identifiers were a mix of Esembl, RefSeq, GeneBank, TIGR and UniGene identifiers. In column **D** the logarithmic fold change to the base 2 of the signal for the probe between mutants and wildtypes in is given. Columns **E** and **F** provide the p-values from the statistical analysis. **F** gives the adjusted p-value using the Benjamini and Hochberg method. In **G** a gene name is linked to the probe. Because each probe (feature) is present on two positions on the array, each probe appears twice on the lists.

Analysis of microarray data

The analysis of the microarray data was performed by the candidate using the tables derived from

Remo's analysis of the raw data. A cut-off for significantly different expressed genes was

defined. The cut-off applied was a logarithmic fold change of >1 (up-regulated) or <-1 (down-

regulated) with an adjusted p-value ≤0.05. Each probe is present twice on the arrays and only

genes for which both probes passed the cut-off were kept for further analysis. The above

mentioned criteria were used to generate lists of significantly up-regulated genes, called Taf8up

and Taf6up. The respective lists for significantly down-regulated genes were called Taf8down

and Taf6down.

For further analysis of the microarray data Ensembl gene IDs were generated for each entry in the

lists of significantly different expressed genes. BioMart and the DAVID ID conversion tool were

used for the ID conversions. A few probe IDs could not be converted into Ensembl IDs using

other identifiers but had a chromosomic position associated with it. Yavor Hadzhiev wrote a

script to retrieve Ensembl gene IDs for them, when this position overlapped with a transcript for an Ensembl gene. The same ID conversions into a unified identifier, Ensembl gene ID, were also applied to the list with the annotations for all probes on the array. That resulted in a list of all genes on the array with an Ensembl gene ID.

I used BioVenn, a web-based bioinformatics tool (Hulsen et al., 2008), for comparison of the gene lists in area-proportional Venn diagrams. The same application was also used to determine the overlap of genes between the different gene lists.

The DAVID Functional Annotation Tool provides enrichment analysis within data sets covering over 40 annotation categories. I used this tool for enrichment analysis within the gene sets from the microarray experiments. As background for the analysis the gene list of all Ensembl genes on the array was used. Genes with Ensembl IDs which are not annotated in the DAVID system are excluded from the analysis using DAVID tool. Thus some genes from the lists are lost during the conversion of Ensembl IDs into DAVID IDs. The percentages of lost genes during the ID conversions were: Taf8down 2.6%, Taf6down 4.7%, Taf8up 15.2%, Taf6up 22.2% and genes on array (background) 9.4%.

## 2.7 Statistical methods

Excel 2007 and SigmaStat 3.5 software were used for statistical analysis of the data.

The arithmetic means of data sets were calculated using the AVERAGE function in Excel.

The standard deviation of data sets was determined using the Excel STDEV function.

Standard errors of the mean (SEM) were calculated by following formula in Excel:

$$SEM = \frac{STDEV\,(data)}{\sqrt{n}}$$

Linear correlation between datasets was estimated using the Excel PEARSON function.

## T-Tests

In this thesis two-tailed t-tests were performed to test for statistically significant difference in the mean between two data sets. Because the test is sensible to normal distribution of the data, the data was always checked for normal distribution using the respective tool in the Sigma Stat software. Only data which passed the test for normal distribution was further analysed by two-tailed t-tests. The hypothesis that the means of two samples are significantly different was rejected, if the p-value returned from t-tests was higher than 0.05.

# 3 Differential requirement of Tafs during zebrafish development suggested by systematic knock down

## 3.1 Introduction and Overview

In the classical model of transcriptional regulation the core promoter plays a passive role. In this model a set of GTFs assembles into a single type of PIC. This is sufficient for the initiation of a low, basal level of transcription. For a robust, high level of transcription additional regulatory input from other sites like enhancers is required. According to this model, transcriptional regulation is mainly driven by sequence-specific activators and repressors binding away from the core promoter.

In the last decades it became clear that multiple layers of transcriptional regulation exist, for example on the level of chromatin (chromatin modifications and remodelling), on the level of the transcription elongation step and also on the level of transcription initiation at the core promoter. The diversity of core promoter structures and of the complexes forming on them suggests a participation of the core promoter in tissue-specific gene expression and development. Several lines of evidence support this hypothesis:

Transcription in early embryos seems to largely follow the classical model for transcription initiation and is mediated by canonical TFIID. There is some evidence suggesting that with the advent of lineage-restricted transcription, this strict requirement for full TFIID gradually diminishes. Partial TFIID complexes and roles for non-prototypical promoter recognition factors have been described. A decrease or complete depletion of TFIID subunits has been observed in several differentiation processes: i) during the all-*trans* retinoic acid induced differentiation of F9

embryonal carcinoma cells into primitive endodermal cell-types (Perletti et al., 2001), ii) the differentiation of 3T3-L1 preadipocytes into adipocytes (Guermah et al., 2003), iii) the differentiation of myoblasts into myotubes (Deato and Tjian, 2007) and iv) the differentiation of hepatoblasts into hepatocytes (D'Alessio et al., 2011). Moreover, it has been demonstrated that certain lineage-restricted and differentiated cell-types do not contain or require prototype full TFIID: Hepatocytes (D'Alessio et al., 2011, Tatarakis et al., 2008), mouse trophoblast cells (Voss et al., 2000), mouse $taf4^{-/-}$ cells (Mengus et al., 2005) and more. In that context it is worth mentioning that also yeast cells growing at high density show reduced levels of several Tafs and Tbp (S. S. Walker et al., 1997).

In the case of myogenesis a complete replacement of TFIID by a TBP2/TAF3 complex has been proposed. An alternative transcription machinery also seems to be acting in the context of meiosis in vertebrates. The two vertebrate TBP-paralogs TBP2 and TLF seem in that respect to play opposing roles in the two sexes, with TBP2 acting in oogenesis and TLF in spermatogenesis (Gazdag et al., 2009, Martianov et al., 2001).

These findings feed into a model where TFIID is required for transcription in the pluripotent state (early embryos) and in mitotically dividing cells, to integrate all possible regulatory input. In differentiated cells not all TFIID subunits are required anymore so that partial TFIID and alternative PRFs are observed in those cell-types. The specialisation of the cells is paralleled by a specialisation of the basal transcription machinery. The transcript levels of zebrafish *tafs* decrease during early development, which might reflect the decreasing deployment of full TFIID in certain lineages (Figure 1.6).

## 3.2    Aims

The natural environment of a metazoan cell is not a Petri dish. In metazoans the cells are embedded in an organism with extensive crosstalk between the cells in the different tissues and organs. Findings made *in vitro* are not always valid *in vivo,* in the context of a whole organism. Therefore the significance of a finding made *in vitro* always needs to be tested in an *in vivo* model.

As described in the introduction, TAFs are expected to have specific functions in the complexity of a metazoan organism. The role of TAFs during early vertebrate development to date not has been comprehensively studied. Zebrafish is an excellent *in vivo* model to study the function of genes during early development, due to the large number of mutants and to the powerful MO-mediated kd technology available in that model. Therefore, I chose zebrafish to study the role of Tafs during development. Besides the relative contribution of distinct TFIID-subunits to early zebrafish development, the study might reveal some interesting specific phenotypes for certain Tafs, similar to the implication of Taf3 in hematopoiesis (Hart et al., 2009). Furthermore it will be interesting to analyse the Taf-morphants in the light of what is already known about their function. This analysis will address questions like:

1. Does systematic knock down of TFIID complex subunits reveal general and specific roles of Tafs in embryo development?

2. Can Taf kd phenotypes reveal core and peripheral functions for TFIID Taf subunits?

3. Do kd phenotypes of TFIID-specific Taf subunits suggest diverged function from Tafs specific for SAGA?

# 3.3    Results

We generated and analysed MO-mediated LOF-phenotypes for the Pol II Tafs annotated in the zebrafish genome (assembly Zv9). The phenotypes were analysed at three developmental stages (1, 2 dpf embryos and 5 dpf larvae) to cover most of early zebrafish development.

In most cases not one very distinct morphant phenotype was observed, but rather a range of very similar phenotypes, varying in the degree of severity. The pictures in Table 3.3, Table 3.5 and Table 3.7 depict representatives of the observed morphant phenotypes. If several distinct groups of phenotypes were observed in one kd experiment, they were analysed separately. When more than 30% of the injected embryos or larvae showed a phenotype, the phenotype was considered as a significant Taf-morphant phenotype. Additionally, when the percentage of abnormal embryos in the larvae injected with the mismatch control MO for the targeting MO remained below the 30% threshold, the phenotype induced by the targeting MO was regarded as a specific phenotype.

# 3.4    1 dpf (Prim-6 stage) phenotypes

Only a small subset of Taf-morphants showed a specific phenotype at 1 dpf in our MO-screen: Taf2/5l/6/6l/9/10/11/12 and 13 (see

Table 3.2 and Table 3.3). This subset contained the orthologs of the SAGA-specific TAF5L and TAF6L. Phenotypes for the core TAFs were observed (Taf6/9/10/11/12 and 13), but this subset was incomplete, as phenotypes for Taf4/5/8 were lacking. Interestingly, there seemed to be a strong requirement for orthologs of the DNA-binding TAFs, TAF2 (Inr) and the TAF6/9 heterodimer (DPE element), for zebrafish development before 1 dpf.

114

The phenotypes observed at 1 dpf after MO-injection are shown in Table 3.3. At this stage; after gastrulation, neurulation and segmentation; the major body plan of the vertebrate embryo has been established. However, only a limited number of organs can be easily studied under the light microscope. Main phenotypes observed at 1 dpf were cell death, the patterns of cell death and a varying degree of underdevelopment, suggesting general cellular defects.

**Table 3.1 – Categories of phenotypes in 1 dpf Taf-morphants**

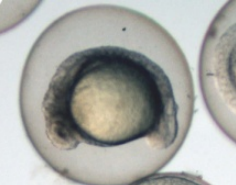| Morphants | Observed phenotype |
|-----------|-------------------|
| Taf2, Taf6 | Underdeveloped and cell death. Body plan not established. |
| Taf5l, Taf6l, Taf11 | Body plan established. Extensive cell death in many parts. |
| Taf9, Taf12, Taf13 | Body plan established. Cell death restricted to anterior part. |
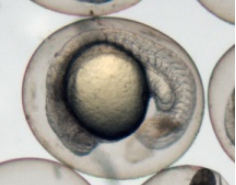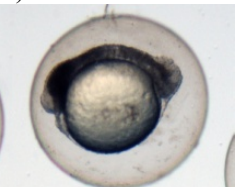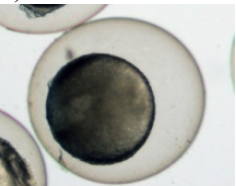
**Table 3.2 – Analysis of Taf-morphant phenotypes at 1 dpf**

N/A = not analysed.
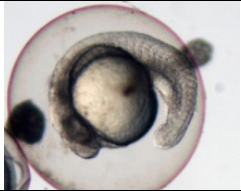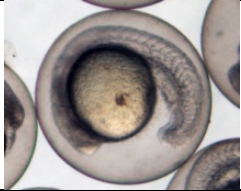
| Gene | MO | Experiments | Embryos | Morphants | % Morphants |
|------|-----|-------------|---------|-----------|-------------|
| *taf1* | *taf1*ATG | 1 | 108 | 13 | 12 |
| | *taf1*ATGmm | 2 | 244 | 0 | 0 |
| | *taf1*UTR | 1 | 96 | 1 | 1 |
| *btaf1* | *btaf1*ATG | 3 | 353 | 0 | 0 |
| | *btaf1*mm | 3 | 227 | 0 | 0 |
| *taf2* | *taf2*ATG | 2 | 122 | 115 | 94 |
| | *taf2*ATGmm | 2 | 211 | 0 | 0 |
| | *taf2*UTR | 2 | 173 | 13 | 8 |
| *taf3* | *taf3*ATG | 2 | 157 | 10 | 6 |
| | *taf3*ATGmm | 1 | 122 | 0 | 0 |
| | *taf3*UTR | 2 | 190 | 9 | 5 |
| *taf4l* | *taf4l*ATG | 2 | 147 | 0 | 0 |
| | *taf4l*mm | 2 | 123 | 0 | 0 |
| *taf5* | *taf5*ATG | 1 | 122 | 29 | 24 |
| | *taf5*ATGmm | 2 | 157 | 0 | 0 |
| *taf5l* | *taf5l*ATG | 1 | 100 | 5 | 5 |
| | *taf5l*UTRmm | 2 | 187 | 0 | 0 |
| | *taf5l*UTR | 1 | 62 | 54 | 87 |

| Gene | MO | Experiments | Embryos | Morphants | % Morphants |
|------|-----|-------------|---------|-----------|-------------|
| *taf6* | *taf6*ATG | 4 | 306 | 289 | 94 |
| | *taf6*ATGmm | 2 | 177 | 0 | 0 |
| | *taf6*UTR | 1 | 91 | 14 | 15 |
| *taf6l* | *taf6l*ATG | 2 | 211 | 189 | 90 |
| | *taf6l*ATGmm | 3 | 342 | 0 | 0 |
| *taf7* | *taf7*ATG | 2 | 146 | 0 | 0 |
| | *taf7*ATGmm | NA | NA | NA | NA |
| | *taf7*UTR | 2 | 148 | 0 | 0 |
| *taf8* | *taf8*ATG | 1 | 125 | 0 | 0 |
| | *taf8*ATGmm | NA | NA | NA | NA |
| *taf9* | *taf9*ATG | 1 | 105 | 80 | 76 |
| | *taf9*ATGmm | 2 | 210 | 0 | 0 |
| | *taf9*UTR | 1 | 70 | 20 | 29 |
| *taf10* | *taf10*ATG | 1 | 81 | 25 | 31 |
| | *taf10*ATGmm | 4 | 369 | 41 | 11 |
| | *taf10*UTR | 1 | 82 | 0 | 0 |
| *taf11* | *taf11*ATG | 4 | 383 | 355 | 93 |
| | *taf11*ATGmm | 2 | 178 | 8 | 4 |
| | *taf11*UTR | 2 | 157 | 60 | 38 |
| *taf12* | *taf12*ATG | 2 | 201 | 102 | 51 |
| | *taf12*ATGmm | 2 | 228 | 0 | 0 |
| | *taf12*UTR | 2 | 217 | 18 | 8 |
| *taf13* | *taf13*ATG | 3 | 272 | 224 | 82 |
| | *taf13*ATGmm | 2 | 265 | 0 | 0 |
| | *taf13*UTR | 2 | 219 | 22 | 10 |
| *taf15* | *taf15*ATG | 3 | 217 | 25 | 12 |
| | *taf15*ATGmm | 2 | 212 | 0 | 0 |
| | *taf15*UTR | 1 | 160 | 0 | 0 |

**Table 3.3 – Taf-morphant phenotypes at 1 dpf**

| MO | Representative experiment[1] | |
|---|---|---|
| | **Picture** | **Phenotypes (Categories A,B ...)** |
| non-injected wildtype |  | reference embryo |
| taf2ATG |  | 92% (70/76)<br>- severely underdeveloped<br>- dark and grainy appearance of body |
| taf5lUTR |  | 87% (54/62)<br>- dark and grainy appearance of body |
| taf6ATG | A)<br><br>B)<br> | A) 62% (36/58)<br>- severely underdeveloped<br>- dark and grainy appearance of body<br>B) 36% (21/58)<br>- Embryonic arrest during gastrulation |
| taf6lATG | A)<br> | A) 67% (63/94)<br>- lots of dark tissue (necrosis) especially in the head<br>- Certain pattern of dark tissue (ring around eye)<br>- Somites misshapen and reduced, slower twitching |

[1] Pictures of dechorionated embryos have been taken at a different magnification.

| | | |
|---|---|---|
| | B)<br> | B) 16% (15/94)<br>- like A but milder with nearly normal twitching<br>- whole body gives a darker grainy appearance<br>- Somites U-shaped |
| *taf9*ATG |  | 72% (76/105)<br>- dark and grainy appearance of body |
| *taf11*ATG |  | 91%<br>- bodies appear dark and grainy<br>- the dark tissue has a more ubiquitous pattern than in the Taf6l-morphant<br>- somites U-shaped |
| *taf12*ATG |  | 96% (71/74)<br>- dark and grainy appearance of body |
| *taf13*ATG |  | 72% (72/100)<br>- dark and grainy appearance of body<br>(picture flipped horizontally) |

## 3.5    2 dpf phenotypes

Most Taf-morphant phenotypes were observed at the 2 dpf stage, which suggests contributions of maternal Tafs to development. Eleven of the 17 Tafs targeted in the MO-screen showed a specific phenotype at this stage: Taf1/2/5l/6/6l/8/9/10/11/12 and 15 (see Table 3.4 and Table 3.5). All the Tafs which displayed a significant phenotype at 1 dpf (Taf2/5L/6/6L/9/11/12 and 13), also displayed a significant phenotype at 2 dpf. The knock down of Taf5 and Taf13 induced a significant phenotype at 2 dpf, but their control MOs induced a significant phenotype as well.

However, in the case of Taf5, the proportion of abnormal embryos was much higher in the targeting MO injected embryos than in the control injected ones.

**Table 3.4 – Analysis of Taf-morphant phenotypes at 2 dpf**

% Morphants: Percentage of phenotype showing embryos
% Survival: Percentage of embryos surviving from 1 to 2 dpf. The number in brackets is the number of experiments from which the survival rate was calculated.
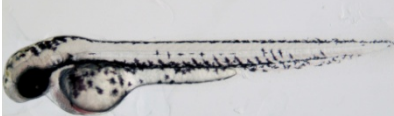N/A = not analysed.
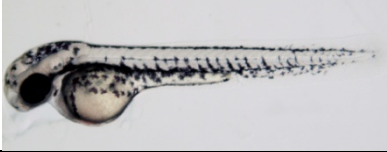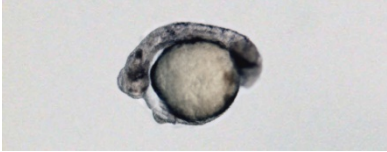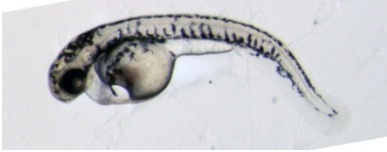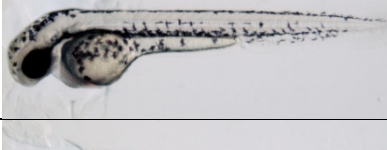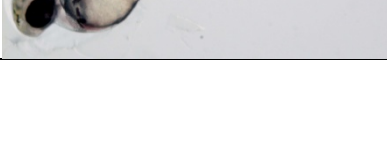
| Gene | MO | Experiments | Embryos | Morphants | % Morphants | % Survival |
|------|-----|-------------|---------|-----------|-------------|------------|
| *taf1* | *taf1*ATG | 3 | 245 | 57 | 23 | 82 (2) |
| | *taf1*ATGmm | 2 | 242 | 10 | 4 | 98 (1) |
| | *taf1*UTR | 3 | 210 | 109 | 52 | 82 (2) |
| *btaf1* | *btaf1*ATG | 3 | 373 | 72 | 19 | 97 (3) |
| | *btaf1*mm | 3 | 195 | 53 | 27 | 85 (3) |
| *taf2* | *taf2*ATG | 3 | 163 | 159 | 98 | 98 (2) |
| | *taf2*ATGmm | 2 | 194 | 54 | 28 | 87 (1) |
| | *taf2*UTR | 3 | 217 | 17 | 8 | 82 (2) |
| *taf3* | *taf3*ATG | 3 | 270 | 14 | 5 | 90 (2) |
| | *taf3*ATGmm | 1 | 122 | 7 | 6 | NA |
| | *taf3*UTR | 3 | 301 | 34 | 11 | 91 (2) |
| *taf4l* | *taf4l*ATG | 2 | 127 | 17 | 13 | 88 (2) |
| | *taf4l*mm | 2 | 94 | 14 | 15 | 78 (2) |
| *taf5* | *taf5*ATG | 3 | 261 | 243 | 93 | 90 (3) |
| | *taf5*ATGmm | 2 | 131 | 44 | 34 | 85 (2) |
| *taf5l* | *taf5l*ATG | 2 | 157 | 24 | 15 | 77 (1) |
| | *taf5l*UTRmm | 2 | 185 | 14 | 8 | 97 (1) |
| | *taf5l*UTR | 2 | 174 | 165 | 95 | 100 (1) |
| *taf6* | *taf6*ATG | 1 | 106 | 86 | 81 | 100 (1) |
| | *taf6*ATGmm | 2 | 148 | 13 | 9 | 78 (2) |
| | *taf6*UTR | 2 | 121 | 4 | 3 | 86 (2) |
| *taf6l* | *taf6l*ATG | 3 | 233 | 192 | 82 | 80 (3) |
| | *taf6l*ATGmm | 3 | 316 | 44 | 14 | 79 (3) |
| *taf7* | *taf7*ATG | 2 | 117 | 12 | 10 | 77 (2) |
| | *taf7*ATGmm | N/A | N/A | N/A | N/A | N/A |
| | *taf7*UTR | 2 | 135 | 17 | 13 | 91 (2) |
| *taf8* | *taf8*ATG | 1 | 125 | 58 | 46 | NA |
| | *taf8*ATGmm | N/A | N/A | N/A | N/A | N/A |

| Gene | MO | Experiments | Embryos | Morphants | % Morphants | % Survival |
|---|---|---|---|---|---|---|
| *taf9* | *taf9*ATG | 2 | 139 | 124 | 89 | 73 (2) |
| | *taf9*ATGmm | 2 | 180 | 48 | 27 | 80 (2) |
| | *taf9*UTR | 2 | 153 | 35 | 23 | 81 (2) |
| *taf10* | *taf10*ATG | 4 | 268 | 106 | 40 | 88 (4) |
| | *taf10*ATGmm | 4 | 313 | 56 | 18 | 82 (4) |
| | *taf10*UTR | 2 | 146 | 13 | 9 | 88 (2) |
| *taf11* | *taf11*ATG | 5 | 447 | 405 | 91 | 88 (5) |
| | *taf11*ATGmm | 3 | 254 | 59 | 23 | 87 (3) |
| | *taf11*UTR | 3 | 239 | 76 | 32 | 89 (3) |
| *taf12* | *taf12*ATG | 4 | 350 | 260 | 74 | 89 (4) |
| | *taf12*ATGmm | 2 | 178 | 10 | 6 | 80 (2) |
| | *taf12*UTR | 3 | 262 | 28 | 11 | 87 (3) |
| *taf13* | *taf13*ATG | 5 | 594 | 182 | 31 | 96 (5) |
| | *taf13*ATGmm | 2 | 257 | 155 | 60 | 93 (2) |
| | *taf13*UTR | 4 | 322 | 49 | 15 | 94 (4) |
| *taf15* | *taf15*ATG | 5 | 348 | 92 | 26 | 70 (4) |
| | *taf15*ATGmm | 2 | 198 | 36 | 18 | 89 (1) |
| | *taf15*UTR | 2 | 228 | 92 | 40 | 87 (2) |
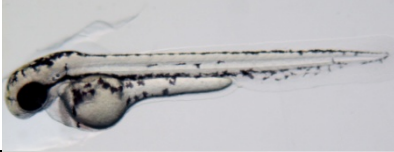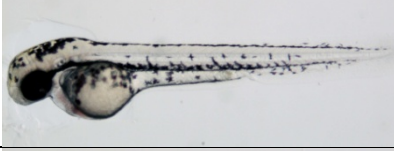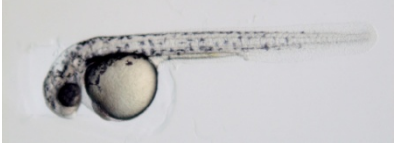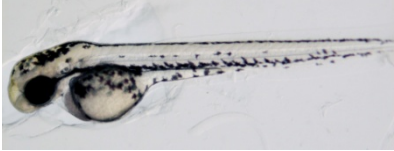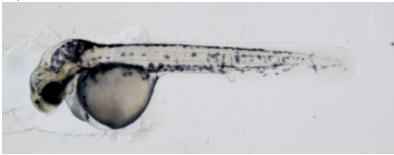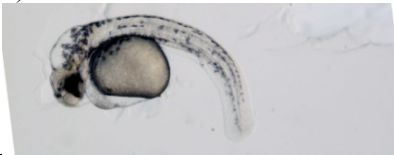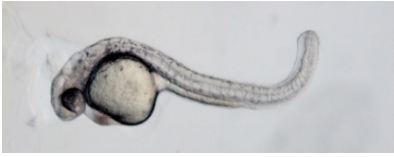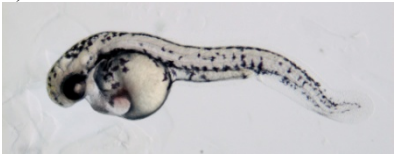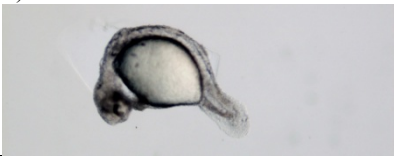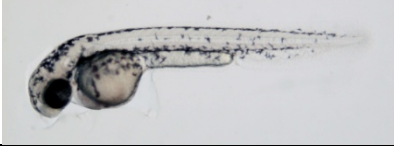
**Table 3.5 – Taf-morphant phenotypes at 2 dpf**
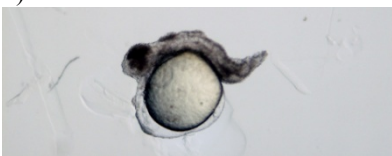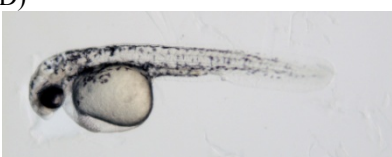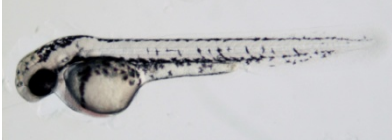
The percentages in the table are the percentages of embryos showing the described phenotype in that particular experiment. If several categories of phenotypes were observed in one experiment, the percentages and descriptions of phenotypes for the different categories are given. Only the phenotype categories with percentages >10% are listed. N/A = not available.
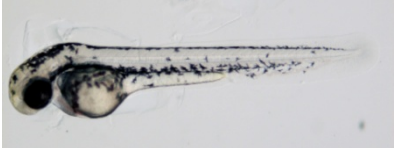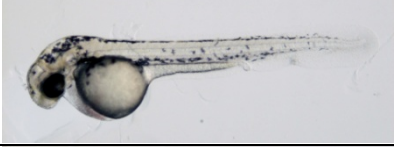
| MO | Representative experiment | | Repeat of experiment | |
| --- | --- | --- | --- | --- |
| | Picture | Phenotype (Categories: A,B…) | Picture | Phenotype (Categories: A,B…) |
| non-injected |  | Reference embryo | | |
| *taf1*ATG |  | No significant phenotype observed | | |
| *taf1*ATGmm |  | No significant phenotype observed | | |
| *taf1*UTR |  | 55% (50/91)<br>- blood accumulation in front of pericardium (maybe more blood)<br>- yolk sac edema<br>- most likely also heart defect<br>- circulation is visible |  | 52% (29/56)<br>- heart defect<br>- circulation range normal -> absent<br>- blood clot in front of the heart or in the ductus cuvieri<br>- otherwise normal |
| *btaf1*ATG |  | No significant phenotype observed | | |

| | | |
|---|---|---|
| *btaf1*mm |  | No significant phenotype observed |
| *taf2*ATG | A)<br><br>B)<br> | A) 90% (28/31)<br>- pleiotropic and degenerating<br>B) 89% (78/88)<br>- circulation absent<br>- axis problem<br>- blood accumulation in a clot in front of the pericardium -> no blood reaches the heart<br>- yolk sac edema (region of blood clot)<br>- head, eyes and yolk extension normal |
| *taf2*ATGmm |  | No significant phenotype observed |
| *taf2*UTR |  | No significant phenotype observed |
| *taf3*ATG |  | No significant phenotype observed |
| *taf3*ATGmm |  | No significant phenotype observed |

| | | |
|---|---|---|
| *taf3*UTR |  | No significant phenotype observed |
| *taf4l*ATG |  | No significant phenotype observed |
| *taf4l*mm |  | No significant phenotype observed |
| *taf5*ATG |  | 85% (63/74)<br>General phenotype<br>- smaller head/eyes<br>- less pigmentation (brownish)<br>- thinner body and yolk extension |  | 93% (75/81)<br>- circulation problem<br>- haemorrhage in head<br>- thin yolk extension<br>- funny shaped yolk |
| *taf5*ATGmm | N/A | 34% of injected embryos exhibit an abnormal phenotype |
| *taf5l*ATG |  | No significant phenotype observed |
| *taf5l*UTRmm |  | No significant phenotype observed |

| | | |
|---|---|---|
| *taf5*UTR | A)  B)  | 67% (70/105)<br>- smaller head/eyes but pigmented<br>- thin trunk with very thin or no yolk extension<br>- big roundish yolk sac<br>- Circulatory problem ranging from normal over reduced to no blood flow (less red blood cells?)<br>- pronounced hydrocephalus<br>B) 30% (31/105)<br>- like A but with curved body axis<br>- shorter body and no or hardly visible blood flow |
| *taf6*ATG | A)  B)  C)  | A) 42% (45/106)<br>- 30% (32/106) S-shaped<br>- 24% (25/106) yolk sac edema<br>- 37% (39/106) less pigmentation and axis problem<br>- heart tubular and reduced or absent circulation<br>B) 19% (20/106)<br>- yolk sac edema and accumulation of blood in front of heart<br>- heart defect (underdeveloped) and axis defect (mix)<br>C) 14% (15/106)<br>- pleiotropic |
| *taf6*ATGmm |  | No significant phenotype observed |
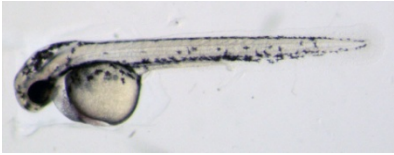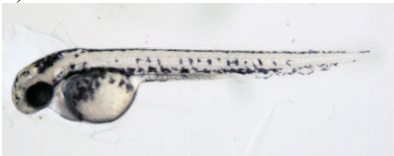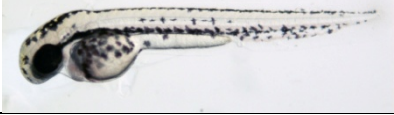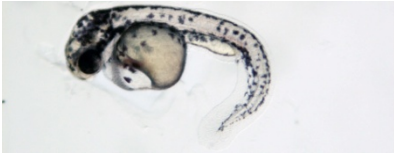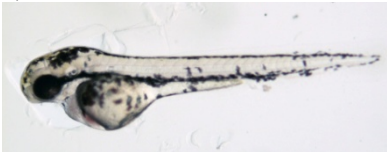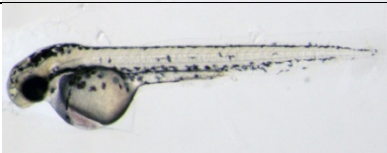
124

| | | |
|---|---|---|
| *taf6*UTR |  | No significant phenotype observed |
| *taf6l*ATG | A)<br><br>B)<br><br>C)<br><br>D)<br> | A) 76% (71/94)<br>- heart is underdeveloped<br>- circulation is absent<br>- eye phenotype (ventral gap and reduced pigment in RPE, retinal pigment epithelium)<br>- yolk sac edema<br>- axis problem<br>- somites sausage-shaped<br>B) 37% (30/82)<br>- dead and necrotic<br>C) 23% (19/82)<br>- necrotic, pleiotropic, no pigment, no circulation<br>- yolk sac edema<br>D) 17% (14/82)<br>- hydrocephalus and yolk sac edema |
| *taf6l*ATGmm |  | No significant phenotype observed |

| | | |
|---|---|---|
| *taf7*ATG |  | No significant phenotype observed |
| *taf7*UTR |  | No significant phenotype observed |
| *taf8*ATG |  | 46% (58/125)<br>- slightly retarded<br>- embryo on picture was PTU-treated (0.003% PTU in E3-medium) |
| *taf9*ATG |  | A) 69% (60/87)<br>- slightly underdeveloped (smaller eyes) and slightly weaker pigment<br>- circulation is reduced<br>B) 26% (23/87)<br>- like A but with a blood clot in the tail |
| *taf9*ATGmm |  | No significant phenotype observed |
| *taf9*UTR |  | No significant phenotype observed |
| *taf10*ATG |  | 30%<br>- barrel-shaped yolk sac |

| | | |
|---|---|---|
| *taf10*ATGmm | | No significant phenotype observed |
| *taf10*UTR | | No significant phenotype observed |
| *taf11*ATG | A)<br><br>B)<br><br>C)<br><br>D)<br>N/A | A) 68% (40/59)<br>- axis problem but notochord is present  (mix but mostly curled upwards)<br>- smaller head/eyes<br>- big yolk sac with edema and no or small extension<br>- heart beat present but no circulation in trunk and tail<br>- eye (RPE) phenotype<br>B) 57% (111/195)<br>- axis problem and hydrocephalus<br>- varying degree of yolk sac edema<br>- big round yolk sac and very thin extension<br>- circulation range normal -> absent<br>- no pigment in RPE sometimes concentrated on ventral half<br>C) 37% (72/195)<br>- like B but:<br>- straight axis<br>- eyes and head slightly bigger<br>- circulation reduced or absent<br>D) 25% (15/59)<br>- 15% (9/59) hydrocephalus<br>- reduced or no circulation<br>- yolk sac edema and axis problem (slightly curved down) |
| *taf11*ATGmm | | No significant phenotype observed |
| *taf11*UTR | N/A | 32% of injected embryos exhibit an abnormal phenotype |

| | | |
|---|---|---|
| *taf12*ATG | A)<br><br>B)<br> | A) 56% (54/97)<br>- slightly less pigmented<br>- mild general phenotype with smaller head and eyes and a thin yolk extension<br>- big roundish yolk sac and reduced or absent circulation<br>- 6% (6/97) hemorrhage<br>- 13% (13/97) hydrocephalus<br>- quite a variation in the phenotype but all have circulation defect<br>B) 52% (33/63)<br>- weak general phenotype<br> - slightly smaller head/eyes<br>- pigmented<br>- thin bodies and yolk extensions |
| *taf12*ATGmm |  | No significant phenotype observed |
| *taf12*UTR |  | No significant phenotype observed |
| *taf13*ATG | A)<br><br>B)<br> | A) 33% (22/67)<br>- yolk and extension are nearly normal<br>- shorter, blood clot in tail and big yolk sac<br>- 12% (8/67) no circulation or reduced circuitry<br>- 16% (11/67) enlarged 4th ventricle<br>B) 15% (10/67)<br>- yolk sac edema and axis problem (bend downwards)<br>- no or reduced circulation<br>- yolk and extension are nearly normal |

| | | |
|---|---|---|
| | C)<br> | C) 12% (8/67)<br>- funny shaped yolk sac<br>- blood accumulation in front of heart |
| *taf13*ATGmm |  | 60% of injected embryos exhibit an abnormal phenotype |
| *taf13*UTR |  | No significant phenotype observed |
| *taf15*ATG |  | No significant phenotype observed |
| *taf15*ATGmm |  | No significant phenotype observed |
| *taf15*UTR | N/A | 40% of injected embryos exhibit an abnormal phenotype |

## 3.6 5 dpf phenotypes

At 5 dpf most of embryos which displayed a strong phenotype already at 1 dpf, morphants for Taf2/5l/6/6l/11, were dead. Some of the morphants which showed a weak significant phenotype at 2 dpf appeared to recover by 5 dpf. This was observed for the morphant phenotypes induced by MOs targeting Taf8/10/13 and for Taf15. Also the significant morphant phenotype induced by injection of the control morpholino for Taf5 recovered by 5 dpf. Taf1/5/912 and the control MO for Taf13, which already displayed a significant phenotype at 2 dpf, also displayed a phenotype at 5 dpf.

**Table 3.6 – Analysis of Taf-morphant phenotypes at 5 dpf**
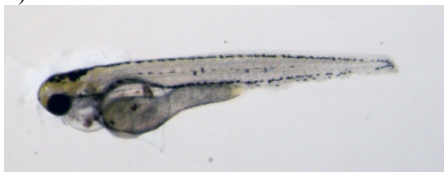
In this table dead embryos were included into the calculation of the percentage of phenotype showing embryos, because death between 2 dpf and 5 dpf is very likely due to the phenotype induced by the MO. N/A = not analysed.
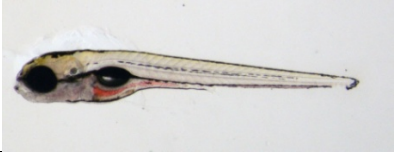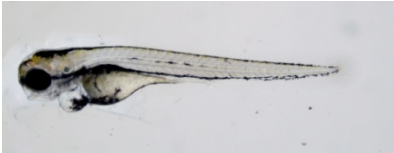
| Gene | MO | Experiments | Embryos | Morphants | Dead | % Phenotype (% Morphants, % Dead) |
|---|---|---|---|---|---|---|
| *taf1* | *taf1*ATG | 3 | 245 | 110 | 3 | 46 (45, 1) |
| | *taf1*ATGmm | 2 | 242 | 11 | 0 | 5 (5, 0) |
| | *taf1*UTR | 3 | 210 | 117 | 10 | 60 (56, 4) |
| *btaf1* | *btaf1*ATG | 3 | 373 | 0 | 0 | 0 (0, 0) |
| | *btaf1*mm | 3 | 195 | 16 | 8 | 12 (8, 4) |
| *taf2* | *taf2*ATG | 2 | 119 | 0 | 119 | 100 (0, 100) |
| | *taf2*ATGmm | 2 | 194 | 27 | 18 | 23 (14, 9) |
| | *taf2*UTR | 1 | 73 | 0 | 0 | 0 (0, 0) |
| *taf3* | *taf3*ATG | 1 | 133 | 0 | 0 | 0 (0, 0) |
| | *taf3*ATGmm | 1 | 122 | 0 | 0 | 0 (0, 0) |
| | *taf3*UTR | 1 | 125 | 0 | 0 | 0 (0, 0) |
| *taf4l* | *taf4l*ATG | 2 | 127 | 0 | 0 | 0 (0, 0) |
| | *taf4l*mm | 2 | 94 | 0 | 0 | 0 (0, 0) |
| *taf5* | *taf5*ATG | 3 | 261 | 210 | 32 | 93 (81, 12) |
| | *taf5*ATGmm | 2 | 131 | 18 | 10 | 21 (14, 7) |

| Gene | MO | Experiments | Embryos | Morphants | Dead | % Phenotype (% Morphants, % Dead) |
|---|---|---|---|---|---|---|
| *taf5l* | *taf5l*ATG | 1 | 80 | 0 | 0 | 0 (0, 0) |
| | *taf5l*UTRmm | 2 | 185 | 0 | 0 | 0 (0, 0) |
| | *taf5l*UTR | 2 | 174 | 39 | 125 | 94 (22, 72) |
| *taf6* | *taf6*ATG | 1 | 106 | 0 | 106 | 100 (0, 100) |
| | *taf6*ATGmm | 2 | 148 | 0 | 0 | 0 (0, 0) |
| | *taf6*UTR | 1 | 54 | 0 | 0 | 0 (0, 0) |
| *taf6l* | *taf6l*ATG | 3 | 233 | 40 | 179 | 94 (17, 77) |
| | *taf6l*ATGmm | 3 | 316 | 22 | 2 | 8 (7, 1) |
| *taf7* | *taf7*ATG | 1 | 81 | 0 | 0 | 0 (0, 0) |
| | *taf7*ATGmm | N/A | N/A | N/A | N/A | N/A |
| | *taf7*UTR | 2 | 135 | 0 | 0 | 0 (0, 0) |
| *taf8* | *taf8*ATG | 1 | 125 | 0 | 0 | 0 (0, 0) |
| | *taf8*ATGmm | N/A | N/A | N/A | N/A | N/A |
| *taf9* | *taf9*ATG | 1 | 87 | 83 | 0 | 95 (95, 0) |
| | *taf9*ATGmm | 1 | 127 | 0 | 0 | 0 (0, 0) |
| | *taf9*UTR | 1 | 107 | 0 | 0 | 0 (0, 0) |
| *taf10* | *taf10*ATG | 3 | 192 | 20 | 2 | 11 (10, 1) |
| | *taf10*ATGmm | 3 | 201 | 16 | 5 | 10 (8, 2) |
| | *taf10*UTR | 1 | 84 | 0 | 0 | 0 (0, 0) |
| *taf11* | *taf11*ATG | 3 | 332 | 114 | 162 | 83 (34, 49) |
| | *taf11*ATGmm | 3 | 254 | 42 | 11 | 21 (17, 4) |
| | *taf11*UTR | 2 | 145 | 0 | 0 | 0 (0, 0) |
| *taf12* | *taf12*ATG | 2 | 160 | 54 | 44 | 61 (34, 27) |
| | *taf12*ATGmm | 2 | 178 | 0 | 0 | 0 (0, 0) |
| | *taf12*UTR | 1 | 73 | 0 | 0 | 0 (0, 0) |
| *taf13* | *taf13*ATG | 2 | 333 | 67 | 0 | 20 (20, 0) |
| | *taf13*ATGmm | 2 | 257 | 257 | 0 | 100 (100, 0) |
| | *taf13*UTR | 2 | 124 | 0 | 0 | 0 (0, 0) |
| *taf15* | *taf15*ATG | 2 | 156 | 0 | 0 | 0 (0, 0) |
| | *taf15*ATGmm | 2 | 198 | 0 | 0 | 0 (0, 0) |
| | *taf15*UTR | 1 | 107 | 0 | 0 | 0 (0, 0) |
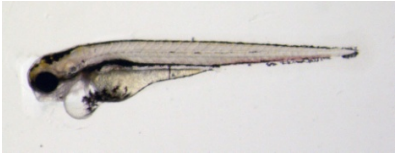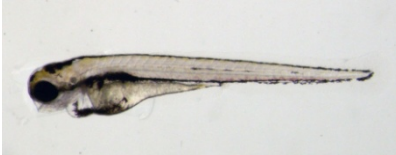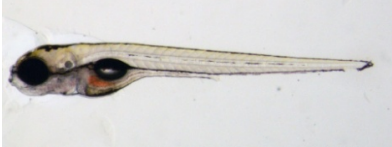
**Table 3.7 – Taf-morphant phenotypes at 5 dpf**
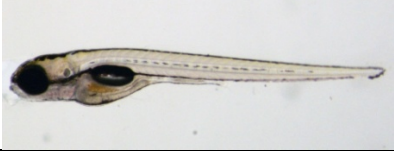
The percentages in the table are the percentages of embryos showing the described phenotype in that particular experiment. If several categories of phenotypes were observed in one experiment, the percentages and descriptions of phenotypes for the different categories are given. Only the phenotype categories with high percentages ≥10% are listed. N/A = not available.

| MO | Representative experiment | | Repeat of experiment | |
| --- | --- | --- | --- | --- |
| | Picture | Phenotype (Categories: A,B…) | Picture | Phenotype (Categories: A,B…) |
| non-injected |  | | | |
| *taf1*ATG |  | 64% (65/102)<br>- non-inflated swim bladder | | |
| *taf1*ATGmm |  | No significant phenotype observed | | |
| *taf1*UTR | A)<br><br>B)<br>N/A | A) 47% (43/91)<br>- whole body edema<br>- generally underdeveloped<br>B) 21% (19/91)<br>- non inflated swim-bladder<br>- underdeveloped liver/gut<br>- slight pericardial edema | A)<br><br>B)<br> | A) 32% (18/56)<br>- non-inflated swim-bladder<br>- appear slightly underdeveloped<br>- 5 % (5/56) pericardial edema and strongly reduced circulation<br>B) 30% (17/56)<br>- total body edema |

132

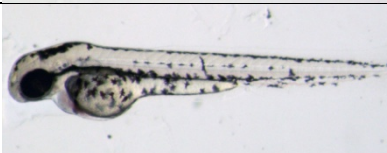| | | |
|---|---|---|
| *btaf1*ATG | N/A | No significant phenotype observed |
| *btaf1*mm |  | No significant phenotype observed |
| *taf2*ATG | N/A | All dead |
| *taf2*ATGmm |  | No significant phenotype observed |
| *taf2*UTR | N/A | No significant phenotype observed |
| *taf3*ATG | N/A | No significant phenotype observed |
| *taf3*ATGmm | N/A | No significant phenotype observed |
| *taf3*UTR | N/A | No significant phenotype observed |
| *taf4l*ATG | N/A | No significant phenotype observed |
| *taf4l*mm | N/A | No significant phenotype observed |
| *taf5*ATG | A)<br><br>B)<br> | A) 32% (24/74) with pigmentation gap<br>- pericardial edema<br>- smaller head/eyes and underdeveloped liver /gut<br>- pointed jaw<br>- sometimes yolk looks like rotting<br>- 15% (11/74) hemorrhage in head<br>- pigmentation gap in tail is lacking<br>B) 46% (34/74) no pigmentation gap<br>- like A1 but without pigmentation gap<br>- 15% (11/74) shorter body axis<br>- 24% (18/74) hemorrhage |

| | | |
|---|---|---|
| | C)  D)  E)  F)  | C) 31% (25/81)<br>- mild to severe whole body edema<br>- circulation is absent<br>- blood clot in tail<br>- severely underdeveloped<br>D) 26% (21/81)<br>- no circulation<br>- 12% (10/81) blood clot in tail<br>- dark yolk<br>- pericardial and beginning total edema<br>- severely underdeveloped<br>- trunk appears rough and dark<br>E) 14% (11/81)<br>- slightly underdeveloped<br>- nearly normal circulation<br>-shiny bodies<br>F) 11% (9/81)<br>- reduced circulation |
| *taf5*ATGmm |  | No significant phenotype observed |
| *taf5l*ATG | N/A | No significant phenotype observed |
| *taf5l*UTRmm | N/A | No significant phenotype observed |
| *taf5l*UTR | N/A | Dead |
| *taf6*ATG | N/A | Dead |
| *taf6*ATGmm | N/A | No significant phenotype observed |
| *taf6*UTR | N/A | No significant phenotype observed |

| | | |
|---|---|---|
| *taf6l*ATG | N/A | Dead |
| *taf6l*ATGmm | N/A | No significant phenotype observed |
| *taf7*ATG | N/A | No significant phenotype observed |
| *taf7*UTR | N/A | No significant phenotype observed |
| *taf8*ATG | N/A | No significant phenotype observed |
| *taf8*ATGmm | NA | NA |
| *taf9*ATG | A)  B)  | A) 46% (40/87) <br> - mild to severe whole body edema <br> - 5% (4/87) hemorrhage in head <br> - pericardial edema <br> - pointed jaw <br> - 18% (16/87) small or no gap in pigmentation <br> B) 25% (22/87) <br> - 15% (13/87) no gap in pigmentation <br> - 1% (1/87) hemorrhage <br> - pericardial edema <br> - no or very mild whole body edema <br> - mild phenotype underdeveloped liver/gut but head looks quite normal except of pointed jaw |
| *taf9*ATGmm | N/A | No significant phenotype observed |
| *taf9*UTR | N/A | No significant phenotype observed |
| *taf10*ATG |  | No significant phenotype observed |
| *taf10*ATGmm |  | No significant phenotype observed |
| *taf10*UTR | N/A | No significant phenotype observed |
| *taf11*ATG | N/A | Dead |

| | | | | |
|---|---|---|---|---|
| *taf11*ATGmm |  | No significant phenotype observed | | |
| *taf11*UTR | N/A | No significant phenotype observed | | |
| *taf12*ATG | A)<br><br>B)<br> | A) 22% (14/63)<br>- non inflated swim bladder<br>- some with underdeveloped liver and gut<br>- 10% (6/63) some with dark yolk<br>B) 22% (14/63)<br>- dark yolk | A)<br> | A) 20% (19/97)<br>- dark yolk<br>- liver and gut are underdeveloped |
| *taf12*ATGmm | N/A | No significant phenotype observed | | |
| *taf12*UTR | N/A | No significant phenotype observed | | |
| *taf13*ATG | N/A | No significant phenotype observed | | |
| *taf13*ATGmm | N/A | 100% of injected larvae exhibit an abnormal phenotype | | |
| *taf13*UTR | N/A | No significant phenotype observed | | |
| *taf15*ATG | N/A | No significant phenotype observed | | |
| *taf15*ATGmm | N/A | No significant phenotype observed | | |
| *taf15*UTR | N/A | No significant phenotype observed | | |

# 3.7    Summary MO-screen
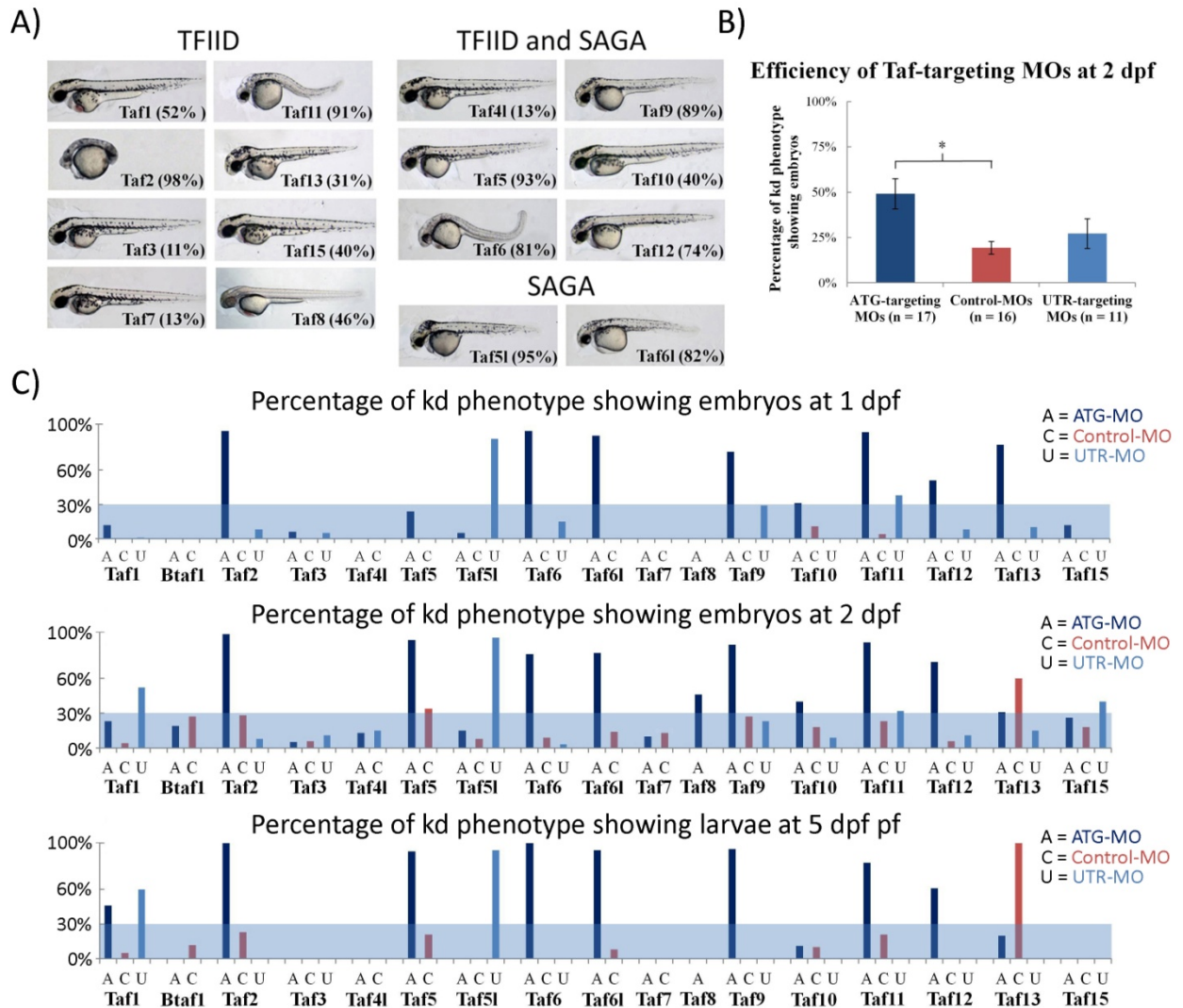


**Figure 3.1 – Summary of Taf-morphant phenotypes at 2 dpf**

**A)** Taf kd phenotypes observed at 2 dpf. The different Tafs are arranged according to the complexes they are found in (TFIID, SAGA and both). The percentage given with the name of the Taf in brackets is the percentage of kd phenotype showing embryos at 2 dpf. **B)** The chart compares the efficiencies of the three types of MOs used in the screen, to induce a phenotype at 2 dpf. Brackets with an asterisk indicate groups with a significantly different efficiency in inducing a kd phenotype at 2 dpf, by two-tailed t-test (p-value ≤0.05). **C)** The charts display the percentages of kd phenotype showing embryos for each Taf at 1, 2 and 5 dpf. If more than 30% of injected embryos were abnormal, the phenotype was considered a significant phenotype.

Most of the Taf-morphant phenotypes manifested at a developmental stage ≤2 dpf, whereas the phenotypes of zygotic mutants of Tafs appear after 2 dpf.

The consistent phenotypes observed for Taf5, Taf6, Taf9 and Taf12 support the presence of a 5 TAF core complex within TFIID. However, the knock down of the TAF4 homolog, Taf4l, did not result in a significant phenotype. The very weak and rather inconsistent phenotypes observed for Taf8/10 argues against a strong participation of that heterodimer in the core complex. The results for the Taf11/13 heterodimer were inconclusive. Taf11 gave a strong specific phenotype, while Taf13 gave a weaker phenotype, which might be unspecific (control shows phenotype).

All the orthologs of TAFs which have been shown to bind to specific core promoter motifs: Taf1, Taf2 and Taf6/9, showed a consistent, specific phenotype.

The phenotypes observed for the orthologs of histone mark binding TAFs, Taf1 and Taf3, are not arguing for a big importance of that function within TFIID during zebrafish development.

The two orthologs of SAGA-specific TAFs tested in our screen, Taf5l and Taf6l, showed a strong, very similar phenotype. Although Taf10 and Taf12 can be found in both complexes, TFIID and SAGA, the phenotypes for their zebrafish orthologs were not stronger than the ones observed for the orthologs of SAGA-specific subunits.

## 3.8   Discussion

In conjunction with a MO-screen targeting 17 different zebrafish Tafs we performed at least 59 kd experiments and I analysed the phenotypes of around 10 000 injected embryos (Table 3.4). The suitability of MOs for medium scale kd screens in zebrafish model was confirmed by the results of our MO-screen. Overall the targeting MOs were more efficient in inducing a phenotype

than the control MOs (Figure 3.1). Interestingly, only the ATG-targeting MOs were significantly more efficient in inducing a phenotype than the control MOs. The slightly higher efficiency of UTR-targeting MOs was not statistically significant.

## 3.8.1    Characteristics of Taf kd phenotypes

Due to the pleiotropy of most of the phenotypes in the MO-screen, it was not practical and the scope of this study, to perform a very detailed characterisation of the morphants. A basic description of the morphants is given in Table 3.3, Table 3.5 and Table 3.7. Reoccurring phenotypes at 2 dpf, the definitive stage of phenotype analysis in the screen, were, amongst others, circulation and heart defects. A functional circulation is required for proper development and organ growth beginning with early larval stages (Korzh et al., 2008). Therefore, some of the defects observed at 5 dpf might be secondary to circulation defects.

This study is the first comprehensive study on the role of TAFs during vertebrate development. There are four zebrafish Taf-mutant phenotypes annotated in the ZFIN database (Taf2, Taf6, Taf7 and Taf8). None of the morphant phenotypes generated in the MO-screen exactly phenocopies their mutant counterparts. Regarding Taf2 and Taf6, the morphant phenotypes are stronger than their mutant counterpart. That can be explained by an additive effect resulting from blocking translation of the zygotic and the maternally derived transcripts by the MO. This additional blocking of the maternally derived transcripts also explains the earlier appearance of the morphant phenotypes for Taf2 and Taf6 than their mutant phenotypes. There is however discrepancy between the morphant phenotypes of Taf7 and Taf8 compared to their mutants.

The Taf8-morphant showed a weak phenotype around 2 dpf (weak retardation), but recovered by 5 dpf. The earlier appearance of the phenotype easily can be explained (see above) but not the lack of a 5 dpf phenotype. It has been shown that the efficiency of early injected MOs to block translation of their targets drops during stages beyond 3 dpf. This has been attributed to dilution of the MO. However, it is not clear why the Taf8 MO would be more diluted than other MOs, which induce a phenotype at 5 dpf. An explanation for this would be that the later phenotypes are a consequence of the efficient block of translation by MOs at earlier stages. If Taf7 is dispensable for embryonic development, it might not be possible to efficiently knock it down by early injection of MOs.

Many injected targeting MOs in the screen did not induce any phenotype. This was observed also for MOs where another MO, targeting the same transcript, induced a phenotype. There are two possible explanations for this: Either the phenotype observed with one of the MOs is caused by off-target effects or the non-phenotype inducing MO is not efficiently targeting the target mRNA. Performing rescue experiment would help to resolve that issue.

## 3.8.2    Limitations of MO antisense technology

Due to limitations of the technology, kd experiments using MOs need to be well controlled for off-target effects. A fully controlled experiment comprises two MOs inducing the same phenotype, no phenotype with the mismatch control MO and a rescue of the phenotype with mRNA of the targeted gene (also see chapter 2.3). Induction of p53-mediated cell death is a common off-target effect of MOs (Robu et al., 2007). It has been suggested by Robu et al. to co-inject a MO against p53 to suppress this off-target effect. The problem with that approach in turn

is that all true phenotypes involving p53-activation are masked. To include all above mentioned controls is quite time consuming and not practical for higher throughput experiments. In a trade off between throughput and controlling specificity, I decided not to perform rescue experiments and to rely on the use of mismatch control MOs for the targeted genes. For similar reasons the concentration of the injected MOs were not optimised. Only one concentration (100 µM) was injected. Another limitation of the MO kd technology is non-efficient targeting of the target sequence by the MO. Non efficient targeting of the mRNA can be caused by:

1. Inaccessibility of the targeted sequence for the MO due to occupation by RNA-binding proteins, or due to the secondary structure of the targeted mRNA.

2. Polymorphisms in the targeted sequence.

3. Poor MO design due to insufficient knowledge about transcripts of the targeted gene.

In respect of point 3 I made an interesting observation in this screen. We know that the majority of the genome is transcribed and that for a given gene there are usually numerous alternative transcripts (Aanes et al., 2011, Birney et al., 2007). It needs to be considered for MO-design, that the MO is efficiently targeting all alternative transcripts of the gene. Our knowledge about the zebrafish transcriptome is incomplete, what can have a significant impact on the success of MO-mediated kd experiments (see Figure 3.2).
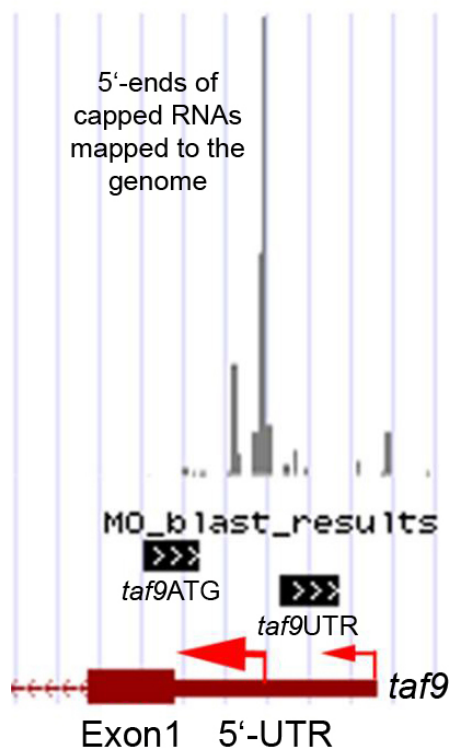
**Figure 3.2 – Implications of CAGE data for MO design**

The figure shows in a histogram the 5'-ends (last base) of capped RNAs mapped to the zebrafish genome. The data is derived from CAGE (capped analysis of gene expression) experiments using RNA from 48 hpf embryos (Christian Previti, Yavor Hadzhiev, Chirag Patel, Nan Li, Vanja Haberle, Hazuki Takahashi, Santosh Amand, Jochen Gehrig, Altuna Akalin, Jan Christian Bryne, Ying Sheng1, Wilfred van IJcken, Olivier Armant, Sepand Rastegar, Uwe Strähle, Elia Stupka, Piero Carninci, Boris Lenhard and Ferenc Müller, unpublished data). This example illustrates how MO design will benefit from improving our knowledge about the zebrafish transcriptome. Because the reference sequence used for MO design is not the predominant transcript, the *taf9*UTR MO does not efficiently target *taf9*. Consequently only the *taf9*ATG MO induces a phenotype and no significant phenotype is observed after injection of the *taf9*UTR MO (Table 3.4).

The mRNAs for all of the Tafs targeted in the MO-screen are maternally provided (unpublished

CAGE data, see Figure 3.2). The already spliced maternal RNA only can be targeted with MOs

against the ATG and the 5'-UTR. It can be assumed, that there is also a maternal supply of the

Taf proteins, which are not affected by MOs. A differential contribution of maternal Taf proteins

to early zebrafish development would mean a major flaw for the conclusions drawn from MO-

142

induced kd experiments. The differences in the strength of the observed phenotypes might not only reflect differential requirement of the Tafs for early development, they might also reflect differential contribution of the maternal proteins.

Because of the limitations in using MOs to study the role of Taf proteins during early zebrafish development, the data and conclusions from the MO-screen have to be taken with caution. The data is rather meant to provide a baseline characterisation of Taf-morphant phenotypes, for further in depth analysis by alternative LOF techniques.

### 3.8.3    Alignment of MO-screen results to the structure of TFIID and SAGA

The results of the MO-screen do not clearly favour one of the three models (chapter 1.1.2.2) suggested for the TFIID core complex. The 7 TAF core complex (TAF4/5/6/8/9/10/12) is, due to the weak phenotypes for Taf8 and Taf10, not well supported by the data. The significant phenotype for the Taf11/13 heterodimer is in line with a participation of this heterodimer in a core complex. However, the control MO for Taf13 also induced a phenotype, so that this result is inconclusive. The data is in line with the existence of a 5 TAF core complex (TAF4/5/6/9/12) *in vivo*. The lack of a significant kd phenotype for Taf4l is disappointing, considering the importance of TAF4 for the integrity of TFIID and viability in other model organism. However, mouse embryonic fibroblasts lacking TAF4 are viable and contain intact TFIID complexes, in which TAF4 is replaced by TAF4b (Mengus et al., 2005). Similarly Taf4b might replace Taf4 in zebrafish TFIID during early development. Knock down experiments targeting *taf4b* could help to clarify that issue.

Knock down of the orthologs of the SAGA subunits TAF5L and TAF6L results in a similar phenotype. This offers the possibility to use their kd as a tool to study specialised roles of SAGA subunits during early zebrafish development.

### 3.8.4    Strong kd phenotypes for orthologs of DNA-binding TAFs

The majority of zebrafish promoters lack a detectable TATA-box. The nucleation of PIC assembly by binding of a PRF to the core promoter is consequently in the majority of the cases not by TBP-binding to the TATA-box. Alternative mechanisms, which have been demonstrated, are the binding of certain TAFs to core promoter motifs and/or chromatin. The data from our MO screen is potentially consistent with a model that the DNA-binding (Taf1, Taf2 and Taf6/9) of Tafs within TFIID is more important during early zebrafish development than chromatin binding (Taf1 and Taf3). A requirement of TAF2 for Inr-dependent transcription has been demonstrated, alone or in a complex with TAF1 (Papai et al., 2009, Verrijzer et al., 1994). Given that the Inr is the most abundant promoter element it is feasible, that loss of TAF2 would cause a lack of recruitment of TFIID to many promoters. In that light the strong phenotype observed for Taf2 is not surprising. The kd of the Taf6/9-heterodimer also induces a strong phenotype. TAF6 has been shown to bind to the DPE in complex with its heterodimer partner TAF9 (Burke and Kadonaga, 1997). These findings suggest that orthologs of the DNA binding TAFs are more rate limiting than non DNA-binding TAFs.

The phenotype for the ortholog of TAF1 suggests a weaker contribution of that Taf to promoter recognition via binding to the Inr or to acetylated histone tails (chromatin). Same is the case for the ortholog of the H3K4me3 binding TAF3.

# 3.9 Conclusions

1. In a MO-screen targeting the majority of the Tafs found in the zebrafish genome, we observed a range of different phenotypes for the different Tafs. This finding suggests differential functions of Tafs during zebrafish development. The results are in line with variant complexes acting during development, but our study did not include biochemical analysis of Taf-containing complexes.

2. The relatively strong phenotypes observed for orthologs of TAFs, which are part of a proposed five TAF core complex (TAF4, 5, 6, 9 and 12), in comparison to the overall weaker kd phenotypes for orthologs of peripheral TAFs (TAF1, 2, 3, 7 and 15), supports the existence of this core complex *in vivo*. However, a significant phenotype for Taf4l, a zebrafish homolog of TAF4, was not observed. This might be explained with substitution of Taf4l by Taf4b during zebrafish development. This question should be addressed in future experiments.

3. The kd of the zebrafish orthologs of the SAGA-specific TAF5L and TAF6L resulted in very similar phenotypes, suggesting specific, non-redundant functions of SAGA-specific Tafs during zebrafish development.

# 4 Mutant phenotype analysis of zebrafish *taf8* compared to *taf6* with focus on a potential coactivator function of Taf8 for Pparγ

## 4.1 Introduction and objectives

The observation that TBP only in conjunction with the higher molecular weight TFIID complex, and not by itself, can mediate activated transcription, let to the establishment of TAFs as coactivators. Many coactivator functions for TAFs have been described in the literature:

An interaction of TAF3 with Antennapedia was found in *Drosophila* (Prince et al., 2008). In mouse an interaction of TAF3 with MyoD has been proposed to drive myogenin transcription (Deato et al., 2008). TAF4 is a mediator of Wnt signalling in *Drosophila* (Wright and Tjian, 2009). Human TAF4 interacts with several activators like SP1 and CREB, via a well conserved domain (TAFH), which binds to a short hydrophobic motif often present in transcriptional regulators (X. Wang et al., 2007).

Several activators apparently target multiple TAFs within TFIID. TAF1 and TAF4 are coactivators for SP1 (Hilton et al., 2005, Rojo-Niersbach et al., 1999). TAF1 and the TAF6/9-heterodimer mediate p53-dependent transactivation (Thut et al., 1995). TAF1 and TAF7 seem to be coactivators for c-Jun (Lively et al., 2004, Munz et al., 2003). Liu et al determined the position of p53, SP1 and c-Jun bound to holo-TFIID by negative stain EM (Liu et al., 2009). In combination with photoactivatable protein cross-linking label transfer assays they were able to also determine the TFIID-subunits in close proximity (within 21 Å) to the bound activator. Their

data validated and extended the multiple TAF-activator contacts found for p53, SP1 and cJun in other studies (Figure 4.1).
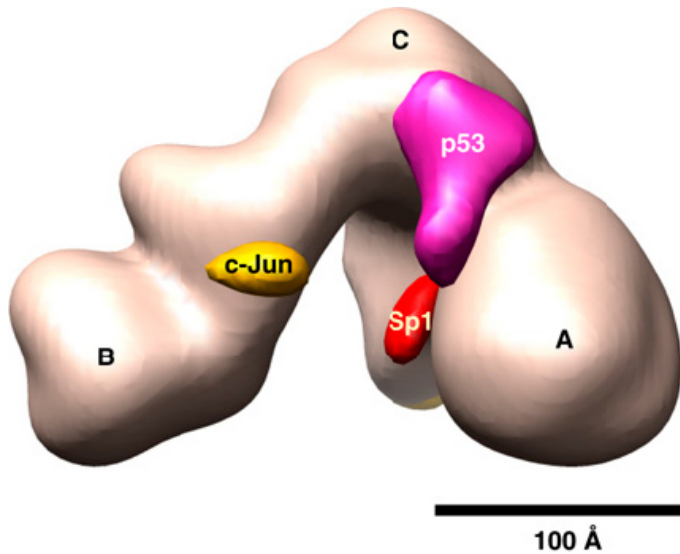


**Figure 4.1 – Structure of complex of TFIID bound to activators**

By a combination of EM and biochemical mapping analysis the position and potential interaction partners of p53, SP1 and c-Jun in complex with holo-TFIID have been determined. SP1 contacts TAF1, TAF4 and TAF6, while p53 contacts TAF1, TAF5, TAF6 and weakly TBP. For c-Jun contacts with TAF1 and TAF6 have been observed. Taken from (Liu et al., 2009).

The nuclear receptor PPARγ is a master regulator of adipocyte biology. PPARγ is essential for the process of adipogenesis and sufficient to drive conversion of fibroblastic precursors into fat cells (Choi et al., 2010). Two major isoforms exist of PPARγ: The broadly expressed PPARγ1 and PPARγ2, which expression is restricted to adipocytes. *Pparγ*$^{-/-}$ mice die before stage E9.5, due to defects in the extraembryonic trophoblast tissue causing cardiomyopathies in the embryo. *Pparγ* ko mutant pups can be obtained by rescue of the trophoblast phenotype via generation of tetraploid aggregate chimeras. They display lipodystrophy, fatty liver and multiple haemorrhages, e.g. in the intestine and in the brain (Barak et al., 1999).

A plethora of co-regulators have been shown to interact with PPARγ: Steroid receptor coactivators (SRC-1, SRC-2), peroxisome proliferator receptor γ coactivator 1 (PGC-1), nuclear receptor corepressor (N-CoR), activating signal cointegrator-2 (ASC-2), silencing mediator of retinoid and thyroid receptors (SMRT), receptor-interacting protein 140 (RIP140) and adenovirus E1A-associated 300 kDa protein (p300)(McKenna and O'Malley, 2010). Furthermore PPARγ connects to the basal transcription machinery via interactions with Mediator subunits 1 and 14 (Ge et al., 2002, Grontved et al., 2010).

Recent findings suggest that the specialisation of cell-types (differentiation) is in part accomplished by a specialisation of the basal transcription machinery. TAFs, as specific mediators of regulatory input from transcriptional activators during ontogeny might play a crucial role in that process. There are several mechanisms proposed for specific roles of TAFs during ontogeny. One mechanism would be a dominant role of specific TAFs in certain lineages, established by retention of those TAFs in the context of depletion of other TFIID components. This for example has been observed for TAF8 in adipocytes and for TAF3 in myotubes. Another mechanism is the cell-type specific expression of non-prototypic TAFs, which replace their prototypic counterparts. An example for this is the gonad-specific expression of certain TAF paralogs. It is therefore important to study the role of TAFs *in vivo*, to potentially discover lineage-specific roles, also as coactivators.

## 4.2 Aims

I chose the zebrafish model to study the role of Taf8 in the complexity of the organism and with special focus on vertebrate development. There is one distinct advantage of using zebrafish as *in*

*vivo* model to investigate specific functions of (general) factors, like Taf8. In zebrafish, due to attenuation of the zygotic mutant phenotype by maternal contribution, late evolving subfunctions of such, otherwise generally required factors may be revealed in specific cell-types and organs. In contrast mouse mutants of these general transcription factors are mostly early embryonic lethal, providing little insight into specific developmental functions.

I compare *taf6*-mutants to *taf8*-mutants to identify general TFIID-dependent functions of *tafs* and to reveal potential *taf*-specific phenotypes that may indicate specialised roles of Taf8 and Taf6. The *taf8*- and *taf6*-mutants (in the following just *taf*-mutants) have been generated by a similar insertional mutagenesis approach and TAF6 is also a subunit of TFIID (and the core complex), like TAF8.

One of the objectives of my PhD is to use zebrafish model to address in an animal model if TAF8 may be a specific coactivator of PPARγ, which was demonstrated *in vitro* with the human TAF8 protein (chapter 1.3). My hypothesis was that if Taf8 is required to mediate Pparγ-activated transcription, then Pparγ-related defects should be observed in zebrafish *taf8*-mutants.

The characterisation of the *taf8*-mutant compared to the *taf6*-mutant addressed the following questions:

1. What are the roles of Taf8 and Taf6 during zebrafish development?

2. Does Taf8 have distinct, specific roles from other TFIID components such as Taf6?

3. Is there a specific requirement of *taf8* for Pparγ-activated transcription?

# 4.3 Results

## 4.3.1 Validation of mutant phenotypes on the level of *taf8* and *taf6* gene expression

The *taf8*- and *taf6*-mutants used in the experiments were generated by insertional mutagenesis. In both mutants the foreign sequence used for mutagenesis has inserted into the first intron of the respective gene. It is not obvious how this would be mutagenic, causing LOF-phenotypes for the respective genes. It has previously been demonstrated that insertions into the first intron of the gene s often cause a significant reduction of the transcript levels of the affected gene.(Amsterdam et al., 2004). I performed qPCR and RT-PCR experiments to investigate whether the analysed *taf8*- and *taf6*-mutant phenotypes are associated with loss of *taf* expression. The experiments were performed with cDNAs prepared from 12 mutant larvae and 12 of their wildtype siblings. The *bactin1* levels served as an internal standard for the normalisation of the *taf* transcript levels in the qPCR and RT-PCR experiments. Mutants were identified by their morphological phenotype. A substantial reduction in the transcript-levels for *taf8* and *taf6* in their mutants was observed by qPCR and RT-PCR, while the transcript levels of the respective other *taf* were largely unaffected. For *taf8* this was validated by WISH (whole-mount *in situ* hybridisation, data not shown). That finding confirmed the hypothesis, that the insertion of the transgene into the first intron of *taf8* and that of *taf6* causes depletion of their transcript levels.
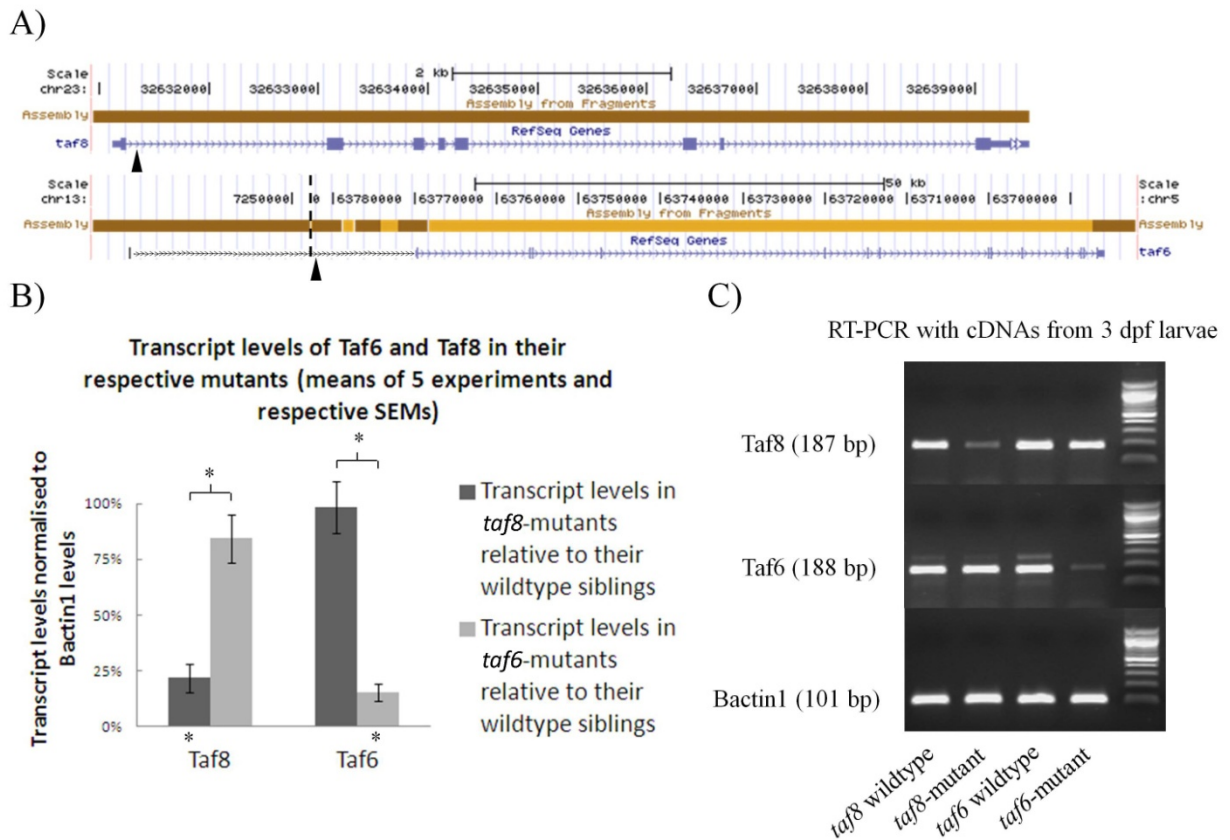
**Figure 4.2 – Validation of LOF of *taf8*- and *taf6* in the respective mutants**

**A)** UCSC browser view of the *taf8* and *taf6* loci in zebrafish genome assembly Zv9. The black arrow heads point to the insertion sites of the foreign sequences in the mutant alleles. Note that there is a presumptive mis-assembly of fragments for the 5'-sequence of the *taf6* locus. Due to that mis-assembly, exon1 and intron1 of the reference sequence for *taf6* are missing. For this figure the correct fragment from another locus was added. The dashed line indicates where the added sequence begins. The results from comparative gene expression analysis experiments using cDNAs from 3 dpf *taf*-mutants and their wildtype siblings are shown. The chart in **B)** summarises the results for five qPCR experiments and **C)** shows the results of a RT-PCR using cDNAs from one of the qPCR experiments. PCR and gel in **C)** were done by Irene Miguel.

## 4.3.2    Comparison of Taf8, Taf6 and Pparγ LOF-phenotypes

In this subchapter results for the morphological and anatomical characterisation of the *taf8*- and

*taf6*-mutant phenotypes are presented. As it was also an objective of the PhD-project to address

the putative role of Taf8 in Pparγ signalling, the focus of the mutant characterisation has been on general morphology followed by analysis of PPARγ-related processes and defects.

## 4.3.2.1 Distinct craniofacial defects in *taf8*- and *taf6*-mutants suggest differential functions

The *taf8*- and *taf6*-mutants are recessive mutants and their phenotype manifests in the 25% of embryos from crossing of heterozygous parents which are homozygous for the mutant allele. Those homozygous embryos are not viable and cannot be grown to adulthood. There is no obvious heterozygous phenotype. Also, there is no additive effect of heterozygosity for the *tafs*. All larvae from 7 crosses of heterozygous *taf8*-mutants with heterozygous *taf6*-mutants show normal wildtype phenotype (data not shown).

The morphological phenotypes of zebrafish *taf8* and *taf6* are very similar. Like the phenotypes for many other essential genes they resemble the category of the "general phenotype" described in chapter 1.2.1. The morphological phenotype manifests at 3 dpf in a general underdevelopment of most of the organs and structures (Figure 4.3). This general underdevelopment seems to be somewhat more pronounced in the anterior part of the embryo. Most anterior organs and structures in the mutants are smaller than their wildtype counterparts: The head, the eyes, the jaws, the liver and the intestinal bulb (Figure 4.3). What also can be observed is a swelling of the pericardium (pericardial edema) in the mutants appearing at 4 dpf (Figure 4.3). Also the endodermal organs liver, intestine and pancreas are severely underdeveloped. The drunk and tail have an almost normal appearance. Also the somites appear normal and the *taf*-mutant larvae have no obvious defects in motility. At 5 dpf the diameter of the trunk of *taf8*- and *taf6*-mutants is

significantly larger then the one of their respective wildtype siblings (Marko Saric, unpublished data).

Besides the similarities of the two *taf*-mutant phenotypes there are also differences in the detail and degree of the defects observed. Both mutants have a circulation defect and develop pericardial edema. But this defect is more severe in *taf6*-mutants, were in approximately 50% of the larvae it develops into whole body edema around 5 dpf (data not shown). The head-morphology of the mutants differs throughout the examined stages, partly due to differential defects in the cartilaginous head skeleton. Overall, the pharyngeal skeleton of *taf8*-mutants appears larger than the one of *taf6*-mutants in side views (Figure 4.6). The cartilaginous head skeleton appears somewhat compressed along the anterior-posterior axis in *taf8*-mutants compared to *taf6*-mutants and wildtype siblings (Figure 4.4). There is a kink in the neurocranium of 5 dpf *taf8*-mutant larvae, at the level where the trabeculae join the parachordals (polar cartilage region) (Figure 4.5). The region of the abc cartilage (anterior basicranial comissure) appears larger in side views pictures of 5 dpf *taf8*-mutants compared to *taf6*-mutants and wildtype siblings (Figure 4.5). The ceratohyal cartilage in ventral views of *taf8*-mutants has a larger diameter than the ceratohyal of *taf6*-mutants (Figure 4.5).
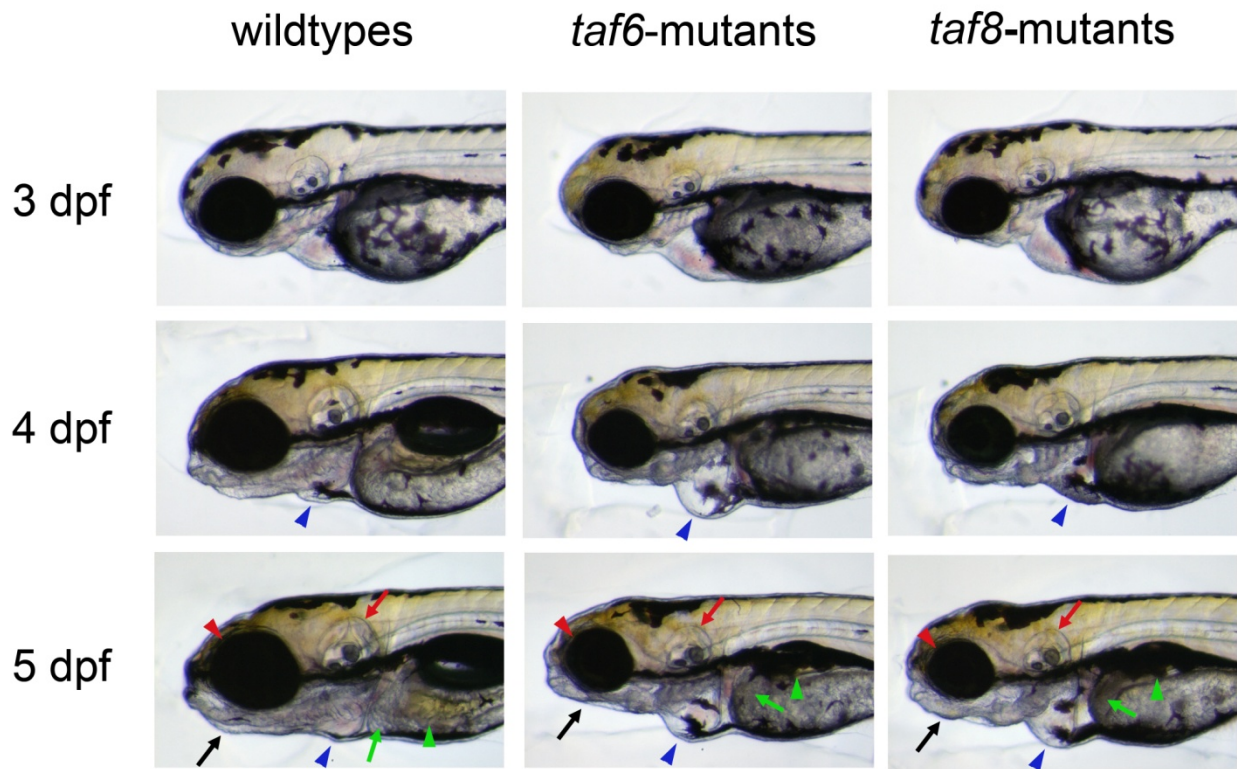
**Figure 4.3 – Morphological differences between the *taf8*- and *taf6*-mutant phenotypes**

Representative *taf8*-mutant larvae compared to *taf6*-mutants and wildtypes at different developmental stages. Shown are side view (left side) pictures of the anterior halves of the larvae, with anterior to the left and dorsal to the top. Markers in the figure point to eyes (red arrow heads), ears (red arrows), jaws (black arrow), pericardium (blue arrow heads), liver (green arrows) and intestine (green arrow heads).
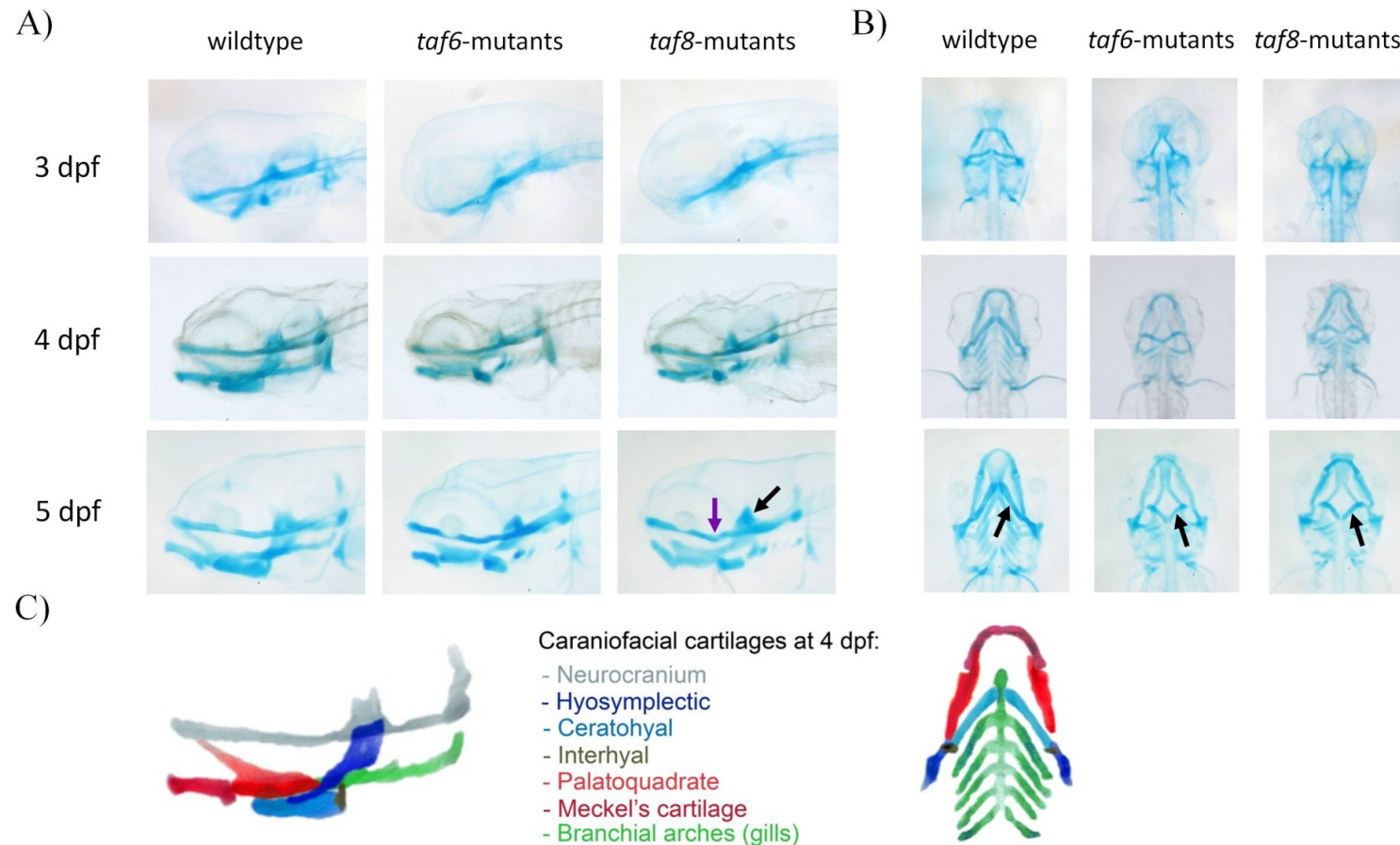
**Figure 4.4 – Differences in cartilaginous head skeleton between *taf8*- and *taf6*-mutants**

**A)** and **B)** show whole-mounted larvae at different stages. Their cartilage is stained blue by alcian blue staining. **A)** Side view pictures with anterior to the left and dorsal to the top. **B)** Ventral view pictures with anterior to the top.
Black arrows point to the anterior basicranial comissure cartilage in **A)** and to the ceratohyal cartilage in **B)**. The purple arrow in **A)** points to a kink in the neurocranium. **C)** Camera lucida drawing of the cartilage elements from the 4 dpf wildtype in side view and ventral view. Distinct cartilage elements are depicted in different colours and their names are given.

155

**A) Diameter of ceratohyal in 5 dpf *taf*-mutants**

**B) Kink in neurocranium of 5 dpf *taf*-mutants**

**C) Size of anterior basicranial commissure cartilage (abc) in 5 dpf *taf*-mutants**
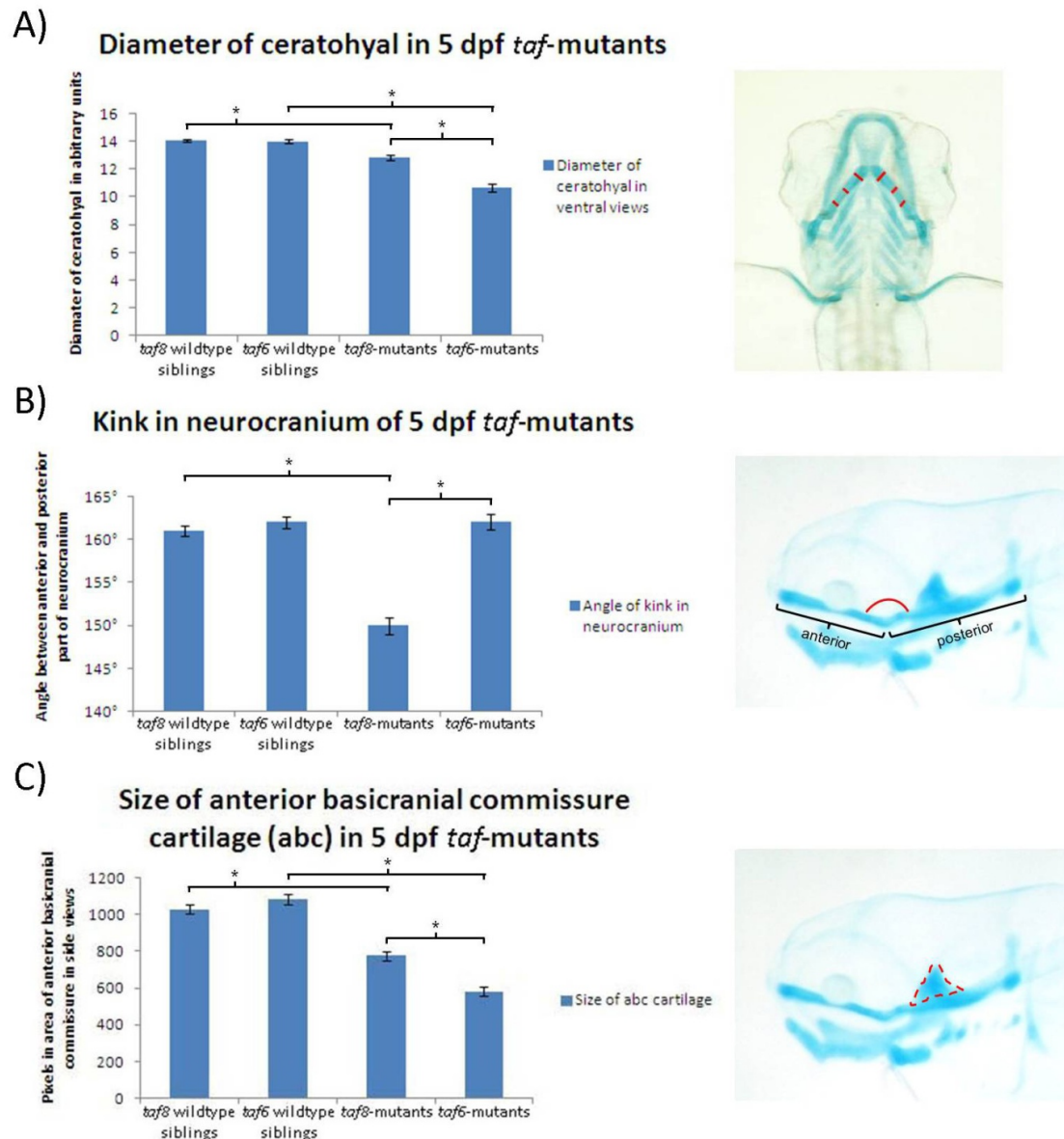
**Figure 4.5 – Defects in the cartilaginous head skeleton of 5 dpf *taf8*-mutants**

Shown in this figure is the quantification of defects in the cartilaginous head skeleton of 5 dpf *taf*-mutants. Features of craniofacial cartilages are compared between *taf*-mutants and their wildtype siblings. The pictures of alcian blue stained lavae on the right side of each bar chart illustrate what feature was quantified Brackets with asterisks indicate groups which are significantly different for the analysed feature by two-tailed t-test (p-value ≤0.5). The error bars in the charts are SEMs. The numbers of analysed larvae in each group were: 21 for chart **A)**, 30 for chart **B)** and 22 for chart **C)**. ImageJ straight line selection tool was used to measure the diameter of ceratohyal cartilages in ventral views (mean of six measurements as depicted in **A)** for each larva). The ImageJ angle tool was used to measure angles for chart **B)** and the freehand selection tool was used to measure the area of the abc cartilage in chart **C)**.

156
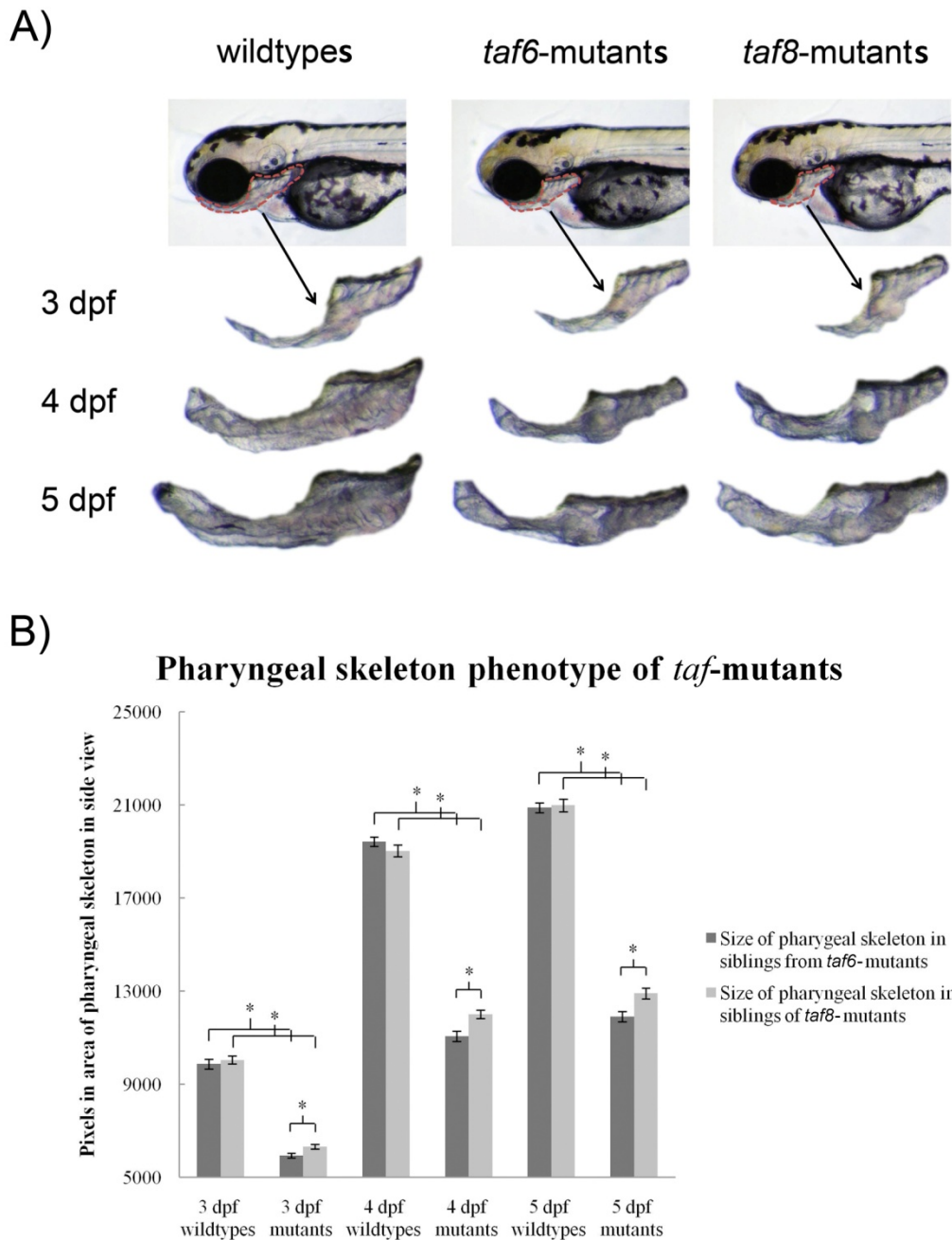
**Figure 4.6 – Larger pharyngeal skeleton of *taf8*-mutants compared to *taf6*-mutants**

The area of the pharyngeal skeleton in side view pictures of 3 dpf, 4 dpf and 5dpf *taf*-mutants and their wildtype siblings was measured using the ImageJ freehand selection tool. The principle of the measurements is shown in **A)** for 3 dpf larvae, where the measured pharyngeal skeleton area is outlined in red. Below examples for the appearance of the pharyngeal skeleton of *taf*-mutants and their wildtype siblings in side view pictures at the examined stages are shown. The results of the measurements are summarised in chart **B)**. Brackets with asterisks indicate groups with a statistically different size of the pharyngeal skeleton by two-tailed t-test (n = 30, p-value ≤0.05). The 5 dpf experiment was carried out with transgenic mutants (*fli1a:EGFP gata1:dsRed*).

157

## 4.3.2.2    Specific defect in Pparγ-dependent lipogenesis in *taf8*-mutants

PPARγ regulates the process of intracellular neutral lipid accumulation (lipogenesis) not only in adipocytes, but also in many other tissues (liver, muscle). Many of the orthologs of mammalian PPARγ target genes involved in lipogenesis are expressed during embryogenesis in zebrafish. At early larval (4-5 dpf) stages an obvious overlap between the expression patterns of these orthologs of PPARγ target genes with the expression patterns of *pparγ* itself emerges (see ZFIN database for expression patterns, http://zfin.org/cgi-bin/webdriver?MIval=aa-xpatselect.apg). This overlap is obvious for the expression of *lpl*, *pparγ*, *cd36*, *fabp11b* and *fabp2* in liver and intestine. This raises the questions, if Pparγ is involved in lipogenesis in those organs during early larval stages and if this Pparγ function requires Taf8, as suggested by Mate Demeny's data (chapter 1.3). To address those questions, I together with Nan Li (Müller group) performed lipid stainings of fixed 5 dpf larvae with Oil Red O, which is commonly used to visualise intracellular neutral lipid accumulations (lipid droplets).

First we determined the lipid staining patterns in *taf8*-mutants compared to *taf6*-mutants and their respective wildtype siblings at 5 dpf. At that stage, wildtype larvae display ORO staining of the swim bladder, the yolk, the heart, the liver, the vasculature and head structures (Imrie and Sadler, 2010, N. Li et al., 2010, Schlegel and Stainier, 2006). In our experiments we observed much fewer lipid droplets in the liver and intestine of *taf8*-mutants compared to their wildtype siblings and *taf6*-mutants (Figure 4.7, Figure 4.8). Note that the strongly stained, lipid rich yolk sac is much bigger in mutant larvae, while liver and intestine are much smaller. This suggests a specific defect in lipogenesis in liver and intestine of 5 dpf *taf8*-mutants. Liver and intestine are organs which strongly express *pparγ* at 5 dpf (Figure 4.7, panels B and C). Interestingly, there was also a

clear difference in the staining behaviour of the wildtype phenotype showing larvae, between the two mutant lines. The wildtype siblings of *taf8*-mutants display much more lipid droplets in the liver and intestine than the wildtype siblings of *taf6*-mutants (Figure 4.8).

The strong expression of *pparγ* in liver and intestine of 5 dpf larvae suggests a possible involvement of Pparγ in lipogenesis in those tissues, at that stage. We hypothesised that, if the observed lipid droplets are formed by Pparγ-dependent lipogenesis, then they should be removed by treatment with a PPARγ inhibitor. To test the hypothesis, we performed drug treatments of *taf6*-mutants and their wildtype siblings with the selective and irreversible PPARγ antagonist GW9662 (Leesnitzer et al., 2002). We did not include *taf8*-mutants into those experiments, because they already display a very low amount of lipid droplets in their livers and intestine. Larvae derived from crosses of heterozygous *taf6*-mutants were incubated in E3-medium containing either 500 nM or 5 µM GW9662 for approximately 75 h, from 2 dpf till 5 dpf. As controls served larvae treated with the same amount of DMSO, which has been introduced with the GW9662 treatments.

Treatment with the PPARγ inhibitor GW9662 efficiently reduces the number of lipid droplets observed in liver and intestine of *taf6*-mutants (Figure 4.7, Figure 4.8). The DMSO treated larvae stained similar to non-treated *taf6*-mutant larvae. Also the wildtype siblings showed reduction of the lipid droplets observed in intestine and liver. Taken together the data suggests a requirement of Pparγ for the lipogenic process leading to lipid droplet accumulation in liver and intestine at 5 dpf.
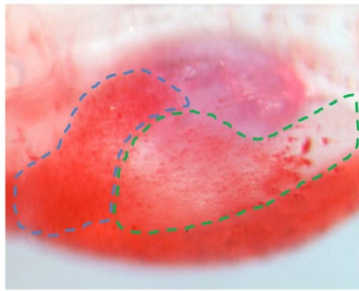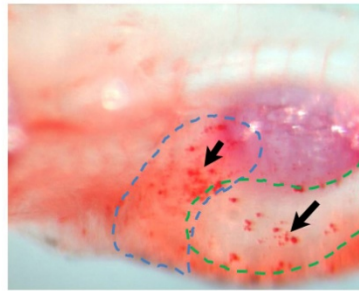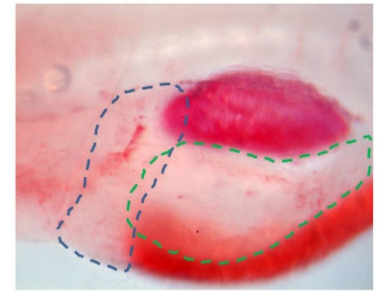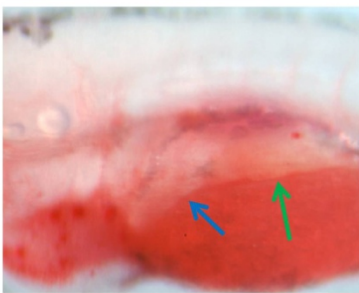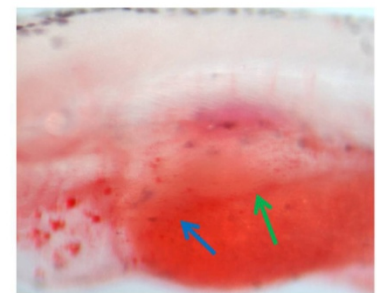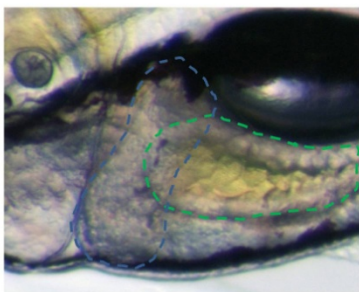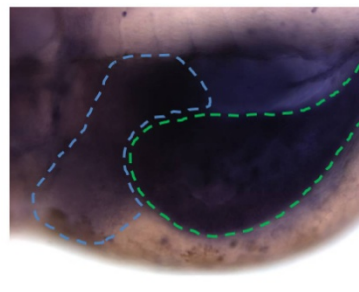
**Figure 4.7 – Specific defect in Pparγ-dependent lipogenesis in *taf8*-mutants**

Shown are side view pictures (left side) of the region containing the liver and intestine (intestinal bulb) in 5 dpf larvae. Anterior is to the left and dorsal is to the top. **A)** depicts whole-mounted larvae stained for lipids with Oil Red O. **B)** shows a bright field image of a wildtype larva and **C)** a wildtype larva from a whole-mount *in situ* staining against *pparγ*-mRNA (purple staining). The blue dashed lines outline the liver and the green dashed lines outline the intestine in **A)**, **B)** and **C)**. Accordingly, the blue and the green arrows in **A)** point to the respective organs in the mutant larvae. Black arrows point to lipid droplets in liver and intestine in **A)**. Oil Red O staining of fixed embryos was performed by Nan Li.

**A)**

**Percentage of mutant larvae falling into different categories of lipid staining (means of three experiments with respective SEMs)**

Legend:
- *taf6*-mutants (n = 110)
- *taf6*-mutants treated with DMSO (n = 9)
- *taf8*-mutants (n = 86)
- *taf6*-mutants treated with 500 nM GW9662 (n = 45)
- *taf6*-mutants treated with 5 000 nM GW9662 (n = 29)

**B)**

weak          medium          strong
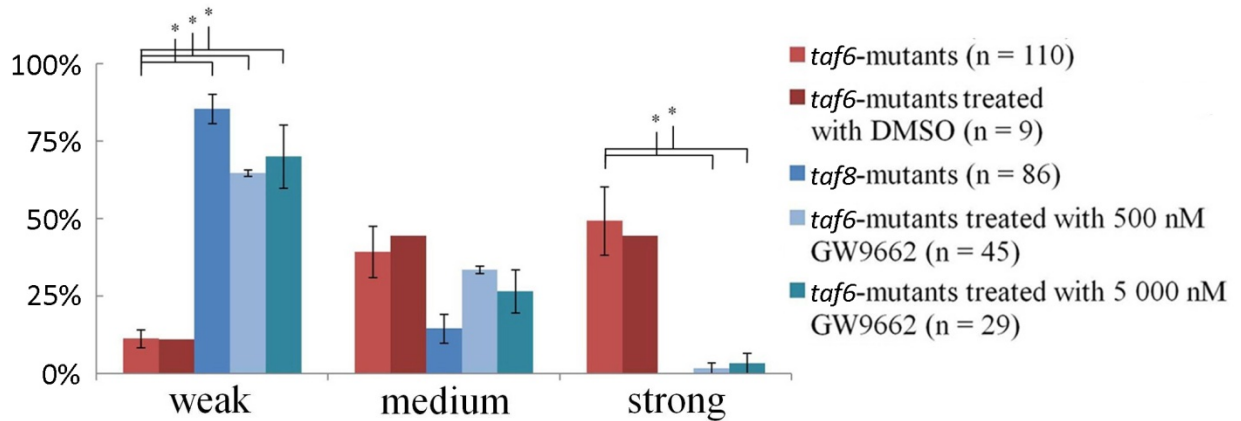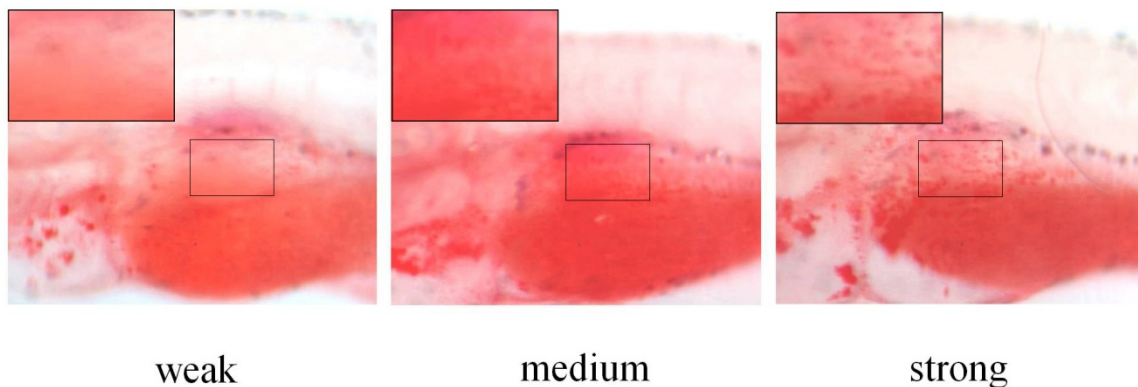
**Figure 4.8 – Lipogenesis in liver and intestinal bulb of *taf6*-mutants is Pparγ-dependent and *taf6*-independent**

Shown are side view pictures (left side) of the region containing the liver and intestine (intestinal bulb) in 5 dpf larvae. Anterior is to the left and dorsal is to the top. **B)** defines three categories for lipid staining with ORO in mutant livers and intestine. The measure for the strength of the staining is not the overall strength of the red staining, but the number of stained lipid droplets (Figure 4.7) that can be seen in the intestine and liver area in side views. The bar chart in **A)** shows the proportion of larvae from different treatment groups falling into the different lipid staining categories. Brackets with an asterisk indicate treatment groups, which are significantly different for lipid staining within the respective category, by two-tailed t-test. Oil Red O staining of fixed embryos and scoring of the stained embryos were performed by Nan Li.

A)

**Percentage of wildtype siblings falling into different categories of lipid staining (means of three experiments with respective SEMs)**

- *taf6*-mutant wildtype siblings (n = 302)
- *taf6*-mutant wildtype siblings treated with DMSO (n = 23)
- *taf8*-mutant wildtype siblings (n = 275)
- *taf6*-mutant wildtype siblings treated with 500 nM GW9662 (n = 76)
- *taf6*-mutant wildtype siblings treated with 5 000 nM GW9662 (n = 82)

weak    medium    strong

B)

weak    medium    strong
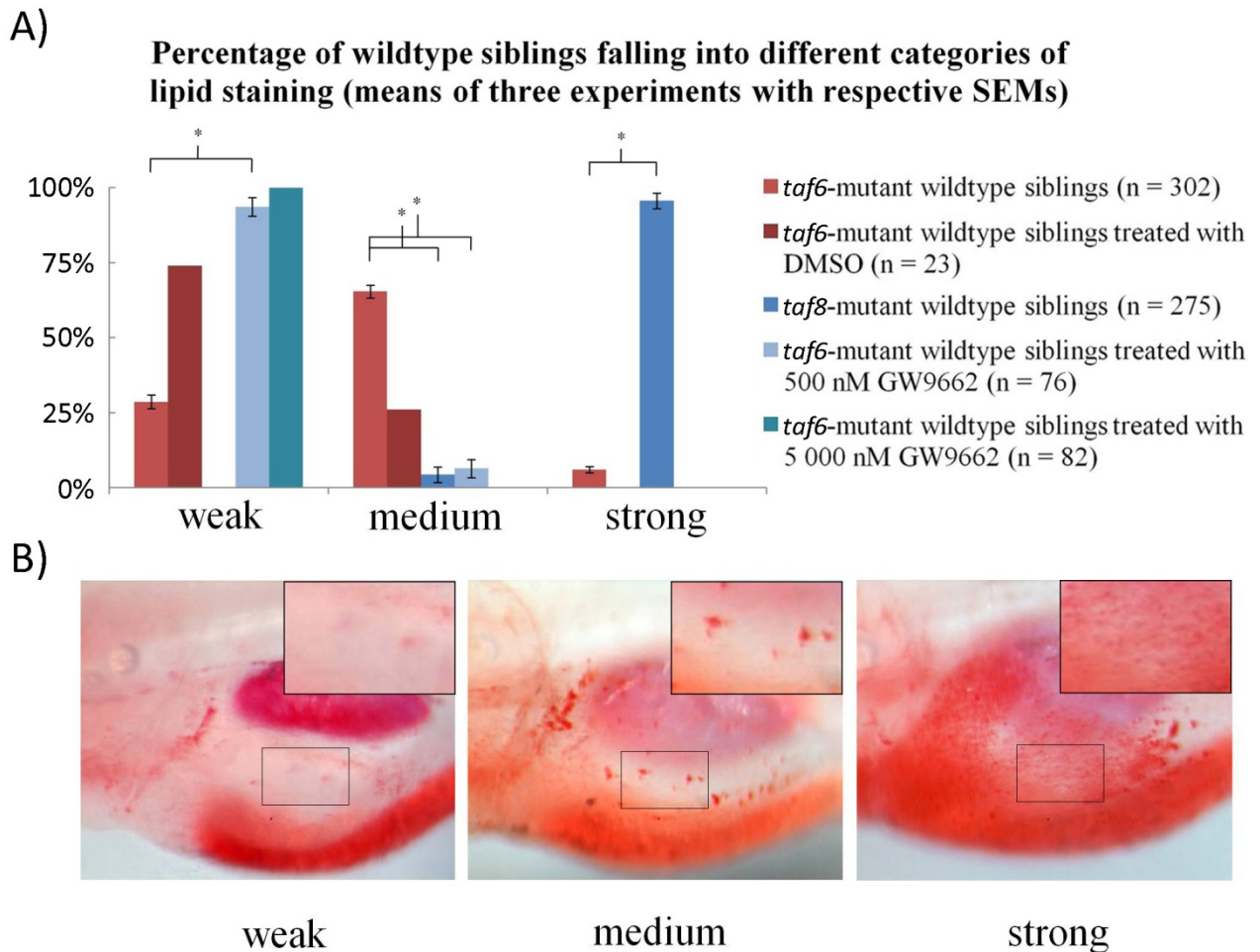
**Figure 4.9 – Lower level of lipogenesis in wildtype siblings of *taf6*-mutants compared to wildtype siblings of *taf8*-mutants**

Shown are side view pictures (left side) of the region containing the liver and intestine (intestinal bulb) in 5 dpf larvae. Anterior is to the left and dorsal is to the top. **B)** defines three categories for lipid staining with ORO in wildtype (sibling) livers and intestine. The measure for the strength of the staining is not the overall strength of the red staining, but the number of stained lipid droplets (Figure 4.7), that can be seen in the intestine and liver area in side views. The bar chart in **A)** shows the proportion of larvae from different treatment groups falling into the different lipid stainig categories. Brackets with an asterisk indicate treatment groups, which are significantly different for lipid staining within the respective category, by two-tailed t-test. Oil Red O staining of fixed embryos and scoring of the stained embryos were performed by Nan Li.

## 4.3.3 Similarities and differences of gene expression in *taf*-mutants revealed by comparative gene expression analysis

We investigated the consequences of loss of Taf8 and Taf6 on transcription in their respective mutants by comparative gene expression analysis between the respective mutants and their wildtype siblings. We addressed this question globally by performing microarray analysis using cDNAs from 4 dpf larvae. In qPCR experiments with cDNAs fom 2 and 3 dpf larvae we focused on the expression of a set of orthologs of bona fide PPARγ target genes, to address a possible requirement of Taf8 for Pparγ-activated transcription, as suggested by Mate Demeny's data.
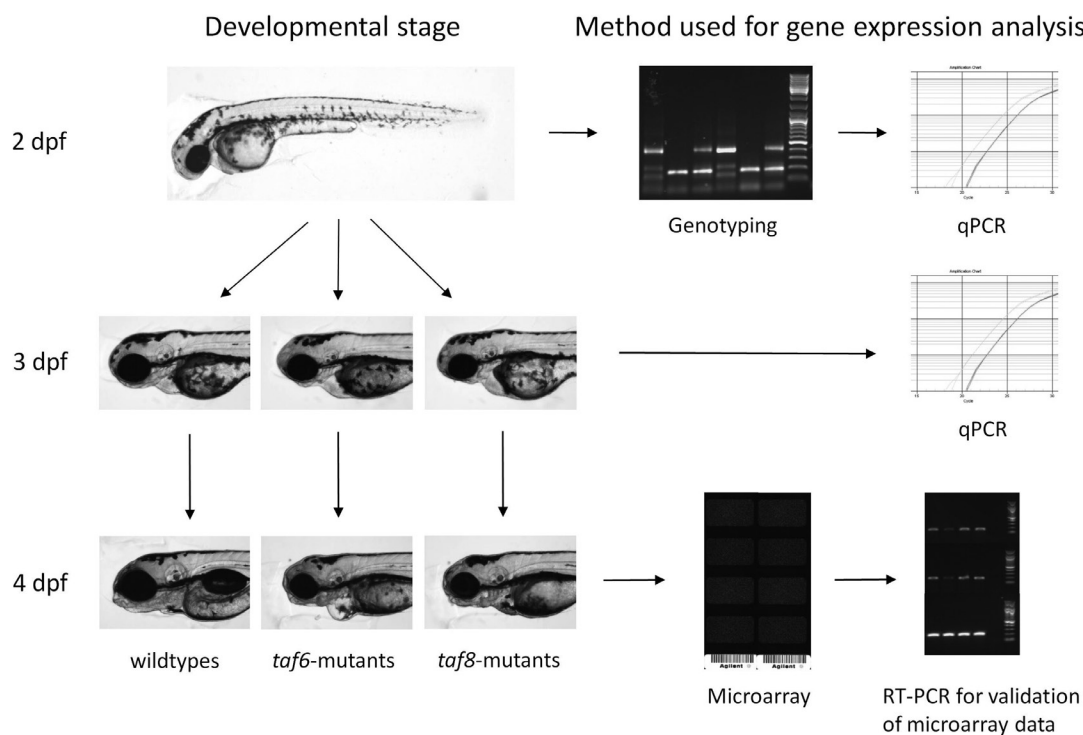


**Figure 4.10 – Stages and methods of comparative gene expression analysis**

This figure depicts the developmental stages together with the respective method used for comparative gene expression experiments with *taf*-mutants. For the 2 dpf experiment the larvae needed to be genotyped prior to cDNA preparation for qPCR. In the 2 and 3 dpf experiments the transcript levels of a selected set of orthologs of mammalian PPARγ target genes in *taf*-mutants were analysed. In the 4 dpf experiment the set of genes analysed was expanded to more than 10 000 by the use of microarray technology.

163

## 4.3.3.1 Transcriptome analysis indicates common and distinct roles of Taf8 and Taf6 in regulating gene expression during larval development

At 4 dpf, the *taf8*- and *taf6*-mutant larvae are well distinguishable from their wildtype siblings, but are not displaying the severe circulation defect, which appears at later stages. Many orthologs of mammalian PPARγ target genes and *pparγ* are co-expressed at this stage (ZFIN database). I therefore selected the 4 dpf stage for comparing the transcriptomes of *taf8*- and *taf6*-mutants to the ones of their wildtype siblings, and to each other.

I prepared total RNA from 4 dpf *taf8*-mutants, *taf6*-mutants and their wildtype siblings. This total RNA was used to prepare fluorescent labelled cRNA (complementary RNA), which then was hybridised to G2519F microarrays (Agilent, Waldbronn, Germany). Three experiments for the microarray analysis of the transcriptome of *taf8*-mutants compared to their wildtype siblings were performed. Because the three experiments included a dye swap, six microarrays were hybridised. For the comparison of the transcriptome of *taf6*-mutants to the transcriptome of their wildtype siblings only one experiment was performed (two microarrays hybridised).

Remo Sanges (Stazione Zoologica Anton Dohrn, Napoli) carried out a bioinformatic analysis of the microarray raw data, which provided lists of genes, which are significantly different expressed between mutants and wildtypes. In the case of *taf8* this list is derived from combined statistical analysis of all three experiments performed for *taf8*. For *taf6* only one experiment was performed and analysed. That means that the analysis of the microarrays comprised 12 spots for each probe in the case of *taf8*, and 4 spots for each probe in the case of *taf6* (chapter 2.6.4.3).

As expected from RT-PCR and qPCR data, *taf8* appears in the set of down-regulated genes from the *taf8*-microarray experiment and is not affected in *taf6*-mutants. This validates the reliability

of the microarray data. Unfortunately *taf6* is not represented on the array. Only a small

percentage of the 11 972 Ensembl genes represented on the microarray, approximately 2 %, are

significantly different expressed in the *taf*-mutants. There is a substantial overlap of the sets of

down-regulated genes in both mutants. About two thirds of the set of down-regulated genes in

*taf8*-mutants overlaps with the corresponding set of *taf6*-mutants. In contrast the overlap between

the respective sets of up-regulated genes is much smaller (Figure 4.11).

A)

*taf8*-mutant
*taf6*-mutant
genes on array

differentially expressed        down-regulated    up-regulated

B)

| Experiment | TAF8 microarray | | TAF6 microarray |
| --- | --- | --- | --- |
| Information | Number (Percentage) | Overlap | Number (Percentage) |
| Differentially expressed genes | 213 (1.78%) | 82 | 231 (1.93%) |
| Down-regulated genes | 114 (0.95%) | 78 | 213 (1.78%) |
| Up-regulated genes | 99 (0.83%) | 3 | 18 (0.15%) |
| Genes on array | 11 972 genes with Ensembl accession number on the array | | |

**Figure 4.11 – Overlap of the sets of regulated genes from microarray experiments**

In **A)** gene lists from the 4 dpf microarray experiments are compared to each other for overlap in Venn diagrams. The table in **B)** gives information about the number of genes in the different gene lists and about the extent of overlap between the gene lists. The numbers in the table are the numbers of genes in the respective gene lists, which have an Ensembl accession number. The associated percentage is the respective percentage of all genes with Ensembl accession number on the array. Less than 2% of the genes queried by the *taf8* and *taf6* microarray experiments are significantly different expressed in the respective mutant. The overlap between the significantly different expressed genes is substantial. More than one third of the differentially expressed genes in both mutants overlap. This overlap is due to an extensive similarity of the down-regulated genes in the two mutants. The up-regulated genes differ between the two mutants. The overlap of down- and up-regulated genes does not add up to the number of the total overlap because one gene is part of Taf8up and Taf6down.

I used the Functional Annotation Tool of the DAVID Bioinformatics Database to analyse the gene sets from the microarray experiments for enrichment of ZFIN anatomical terms, KEGG pathways and GO-terms (data not shown). The results from this analysis are in line with Figure 4.11. There is a substantial overlap of enriched anatomical terms in the set of down-regulated genes from both mutants and hardly any overlap in respect of the up-regulated genes. Only three of the enriched anatomical terms in Taf8down are not also enriched in Taf6down: Fat cell, lens, lens vesicle (Table 4.2). The appearance of the anatomical term "fat cell" only in Taf8down is a specific link of Taf8 to Ppar$\gamma$-function. PPAR$\gamma$ has been shown to regulate transcription of many genes in fat cells (Nielsen et al., 2008). Taf8down is enriched for genes which are part of the PPAR pathway. Because also Taf6down is enriched for genes belonging to the PPAR pathway, this finding does not provide a specific link of Taf8 to Ppar$\gamma$ function (Table 7.6). Furthermore, only two of the genes belonging to the PPAR pathway in Taf8down, are orthologs of bona fide PPAR$\gamma$ target genes (Table 4.6).

The anatomical term "pharyngeal arch" is enriched in Taf8down (Table 4.1). This finding is in line with the differential craniofacial defects described in chapter 4.3.2.1. The appearance of anatomical terms linked to muscle in Taf8up and Taf6up might reflect the larger diameter of the trunk observed in side views of *taf*-mutants. The KEGG pathways enriched in Taf8up strongly suggest an up-regulation of p53-dependent apoptosis in *taf8*-mutants (Table 4.5).

**Table 4.1 – Enriched ZFIN anatomical terms in the sets of up-regulated genes**

The table depicts the results of the enrichment analysis of the microarray data for ZFIN anatomical terms using the DAVID functional annotation tool. The columns in the table contain following information: Term is a specific ZFIN anatomical term. Count contains the number of genes in the analysed gene list linked to that anatomical term. The percentage (%) is the percentage of genes from the analysed list falling into the respective category (anatomical term). The p-value is a measure to assess the significance of the enrichment of genes in the analysed gene list falling into the respective category. The DAVID functional annotation tool uses a modified Fisher Exact test (EASE Score) for calculation of p-values. The default cut-off in DAVID for categories being listed is at least two genes falling into respective category and a p-value <0.1.

| Taf8 microarray | | | | Taf6 microarray | | | |
|---|---|---|---|---|---|---|---|
| **Term** | **Count** | **%** | **P-value** | **Term** | **Count** | **%** | **P-value** |
| musculature system | 6 | 17.1 | 7.86E-04 | mesoderm | 5 | 45.5 | 2.35E-05 |
| pharynx | 5 | 14.3 | 0.002885 | presumptive blood | 3 | 27.3 | 1.00E-04 |
| sternohyoid | 2 | 5.7 | 0.016241 | sternohyoid | 2 | 18.2 | 0.003766 |
| gut | 6 | 17.1 | 0.019195 | intermediate cell mass of mesoderm | 3 | 27.3 | 0.005534 |
| epidermal superficial stratum | 2 | 5.7 | 0.028255 | blood | 3 | 27.3 | 0.006424 |
| liver | 7 | 20.0 | 0.042052 | nucleate erythrocyte | 2 | 18.2 | 0.008456 |
| pharyngeal arch | 5 | 14.3 | 0.044214 | fast muscle cell | 2 | 18.2 | 0.021491 |
| proliferative region | 3 | 8.6 | 0.04557 | blood island | 2 | 18.2 | 0.027034 |
| somite | 7 | 20.0 | 0.087047 | axial chorda mesoderm | 2 | 18.2 | 0.061533 |
| fast muscle cell | 2 | 5.7 | 0.089983 | hypaxial myotome region | 2 | 18.2 | 0.069553 |
| epidermis | 4 | 11.4 | 0.096562 | | | | |

**Table 4.2 – Enriched ZFIN anatomical terms in the sets of down-regulated genes**

The columns in this table are organised like in Table 4.1

| Taf8 microarray | | | | Taf6 microarray | | | |
|---|---|---|---|---|---|---|---|
| **Term** | **Count** | **%** | **P-value** | **Term** | **Count** | **%** | **P-value** |
| **intestinal bulb** | 16 | 15.1 | 2.80E-10 | **intestinal bulb** | 37 | 19.8 | 4.35E-26 |
| **pancreas** | 12 | 11.3 | 4.47E-08 | **liver** | 44 | 23.5 | 1.13E-11 |
| **exocrine pancreas** | 6 | 5.7 | 1.77E-06 | **retinal photoreceptor layer** | 14 | 7.5 | 1.83E-08 |
| **liver** | 22 | 20.8 | 2.42E-06 | **retinal cone cell** | 7 | 3.7 | 1.07E-06 |
| **pronephric proximal straight tubule** | 3 | 2.8 | 0.004926 | **gut** | 25 | 13.4 | 4.00E-06 |
| **pronephric proximal convoluted tubule** | 3 | 2.8 | 0.005979 | **pancreas** | 13 | 7.0 | 1.09E-05 |
| **gut** | 10 | 9.4 | 0.024315 | **retinal outer nuclear layer** | 6 | 3.2 | 5.89E-05 |
| **lens** | 8 | 7.5 | 0.04881 | **eye** | 25 | 13.4 | 7.69E-04 |
| **retinal photoreceptor layer** | 4 | 3.8 | 0.057136 | **exocrine pancreas** | 5 | 2.7 | 8.48E-04 |
| **lens vesicle** | 7 | 6.6 | 0.060716 | **pronephric proximal straight tubule** | 4 | 2.1 | 0.001139 |
| **fat cell** | 2 | 1.9 | 0.06332 | **pronephric proximal convoluted tubule** | 4 | 2.1 | 0.001541 |
| | | | | **YSL** | 19 | 10.2 | 0.002831 |
| | | | | **epiphysis** | 16 | 8.6 | 0.003625 |
| | | | | **retina** | 30 | 16.0 | 0.017006 |
| | | | | **intestine** | 8 | 4.3 | 0.029788 |
| | | | | **gill** | 8 | 4.3 | 0.059054 |
| | | | | **stratum fibrosum et griseum superficiale** | 2 | 1.1 | 0.064996 |

**Table 4.3 – KEGG pathways enriched in Taf8down**

The columns in this table are organised like in Table 4.1

| Term | Count | % | P-value |
|---|---|---|---|
| dre03320:PPAR signaling pathway | 4 | 3.8 | 0.006083 |

**Table 4.4 – KEGG pathways enriched in Taf6down**

The columns in this table are organised like in Table 4.1

| Term | Count | % | P-value |
|---|---|---|---|
| dre03320:PPAR signaling pathway | 6 | 3.2 | 9.86E-04 |
| dre00982:Drug metabolism | 4 | 2.1 | 0.003867 |
| dre00980:Metabolism of xenobiotics by cytochrome P450 | 4 | 2.1 | 0.004686 |
| dre00591:Linoleic acid metabolism | 3 | 1.6 | 0.023287 |
| dre00520:Amino sugar and nucleotide sugar metabolism | 4 | 2.1 | 0.040761 |
| dre00260:Glycine, serine and threonine metabolism | 3 | 1.6 | 0.070900 |
| dre00140:Steroid hormone biosynthesis | 3 | 1.6 | 0.077280 |
| dre00250:Alanine, aspartate and glutamate metabolism | 3 | 1.6 | 0.083835 |

**Table 4.5 – KEGG pathways enriched in Taf8up**

The columns in this table are organised like in Table 4.1

| Term | Count | % | P-value |
|---|---|---|---|
| dre04115:p53 signaling pathway | 3 | 8.6 | 0.006307 |
| dre04110:Cell cycle | 3 | 8.6 | 0.024537 |
| dre04010:MAPK signaling pathway | 3 | 8.6 | 0.067443 |

**Table 4.6 – Genes belonging to the PPAR pathway down-regulated in *taf*-mutants**

Shown in the first two columns are the genes belonging to the KEGG PPAR pathway and the mutants, in which they are down-regulated. The third column gives the full gene names. The third column gives information about which PPAR isotype has been shown to regulate the respective gene. This information is derived from the nuclear receptor resource database.

| Genes belonging to PPAR pathway | | | |
|---|---|---|---|
| *taf6*-mutants | *taf8*-mutants | Gene Name | PPARγ target? (nrresource.org) |
| cd36 | cd36 | CD36 antigen | PPARα, β and γ |
| fabp6 | fabp6 | fatty acid-binding protein 6, ileal | PPARα and β |
| scp2a | scp2a | sterol carrier protein 2 | PPARα |
| - | fads2 | fatty acid desaturase 2 | PPARα and γ |
| cyp8b1 | | cytochrome P450, family 8, subfamily B, polypeptide 1 | PPARα |
| acsl5 | | acyl-CoA synthetase long-chain family member 5 | PPARγ |
| pck2 | | phosphoenolpyruvate carboxykinase 2 (mitochondrial) | PPARα and γ |

## 4.3.3.2    Gene expression in 2 dpf and 3 dpf mutants

The 4 dpf microarray analysis did not convincingly demonstrate a requirement of Taf8 for Pparγ-dependent transcription. However, some findings are suggestive for a link between both factors, for example the enrichment of the anatomical term "fat cell" in Taf8down. To exclude the possibility, that a requirement of Taf8 for Pparγ-dependent transcription was missed due to the limitations of microarrays, I decided to analyse the expression of a small set of zebrafish othologs of well established PPARγ target genes by qPCR. This method has higher specificity, sensitivity and covers a wider dynamic range for the quantification than microarray analysis.

Transcription regulation has direct and indirect consequences due to epistatic relationships of genes. It is therefore important to aim for the earliest possible detection of changes, when looking

for direct regulatory roles of a factor. I decided to analyse the expression of orthologs of PPARγ target genes at two stages, 2 dpf and 3 dpf. At 2 dpf, *taf8*-mutants and *taf6*-mutants are indistinguishable from each other. However, transcriptional mis-regulation, causative for the later appearing morphological phenotype, might already occur at this stage. Three dpf is the developmental stage when the *taf*-mutant phenotypes manifest morphologically. Because the morphological differences between mutants and wildtypes are rather subtle at that stage, it can be assumed, that differences in the quantification of tanscript levels, due to differences in the morphology between wildtypes and mutants, will be minimal. The transcript levels of following othologs of PPARγ target genes were analysed by qPCR:

LPL (lipoprotein lipase):

LPL is an enzyme which is hydrolysing the TGs in chylomicrons and in VLDL. The TG depletion turns VLDL into IDL (LDL) and chylomicrons into chylomicron remnants (Eckel, 1989, Goldberg and Merkel, 2001). The TGs are hydrolysed into two FFA (free fatty acid) molecules and into one monoacylglycerol molecule. LPL is a secreted protein, which is produced in the parenchymal cells of heart, skeletal muscle and adipose tissue. The secreted enzyme transverses the endothelial layer and gets anchored to the luminal surface of vascular endothelial cells via interactions with proteoglycans and GPIHBP1 (glycosylphosphatidylinositol-anchored high-density lipoprotein-binding protein 1) (H. Wang and Eckel, 2009).

CD36 molecule (thrombospondin receptor):

CD36 is a surface protein present on many mammalian cell-types including platelets, macrophages, hepatocytes, adipocytes and enterocytes (Febbraio et al., 2001). It is the fourth major glycoprotein on the platelet surface (Clemetson et al., 1977). CD36 seems to play a role in cell adhesion, because it is a receptor for thrombospondins, proteins involved in cell adhesion

(Asch et al., 1987, Silverstein et al., 1992) . Furthermore, CD36 also functions as a scavenger receptor, which is recognising molecular patterns on potential pathogens, which are then cleared by phagocytosis. CD36 was shown to be a negative regulator of angiogenesis (Dawson et al., 1997). Another important function of CD36 is promoting fatty acid uptake in adipocytes, muscle, liver and intestine (Abumrad et al., 1993, Coburn et al., 2000, Nassir et al., 2007, Zhou et al., 2008).

FABP2 and FABP4 (fatty acid-binding proteins):

FABPs are intracellular fatty acid-binding proteins. They are thought to associate with lipids to guide them to their destination in the cell (e.g. lipid droplets, endoplasmatic reticulum and nucleus). Therefore they are also regarded as lipid chaperones. The FABP-family contains at least nine members: FABP1 (Liver FABP, L-FABP), FABP2 (Intestinal FABP, I-FABP), FABP3 (Heart FABP, H-FABP), FABP4 (Adipocyte FABP, A-FABP), FABP5 (Epidermal FABP, E-FABP), FABP6 (Ileal FABP, Il-FABP), FABP7 (Brain FABP, B-FABP), FABP8 (Myelin FABP, M-FABP), FABP9 (Testis FABP, T-FABP). This nomenclature is misleading because the FABPs are not exclusively expressed in the name giving tissue. Liver FABP is for example also expressed in pancreas and kidney.

FABP2 (I-FABP) is expressed throughout the intestine and in the liver. Its Mouse knock out suggest that FABP2 is not essential for dietary fat absorption, which is likely due to compensation by the other two FABPs expressed in the intestine, FABP1 (L-FABP) and FABP6 (Il-FABP).

FABP4 is used as a molecular marker for differentiated adipocytes, where its expression is regulated by PPARγ (Hunt et al., 1986, Nielsen et al., 2008). It is also expressed at lower levels in macrophages (Makowski et al., 2001), dendritic cells (Rolph et al., 2006) and in bronchial

epithelial cells (Shum et al., 2006). Because FABP4 deficiency in mouse models and humans seems to have a protective effect against disorders associated with the metabolic syndrome, insulin resistance (diabetes 2) and atherosclerosis, it was suggested as a drug target against those disorders (Furuhashi and Hotamisligil, 2008, Tuncman et al., 2006, Uysal et al., 2000).

The fish-specific whole genome duplication event in the actinopterygian lineage (Meyer and Van de Peer, 2005) has resulted in two copies of the ortholog of the mammalian FABP4 gene, *fabp11a* and *fabp11b*, in zebrafish. The co-expression of *fabp11a* with *pparγ* in neutral lipid accumulating cells, presumptive adipocytes, suggests that this gene is the functional as well as the evolutionary ortholog of FABP4 (Flynn et al., 2009). However, also *fabp11b* is co-expressed with *pparγ*, in the liver and intestine, and its expression can be stimulated by administration of a PPARγ agonist (Jones et al., 2008).

SLC27A1 (solute carrier family 27 (fatty acid transporter), member 1; FATP1):

FATPs are integral membrane proteins, which facilitate the uptake of long-chain fatty acids. Because they possess acyl-CoA synthetase activity, they are thought to combine the uptake with CoA-esterification of the fatty acids (Wiczer and Bernlohr, 2009). The FATP-family comprises six members in mammals, which show tissue-specific expression patterns (Hirsch et al., 1998).

FATP1 was initially identified as a fatty acid transporter in adipocytes (Schaffer and Lodish, 1994). FATP1 is expressed in tissues with high fatty acid uptake like adipose, skeletal muscle and heart (Kim et al., 2004). The majority of FATP1 seems to be associated with intracellular structures and it tanslocates to the plasmamembrane in response to insulin (Stahl et al., 2002).

Due to the aforementioned genome dublication event, zebrafish contains two genes encoding for mammalian FATP-1 orthologs, *slc27a1a* and *slc27a1b*. The gene analysed in the comparative gene expression experiments at 2 and 3 dpf was *slc27a1a*. Its duplicate, *slc27a1b,* was not

174

differentially expressed between *taf8*-mutants and their wildtype siblings in the 4 dpf microarray experiments.

The results of the 2 dpf analysis of transcription are shown in Figure 4.12. The transcript levels of Taf8 and Taf6 are severely reduced in their mutants, while they are unaffected in the respective other mutant. There are no significant changes in the transcript levels of the other genes.

The study of transcription in 3 dpf *taf*-mutants revealed a tendency of orthologs of PPARγ target genes to be down-regulated in *taf8*-mutants at that stage (see Figure 4.12). However, after statistical analysis of the data, the 3 dpf experiments fail to demonstrate a convincing defect in Pparγ-activated transcription in *taf8*-mutants compared to their wildtype siblings and *taf6*-mutants. There is only one statistically significant down-regulated gene besides the respective *taf* gene in both *taf*-mutants. That gene is *cd36*. It is not significant different regulated between the two mutants by two-tailed t-test. Lpl levels are significantly different between the mutants, but it is not significantly down-regulated in *taf8*-mutants.

**A)**

Transcript levels of orthologs of mammalian PPARγ target genes in zebrafish *taf*-mutants (means of 3 experiments and respective SEMs)

**B)**

Transcript levels of orthologs of mammalian PPARγ target genes in zebrafish *taf*-mutants (means of 5 experiments and respective SEMs)
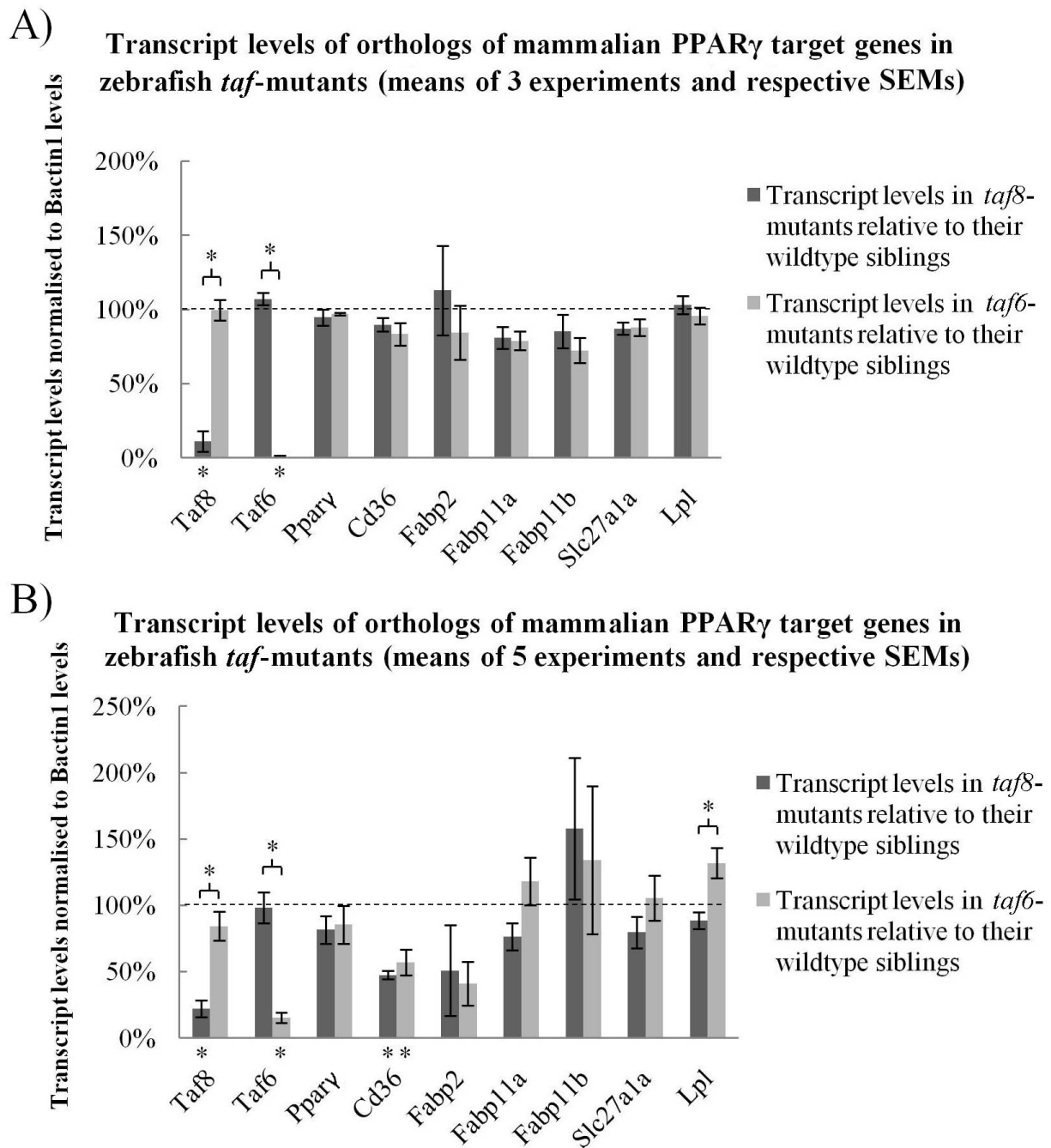
**Figure 4.12 – Expression of orthologs of PPARγ target genes in *taf8*- and *taf6*-mutants**

Shown are bar charts depicting relative transcript levels of Taf8, Taf6, Pparγ and orthologs of PPARγ target genes at 2 dpf **A)** and 3 dpf **B)**, comparing mutants to wildtypes. The transcript levels were normalised to Bactin1 levels. Brackets with an asterisk indicate genes which are significantly different regulated between *taf8*- and *taf6*-mutants by two-tailed t-test. Asterisks below the x-axis label genes which are significantly different regulated between mutant and wildtype siblings by two-tailed t-test. The Fabp2 qPCRs were performed by Irene Miguel.

176

## 4.4 Discussion

### 4.4.1 Similarities and differences in the mutant phenotypes for *taf8* and *taf6*

The *taf8*- and *taf6*-mutants display very similar morphological defects (see Figure 4.3). Their mutant phenotype manifests beginning with early larval stages (around 3 dpf) and from then onwards subsequent developmental processes are generally impaired in zygotic mutants due to the lack of essential gene function. Most of the anterior organs and structures are smaller comparing mutants to wildtypes. They share this phenotype with many other zebrafish mutants for essential genes (Amsterdam et al., 2004). An explanation for this phenomenon would be the following:

There is a substantial maternal supply of the gene products for housekeeping genes (essential genes) which is sufficient for most of zebrafish embryonic development up into early larval stages. The maternal supply runs out during early larval stages and beginning from then on developmental processes (proliferation, cell and organ growth, differentiation) are generally impaired, because of the lack of a cell-essential gene. That would lead to the phenotype observed for many essential genes because the developmental changes in size and shape of the organs are more dramatic at the anterior part than in trunk and tail. The general phenotype is actually the manifestation of a general cellular defect, delayed by maternal supply of the gene product.

That the principle described above, to a certain extend applies to the *taf*-mutants, cannot be excluded. Full TFIID might be required for mitotically dividing cells. Partial TFIID complexes

and/or alternative complexes might be required to restrict transcriptional programmes to specific cell-types, during differentiation and meiosis (Deato and Tjian, 2007, Gazdag et al., 2009).

Most likely the phenotypes for *taf8* and *taf6* are mixtures of both, a general phenotype and a *taf*-specific phenotype. The general cellular defect is mostly affecting mitotically dividing cells (cell cycle defect) and the resulting general phenotype is similar for both mutants. Cell cycle defects have been demonstrated for yeast Taf-mutants (Green, 2000). Additionally to the similarities there are subtle differences due to a specific function of the particular Taf in certain cell lineages. Both mutants develop a circulation defect and pericardial edema around 4 dpf. As a prerequisite to address the question whether this circulation defect is caused by a heart defect of by a mis-development of the vasculature I crossed the *taf*-mutants to the *fli1a:EGFP gata1:dsRed* transgenic line. In this transgenic line the *fli1a:EGFP* transgene labels the vasculature and the *gata1:dsRed* transgene labels red blood cells. The mutant transgenic lines to date not were fully analysed for defects in the vasculature. The overall pattern of the vasculature looks similar between both, mutant transgenics and their wildtype siblings (data not shown). However, a relatively high incidence of haemorrhages, predominantly in the brain, was observed in the *taf8*-mutant line (72 mutants and 38 wildtype siblings out of 2982 examined larvae). This hemorrhage phenotype is literally absent in the *taf6*-mutant line. Considering the expression of some zebrafish orthologs of PPARγ target genes in the head vasculature and the hemorrhage phenotype of *pparγ* ko mice, this would be interesting to follow up. Adipogenesis is coordinated with angiogenesis and a vascular niche has been suggested for preadipocytes (Billon et al., 2010, Hausman and Richardson, 2004). The *taf8*-mutant transgenic line might prove in the future useful in establishing a link between Taf8 and Pparγ.

The circulation defect might be the primary cause of death of the *taf*-mutants starting at stages beyond 5 dpf. At 5 dpf the edema restricted to the pericardium at 4 dpf has developed into whole-body edema in a certain proportion of the mutants. The mutants displaying whole body edema also display a strong circulation defect. The lack of circulation is causing a lack of supply of peripheral tissues with nutrients and oxygen. Consequently the peripheral tissue is dying and shows opaque appearance by light microscopy. At stages beyond 5 dpf, dead mutant embryos, completely lacking a visible heart beat are observed. There is a difference in the proportion of whole body edema displaying embryos at 5 dpf between *taf6* and *taf8*-mutants.

In this thesis I describe a statistically different phenotype between *taf8*- and *taf6*-mutants regarding the pharyngeal skeleton. The pharyngeal skeleton of *taf8*-mutants appears larger throughout early larval stages (3-5 dpf) in side views (Figure 4.6). I also found a corresponding difference in the mutant phenotypes regarding craniofacial cartilages at 5 dpf. Some of the cartilaginous elements appear larger in side views of *taf8*-mutants than in side views *taf6*-mutants (Figure 4.4, Figure 4.5). This is unlikely to be explained simply by differences in position and orientation of the respective elements, because differences are also observed in ventral views and side views.

Most of the zebrafish head skeleton develops from CNC. The CNC migrates to specific positions in the head, where the postmigratory CNC then develops into specific cartilaginous elements (Kimmel et al., 2001). The patterning of the skeletal derivatives of the postmigratory CNC is achieved via a combination of intrinsic signals, depending on the origin of the premigratory CNC in the brain, and extrinsic signals from adjacent tissues (Knight and Schilling, 2006).

The craniofacial defects observed in the *taf*-mutants do not clearly suggest a defect in the patterning of the craniofacial cartilages. There is no clear difference in the degree of defects

along the anterior-posterior axis, or along the dorsal ventral axis. Also the shape of the neurocranium in the mutants does not suggest a defect in the midline. However, the kink in the neurocranium of *taf8*-mutants might be caused by a lack or overgrowth of the overlying brain tissues. There is also no obvious fusion of head cartilages, but their presence was not thoroughly investigated by flat mouting of dissected alcian blue stained head skeletons on slides. Whether there is a defect in CNC was not addressed in this study, where the mutant phenotype analysis focused on early larval stages, after the migration of CNC (Yelick and Schilling, 2002).

## 4.4.2 Link of Taf8 to Pparγ function

A functional interaction of TAF8 with PPARγ has been demonstrated *in vitro* for the human proteins by Mate Demeny (Tora lab, Strasburg). One objective of this thesis was to establish a link of Taf8 to Pparγ function *in vivo* using zebrafish model. Both factors have been implicated in adipogenesis (see chapter 1.3). Because of this biological link of TAF8 and PPARγ via adipogenesis, the focus of the phenotype characterisation exploring a potential role of Taf8 for Pparγ was on aspects of PPARγ linked to fat cells and their function (lipogenesis, adipocyte PPARγ target genes).

### 4.4.2.1 Craniofacial defect might be linked to Pparγ

To date, only a few studies on adipogenesis during early zebrafish development have been carried out. There is conflicting data about the first appearance of adipocytes during early zebrafish development. One study observed the first preadipocytes at 6 dpf in the pancreas. These cells begin to accumulate neutral lipids at 8 dpf. They also found that feeding is required for the

formation of the visceral preadipocytes (Flynn et al., 2009). Another study described the appearance of lipid accumulating cephalic adipocytes at an earlier stage, at 120 hpf. These adipocytes reside in the region of the developing hyomandibular skeleton which expresses the adipocyte marker *cebpa* beginning with 48 hpf. One of those regions is the second pharyngeal arch (N. Li et al., 2010). The 4 dpf microarray data is in line with the differential pharyngeal skeleton phenotypes of the *taf*-mutants (see chapter 4.3.3.1).

This provides a possible link of the *taf8*-mutant phenotype to Ppar𝛾. There is a differential phenotype of the pharyngeal skeleton between the two *taf*-mutants. The pharyngeal skeleton of *taf8*-mutants is significantly larger. It has been previously demonstrated that cephalic adipocytes and osteoblasts share a common ancestor, mesenchymal stem cells (MSC) derived from cephalic neural crest. There is a reciprocal relationship between the differentiation of those MSC into adipocytes or osteoblasts. One goes on the expense of the other ((N. Li et al., 2010). To address the question, if there is increased osteogenesis in *taf8*-mutants compared to *taf6*-mutants and their wildtype siblings, Nan Li (Mueller group, University of Birmingham) performed alizarin red stainings of calcified bones with 5 dpf larvae. The results were negative. There is a comparably defect in osteogenesis in both mutants (data not shown). However, MSC can also differentiate into chondrocytes. If adipogenic differentiation is blocked due to impaired function of Ppar𝛾 in *taf8*-mutants, this might cause an increase of chondrogenesis and a relative enlargement of the pharyngeal skeleton in *taf8*-mutants compared to *taf6*-mutants.

## 4.4.2.2    Specific defect in Pparγ-dependent lipogenesis in *taf8*-mutants

The strongest link between Taf8 and Pparγ function found in this thesis is the specific defect in lipogenesis in *taf8*-mutants relative to their wildtype siblings and *taf6*-mutants (see chapter 4.3.2.2). The *taf8*-mutants display a defect in the accumulation of Oil Red O stainable lipid droplets in liver and intestinal bulb. This lipogenic process in liver and intestinal bulb can be blocked in *taf6*-mutants with a PPARγ inhibitor. Taken together the data suggests that the observed lipogenic process is *taf8*-and Pparγ-dependent, but *taf6*-independent.

The PPARγ inhibitor used for those experiments was GW9662, which binds irreversibly to the LBD of all three PPAR subtypes by forming a covalent bond (arylation) with a conserved cysteine residue (Leesnitzer et al., 2002). This cysteine residue is not present in zebrafish Pparγ, although there is another cysteine residue present in close vicinity in the primary structure of zebrafish Pparγ. It has been demonstrated by reporter gene assays with full length PPARs that GW9662 is functionally a subtype selective PPARγ antagonist, with a nanomolar $IC_{50}$ (half maximal inhibitory concentration) (Leesnitzer et al., 2002).

Another finding was a clear difference in the staining behaviour of the wildtype siblings of the *taf*-mutants compared to the wildtype siblings of *taf8*-mutants. The data suggests reduced lipogenesis in liver and intestine in the *taf6*-mutant line.

Interestingly, in a study on a gene important for fat storage, a similar lipogenesis phenotype was observed. In this study *fit2* (fat induced transcript 2) morphants showed severely reduced ORO staining in intestine and liver compared to control larvae, after feeding of 6 dpf larvae with a high fat diet (Kadereit et al., 2008).

## 4.4.2.3     Similarities and differences in Taf8- and Taf6-dependent transcription of genes expressed in larval zebrafish

The results from the comparative gene expression experiments with *taf*-mutants give some support to the hypothesis that Taf8 is required for Ppar function. But the data is not entirely convincing. The Taf8down gene set from the 4 dpf microarray experiments is enriched for genes belonging to the PPAR pathway. But the same is the case for Taf6down. Taf8down is also enriched for genes linked to the anatomical term "fat cell", a cell-type in which PPARγ plays a crucial role for the transcription of many genes (Nielsen et al., 2008). Taken together, the link of Taf8down to Pparγ is there, but it is not very convincing.

The Taf8up and Taf6up gene sets are dissimilar and so are the enriched anatomical terms and KEGG pathways within them. The exception is that genes linked to muscle are enriched in both sets, what might reflect the larger diameter of the trunk observed in side views of *taf*-mutants compared to their respective wildtype siblings. The enriched p53 pathway in Taf8up strongly suggests substantial apoptosis in *taf8*-mutants. Interestingly, this up-regulation of genes indicating p53-mediated apoptosis is not observed in 4 dpf *taf6*-mutants. This finding is in line with the proposed coactivator function of TAF6 for p53.

The comparative gene expression experiments performed with 2 dpf and 3 dpf larvae failed to reveal a convincing specific down-regulation of orthologs of PPARγ target genes in *taf8*-mutants. At 2 dpf, most of the examined genes are not significantly different expressed between wildtypes and mutants. This suggests that parallel to the phenotypes, there is also hardly any difference in gene expression between mutants and wildtypes. The picture changes at 3 dpf. Now more mis-regulation of transcription appears. The ortholog of the PPARγ target gene LPL is significantly

different regulated between *taf8*-mutants and *taf6*-mutants. However, Lpl is not significantly down-regulated between *taf8*-mutants and their wildtype siblings.

In conclusion the 2 dpf and 3 dpf experiments did not reveal a specific requirement of Taf8 for Pparγ-dependent transcription. However, there is a tendency of orthologs of PPARγ target genes in *taf8*-mutants to be lower expressed relative to their wildtype siblings and to *taf6*-mutants at 3 dpf. The addition of more biological repeats might turn these tendencies into statistically significant differences.

## 4.5    Conclusions

1. Zebrafish *taf8* and *taf6* are both essential genes for development. Their zygotic mutant phenotypes morhologically manifest around 3 dpf. The fact that the first defects appear after embryogenesis, during early larval stages, suggests contribution of maternally supplied Taf8 and Taf6 protein to development. The *taf8* and *taf6* transcript levels are already severely reduced at 2 dpf, as a consequence of the insertional mutation. The mutants display a general underdevelopment of most structures and organs, which is more pronounced in the anterior part of the larvae. In both mutants the diameter of the trunk is significantly larger than the one of their wildtype siblings, what might reflect the up-regulation of genes linked to muscle at 4 dpf.

2. There is clearly a high degree of similarity on the global morphologies between the *taf8*- and *taf6*-mutants. This similarity might be explained by a general cellular defect, which is attenuated and delayed by a substantial maternal supply of the respective gene products. However, a more detailed characterisation of the phenotypes revealed subtle differences in the phenotypes. Those differences are not simply differences in the degree of the observed defects, resulting from a

different degree of LOF for a TFIID core subunit. If this was the case, then all defects would be stronger in one of the mutants. However, some of the observed defects are more severe in *taf8*-mutants (lipogenesis defect, kink in neurocranium) and others are more severe in *taf6*-mutants (edema, diameter of ceratohyal). That argues against the possibility that both mutants merely reflect different degrees of the same phenotype, caused be destabilisation of TFIID. It more likely reflects differential functions of those two Tafs during zebrafish development.

3. This study did not convincingly demonstrate a requirement of Taf8 for Pparγ function. Future work must link the lipogenesis defect observed in liver and intestine of 5 dpf *taf8*-mutants to down-regulation of Pparγ target genes in those tissues. It also might be worth to explore the significance of the increased incidence of hemorrhages observed in the brain of *taf8*-mutants, given the expression of some orthologs of PPARγ target genes in the head vasculature.

The transcriptome analysis indicates that some aspects of Taf8 regulated gene expression are distinct from that of Taf6 and include a specific requirement for fat cell differentiation. This observation suggests that at least some aspects of Pparγ regulated gene expression are likely specifically Taf8-dependent. However, other aspects of Pparγ-dependent gene expression require both Taf8 and 6 (genes in KEGG PPAR pathway).

# 5 Generation of a zebrafish model for ARC-syndrome

## 5.1 Introduction and Overview

Zebrafish is becoming increasingly used as a model for lipid-metabolism and the development and pathologies of associated organs, such as the liver. Liver development in zebrafish is rapid and at 5 dpf the liver is nearly fully functional, displaying bile production, serum protein secretion, glycogen storage, lipogenesis and xenobiotic metabolism (Chu and Sadler, 2009). The transcriptional networks controlling hepatogenesis appear to be very similar between zebrafish and mammals. The same is true for liver function, cellular composition and many pathologies like hepatocarcinogenesis (Lam et al., 2006). But there are also differences, which are not necessarily disadvantages for using zebrafish as a model for liver biology.

The teleost liver has a different architecture from the mammalian liver. The arrangement of vasculature, the biliary network and other liver cell-types into an organ differs, but the function of the organ is conserved. An exception is embryonic hematopoiesis, which takes place in the liver of mammals but not in the liver of zebrafish. Therefore defects in liver development in zebrafish will not lead to early lethality associated with hematopoietic dysfunction. Also, early liver development in zebrafish is independent from vasculogenesis and therefore not affected by a defective vasculogenesis. Because of the substantial maternal contribution to early development, zebrafish mutant phenotypes are often milder than their mammalian counterparts. This enables one to study the role of genes, which are early embryonic lethal when mutated in mouse, at later stages of development, e.g. during organogenesis, in zebrafish model. For instance, the

requirement of Hdac1 in liver and pancreas formation could only be revealed in the context of the milder zebrafish *hdac1* mutant phenotype and not in the more severe mouse mutant phenotype (Noel et al., 2008).

In the last decade zebrafish became increasingly used as a model for hepatobiliary development and diseases. Matthews et al. showed that zebrafish members of the onecut family of transcription factors, *onecut1* (Hnf6 ortholog) and *onecut3* play a role in intrahepatic biliary development (Matthews et al., 2008, Matthews et al., 2004). Analysis of the kd phenotypes of zebrafish *jagged* and *notch* genes established a role of Jagged-mediated Notch signalling in biliary development. The defects observed in the *jagged* and *notch* morphants were also in line with a phenocopy of the multisystem disorder Allagille syndrome, which is in the majority of the cases caused by haploinsufficiency for Jagged 1 (Lorent et al., 2004). Sadler et al. screened, in conjunction with a large scale mutagenesis screen, for mutants displaying hepatomegaly, which is a hallmark of many liver diseases (Sadler et al., 2005). They identified three mutants displaying signs of hepatic pathology. The mutant for the tumor suppressor *nf2* (*neurofibromatosis2*) displays type I and type II choledochal cysts. The *fgr*-mutant (*foie gras*) showed defects resembling non-alcoholic steatohepatitis (NASH, hepatocyte enlargement, steatosis and death), but displayed no signs of hepatic inflammation. Pigmentation defects, hepatomegaly and biliary paucity were observed in the third mutant, the mutant for *vps18*. The pigmentation defects and the hepatomegaly might be caused by the failure of targeting endosomes to pigment granules in melanocytes and to lysosomes in hepatocytes.

The congenital metabolic disease ARC syndrome comprises the disorders arthrogryposis (joint contractures), renal dysfunction (wasting of sugars and amino acids in the urine) and cholestasis (reduced bile flow). Other defects observed in ARC are lipid malabsorption, diarrhea, poor

187

growth, dysmorphic facial features, reduced motor neuron density, ichthyosis and platelet defects (Eastham et al., 2001). Most cases of ARC-syndrome are caused by mutations in the *VPS33B* gene, an otholog of the yeast class C vacuolar protein sorting protein Vps33p. Hepatic defects observed in ARC-syndrome comprise hepatomegaly, severely reduced intrahepatic bile flow (cholestasis) associated with mislocalisation of canalicular markers, biliary paucity (hypoplastic peripheral biliary radicles), hepatocyte giant-cell transformation and intrahepatocyte pigment accumulation (Gissen et al., 2004, Gissen et al., 2006, Horslen et al., 1994).

Matthews et al. analysed the kd phenotype of zebrafish *vps33b* and found that the morphants display a phenotype in line with a partial phenocopy of the digestive defects in ARC-syndrome (Matthews et al., 2005). They determined the expression patterns of *vps33b* by whole-mount *in situ* hybridisation. At early stages *vps33b* is broadly expressed. Beginning with 48 hpf the expression patterns becomes more restricted to the brain, retina, ear, liver and proximal intestine. The reticular pattern of *vps33b* expression in the liver suggested expression predominantly in biliary epithelial cells. Electron micrographs showed a disrupted ultrastructure of biliary epithelial cells and the accumulation of vesicles in their cytoplasm. Keratin 18 immunostaining of livers revealed a reduction in the terminal branches of the biliary tree, a reduction in interhepatic interconnecting ducts and terminal ductules in the morphants. Ultrastructural defects also have been observed in enterocytes, which display Golgi abnormalities and accumulation of cytoplasmic vesicles. Furthermore labelling experiments using a fluorescent lipid (AM1-43) used to track exocytosis showed evidence of altered vesicle transport in enterocytes. The defects observed in biliary epithelial cells and in enterocytes point to a defect in intracellular trafficking.

PED6 is a fluorescent phospholipid, which green fluorescence is quenched until the quencher is cleaved off by the intestinal enzyme phospholipase A2. Processed PED6 accumulates in the

188

intestine and in the gall bladder via the hepatobiliay system. The PED6 assay can be used in zebrafish to visualise biliary morphology, and to test biliary secretion and intestinal lipid absorption. Zebrafish *vps33b*-morphants display reduced PED6 fluorescence in the gall bladder. The observed biliary and intestinal defects probably both contribute to the PED6 phenotype.

## 5.2  Aims

It was one of my personal objectives for my PhD, to receive training and gain experience in using zebrafish as a model to study genes linked to lipid-metabolism and metabolic disorders, like *pparγ*. A collaborative project with the group of Paul Gissen (University of Birmingham) offered an opportunity to generate a zebrafish model for a metabolic disease, ARC-syndrome.

A human *VPS33B* interacting protein, identified by yeast two-hybrid assay, was found to be the causative mutation in patients with classical ARC without mutations in *VPS33B*. This gene was named *VIPAR* (VPS33b-interacting protein involved in polarity and apical protein restriction). In his PhD-project Andrew R. Cullinane (Paul Gissen-group, University of Birmingham) functionally characterised this new gene and placed it in a novel intracellular trafficking pathway together with *VPS33B* and *Rab11a*. This pathway is required for normal epithelial polarisation and development in liver and kidney. We chose zebrafish to test the cell culture and ARC-patient data based finding that VIPAR and VPS33b act in the same pathway, which is disrupted in the pathogenesis of ARC-syndrome, in an *in vivo* model. We functionally characterised the zebrafish *vipar* LOF-phenotype in comparison to the published *vps33b* LOF-phenotype (Matthews et al., 2005) in collaboration with the Gissen-group. Similarities of the phenotypes would argue for both genes playing a role in the same pathway, in support of the findings of Andrew R. Cullinane.

Furthermore the work on *vipar* would additionally to the work on *ppar γ* explore the suitability of zebrafish as a model for genes linked to lipid-metabolism and metabolic diseases.

Major aims and questions to answer by this study were:

1. What are the expression patterns of *vipar*? Are they overlapping with the expression patterns of *vps33b*?

2. What is the effect of LOF of *vipar* on lipid-metabolism and biliary development?

# 5.3    Results

First we determined the expression patterns of *vipar*-mRNA by whole-mount *in situ* hybridisation. The *vipar* message is broadly expressed at embryonic stages and later becomes more restricted. At 5 dpf there is substantial expression of *vipar* in the liver, intestine and also pancreas (Figure 5.1). The expression patterns of *vipar* and *vps33b* overlap during embryonic and early larval stages.

We performed MO-mediated kd experiments of *vipar*, by injections of MOs targeting the ATG and the splice site for exon 3 into one cell stage embryos. At a concentration of 100 µM in the injection solution the *vipar* ATG MO caused a severe growth defect phenotype (data not shown). At a concentration of 10 µM (ATG MO) and 100 µM (Exon 3 MO) the targeting MOs caused a milder phenotype compatible with a partial phenocopy of ARC-syndrome at 5 dpf.

Like the *vps33b*-morphant the *vipar*-morphants display defects resembling the digestive and hepatobiliary defects observed in ARC (Figure 5.1). The terminal part of the intrahepatic biliary tree is underdeveloped in *vipar*-morphants and they accumulate less PED6 through the hepatobiliary system in their gall bladders than control MO injected and non-injected larvae (Figure 5.1). Additionally, decreased expression of the adherens junction protein E-cadherin was observed by immunohistochemistry in livers of *vipar*-morphants, similar to what was observed in the livers of ARC-patients (Figure 5.1).

The similarities between the defects observed in *vipar*/*vps33b* morphants and the hepatobiliary defects observed in ARC-patients are in line with the finding of Andrew R. Cullinane, that a (conserved) VPS33b/VIPAR-complex plays a role in the hepatopathology of ARC syndrome.
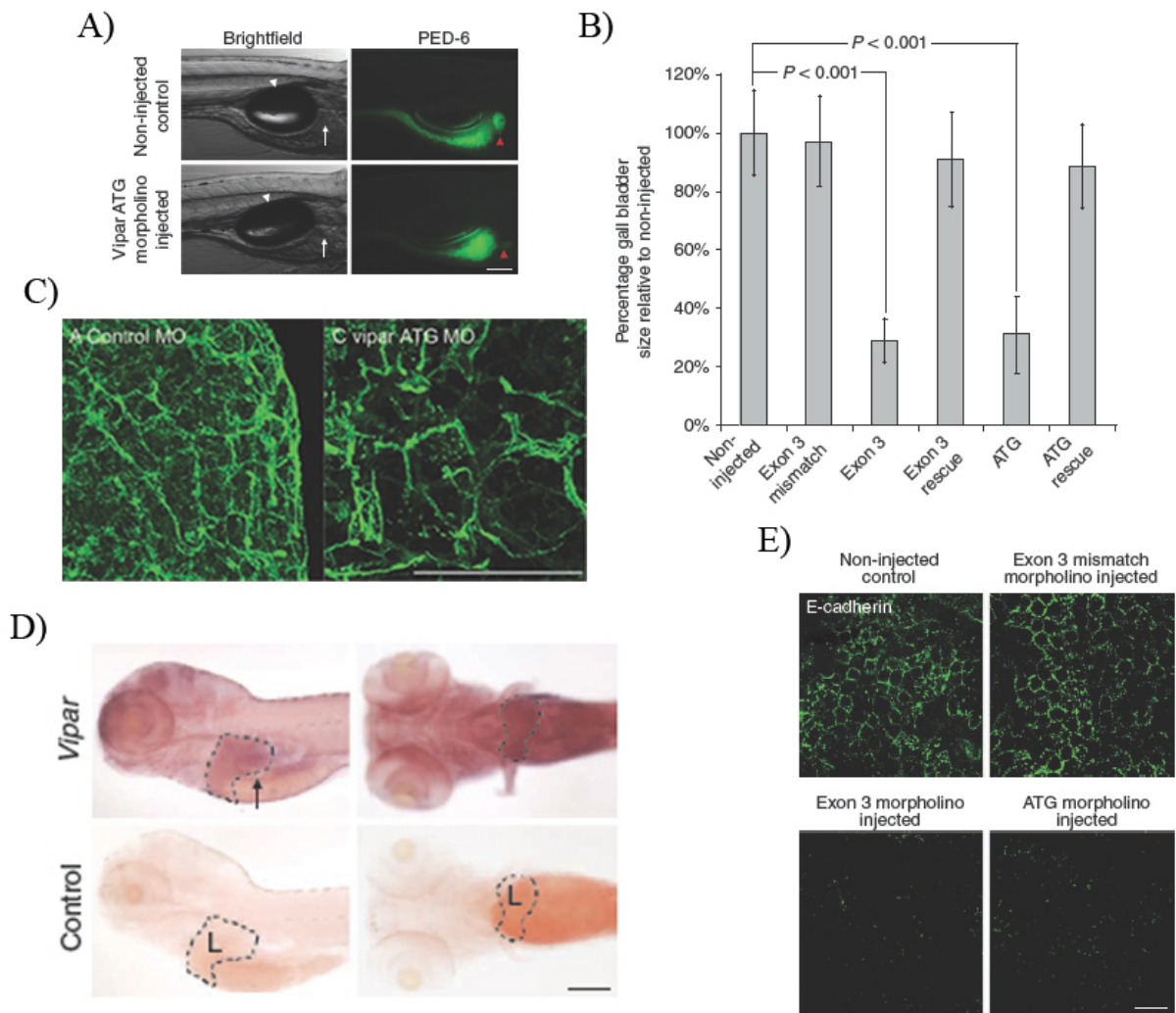
**Figure 5.1 – Phenotype for *vipar* resembles hepatobiliary defects of ARC**

**A)** Brightfield and green fluorescence images of PED6-treated non-injected and *vipar* ATG MO injected 5 dpf larvae. Liver (white arrow), swim bladder (white arrowhead) and gallbladder (red arrowhead) are indicated. **B)** Bar chart showing that the size of the gall bladder in side views is significantly smaller in ATG and Exon3 MO injected larvae than in non-injected control larvae, or in control MO injected larvae. Co-injection of *vipar*-mRNA but not an unrelated RNA (RFP) rescued the phenotype (n = 90 for each treatment group (3 independent injections with 30 larvae in each clutch); error bars, ± 1 s.d., *P<.0.001 by z-test). **C)** Keratin 18 immunostaining (green fluorescence) of livers from 5 dpf *vipar* ATG MO injected and control MO injected larvae. **D)** Lateral and ventral views of 5 dpf wildtype larvae after WISH against *vipar*-mRNA using DIG-labelled antisense and sense (control) *vipar* RNA probes. Substantial expression in liver (L, outlined) and intestine (arrow) is seen. **E)** Immunostaining of 5 dpf larvae livers for E-cadherin showing markedly reduced E-cadherin staining in morpholino-injected larvae compared with controls. Scale bars, 200 μm (A, D), 50 μm (C) or 10 μm (E). The immunostainings and imaging in C and E were performed by Anna Straatman-Iwanowska and Andrew R. Cullinane (Gissen group).

## 5.4 Discussion

The work on the role of *vipar* during zebrafish development produced a zebrafish model for cholestasis. The morphant phenotype for *vipar* was in line with a partial phenocopy of ARC-syndrome. It would be interesting to test if the more severe phenotype observed after injection of a higher dose of *vipar* MO is rescuable with *vipar*-mRNA. The more severe phenotype might display features of ARC, which are not found in the mild phenotype. Another interesting question is whether *vipar* is also regulated by *hnf6* and its downstream target *vhnf1*, like it was shown for *vps33b*.

The *vipar*-morphants display hepatobiliary defects reminiscent of the ones observed in ARC-patients. The morphants show reduced numbers of terminal branches of intrahepatic bile ducts and they have smaller gall bladders in side views. This suggests that the filling state of the gall bladder differs between morphants and controls, presumeably due to reduced excretion of PED6 into the gall bladder. However, it cannot be excluded that the gall bladder is underdeveloped. In that respect the *vipar*-morphants differ slightly from the *vps33b*-morphants, which display a reduced intensity of the PED6 fluorescence in the gall bladder. Overall morphology of the larvae and the liver size between morphants and controls used for the *vipar* experiments were comparable.

The cause of the reduced PED6 accumulation in the gall bladders of *vipar*-morphants is not entirely clear. The PED6-assay does not distinguish between a defective lipid absorption in the intestine and defective excretion through the hepatobiliary system. There is some evidence for lipid malabsorption in *vps33b*-morphants. Electron micrographs revealed Golgi abnormalities and the accumulation of cytoplasmic vesicles in *vps33b*-morphant enterocytes. After ingestion of a

fluorescent lipid (AM1-43), more fluorescent vesicles were seen in the cytoplasm of *vps33b*-morphant enterocytes than in the cytoplasm of wildtypes. These findings suggest that lipid malabsorption contributes to the PED6 phenotype in *vps33b*-morphants and likely also in *vipar*-morphants.

A number of hepatopathologies are observed in ARC. A hallmark of ARC is the mis-sorting of apical proteins in polarised cells of the liver. If there is mis-sorting of apical proteins in the livers of *vipar* or *vps33b* morphants was not investigated. Interestingly the zebrafish *vps18*-mutant displays mis-sorting of the canalicular marker MDR-1 (multi drug resistance, member 1) (Sadler et al., 2005). Like in the livers of ARC-patients the expression of the adherens junction protein E-cadherin is severely reduced in the livers of *vipar*-morphants. The observed reduced immunodetection of E-cadherin in the AJC (apical junction complex) of hepatocytes cannot directly be attributed to a defect in intracellular trafficking, because it is due to reduced transcription of E-cadherin. However, *vps33b*-morphants display accumulation of cytoplasmic vesicles, which points to defective intracellular trafficking.

Injection of the *vipar* ATG MO at concentration of 10 μM in the injection solution induced a specific hepatobiliary phenotype, while at a concentration of 100 μM in induces a severe growth arrest phenotype. A similar phenomenon has been observed for the MO-mediated knock down of *vps18*. Injection of the lower dose of *vps18* MO induced a hepatomegaly, while a higher dose caused global developmental defects and albinism. The *vps18*-mutant displayed a compound phenotype, with hepatomegaly and albinism. The stronger developmental defects could be explained with an additionally effect by knocking down the maternal transcript. These findings suggest that the *vps18*-morphants displayed a dose-dependent degree of severity of a specific

phenotype. The same might be true for the *vipar*-morphants, but a mutant as a reference was not available.

Other features of ARC are renal dysfunction and motor axon defects. Neither kidney defects nor motor neuron defects were obvious in *vipar*- and *vps33b*-morphants. The motoric behaviour of *vipar*-morphants did not differ from that of controls. Kidney function in the morphant larvae could not be addressed, because of a lack of suitable assays. It would be interesting to test the presence of platelet defects in the morphants. An assay to test the function of zebrafish thrombocytes has been developed (Jagadeeswaran et al., 2005).

## 5.5 Conclusions

1. Analysis of the expression patterns of *vipar* revealed a ubiquitous expression of *vipar* at Prim-5 stage (24 hpf). The 5 dpf expression patterns are more restricted, with substantial expression in liver and intestine. The observed expression patterns for *vipar* resemble the ones described for *vps33b*.

2. The characterisation of the *vipar*-morphants revealed a role of *vipar* in biliary development. Knock down of *vipar* causes a reduction of the terminal branches of the intrahepatic biliary tree. We demonstrated that a lower volume of the fluorescent lipid reporter PED6 accumulates in the gall bladders of *vipar*-morphants, which suggests a defect in bile secretion in *vipar*-morphants.

# 6 Development of a method to culture and transplant stage I and stage II oocytes to allow manipulation of maternal gene products

## 6.1 Introduction and Overview

During my PhD I have recognised how interference with zygotic gene activity may only partially address the function of genes during development and the importance to study the contribution of maternal gene products to zebrafish embryonic development. However, to interfere with maternal gene function remains a technically challenging task. The difficulty in inhibiting maternal genes, contributes to our lack of understanding of the degree of maternal contribution to embryo development.

Early zebrafish development until the MBT is almost entirely driven by maternal factors. Besides supporting all basic cellular functions those maternal factors are also involved in processes like fertilisation, egg activation, the first cell divisions and the ZGA. Maternal factors also contribute to the establishment of the axes in zebrafish embryos: The animal-vegetal axis (Marlow and Mullins, 2008), the dorsal-ventral axis (Lu et al., 2011) and anterior-posterior axis (Pelegri, 2003). But maternal contribution to development reaches far beyond the MBT. Most of the maternal mutant phenotypes manifest at post MBT stages, although they might be initiated at earlier stages (Wagner et al., 2004). There are numerous examples for maternal zygotic (MZ) mutants, which display a more severe phenotype than the zygotic mutant or the maternal mutant alone: For example the MZ mutant *oep* (one-eyed pinhead), *pou5f1* (POU domain, class 5,

transcription factor 1), *gart* (phosphoribosylglycinamide formyltransferase) and *paics* (phosphoribosylaminoimidazole succinocarboxamide synthetase) (Gritsman et al., 1999, Lunde et al., 2004, Ng et al., 2009) all show dramatically enhanced phenotypes as compared to the zygotic counterparts.

There are several strategies used in zebrafish to generate maternal mutants. Maternal mutants can be obtained simply by inbreeding, of homozygous zygotic mutants when those are viable. This strategy was applied in a four-generation maternal-effect mutant screen carried out in the lab of Mary C. Mullins ((Dosch et al., 2004, Wagner et al., 2004). If homozygous zygotic mutants are not viable, the generation of maternal mutants is still possible in some cases. Maternal mutants for genes required for early development can be obtained by rescue of early phenotypes by microinjection of synthetic wildtype mRNA (Gritsman et al., 1999). If the zygotic phenotype is not rescuable by mRNA injection the generation of a maternal mutant is more complicated. In those cases a PGC (primordial germ cell) replacement method can be used to generate chimeric fish with a mutant germline in a wildtype background (Ciruna et al., 2002), which then generates functionally null mutant gametes in the mother.

The above mentioned methods are either not applicable for all genes (rescue of zygotic mutants and imbreeding) or are time consuming and tedious (PGC-replacement). Therefore there is a need for new methods to interfere with maternal gene function, which circumvent the need of a zygotic mutant as a prerequisite and which are easily applicable to all genes.

## 6.2    Aims

Antisense technologies using MOs or RNAi are universally applicable to interfere with gene function. Many maternal RNAs and proteins are produced during early stages of oogenesis, in stages I and II (Pelegri, 2003). Thus, to utilise antisense effectors to efficiently block maternal genes they need to be introduced into early stage oocytes. In collaboration with Zsolt Csenki we aimed to establish an early stage oocyte transplantation protocol as a prerequisite to interfere with maternal gene function in the oocytes. In those experiments we addressed the following questions:

1. Can stage I-II oocytes be recovered and transplanted into the ovary of recipient mothers?

2. Do those transplanted oocytes resume and complete oogenesis? Can viable embryos be obtained by oocyte transplantation?

3. Can this transplantation protocol be used as a tool to interfere with maternal gene function?

## 6.3    Results

This work composed part of the PhD-project of Zsolt Csenki. A substantial part of this work was carried out during visits of Zsolt in the ITG (Institute of Toxicology and Genetics) at the KIT (Karlsruhe Institute of Technology). The below described results were the outcome of my joint work with Zsolt in the ITG. I isolated oocytes for transplantations and microinjections and I performed whole-mount *in situ* analysis of expression of reporter and endogenous gene products in ovaries.

First we asked whether early stage oocytes can be transplanted into recipient females. We transplanted YFP-positive stage I-II follicles, dissected from transgenic donor females with ubiquitous YFP expression (*bactin:yfp*), into the ovaries of YFP-negative wildtype recipient mothers. The YFP transgene enabled us to monitor the fate of the transplanted follicles, because they can be distinguished from the non-transgenic follicles of the recipient mother by YFP-fluorescence under a fluorescence microscope and by detection of the YFP-mRNA with WISH (Figure 6.1).

We assessed the retention of transplanted early stage oocytes in the recipient ovaries at several time points after the transplantation (dpt, days post transplantation). The number of recovered transplanted follicles is initially high, 47.5% (171/360) at 1 dpt, but steadily drops with further days post transplantation. At 14 dpt just 2.6% (9/350) of transplanted oocytes were recovered.

We then investigated whether the transplanted oocytes fully integrate into the recipient ovaries and continue with oogenesis. We hypothesised that the transplanted oocytes (follicles) would increase in size, if they continued with oogenesis after transplantation. To test that hypothesis we measured the diameter of follicles before transplantation and compared it to the diameter of transplanted follicles, recovered at certain time points post transplantation. Follicle diameter is commonly used for staging of oocytes (Selman et al., 1993). Follicles matching the histological and the size criteria for stage III follicles were recovered at 1 week and 2 weeks after transplantation of stage I follicles. This suggests that transplanted follicles can integrate into recipient ovaries and continue with oogenesis.

Finally, we asked whether normally developing embryos can be obtained from transplanted oocytes. We injected 10 recipient females with up to 100 stage I follicles and mated them weekly with wildtype males over a course of six weeks. Four YFP-positive embryos were obtained from

199

the 3$^{rd}$ and 4$^{th}$ week's matings. Microsatellite marker analysis confirmed that those embryos'

maternal genome was derived from the donor females and not from the recipient mothers.

We also addressed the question, if the oocytes can be microinjected prior to transplantation.

Microinjetion is a widely used method in zebrafish, to introduce molecules interfering with gene

function, like MOs. We injected stage I and II oocytes with mRNA encoding for DsRed, a red

fluorescent protein. DsRed-fluorescence was observed in 10.3% (5/58) of DsRed-mRNA injected

oocytes, after one day of *in vitro* incubation in agarose-plates with Ringer solution. We also

recovered microinjected and then transplanted oocytes (YFP- and DsRed-positive) one day after

transplantation from recipient mothers.
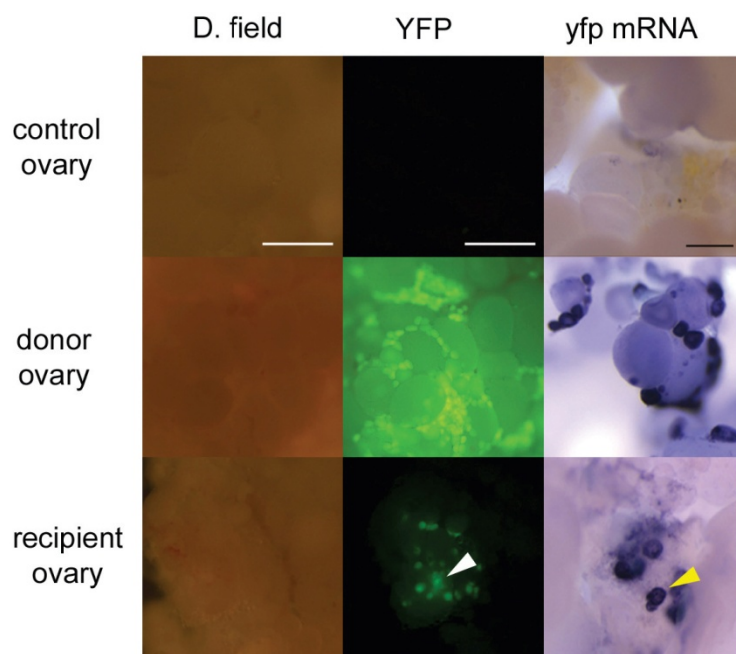


**Figure 6.1 – Recovery of transplanted follicles from recipient ovaries**

Dark field (left), YFP filter view (middle) and whole-mount *in situ* analysis against YFP-mRNA
of ovaries which are specified by the labels of the rows. Transgenic, YFP-positive donor follicles
are yellowish green in YFP filter view and purple in the whole-mount *in situ* hybridisation
analysis, while no YFP-signal is detected in ovaries from wildtypes which not have be subjected
to transplantation.

## 6.4 Discussion

In collaboration with Zsolt Cenki we developed a transplantation protocol for early stage oocytes into surrogate mothers. With a very low frequency, viable embryos from those transplanted oocytes were obtained, which later developed into fertile adults. Furthermore we showed that it is possible to microinject the oocytes prior to transplantation. The combination of microinjection and transplantation could be further developed into an experimental tool to block maternal factors, if the recovery rate of embryos from transplanted oocytes can be improved.

The milder zygotic phenotypes of many zebrafish genes compared to their mouse counterparts enables zebrafish researchers to study the role of those genes in developmental processes, which cannot be studied in the more severe mouse ko phenotypes. On the other hand it is very likely that many zygotic mutant phenotypes are not full LOF-phenotypes. Because only maternal mRNA, not maternal protein, can be efficiently targeted with MOs, the same might be true for many morphants. This is a major problem for studies where phenotypes for different zebrafish genes are compared to each other, like in our MO-screen (see chapter 3). Without assessing maternal contribution it is not clear, whether differences, especially in the severity of phenotypes, are due to differential maternal contribution, or due to differential gene function. Methods to interrogate maternal contribution to development, easily applicable to all genes, would help to resolve such issues. The early stage oocyte transplantation protocol might be developed into such a method.

# 6.5    Conclusions

1. Using a novel transplantation protocol we demonstrated that stage I-II oocytes derived from donor females can be transplanted into surrogate mothers.

2. Some of the transplanted oocytes fully integrate into the ovary of the surrogate mothers and continue with oogenesis. With a very low frequency, viable, normal developing embryos were recovered from transplanted oocytes.

3. The recovery rate of embryos from transplanted oocytes needs to be improved to develop the transplantation protocol further, into a method to study maternal gene function in oocyte and embryonic development.

# 7 Appendices

## 7.1 Tables from microarray analysis

The results from the enrichment analysis of the microarray data using the DAVID functional annotation tool can be retrieved as tables. Those tables contain following information:

1. Category

   The category is the term-based annotation system (database, resource) within which the enrichment analysis is performed by the tool.

2. Term

   In this column the enriched terms associated with the analysed gene lists are listed.

3. Count

   The number in this column is the number of genes in the analysed list, which are involved in the respective term.

4. %

   This is the percentage of genes in List Total which are involved in the respective term.

5. Genes

   Here the individual genes involved in the respective term are listed. Because of space limitations they were not included into the tables of this thesis.

6. List Total

   The number in this column is the total number of genes which are involved in at least one of the terms in the category.

7. Pop Hits

Pop Hits contains the number of genes involved in the respective term within the specific background for the analysis.

8. Pop Total

The DAVID tool applies a dynamic background. The background for microarray analysis using DAVI Functional Annotation tool was all genes on the microarray. Pop Total is the specific background for calculations within the specific category. For example all genes on the microarray which are involved in at least one of the terms in the category KEGG pathways.

9. P-value

The p-value is derived from a modified Fisher Exact test (EASE Score) to test the significance of the enrichment of terms within gene lists. The cut-off applied by the default setting to include a term is $\leq 0.1$. The p-value is calculated by comparing the enrichment of Count in List Total to the enrichment of Pop Hits in Pop Total using the modified Fisher Exact test.

10. Fold Enrichment

The fold enrichment is the observed enrichment over the enrichment by chance.

11. Bonferroni, Benjamini(-Hochberg) and FDR (False Discovery Rate)

These are additional standard statistics provided for the assessment of the significance of the results from the enrichment analysis.

**Table 7.1 – Anatomical terms enriched in Taf8down**

| Term | Count | % | P-value | List Total | Pop Hits | Pop Total | Fold Enrichment | Bonferroni | Benjamini | FDR |
|---|---|---|---|---|---|---|---|---|---|---|
| intestinal bulb | 16 | 15.1 | 2.80E-10 | 70 | 173 | 6366 | 8.4109 | 2.66E-08 | 2.66E-08 | 3.08E-07 |
| pancreas | 12 | 11.3 | 4.47E-08 | 70 | 119 | 6366 | 9.170708 | 4.25E-06 | 2.12E-06 | 4.92E-05 |
| exocrine pancreas | 6 | 5.7 | 1.77E-06 | 70 | 20 | 6366 | 27.28286 | 1.68E-04 | 5.59E-05 | 0.001941 |
| liver | 22 | 20.8 | 2.42E-06 | 70 | 646 | 6366 | 3.097125 | 2.29E-04 | 5.74E-05 | 0.002655 |
| pronephric proximal straight tubule | 3 | 2.8 | 0.004926 | 70 | 10 | 6366 | 27.28286 | 0.374456 | 0.089559 | 5.283444 |
| pronephric proximal convoluted tubule | 3 | 2.8 | 0.005979 | 70 | 11 | 6366 | 24.8026 | 0.434297 | 0.09058 | 6.379048 |
| gut | 10 | 9.4 | 0.024315 | 70 | 391 | 6366 | 2.325904 | 0.903528 | 0.283998 | 23.7062 |
| lens | 8 | 7.5 | 0.04881 | 70 | 309 | 6366 | 2.354508 | 0.991383 | 0.448021 | 42.30857 |
| retinal photoreceptor layer | 4 | 3.8 | 0.057136 | 70 | 81 | 6366 | 4.491005 | 0.996262 | 0.462604 | 47.62288 |
| lens vesicle | 7 | 6.6 | 0.060716 | 70 | 259 | 6366 | 2.457915 | 0.997396 | 0.448468 | 49.76781 |
| fat cell | 2 | 1.9 | 0.06332 | 70 | 6 | 6366 | 30.31429 | 0.997999 | 0.431604 | 51.27763 |

**Table 7.2 – Anatomical terms enriched in Taf6down**

| Term | Count | % | P-value | List Total | Pop Hits | Pop Total | Fold Enrichment | Bonferroni | Benjamini | FDR |
|---|---|---|---|---|---|---|---|---|---|---|
| intestinal bulb | 37 | 19.8 | 4.35E-26 | 142 | 173 | 6366 | 9.588129936 | 9.05E-24 | 9.05E-24 | 5.49E-23 |
| liver | 44 | 23.5 | 1.13E-11 | 142 | 646 | 6366 | 3.053503685 | 2.36E-09 | 1.18E-09 | 1.43E-08 |
| retinal photoreceptor layer | 14 | 7.5 | 1.83E-08 | 142 | 81 | 6366 | 7.748565467 | 3.81E-06 | 1.27E-06 | 2.31E-05 |
| retinal cone cell | 7 | 3.7 | 1.07E-06 | 142 | 17 | 6366 | 18.45981773 | 2.24E-04 | 5.59E-05 | 0.001356 |
| gut | 25 | 13.4 | 4.00E-06 | 142 | 391 | 6366 | 2.866431325 | 8.31E-04 | 1.66E-04 | 0.005041 |
| pancreas | 13 | 7.0 | 1.09E-05 | 142 | 119 | 6366 | 4.897502663 | 0.0022615 | 3.77E-04 | 0.01373 |

| | Count | % | P-value | List Total | Pop Hits | Pop Total | Fold Enrichment | Bonferroni | Benjamini | FDR |
|---|---|---|---|---|---|---|---|---|---|---|
| retinal outer nuclear layer | 6 | 3.2 | 5.89E-05 | 142 | 20 | 6366 | 13.44929577 | 0.0121727 | 0.0017481 | 0.074248 |
| eye | 25 | 13.4 | 7.69E-04 | 142 | 544 | 6366 | 2.060247514 | 0.1479221 | 0.0198108 | 0.966112 |
| exocrine pancreas | 5 | 2.7 | 8.48E-04 | 142 | 20 | 6366 | 11.20774648 | 0.1617303 | 0.0194108 | 1.064191 |
| pronephric proximal straight tubule | 4 | 2.1 | 0.001139 | 142 | 10 | 6366 | 17.93239437 | 0.21101 | 0.0234215 | 1.427047 |
| pronephric proximal convoluted tubule | 4 | 2.1 | 0.001541 | 142 | 11 | 6366 | 16.3021767 | 0.274343 | 0.0287317 | 1.926003 |
| YSL | 19 | 10.2 | 0.002831 | 142 | 398 | 6366 | 2.140172694 | 0.4455317 | 0.0479574 | 3.513385 |
| epiphysis | 16 | 8.6 | 0.003625 | 142 | 312 | 6366 | 2.299024919 | 0.5302103 | 0.0564568 | 4.478274 |
| retina | 30 | 16.0 | 0.017006 | 142 | 882 | 6366 | 1.524863467 | 0.9717759 | 0.2249494 | 19.4555 |
| intestine | 8 | 4.3 | 0.029788 | 142 | 135 | 6366 | 2.656651017 | 0.9981452 | 0.3425139 | 31.71389 |
| gill | 8 | 4.3 | 0.059054 | 142 | 157 | 6366 | 2.284381448 | 0.9999968 | 0.5467454 | 53.5982 |
| stratum fibrosum et griseum superficiale | 2 | 1.1 | 0.064996 | 142 | 3 | 6366 | 29.88732394 | 0.9999992 | 0.5605647 | 57.16199 |

**Table 7.3 – Anatomical terms enriched in Taf8up**

| Term | Count | % | P-value | List Total | Pop Hits | Pop Total | Fold Enrichment | Bonferroni | Benjamini | FDR |
|---|---|---|---|---|---|---|---|---|---|---|
| musculature system | 6 | 17.1 | 7.86E-04 | 27 | 185 | 6366 | 7.646847 | 0.090727 | 0.090727 | 0.899598 |
| pharynx | 5 | 14.3 | 0.002885 | 27 | 149 | 6366 | 7.912006 | 0.295013 | 0.160365 | 3.266868 |
| sternohyoid | 2 | 5.7 | 0.016241 | 27 | 4 | 6366 | 117.8889 | 0.862106 | 0.483367 | 17.15891 |
| gut | 6 | 17.1 | 0.019195 | 27 | 391 | 6366 | 3.618073 | 0.904175 | 0.443622 | 19.97469 |
| epidermal superficial stratum | 2 | 5.7 | 0.028255 | 27 | 7 | 6366 | 67.36508 | 0.968822 | 0.50023 | 28.07228 |
| liver | 7 | 20.0 | 0.042052 | 27 | 646 | 6366 | 2.554868 | 0.994474 | 0.579532 | 38.97629 |
| pharyngeal arch | 5 | 14.3 | 0.044214 | 27 | 333 | 6366 | 3.540207 | 0.995796 | 0.542367 | 40.54164 |
| proliferative region | 3 | 8.6 | 0.04557 | 27 | 84 | 6366 | 8.420635 | 0.99646 | 0.506109 | 41.50375 |

| | | | | | | | | | | |
|---|---|---|---|---|---|---|---|---|---|---|
| somite | 7 | 20.0 | 0.087047 | 27 | 774 | 6366 | 2.132357 | 0.999984 | 0.706065 | 64.90111 |
| fast muscle cell | 2 | 5.7 | 0.089983 | 27 | 23 | 6366 | 20.50242 | 0.999989 | 0.68048 | 66.17728 |
| epidermis | 4 | 11.4 | 0.096562 | 27 | 271 | 6366 | 3.480115 | 0.999995 | 0.672747 | 68.88397 |

**Table 7.4 – Anatomical terms enriched in Taf6up**

| Term | Count | % | P-value | List Total | Pop Hits | Pop Total | Fold Enrichment | Bonferroni | Benjamini | FDR |
|---|---|---|---|---|---|---|---|---|---|---|
| mesoderm | 5 | 45.5 | 2.35E-05 | 7 | 230 | 6366 | 19.770186 | 0.0011051 | 0.0011051 | 0.0223423 |
| presumptive blood | 3 | 27.3 | 1.00E-04 | 7 | 17 | 6366 | 160.48739 | 0.004692 | 0.0023488 | 0.0949993 |
| sternohyoid | 2 | 18.2 | 0.003765 | 7 | 4 | 6366 | 454.71429 | 0.1624855 | 0.0573927 | 3.5199407 |
| intermediate cell mass of mesoderm | 3 | 27.3 | 0.005534 | 7 | 126 | 6366 | 21.653061 | 0.2295839 | 0.0631257 | 5.1344804 |
| blood | 3 | 27.3 | 0.006424 | 7 | 136 | 6366 | 20.060924 | 0.261327 | 0.0587815 | 5.9377038 |
| nucleate erythrocyte | 2 | 18.2 | 0.008455 | 7 | 9 | 6366 | 202.09524 | 0.3290894 | 0.0643557 | 7.7490721 |
| fast muscle cell | 2 | 18.2 | 0.021491 | 7 | 23 | 6366 | 79.080745 | 0.6398004 | 0.1357308 | 18.645411 |
| blood island | 2 | 18.2 | 0.027033 | 7 | 29 | 6366 | 62.719212 | 0.7242 | 0.1487164 | 22.918529 |
| axial chorda mesoderm | 2 | 18.2 | 0.061533 | 7 | 67 | 6366 | 27.147122 | 0.9494535 | 0.2822625 | 45.294682 |
| hypaxial myotome region | 2 | 18.2 | 0.069552 | 7 | 76 | 6366 | 23.932331 | 0.9662317 | 0.2873915 | 49.577162 |

**Table 7.5 – Pathways enriched in Taf8down**

| Term | Count | % | P-value | List Total | Pop Hits | Pop Total | Fold Enrichment | Bonferroni | Benjamini | FDR |
|---|---|---|---|---|---|---|---|---|---|---|
| dre03320:PPAR signaling pathway | 4 | 3.8 | 0.006083 | 27 | 36 | 2439 | 10.03704 | 0.1923 | 0.1923 | 5.261333 |

**Table 7.6 – Pathways enriched in Taf6down**

| Term | Count | % | P-value | List Total | Pop Hits | Pop Total | Fold Enrichment | Bonferroni | Benjamini | FDR |
|---|---|---|---|---|---|---|---|---|---|---|
| dre03320:PPAR signaling pathway | 6 | 3.2 | 9.86E-04 | 55 | 36 | 2439 | 7.3909091 | 0.059351 | 0.0593511 | 0.990947 |
| dre00982:Drug metabolism | 4 | 2.1 | 0.003867 | 55 | 15 | 2439 | 11.825455 | 0.213576 | 0.1131946 | 3.835134 |
| dre00980: Metabolism of xenobiotics by cytochrome P450 | 4 | 2.1 | 0.004686 | 55 | 16 | 2439 | 11.086364 | 0.252651 | 0.0925115 | 4.629537 |
| dre00591:Linoleic acid metabolism | 3 | 1.6 | 0.023287 | 55 | 11 | 2439 | 12.094215 | 0.767977 | 0.3059632 | 21.16306 |
| dre00520:Amino sugar and nucleotide sugar metabolism | 4 | 2.1 | 0.040761 | 55 | 35 | 2439 | 5.0680519 | 0.924237 | 0.4031151 | 34.29281 |
| dre00260:Glycine, serine and threonine metabolism | 3 | 1.6 | 0.070900 | 55 | 20 | 2439 | 6.6518182 | 0.989532 | 0.5322925 | 52.39002 |
| dre00140:Steroid hormone biosynthesis | 3 | 1.6 | 0.077280 | 55 | 21 | 2439 | 6.3350649 | 0.993171 | 0.5095257 | 55.58808 |
| dre00250:Alanine, aspartate and glutamate metabolism | 3 | 1.6 | 0.083835 | 55 | 22 | 2439 | 6.0471074 | 0.995611 | 0.4926658 | 58.67100 |

**Table 7.7 – Pathways enriched in Taf8up**

| Term | Count | % | P-value | List Total | Pop Hits | Pop Total | Fold Enrichment | Bonferroni | Benjamini | FDR |
|---|---|---|---|---|---|---|---|---|---|---|
| dre04115:p53 signaling pathway | 3 | 8.6 | 0.006307 | 8 | 44 | 2439 | 20.786932 | 0.096284 | 0.096284 | 4.3939237 |

| | | | | | | | | | |
|---|---|---|---|---|---|---|---|---|---|
| dre04110:Cell cycle | 3 | 8.6 | 0.024537 | 8 | 89 | 2439 | 10.276685 | 0.328002 | 0.180245 | 16.173748 |
| dre04010:MAPK signaling pathway | 3 | 8.6 | 0.067443 | 8 | 154 | 2439 | 5.9391234 | 0.672805 | 0.310921 | 39.094802 |

# 8 References

Aanes, H., Winata, C.L., Lin, C.H., et al. (2011) Zebrafish mRNA sequencing deciphers novelties in transcriptome dynamics during maternal to zygotic transition. **Genome Res**, 21: (8): 1328-1338.

Abe, G., Suster, M.L. and Kawakami, K. (2011) Tol2-mediated Transgenesis, Gene Trapping, Enhancer Trapping, and the Gal4-UAS System. **Methods Cell Biol**, 104: 23-49.

Abumrad, N.A., el-Maghrabi, M.R., Amri, E.Z., et al. (1993) Cloning of a rat adipocyte membrane protein implicated in binding or transport of long-chain fatty acids that is induced during preadipocyte differentiation. Homology with human CD36. **J Biol Chem**, 268: (24): 17665-17668.

Akhtar, W. and Veenstra, G.J. (2009) TBP2 is a substitute for TBP in Xenopus oocyte transcription. **BMC Biol**, 7: 45.

Amsterdam, A., Burgess, S., Golling, G., et al. (1999) A large-scale insertional mutagenesis screen in zebrafish. **Genes Dev**, 13: (20): 2713-2724.

Amsterdam, A., Nissen, R.M., Sun, Z., et al. (2004) Identification of 315 genes essential for early zebrafish development. **Proc Natl Acad Sci U S A**, 101: (35): 12792-12797.

Anamika, K., Krebs, A.R., Thompson, J., et al. (2010) Lessons from genome-wide studies: an integrated definition of the coactivator function of histone acetyl transferases. **Epigenetics Chromatin**, 3: (1): 18.

Asch, A.S., Barnwell, J., Silverstein, R.L., et al. (1987) Isolation of the thrombospondin membrane receptor. **J Clin Invest**, 79: (4): 1054-1061.

Barak, Y., Nelson, M.C., Ong, E.S., et al. (1999) PPAR gamma is required for placental, cardiac, and adipose tissue development. **Mol Cell**, 4: (4): 585-595.

Bartfai, R., Balduf, C., Hilton, T., et al. (2004) TBP2, a vertebrate-specific member of the TBP family, is required in embryonic development of zebrafish. **Curr Biol**, 14: (7): 593-598.

Bashirullah, A., Lam, G., Yin, V.P., et al. (2007) dTrf2 is required for transcriptional and developmental responses to ecdysone during Drosophila metamorphosis. **Dev Dyn**, 236: (11): 3173-3179.

Bernstein, B.E., Mikkelsen, T.S., Xie, X., et al. (2006) A bivalent chromatin structure marks key developmental genes in embryonic stem cells. **Cell**, 125: (2): 315-326.

Bertrand, J.Y., Chi, N.C., Santoso, B., et al. (2010) Haematopoietic stem cells derive directly from aortic endothelium during development. **Nature**, 464: (7285): 108-111.

Bertrand, S., Thisse, B., Tavares, R., et al. (2007) Unexpected novel relational links uncovered by extensive developmental profiling of nuclear receptor expression. **PLoS Genet**, 3: (11): e188.

Billon, N., Kolde, R., Reimand, J., et al. (2010) Comprehensive transcriptome analysis of mouse embryonic stem cell adipogenesis unravels new processes of adipocyte development. **Genome Biol**, 11: (8): R80.

Birney, E., Stamatoyannopoulos, J.A., Dutta, A., et al. (2007) Identification and analysis of functional elements in 1% of the human genome by the ENCODE pilot project. **Nature**, 447: (7146): 799-816.

Bonasio, R., Lecona, E. and Reinberg, D. (2010) MBT domain proteins in development and disease. **Semin Cell Dev Biol**, 21: (2): 221-230.

Burke, T.W. and Kadonaga, J.T. (1997) The downstream core promoter element, DPE, is conserved from Drosophila to humans and is recognized by TAFII60 of Drosophila. **Genes Dev**, 11: (22): 3020-3031.

Burket, C.T., Montgomery, J.E., Thummel, R., et al. (2008) Generation and characterization of transgenic zebrafish lines using different ubiquitous promoters. **Transgenic Res**, 17: (2): 265-279.

Carter, D., Chakalova, L., Osborne, C.S., et al. (2002) Long-range chromatin regulatory interactions in vivo. **Nat Genet***, 32: (4): 623-626.

Chakrabarti, S., Streisinger, G., Singer, F., et al. (1983) Frequency of gamma-Ray Induced Specific Locus and Recessive Lethal Mutations in Mature Germ Cells of the Zebrafish, BRACHYDANIO RERIO. **Genetics***, 103: (1): 109-123.

Chalkley, G.E. and Verrijzer, C.P. (1999) DNA binding site selection by RNA polymerase II TAFs: a TAF(II)250-TAF(II)150 complex recognizes the initiator. **EMBO J***, 18: (17): 4835-4845.

Champagne, K.S. and Kutateladze, T.G. (2009) Structural insight into histone recognition by the ING PHD fingers. **Curr Drug Targets***, 10: (5): 432-441.

Chandra, V., Huang, P., Hamuro, Y., et al. (2008) Structure of the intact PPAR-gamma-RXR-alpha nuclear receptor complex on DNA. **Nature***, 350-356.

Chawla, A., Repa, J.J., Evans, R.M., et al. (2001) Nuclear receptors and lipid physiology: opening the X-files. **Science***, 294: (5548): 1866-1870.

Chiang, C.M. and Roeder, R.G. (1995) Cloning of an intrinsic human TFIID subunit that interacts with multiple transcriptional activators. **Science***, 267: (5197): 531-536.

Choi, J.H., Banks, A.S., Estall, J.L., et al. (2010) Anti-diabetic drugs inhibit obesity-linked phosphorylation of PPARgamma by Cdk5. **Nature***, 466: (7305): 451-456.

Chu, J. and Sadler, K.C. (2009) New school in liver development: lessons from zebrafish. **Hepatology***, 50: (5): 1656-1663.

Ciruna, B., Weidinger, G., Knaut, H., et al. (2002) Production of maternal-zygotic mutant zebrafish by germ-line replacement. **Proc Natl Acad Sci U S A***, 99: (23): 14919-14924.

Clemetson, K.J., Pfueller, S.L., Luscher, E.F., et al. (1977) Isolation of the membrane glycoproteins of human blood platelets by lectin affinity chromatography. **Biochim Biophys Acta***, 464: (3): 493-508.

Cler, E., Papai, G., Schultz, P., et al. (2009) Recent advances in understanding the structure and function of general transcription factor TFIID. **Cell Mol Life Sci***, 66: (13): 2123-2134.

Coburn, C.T., Knapp, F.F., Jr., Febbraio, M., et al. (2000) Defective uptake and utilization of long chain fatty acids in muscle and adipose tissues of CD36 knockout mice. **J Biol Chem***, 275: (42): 32523-32529.

Crowley, T.E., Hoey, T., Liu, J.K., et al. (1993) A new factor related to TATA-binding protein has highly restricted expression patterns in Drosophila. **Nature***, 361: (6412): 557-561.

D'Alessio, J.A., Ng, R., Willenbring, H., et al. (2011) Core promoter recognition complex changes accompany liver development. **Proc Natl Acad Sci U S A***, 108: (10): 3906-3911.

Dantonel, J.C., Wurtz, J.M., Poch, O., et al. (1999) The TBP-like factor: an alternative transcription factor in metazoa? **Trends Biochem Sci***, 24: (9): 335-339.

Dawson, D.W., Pearce, S.F., Zhong, R., et al. (1997) CD36 mediates the In vitro inhibitory effects of thrombospondin-1 on endothelial cells. **J Cell Biol***, 138: (3): 707-717.

Deato, M.D., Marr, M.T., Sottero, T., et al. (2008) MyoD targets TAF3/TRF3 to activate myogenin transcription. **Mol Cell***, 32: (1): 96-105.

Deato, M.D. and Tjian, R. (2007) Switching of the core transcription machinery during myogenesis. **Genes Dev***, 21: (17): 2137-2149.

Demeny, M.A., Soutoglou, E., Nagy, Z., et al. (2007) Identification of a small TAF complex and its role in the assembly of TAF-containing complexes. **PLoS One***, 2: (3): e316.

Desreumaux, P., Dubuquoy, L., Nutten, S., et al. (2001) Attenuation of colon inflammation through activators of the retinoid X receptor (RXR)/peroxisome proliferator-activated receptor gamma (PPARgamma) heterodimer. A basis for new therapeutic strategies. **J Exp Med***, 193: (7): 827-838.

Desvergne, B. and Wahli, W. (1999) Peroxisome proliferator-activated receptors: nuclear control of metabolism. **Endocr Rev***, 20: (5): 649-688.

Dosch, R., Wagner, D.S., Mintzer, K.A., et al. (2004) Maternal control of vertebrate development before the midblastula transition: mutants from the zebrafish I. **Dev Cell**, 6: (6): 771-780.

Dynlacht, B.D., Hoey, T. and Tjian, R. (1991) Isolation of coactivators associated with the TATA-binding protein that mediate transcriptional activation. **Cell**, 66: (3): 563-576.

Eastham, K.M., McKiernan, P.J., Milford, D.V., et al. (2001) ARC syndrome: an expanding range of phenotypes. **Arch Dis Child**, 85: (5): 415-420.

Eckel, R.H. (1989) Lipoprotein lipase. A multifunctional enzyme relevant to common metabolic diseases. **N Engl J Med**, 320: (16): 1060-1068.

Elo, B., Villano, C.M., Govorko, D., et al. (2007) Larval zebrafish as a model for glucose metabolism: expression of phosphoenolpyruvate carboxykinase as a marker for exposure to anti-diabetic compounds. **J Mol Endocrinol**, 38: (4): 433-440.

Evans, R.M. (2004) 2003 Keio Medical Science Prize commemorative lecture. PPARs and the complex journey to obesity. **Keio J Med**, 53: (2): 53-58.

Evans, R.M., Barish, G.D. and Wang, Y.X. (2004) PPARs and the complex journey to obesity. **Nat Med**, 10: (4): 355-361.

Falender, A.E., Freiman, R.N., Geles, K.G., et al. (2005) Maintenance of spermatogenesis requires TAF4b, a gonad-specific subunit of TFIID. **Genes Dev**, 19: (7): 794-803.

Febbraio, M., Hajjar, D.P. and Silverstein, R.L. (2001) CD36: a class B scavenger receptor involved in angiogenesis, atherosclerosis, inflammation, and lipid metabolism. **J Clin Invest**, 108: (6): 785-791.

Ferg, M., Sanges, R., Gehrig, J., et al. (2007) The TATA-binding protein regulates maternal mRNA degradation and differential zygotic transcription in zebrafish. **EMBO J**, 26: (17): 3945-3956.

Field, H.A., Ober, E.A., Roeser, T., et al. (2003) Formation of the digestive system in zebrafish. I. Liver morphogenesis. **Dev Biol**, 253: (2): 279-290.

Flynn, E.J., 3rd, Trent, C.M. and Rawls, J.F. (2009) Ontogeny and nutritional control of adipogenesis in zebrafish (Danio rerio). **J Lipid Res**, 50: (8): 1641-1652.

Flynt, A.S., Li, N., Thatcher, E.J., et al. (2007) Zebrafish miR-214 modulates Hedgehog signaling to specify muscle cell fate. **Nat Genet**, 39: (2): 259-263.

Fuentes, R. and Fernandez, J. (2010) Ooplasmic segregation in the zebrafish zygote and early embryo: pattern of ooplasmic movements and transport pathways. **Dev Dyn**, 239: (8): 2172-2189.

Furuhashi, M. and Hotamisligil, G.S. (2008) Fatty acid-binding proteins: role in metabolic diseases and potential as drug targets. **Nat Rev Drug Discov**, 7: (6): 489-503.

Garbett, K.A., Tripathi, M.K., Cencki, B., et al. (2007) Yeast TFIID serves as a coactivator for Rap1p by direct protein-protein interaction. **Mol Cell Biol**, 27: (1): 297-311.

Gazdag, E., Rajkovic, A., Torres-Padilla, M.E., et al. (2007) Analysis of TATA-binding protein 2 (TBP2) and TBP expression suggests different roles for the two proteins in regulation of gene expression during oogenesis and early mouse development. **Reproduction**, 134: (1): 51-62.

Gazdag, E., Santenard, A., Ziegler-Birling, C., et al. (2009) TBP2 is essential for germ cell development by regulating transcription and chromatin condensation in the oocyte. **Genes Dev**, 23: (18): 2210-2223.

Ge, K., Guermah, M., Yuan, C.X., et al. (2002) Transcription coactivator TRAP220 is required for PPAR gamma 2-stimulated adipogenesis. **Nature**, 417: (6888): 563-567.

Gissen, P., Johnson, C.A., Morgan, N.V., et al. (2004) Mutations in VPS33B, encoding a regulator of SNARE-dependent membrane fusion, cause arthrogryposis-renal dysfunction-cholestasis (ARC) syndrome. **Nat Genet**, 36: (4): 400-404.

Gissen, P., Tee, L., Johnson, C.A., et al. (2006) Clinical and molecular genetic features of ARC syndrome. **Hum Genet**, 120: (3): 396-409.

Gleeson, M., Connaughton, V. and Arneson, L.S. (2007) Induction of hyperglycaemia in zebrafish (Danio rerio) leads to morphological changes in the retina. **Acta Diabetol**, 44: (3): 157-163.

Goldberg, I.J. and Merkel, M. (2001) Lipoprotein lipase: physiology, biochemistry, and molecular biology. **Front Biosci**, 6: D388-405.

Goodrich, J.A. and Tjian, R. (2010) Unexpected roles for core promoter recognition factors in cell-type-specific transcription and gene regulation. **Nat Rev Genet**, 11: (8): 549-558.

Green, M.R. (2000) TBP-associated factors (TAFIIs): multiple, selective transcriptional mediators in common complexes. **Trends Biochem Sci**, 25: (2): 59-63.

Gritsman, K., Zhang, J., Cheng, S., et al. (1999) The EGF-CFC protein one-eyed pinhead is essential for nodal signaling. **Cell**, 97: (1): 121-132.

Grontved, L., Madsen, M.S., Boergesen, M., et al. (2010) MED14 tethers mediator to the N-terminal domain of peroxisome proliferator-activated receptor gamma and is required for full transcriptional activity and adipogenesis. **Mol Cell Biol**, 30: (9): 2155-2169.

Guermah, M., Ge, K., Chiang, C.M., et al. (2003) The TBN protein, which is essential for early embryonic mouse development, is an inducible TAFII implicated in adipogenesis. **Mol Cell**, 12: (4): 991-1001.

Guven-Ozkan, T., Nishi, Y., Robertson, S.M., et al. (2008) Global transcriptional repression in C. elegans germline precursors by regulated sequestration of TAF-4. **Cell**, 135: (1): 149-160.

Haffter, P., Granato, M., Brand, M., et al. (1996) The identification of genes with unique and essential functions in the development of the zebrafish, Danio rerio. **Development**, 123: 1-36.

Hansen, S.K., Takada, S., Jacobson, R.H., et al. (1997) Transcription properties of a cell type-specific TATA-binding protein, TRF. **Cell**, 91: (1): 71-83.

Hart, D.O. and Green, M.R. (2008) Targeting a TAF to make muscle. **Mol Cell**, 32: (2): 164-166.

Hart, D.O., Raha, T., Lawson, N.D., et al. (2007) Initiation of zebrafish haematopoiesis by the TATA-box-binding protein-related factor Trf3. **Nature**, 450: (7172): 1082-1085.

Hart, D.O., Santra, M.K., Raha, T., et al. (2009) Selective interaction between Trf3 and Taf3 required for early development and hematopoiesis. **Dev Dyn**, 238: (10): 2540-2549.

Hausman, G.J. and Richardson, R.L. (2004) Adipose tissue angiogenesis. **J Anim Sci**, 82: (3): 925-934.

Heinaniemi, M., Uski, J.O., Degenhardt, T., et al. (2007) Meta-analysis of primary target genes of peroxisome proliferator-activated receptors. **Genome Biol**, 8: (7): R147.

Hilton, T.L., Li, Y., Dunphy, E.L., et al. (2005) TAF1 histone acetyltransferase activity in Sp1 activation of the cyclin D1 promoter. **Mol Cell Biol**, 25: (10): 4321-4332.

Hinton, D.E. and Couch, J.A. (1998) Architectural pattern, tissue and cellular morphology in livers of fishes: relationship to experimentally-induced neoplastic responses. **EXS**, 86: 141-164.

Hirsch, D., Stahl, A. and Lodish, H.F. (1998) A family of fatty acid transporters conserved from mycobacterium to man. **Proc Natl Acad Sci U S A**, 95: (15): 8625-8629.

Hochheimer, A. and Tjian, R. (2003) Diversified transcription initiation complexes expand promoter selectivity and tissue-specific gene expression. **Genes Dev**, 17: (11): 1309-1320.

Hochheimer, A., Zhou, S., Zheng, S., et al. (2002) TRF2 associates with DREF and directs promoter-selective gene expression in Drosophila. **Nature**, 420: (6914): 439-445.

Holmes, M.C. and Tjian, R. (2000) Promoter-selective properties of the TBP-related factor TRF1. **Science**, 288: (5467): 867-870.

Holtta-Vuori, M., Salo, V.T., Nyberg, L., et al. (2010) Zebrafish: gaining popularity in lipid research. **Biochem J**, 429: (2): 235-242.

Horslen, S.P., Quarrell, O.W. and Tanner, M.S. (1994) Liver histology in the arthrogryposis multiplex congenita, renal dysfunction, and cholestasis (ARC) syndrome: report of three new cases and review. **J Med Genet**, 31: (1): 62-64.

Hulsen, T., de Vlieg, J. and Alkema, W. (2008) BioVenn - a web application for the comparison and visualization of biological lists using area-proportional Venn diagrams. **BMC Genomics***, 9: 488.

Hunt, C.R., Ro, J.H., Dobson, D.E., et al. (1986) Adipocyte P2 gene: developmental expression and homology of 5'-flanking sequences among fat cell-specific genes. **Proc Natl Acad Sci U S A***, 83: (11): 3786-3790.

Ibabe, A., Grabenbauer, M., Baumgart, E., et al. (2002) Expression of peroxisome proliferator-activated receptors in zebrafish (Danio rerio). **Histochem Cell Biol***, 118: (3): 231-239.

Imrie, D. and Sadler, K.C. (2010) White adipose tissue development in zebrafish is regulated by both developmental time and fish size. **Dev Dyn***, 239: (11): 3013-3023.

Isogai, Y., Keles, S., Prestel, M., et al. (2007a) Transcription of histone gene cluster by differential core-promoter factors. **Genes Dev***, 21: (22): 2936-2949.

Isogai, Y., Takada, S., Tjian, R., et al. (2007b) Novel TRF1/BRF target genes revealed by genome-wide analysis of Drosophila Pol III transcription. **EMBO J***, 26: (1): 79-89.

Issemann, I. and Green, S. (1990) Activation of a member of the steroid hormone receptor superfamily by peroxisome proliferators. **Nature***, 347: (6294): 645-650.

Jacobi, U.G., Akkers, R.C., Pierson, E.S., et al. (2007) TBP paralogs accommodate metazoan- and vertebrate-specific developmental gene regulation. **EMBO J***, 26: (17): 3900-3909.

Jacobson, R.H., Ladurner, A.G., King, D.S., et al. (2000) Structure and function of a human TAFII250 double bromodomain module. **Science***, 288: (5470): 1422-1425.

Jagadeeswaran, P., Gregory, M., Day, K., et al. (2005) Zebrafish: a genetic model for hemostasis and thrombosis. **J Thromb Haemost***, 3: (1): 46-53.

Jallow, Z., Jacobi, U.G., Weeks, D.L., et al. (2004) Specialized and redundant roles of TBP and a vertebrate-specific TBP paralog in embryonic gene regulation in Xenopus. **Proc Natl Acad Sci U S A***, 101: (37): 13525-13530.

Jennewein, C., Kuhn, A.M., Schmidt, M.V., et al. (2008) Sumoylation of peroxisome proliferator-activated receptor gamma by apoptotic cells prevents lipopolysaccharide-induced NCoR removal from kappaB binding sites mediating transrepression of proinflammatory cytokines. **J Immunol***, 181: (8): 5646-5652.

Jones, K.S., Alimov, A.P., Rilo, H.L., et al. (2008) A high throughput live transparent animal bioassay to identify non-toxic small molecules or genes that regulate vertebrate fat metabolism for obesity drug development. **Nutr Metab (Lond)***, 5: 23.

Kadereit, B., Kumar, P., Wang, W.J., et al. (2008) Evolutionarily conserved gene family important for fat storage. **Proc Natl Acad Sci U S A***, 105: (1): 94-99.

Kagey, M.H., Newman, J.J., Bilodeau, S., et al. (2010) Mediator and cohesin connect gene expression and chromatin architecture. **Nature***, 467: (7314): 430-435.

Kaltenbach, L., Horner, M.A., Rothman, J.H., et al. (2000) The TBP-like factor CeTLF is required to activate RNA polymerase II transcription during C. elegans embryogenesis. **Mol Cell***, 6: (3): 705-713.

Kim, J.K., Gimeno, R.E., Higashimori, T., et al. (2004) Inactivation of fatty acid transport protein 1 prevents fat-induced insulin resistance in skeletal muscle. **J Clin Invest***, 113: (5): 756-763.

Kimmel, C.B., Ballard, W.W., Kimmel, S.R., et al. (1995) Stages of embryonic development of the zebrafish. **Dev Dyn***, 203: (3): 253-310.

Kimmel, C.B., Miller, C.T. and Moens, C.B. (2001) Specification and morphogenesis of the zebrafish larval head skeleton. **Dev Biol***, 233: (2): 239-257.

Knight, R.D. and Schilling, T.F. (2006) Cranial neural crest and development of the head skeleton. **Adv Exp Med Biol***, 589: 120-133.

Kodera, Y., Takeyama, K., Murayama, A., et al. (2000) Ligand type-specific interactions of peroxisome proliferator-activated receptor gamma with transcriptional coactivators. **J Biol Chem**, 275: (43): 33201-33204.

Konig, H., Matter, N., Bader, R., et al. (2007) Splicing segregation: the minor spliceosome acts outside the nucleus and controls cell proliferation. **Cell**, 131: (4): 718-729.

Kopytova, D.V., Krasnov, A.N., Kopantceva, M.R., et al. (2006) Two isoforms of Drosophila TRF2 are involved in embryonic development, premeiotic chromatin condensation, and proper differentiation of germ cells of both sexes. **Mol Cell Biol**, 26: (20): 7492-7505.

Korzh, S., Pan, X., Garcia-Lecea, M., et al. (2008) Requirement of vasculogenesis and blood circulation in late stages of liver growth in zebrafish. **BMC Dev Biol**, 8: 84.

Lam, S.H., Wu, Y.L., Vega, V.B., et al. (2006) Conservation of gene expression signatures between zebrafish and human liver tumors and tumor progression. **Nat Biotechnol**, 24: (1): 73-75.

Lee, B.M. and Mahadevan, L.C. (2009) Stability of histone modifications across mammalian genomes: implications for 'epigenetic' marking. **J Cell Biochem**, 108: (1): 22-34.

Lee, D.H., Gershenzon, N., Gupta, M., et al. (2005) Functional characterization of core promoter elements: the downstream core element is recognized by TAF1. **Mol Cell Biol**, 25: (21): 9674-9686.

Leesnitzer, L.M., Parks, D.J., Bledsoe, R.K., et al. (2002) Functional consequences of cysteine modification in the ligand binding sites of peroxisome proliferator activated receptors by GW9662. **Biochemistry**, 41: (21): 6640-6650.

Lefterova, M.I., Zhang, Y., Steger, D.J., et al. (2008) PPARgamma and C/EBP factors orchestrate adipocyte biology via adjacent binding on a genome-wide scale. **Genes Dev**, 22: (21): 2941-2952.

Levine, M. (2011) Paused RNA polymerase II as a developmental checkpoint. **Cell**, 145: (4): 502-511.

Li, N., Kelsh, R.N., Croucher, P., et al. (2010) Regulation of neural crest cell fate by the retinoic acid and Pparg signalling pathways. **Development**, 137: (3): 389-394.

Li, V.C., Davis, J.C., Lenkov, K., et al. (2009) Molecular evolution of the testis TAFs of Drosophila. **Mol Biol Evol**, 26: (5): 1103-1116.

Liu, W.L., Coleman, R.A., Ma, E., et al. (2009) Structures of three distinct activator-TFIID complexes. **Genes Dev**, 23: (13): 1510-1521.

Lively, T.N., Nguyen, T.N., Galasinski, S.K., et al. (2004) The basic leucine zipper domain of c-Jun functions in transcriptional activation through interaction with the N terminus of human TATA-binding protein-associated factor-1 (human TAF(II)250). **J Biol Chem**, 279: (25): 26257-26265.

Lorent, K., Yeo, S.Y., Oda, T., et al. (2004) Inhibition of Jagged-mediated Notch signaling disrupts zebrafish biliary development and generates multi-organ defects compatible with an Alagille syndrome phenocopy. **Development**, 131: (22): 5753-5766.

Lu, F.I., Thisse, C. and Thisse, B. (2011) Identification and mechanism of regulation of the zebrafish dorsal determinant. **Proc Natl Acad Sci U S A**.

Lunde, K., Belting, H.G. and Driever, W. (2004) Zebrafish pou5f1/pou2, homolog of mammalian Oct4, functions in the endoderm specification cascade. **Curr Biol**, 14: (1): 48-55.

Makowski, L., Boord, J.B., Maeda, K., et al. (2001) Lack of macrophage fatty-acid-binding protein aP2 protects mice deficient in apolipoprotein E against atherosclerosis. **Nat Med**, 7: (6): 699-705.

Maldonado, E. (1999) Transcriptional functions of a new mammalian TATA-binding protein-related factor. **J Biol Chem**, 274: (19): 12963-12966.

Marlow, F.L. (2010).

Marlow, F.L. and Mullins, M.C. (2008) Bucky ball functions in Balbiani body assembly and animal-vegetal polarity in the oocyte and follicle cell layer in zebrafish. **Dev Biol**, 321: (1): 40-50.

Martianov, I., Fimia, G.M., Dierich, A., et al. (2001) Late arrest of spermiogenesis and germ cell apoptosis in mice lacking the TBP-like TLF/TRF2 gene. **Mol Cell**, 7: (3): 509-515.

Martianov, I., Viville, S. and Davidson, I. (2002) RNA polymerase II transcription in murine cells lacking the TATA binding protein. **Science**, 298: (5595): 1036-1039.

Martinez, E. (2002) Multi-protein complexes in eukaryotic gene transcription. **Plant Mol Biol**, 50: (6): 925-947.

Matthews, R.P., Lorent, K., Manoral-Mobias, R., et al. (2009) TNFalpha-dependent hepatic steatosis and liver degeneration caused by mutation of zebrafish S-adenosylhomocysteine hydrolase. **Development**, 136: (5): 865-875.

Matthews, R.P., Lorent, K. and Pack, M. (2008) Transcription factor onecut3 regulates intrahepatic biliary development in zebrafish. **Dev Dyn**, 237: (1): 124-131.

Matthews, R.P., Lorent, K., Russo, P., et al. (2004) The zebrafish onecut gene hnf-6 functions in an evolutionarily conserved genetic pathway that regulates vertebrate biliary development. **Dev Biol**, 274: (2): 245-259.

Matthews, R.P., Plumb-Rudewiez, N., Lorent, K., et al. (2005) Zebrafish vps33b, an ortholog of the gene responsible for human arthrogryposis-renal dysfunction-cholestasis syndrome, regulates biliary development downstream of the onecut transcription factor hnf6. **Development**, 132: (23): 5295-5306.

McCurley, A.T. and Callard, G.V. (2008) Characterization of housekeeping genes in zebrafish: male-female differences and effects of tissue type, developmental stage and chemical treatment. **BMC Mol Biol**, 9: 102.

McKenna, N.J. and O'Malley, B.W. (2010) SnapShot: NR coregulators. **Cell**, 143: (1): 172-172 e171.

Mengus, G., Fadloun, A., Kobi, D., et al. (2005) TAF4 inactivation in embryonic fibroblasts activates TGF beta signalling and autocrine growth. **EMBO J**, 24: (15): 2753-2767.

Meyer, A. and Van de Peer, Y. (2005) From 2R to 3R: evidence for a fish-specific genome duplication (FSGD). **Bioessays**, 27: (9): 937-945.

Mikkelsen, T.S., Ku, M., Jaffe, D.B., et al. (2007) Genome-wide maps of chromatin state in pluripotent and lineage-committed cells. **Nature**, 448: (7153): 553-560.

Moore, P.A., Ozer, J., Salunek, M., et al. (1999) A human TATA binding protein-related protein with altered DNA binding specificity inhibits transcription from multiple promoters and activators. **Mol Cell Biol**, 19: (11): 7610-7620.

Morcos, P.A. (2007) Achieving targeted and quantifiable alteration of mRNA splicing with Morpholino oligos. **Biochem Biophys Res Commun**, 358: (2): 521-527.

Mujtaba, S., Zeng, L. and Zhou, M.M. (2007) Structure and acetyl-lysine recognition of the bromodomain. **Oncogene**, 26: (37): 5521-5527.

Muller, F., Lakatos, L., Dantonel, J., et al. (2001) TBP is not universally required for zygotic RNA polymerase II transcription in zebrafish. **Curr Biol**, 11: (4): 282-287.

Muller, F. and Tora, L. (2004) The multicoloured world of promoter recognition complexes. **EMBO J**, 23: (1): 2-8.

Munz, C., Psichari, E., Mandilis, D., et al. (2003) TAF7 (TAFII55) plays a role in the transcription activation by c-Jun. **J Biol Chem**, 278: (24): 21510-21516.

Nassir, F., Wilson, B., Han, X., et al. (2007) CD36 is important for fatty acid and cholesterol uptake by the proximal but not distal intestine. **J Biol Chem**, 282: (27): 19493-19501.

Ng, A., Uribe, R.A., Yieh, L., et al. (2009) Zebrafish mutations in gart and paics identify crucial roles for de novo purine synthesis in vertebrate pigmentation and ocular development. **Development**, 136: (15): 2601-2611.

Nicolakakis, N. and Hamel, E. (2010) The Nuclear Receptor PPARgamma as a Therapeutic Target for Cerebrovascular and Brain Dysfunction in Alzheimer's Disease. **Front Aging Neurosci**, 2.

Nielsen, R., Pedersen, T.A., Hagenbeek, D., et al. (2008) Genome-wide profiling of PPARgamma:RXR and RNA polymerase II occupancy reveals temporal activation of distinct metabolic pathways and changes in RXR dimer composition during adipogenesis. **Genes Dev**, 22: (21): 2953-2967.

Noel, E.S., Casal-Sueiro, A., Busch-Nentwich, E., et al. (2008) Organ-specific requirements for Hdac1 in liver and pancreas formation. **Dev Biol**, 322: (2): 237-250.

Ohler, U. and Wassarman, D.A. (2010) Promoting developmental transcription. **Development**, 137: (1): 15-26.

Panne, D. (2008) The enhanceosome. **Curr Opin Struct Biol**, 18: (2): 236-242.

Papai, G., Tripathi, M.K., Ruhlmann, C., et al. (2009) Mapping the initiator binding Taf2 subunit in the structure of hydrated yeast TFIID. **Structure**, 17: (3): 363-373.

Pascual, G., Fong, A.L., Ogawa, S., et al. (2005) A SUMOylation-dependent pathway mediates transrepression of inflammatory response genes by PPAR-gamma. **Nature**, 437: (7059): 759-763.

Passeri, M.J., Cinaroglu, A., Gao, C., et al. (2009) Hepatic steatosis in response to acute alcohol exposure in zebrafish requires sterol regulatory element binding protein activation. **Hepatology**, 49: (2): 443-452.

Pelegri, F. (2003) Maternal factors in zebrafish development. **Dev Dyn**, 228: (3): 535-554.

Perletti, L., Kopf, E., Carre, L., et al. (2001) Coordinate regulation of RARgamma2, TBP, and TAFII135 by targeted proteolysis during retinoic acid-induced differentiation of F9 embryonal carcinoma cells. **BMC Mol Biol**, 2: 4.

Persengiev, S.P., Zhu, X., Dixit, B.L., et al. (2003) TRF3, a TATA-box-binding protein-related factor, is vertebrate-specific and widely expressed. **Proc Natl Acad Sci U S A**, 100: (25): 14887-14891.

Pfaffl, M.W. (2001) A new mathematical model for relative quantification in real-time RT-PCR. **Nucleic Acids Res**, 29: (9): e45.

Phillips, J.E. and Corces, V.G. (2009) CTCF: master weaver of the genome. **Cell**, 137: (7): 1194-1211.

Pijnappel, W.W. and Timmers, H.T. (2008) Dubbing SAGA unveils new epigenetic crosstalk. **Mol Cell**, 29: (2): 152-154.

Pointud, J.C., Mengus, G., Brancorsini, S., et al. (2003) The intracellular localisation of TAF7L, a paralogue of transcription factor TFIID subunit TAF7, is developmentally regulated during male germ-cell differentiation. **J Cell Sci**, 116: (Pt 9): 1847-1858.

Prince, F., Katsuyama, T., Oshima, Y., et al. (2008) The YPWM motif links Antennapedia to the basal transcriptional machinery. **Development**, 135: (9): 1669-1679.

Rabenstein, M.D., Zhou, S., Lis, J.T., et al. (1999) TATA box-binding protein (TBP)-related factor 2 (TRF2), a third member of the TBP family. **Proc Natl Acad Sci U S A**, 96: (9): 4791-4796.

Rampon, C., Bouzaffour, M., Ostuni, M.A., et al. (2009) Translocator protein (18 kDa) is involved in primitive erythropoiesis in zebrafish. **FASEB J**, 23: (12): 4181-4192.

Reeves, W.M. and Hahn, S. (2005) Targets of the Gal4 transcription activator in functional transcription complexes. **Mol Cell Biol**, 25: (20): 9092-9102.

Robu, M.E., Larson, J.D., Nasevicius, A., et al. (2007) p53 activation by knockdown technologies. **PLoS Genet**, 3: (5): e78.

Roh, T.Y., Cuddapah, S. and Zhao, K. (2005) Active chromatin domains are defined by acetylation islands revealed by genome-wide mapping. **Genes Dev**, 19: (5): 542-552.

Rojo-Niersbach, E., Furukawa, T. and Tanese, N. (1999) Genetic dissection of hTAF(II)130 defines a hydrophobic surface required for interaction with glutamine-rich activators. **J Biol Chem**, 274: (47): 33778-33784.

Rolph, M.S., Young, T.R., Shum, B.O., et al. (2006) Regulation of dendritic cell function and T cell priming by the fatty acid-binding protein AP2. **J Immunol**, 177: (11): 7794-7801.

Rosenfeld, J.A., Wang, Z., Schones, D.E., et al. (2009) Determination of enriched histone modifications in non-genic portions of the human genome. **BMC Genomics**, 10: 143.

Ryu, S., Holzschuh, J., Erhardt, S., et al. (2005) Depletion of minichromosome maintenance protein 5 in the zebrafish retina causes cell-cycle defect and apoptosis. **Proc Natl Acad Sci U S A**, 102: (51): 18467-18472.

Sadler, K.C., Amsterdam, A., Soroka, C., et al. (2005) A genetic screen in zebrafish identifies the mutants vps18, nf2 and foie gras as models of liver disease. **Development**, 132: (15): 3561-3572.

Sakaguchi, T.F., Sadler, K.C., Crosnier, C., et al. (2008) Endothelial signals modulate hepatocyte apicobasal polarization in zebrafish. **Curr Biol**, 18: (20): 1565-1571.

Schaffer, J.E. and Lodish, H.F. (1994) Expression cloning and characterization of a novel adipocyte long chain fatty acid transport protein. **Cell**, 79: (3): 427-436.

Schlegel, A. and Stainier, D.Y. (2006) Microsomal triglyceride transfer protein is required for yolk lipid utilization and absorption of dietary lipids in zebrafish larvae. **Biochemistry**, 45: (51): 15179-15187.

Schlombs, K., Wagner, T. and Scheel, J. (2003) Site-1 protease is required for cartilage development in zebrafish. **Proc Natl Acad Sci U S A**, 100: (24): 14024-14029.

Schmidt, M.V., Brune, B. and von Knethen, A. (2010) The nuclear hormone receptor PPARgamma as a therapeutic target in major diseases. **ScientificWorldJournal**, 10: 2181-2197.

Schmitz, K.M., Schmitt, N., Hoffmann-Rohrer, U., et al. (2009) TAF12 recruits Gadd45a and the nucleotide excision repair complex to the promoter of rRNA genes leading to active DNA demethylation. **Mol Cell**, 33: (3): 344-353.

Selman, K., Wallace, R.A., Sarka, A., et al. (1993) Stages of oocyte development in the zebrafish, Brachydanio rerio. **Journal of Morphology**, 218: (2): 203-224.

Seyffert, W. (2003) Lehrbuch der Genetik. **Spektrum Akademischer Verlag**.

Shum, B.O., Mackay, C.R., Gorgun, C.Z., et al. (2006) The adipocyte fatty acid-binding protein aP2 is required in allergic airway inflammation. **J Clin Invest**, 116: (8): 2183-2192.

Silverstein, R.L., Baird, M., Lo, S.K., et al. (1992) Sense and antisense cDNA transfection of CD36 (glycoprotein IV) in melanoma cells. Role of CD36 as a thrombospondin receptor. **J Biol Chem**, 267: (23): 16607-16612.

Smith, E. and Shilatifard, A. (2010) The chromatin signaling pathway: diverse mechanisms of recruitment of histone-modifying enzymes and varied biological outcomes. **Mol Cell**, 40: (5): 689-701.

Song, Y. and Cone, R.D. (2007) Creation of a genetic model of obesity in a teleost. **FASEB J**, 21: (9): 2042-2049.

Soutoglou, E., Demeny, M.A., Scheer, E., et al. (2005) The nuclear import of TAF10 is regulated by one of its three histone fold domain-containing interaction partners. **Mol Cell Biol**, 25: (10): 4092-4104.

Stahl, A., Evans, J.G., Pattel, S., et al. (2002) Insulin causes fatty acid transport protein translocation and enhanced fatty acid uptake in adipocytes. **Dev Cell**, 2: (4): 477-488.

Stoletov, K., Fang, L., Choi, S.H., et al. (2009) Vascular lipid accumulation, lipoprotein oxidation, and macrophage lipid uptake in hypercholesterolemic zebrafish. **Circ Res**, 104: (8): 952-960.

Streisinger, G., Walker, C., Dower, N., et al. (1981) Production of clones of homozygous diploid zebra fish (Brachydanio rerio). **Nature**, 291: (5813): 293-296.

Takada, S., Lis, J.T., Zhou, S., et al. (2000) A TRF1:BRF complex directs Drosophila RNA polymerase III transcription. **Cell**, 101: (5): 459-469.

Tatarakis, A., Margaritis, T., Martinez-Jimenez, C.P., et al. (2008) Dominant and redundant functions of TFIID involved in the regulation of hepatic genes. **Mol Cell**, 31: (4): 531-543.

Thisse, B., Thisse, C. (2004) Fast Release Clones: A High Throughput Expression Analysis. **ZFIN Direct Data Submission ([http://zfin.org](http://zfin.org)).**

Thomas, M.C. and Chiang, C.M. (2006) The general transcription machinery and general cofactors. **Crit Rev Biochem Mol Biol***,* 41: (3): 105-178.

Thut, C.J., Chen, J.L., Klemm, R., et al. (1995) p53 transcriptional activation mediated by coactivators TAFII40 and TAFII60. **Science***,* 267: (5194): 100-104.

Tora, L. (2002) A unified nomenclature for TATA box binding protein (TBP)-associated factors (TAFs) involved in RNA polymerase II transcription. **Genes Dev***,* 16: (6): 673-675.

Tuncman, G., Erbay, E., Hom, X., et al. (2006) A genetic variant at the fatty acid-binding protein aP2 locus reduces the risk for hypertriglyceridemia, type 2 diabetes, and cardiovascular disease. **Proc Natl Acad Sci U S A***,* 103: (18): 6970-6975.

Uysal, K.T., Scheja, L., Wiesbrock, S.M., et al. (2000) Improved glucose and lipid metabolism in genetically obese mice lacking aP2. **Endocrinology***,* 141: (9): 3388-3396.

van Beekum, O., Fleskens, V. and Kalkhoven, E. (2009) Posttranslational modifications of PPAR-gamma: fine-tuning the metabolic master regulator. **Obesity (Silver Spring)***,* 17: (2): 213-219.

Veenstra, G.J., Weeks, D.L. and Wolffe, A.P. (2000) Distinct roles for TBP and TBP-like factor in early embryonic gene transcription in Xenopus. **Science***,* 290: (5500): 2312-2315.

Vermeulen, M., Mulder, K.W., Denissov, S., et al. (2007) Selective anchoring of TFIID to nucleosomes by trimethylation of histone H3 lysine 4. **Cell***,* 131: (1): 58-69.

Verrijzer, C.P., Yokomori, K., Chen, J.L., et al. (1994) Drosophila TAFII150: similarity to yeast gene TSM-1 and specific binding to core promoter DNA. **Science***,* 264: (5161): 933-941.

Visel, A., Blow, M.J., Li, Z., et al. (2009) ChIP-seq accurately predicts tissue-specific activity of enhancers. **Nature***,* 457: (7231): 854-858.

Viswakarma, N., Jia, Y., Bai, L., et al. (2010) Coactivators in PPAR-Regulated Gene Expression. **PPAR Res***,* 2010.

Voss, A.K., Thomas, T., Petrou, P., et al. (2000) Taube nuss is a novel gene essential for the survival of pluripotent cells of early mouse embryos. **Development***,* 127: (24): 5449-5461.

Wagner, D.S., Dosch, R., Mintzer, K.A., et al. (2004) Maternal control of development at the midblastula transition and beyond: mutants from the zebrafish II. **Dev Cell***,* 6: (6): 781-790.

Walker, C. and Streisinger, G. (1983) Induction of Mutations by gamma-Rays in Pregonial Germ Cells of Zebrafish Embryos. **Genetics***,* 103: (1): 125-136.

Walker, S.S., Shen, W.C., Reese, J.C., et al. (1997) Yeast TAF(II)145 required for transcription of G1/S cyclin genes and regulated by the cellular growth state. **Cell***,* 90: (4): 607-614.

Wang, H. and Eckel, R.H. (2009) Lipoprotein lipase: from gene to obesity. **Am J Physiol Endocrinol Metab***,* 297: (2): E271-288.

Wang, P., Anderson, P.O., Chen, S., et al. (2001) Inhibition of the transcription factors AP-1 and NF-kappaB in CD4 T cells by peroxisome proliferator-activated receptor gamma ligands. **Int Immunopharmacol***,* 1: (4): 803-812.

Wang, X., Truckses, D.M., Takada, S., et al. (2007) Conserved region I of human coactivator TAF4 binds to a short hydrophobic motif present in transcriptional regulators. **Proc Natl Acad Sci U S A***,* 104: (19): 7839-7844.

Wiczer, B.M. and Bernlohr, D.A. (2009) A novel role for fatty acid transport protein 1 in the regulation of tricarboxylic acid cycle and mitochondrial function in 3T3-L1 adipocytes. **J Lipid Res***,* 50: (12): 2502-2513.

Wilhelm, E., Pellay, F.X., Benecke, A., et al. (2008) TAF6delta controls apoptosis and gene expression in the absence of p53. **PLoS One***,* 3: (7): e2721.

Wright, K.J., Marr, M.T., 2nd and Tjian, R. (2006) TAF4 nucleates a core subcomplex of TFIID and mediates activated transcription from a TATA-less promoter. **Proc Natl Acad Sci U S A**, 103: (33): 12347-12352.

Wright, K.J. and Tjian, R. (2009) Wnt signaling targets ETO coactivation domain of TAF4/TFIID in vivo. **Proc Natl Acad Sci U S A**, 106: (1): 55-60.

Xiao, L., Kim, M. and DeJong, J. (2006) Developmental and cell type-specific regulation of core promoter transcription factors in germ cells of frogs and mice. **Gene Expr Patterns**, 6: (4): 409-419.

Xing, H., Vanderford, N.L. and Sarge, K.D. (2008) The TBP-PP2A mitotic complex bookmarks genes by preventing condensin action. **Nat Cell Biol**, 10: (11): 1318-1323.

Yanagisawa, S. (2004) Dof domain proteins: plant-specific transcription factors associated with diverse phenomena unique to plants. **Plant Cell Physiol**, 45: (4): 386-391.

Yaniv, K., Isogai, S., Castranova, D., et al. (2007) Imaging the developing lymphatic system using the zebrafish. **Novartis Found Symp**, 283: 139-148; discussion 148-151, 238-141.

Yap, K.L. and Zhou, M.M. (2011) Structure and mechanisms of lysine methylation recognition by the chromodomain in gene transcription. **Biochemistry**, 50: (12): 1966-1980.

Yelick, P.C. and Schilling, T.F. (2002) Molecular dissection of craniofacial development using zebrafish. **Crit Rev Oral Biol Med**, 13: (4): 308-322.

Zhang, D., Penttila, T.L., Morris, P.L., et al. (2001) Spermiogenesis deficiency in mice lacking the Trf2 gene. **Science**, 292: (5519): 1153-1155.

Zhou, J., Febbraio, M., Wada, T., et al. (2008) Hepatic fatty acid transporter Cd36 is a common target of LXR, PXR, and PPARgamma in promoting steatosis. **Gastroenterology**, 134: (2): 556-567.

# 9   Publications

Following is a list of my publications with a comment about my contribution to the work:

1. Müller F, **Zaucker A,** Tora L. **(2010)**: *Developmental regulation of transcription initiation: more than just changing the actors.* **Curr Opin Genet Dev.** Review  PMID: 20598874 (minor contribution to the part about TAFs)

2. Csenki Z, **Zaucker A**, Kovács B, Hadzhiev Y, Hegyi A, Lefler KK, Müller T, Kovács R, Urbányi B, Váradi L, Müller F.**(2010)**: *Intraovarian transplantation of stage I-II follicles results in viable zebrafish embryos.* **Int J Dev Biol.** PMID: 20209431 (substantial contribution by planning and performing some of the experiment)

3. Cullinane AR, Straatman-Iwanowska A, **Zaucker A**, Wakabayashi Y, Bruce CK, Luo G, Rahman F, Gürakan F, Utine E, Ozkan TB, Denecke J, Vukovic J, Di Rocco M, Mandel H, Cangul H, Matthews RP, Thomas SG, Rappoport JZ, Arias IM, Wolburg H, Knisely AS, Kelly DA, Müller F, Maher ER, Gissen P. **(2010)**: *Mutations in VIPAR cause an arthrogryposis, renal dysfunction and cholestasis syndrome phenotype with defects in epithelial polarization.* **Nat Genet.** PMID: 20190753 (substantial contribution to the zebrafish part)

4. Gehrig J, Reischl M, Kalmár E, Ferg M, Hadzhiev Y, **Zaucker A**, Song C, Schindler S, Liebel U, Müller F. **(2009)**: *Automated high-throughput mapping of promoter-enhancer interactions in zebrafish embryos.* **Nat Methods.** PMID: 19898487 (minor contribution by conducting basic zebrafish work)